Eur. Phys. J. Plus (2023) 138:709
https://doi.org/10.1140/epjp/s13360-023-04249-x

THE EUROPEAN PHYSICAL JOURNAL PLUS

Regular Article

Nuclear physics midterm plan at Legnaro National Laboratories (LNL)

M. Ballan[1], S. Bottoni[2,3], M. Caamaño[4], A. Caciolli[5,6], M. Campostrini[1], M. Cicerchia[1], F. C. L. Crespi[2,3], S. Cristallo[7,8], D. Dell'Aquila[9,10], R. Depalo[2,3], E. Fioretto[1], F. Galtarossa[1,5], L. R. Gasques[11], A. Gottardo[1], F. Gramegna[1], F. Gulminelli[12], T. Kurtukian-Nieto[13], M. La Cognata[10], S. M. Lenzi[5,6], T. Marchi[1], K. Mazurek[14], D. Mengoni[5,6,a], L. Mou[1,15], R. Nania[16], G. Pupillo[1], J. J. Valiente-Dobón[1,b], I. Zanon[1,15], L. Acosta[17], M. A. G. Alvarez[18], A. Andrighetto[1], A. Arazi[19], A. Arzenton[1,20], M. Assié[21], M. Bagatin[5], F. Barbaro[6,22], C. Barbieri[2,3], S. Barlini[23,24], L. Basiricò[25], G. Battistoni[3], D. Beaumel[20], M. A. Bentley[26], G. Benzoni[3], S. Bertoldo[1], C. Bertulani[27], A. Bonasera[10,28], A. Camaiani[29], L. Canton[6], V. Capirossi[30], M. P. Carante[22,31], C. Carraro[1], S. M. Carturan[1,5], G. Casini[23], F. Cavanna[32], L. Centofante[1], E. R. Chávez[17], A. Chbihi[33], M. Ciemała[14], S. Cisternino[1,34], A. Colombi[22,31], M. Colucci[2,3], A. Compagnucci[35], S. Corradetti[1], L. Corradi[1], G. D'Agata[10,36], G. de Angelis[1], L. De Dominicis[1,5], D. De Salvador[5], E. DeFilippo[37], M. Del Fabbro[6,15], A. Di Nitto[38,39], S. Ditalia Tchernij[40], A. Donzella[31,41], T. Duguet[29,42], J. Esposito[1], F. Favela[17], J. P. Fernández-García[18], F. Flavigny[43], A. Fontana[31], B. Fornal[14], J. Forneris[40], B. Fraboni[25], J. Frankland[33], E. Gamba[2,3], E. Geraci[36,37], S. Gerardin[5], S. A. Giuliani[44], B. Gnoffo[36,37], F. Groppi[2,3], D. Gruyer[42], F. Haddad[45,46], J. Isaak[47], M. Kmiecik[14], A. Koning[48], L. Lamia[10,36], N. Le Neindre[33], S. Leoni[2,3], A. Lépine-Szily[11], G. Lilli[1], I. Lombardo[36,37], M. Loriggiola[1], L. Loriggiola[1], M. Lunardon[5,6], G. Maggioni[1,5], A. Maj[14], S. Manenti[2,3], M. Manzolaro[1], L. E. Marcucci[49,50], D. J. Marín-Lámbarri[17], E. Mariotti[20], G. Martin Hernandez[51], C. Massimi[16,25], P. Mastinu[1], M. Mazzocco[5,6], A. Mazzolari[52], T. Mijatović[53], T. Mishenina[54], K. Mizuyama[55], A. Monetti[1], G. Montagnoli[5,6], L. Morselli[1,15], L. Moschini[56], E. Musacchio Gonzalez[1], A. Nannini[23], Y. F. Niu[57], S. Ota[58], A. Paccagnella[59], S. Palmerini[8,60], L. Pellegri[61], A. Perego[62], S. Piantelli[23], D. Piatti[5,6], F. Picollo[40], M. Pignatari[63,64], F. Pinna[30], S. Pirrone[37], R. G. Pizzone[10], M. Polettini[2,3], G. Politi[36,37], L. Popescu[65], G. Prete[1], A. Quaranta[66,67], R. Raabe[29], J. P. Ramos[65], W. Raniero[1], G. G. Rapisarda[10,36], F. Recchia[5,6], V. Rigato[1], X. Roca Maza[2,3], M. Rocchini[23], T. Rodriguez[44], C. Roncolato[1], D. Rudolph[68], P. Russotto[10], Á. M. Sánchez-Benítez[69], D. Savran[70], D. Scarpa[1], M. Scheck[71], K. Sekizawa[72,73], M. L. Sergi[10,36], F. Sgarbossa[1,5], L. Silvestrin[5,6], O. Singh Khwairakpam[1,20], J. Skowronski[5,6], V. Somà[42], R. Spartà[10], M. Spieker[74], A. M. Stefanini[1], H. Steiger[75,76], L. Stevanato[6], M. R. Stock[76], E. Vardaci[38,39], D. Verney[21], D. Vescovi[7,8,77], E. Vittone[40], V. Werner[47], C. Wheldon[78], O. Wieland[3], K. Wimmer[70], J. Wyss[6,79], L. Zago[1,5], A. Zenoni[31,41]

[1] Laboratori Nazionali di Legnaro, Istituto Nazionale di Fisica Nucleare, Viale dell'Università 2, 35020 Legnaro, Italy
[2] Dipartimento di Fisica, Università degli Studi di Milano, Via Celoria 16, 20133 Milan, Italy
[3] Istituto Nazionale di Fisica Nucleare, Sezione di Milano, Via Celoria 16, 20133 Milan, Italy
[4] IGFAE, Universidade de Santiago de Compostela, Santiago de Compostela, Spain
[5] Dipartimento di Fisica e Astronomia, Università degli Studi di Padova, Via Marzolo 8, 35131 Padua, Italy
[6] Istituto Nazionale di Fisica Nucleare, Sezione di Padova, Via Marzolo 8, 35131 Padua, Italy
[7] INAF - Osservatorio Astronomico d'Abruzzo, Via Mentore Maggini snc, Loc. Collurania, 64100 Teramo, Italy
[8] Istituto Nazionale di Fisica Nucleare, Sezione di Perugia, Via Alessandro Pascoli, 06123 Perugia, Italy
[9] Dipartimento di Fisica "Ettore Pancini", Università degli Studi di Napoli "Federico II", Naples, Italy
[10] Laboratori Nazionali del Sud, Instituto Nazionale di Fisica Nucleare, Via S. Sofia 62, 95123 Catania, Italy
[11] Universidade de Sao Paulo, Instituto de Fisica, Rua do Matao, 1371, Sao Paulo 05508-090, Brazil
[12] LPC (IN2P3-CNRS/Ensicaen et Université), 14076 Caen Cédex, France
[13] CNRS/IN2P3 Université de Bordeaux LP2IB (CENBG), 19 chemin du Solarium, 33170 Gradignan, France
[14] Institute of Nuclear Physics Polish Academy of Sciences, 31342 Kraków, Poland
[15] Dipartimento di Fisica e Scienze della Terra, Università di Ferrara, Ferrara, Italy
[16] Istituto Nazionale di Fisica Nucleare, Sezione di Bologna, Bologna, Italy
[17] Instituto de Física, Universidad Nacional Autónoma de México, Apartado Postal 20-364, 01000 México City, Mexico
[18] Departamento de Física Atómica, Molecular y Nuclear, Universidad de Sevilla, Apartado 1065, 41080 Seville, Spain
[19] Laboratorio TANDAR, Comisión Nacional de Energía Atómica, Avenida General Paz 1499, BKNA1650 San Martín, Argentina
[20] Dipartimento di Scienze Fisiche, della Terra e dell'Ambiente, Università di Siena, Siena, Italy
[21] Université Paris-Saclay, CNRS/IN2P3, IJCLab, 91405 Orsay, France
[22] Dipartimento di Fisica, Università di Pavia, Pavia, Italy
[23] Istituto Nazionale di Fisica Nucleare, Sezione di Firenze, Florence, Italy
[24] Physics and Astronomy Department, University of Firenze, Florence, Italy
[25] Dipartimento di Fisica e Astronomia, Università di Bologna, Bologna, Italy
[26] School of Physics, Engineering and Technology, University of York, Heslington, York YO105DD, UK
[27] Department of Physics and Astronomy, Texas A &M University, Commerce, TX, USA
[28] Cyclotron Institute, Texas A &M University, College Station, TX 77843, USA
[29] Instituut voor Kern- en Stralingsfysica, K.U. Leuven, Celestijnenlaan 200D, 3001 Leuven, Belgium
[30] Department of Applied Science and Technology, Politecnico di Torino, Turin, Italy
[31] Istituto Nazionale di Fisica Nucleare, Sezione di Pavia, Pavia, Italy
[32] Istituto Nazionale di Fisica Nucleare, Sezione di Torino, Via P.Giuria 1, 10125 Turin, Italy
[33] Grand Accélérateur National d'Ions Lourds (GANIL), UPR 3266, CEA-DRF/CNRS-IN2P3, Boulevard Henri Becquerel, 14076 Caen Cedex, France

Published online: 14 August 2023

[34] Dipartimento di Ingegneria Industriale, Università di Padova, Padua, Italy
[35] Gran Sasso Science Institute, L'Aquila, Italy
[36] Dipartimento di Fisica e Astronomia "Ettore Majorana", Università degli Studi di Catania, Via S. Sofia 64, 95123 Catania, Italy
[37] Istituto Nazionale di Fisica Nucleare, Sezione di Catania, Via S. Sofia 62, 95123 Catania, Italy
[38] Physics Department, University of Naples, Naples, Italy
[39] Istituto Nazionale di Fisica Nucleare, Sezione di Napoli, Naples, Italy
[40] Dipartimento di Fisica, Università di Torino, Turin, Italy
[41] Dipartimento di Ingegneria meccanica e industriale, Universitá degli Studi di Brescia, Brescia, Italy
[42] CEA, Saclay, France
[43] Normandie Universitè ENSICAEN, UNICAEN, CNRS/IN2P3, Caen, France
[44] Departamento de Física Teórica, Universidad Autonoma de Madrid (UAM), Ciudad Universitaria de Cantoblanco, 28049 Madrid, Spain
[45] Laboratoire SUBATECH, CNRS/IN2P3, IMT Atlantique, Nantes Université, Nantes, France
[46] GIP ARRONAX, Saint Herblain, Nantes, France
[47] Institut für Kernphysik, Technische Universität Darmstadt, Darmstadt, Germany
[48] International Atomic Energy Agency (IAEA), Wien, Austria
[49] Istituto Nazionale di Fisica Nucleare, Sezione di Pisa, Largo B. Pontecorvo, 3, 56127 Pisa, Italy
[50] Dipartimento di Fisica, Università degli Studi di Pisa, Largo B. Pontecorvo, 3, 56127 Pisa, Italy
[51] Centro de Aplicaciones Tecnológicas y Desarrollo Nuclear, Havana, Cuba
[52] Istituto Nazionale di Fisica Nucleare, Sezione di Ferrara, Ferrara, Italy
[53] Ruder Bošković Institute, Zagreb, Croatia
[54] Astronomical Observatory, Odessa National University, 1v, Marazliyivska st, Odessa 65014, Ukraine
[55] Duy Tan University, Da Nang, Vietnam
[56] Department of Physics, University of Surrey, Stag Hill, Guildford GU2 7XH, UK
[57] Lanzhou University, Lanzhou, China
[58] RCNP Osaka University, Osaka, Japan
[59] Dipartimento di Ingegneria dell' Informazione, Università di Padova, Padua, Italy
[60] Dipartimento di Fisica e Geologia, Università degli Studi di Perugia, Via Alessandro Pascoli, 06123 Perugia, Italy
[61] WITS & iTL South Africa, Cape Town, South Africa
[62] Dipartimento di Fisica, Università degli Studi di Trento, Via Sommarive, 14, 38123 Povo, Italy
[63] Konkoly Observatory, Konkoly-Thege Miklós út 13-17, Budapest 1121, Hungary
[64] Hull University, Hull HU6 7RX, UK
[65] Belgian Nuclear Research Centre SCK CEN, Boeretang 200, 2400 Mol, Belgium
[66] Dipartimento di Ingegneria Industriale, Università di Trento, Trento, Italy
[67] INFN, Trento Institute for Fundamental Physics and Application (TIFPA), Trento, Italy
[68] Department of Physics, Lund University, 22100 Lund, Sweden
[69] Centro de Estudios Avanzados en Física Matemática y Computación, Universidad de Huelva, Calle Dr. Cantero Cuadrado, 6, 21004 Huelva, Spain
[70] GSI Helmholtzzentrum für Schwerionenforschung, Darmstadt, Germany
[71] University of the West of Scotland, Paisley, UK
[72] Department of Physics, School of Science, Tokyo Institute of Technology, Tokyo 152-8551, Japan
[73] Nuclear Physics Division, Center for Computational Sciences, University of Tsukuba, Ibaraki 305-8577, Japan
[74] University of Florida State, Tallahassee, USA
[75] Johannes Gutenberg-Universität Mainz, Mainz, Germany
[76] Technische Universität München, Munich, Germany
[77] Institute for Applied Physics, Goethe University, 60438 Frankfurt, Germany
[78] University of Birmingham, Birmingham, UK
[79] Dipartimento di Ingegneria Civile e Meccanica, Università degli Studi di Cassino e del Lazio Meridionale, Cassino, Frosinone, Italy

Received: 1 February 2023 / Accepted: 2 July 2023

Abstract The next years will see the completion of the radioactive ion beam facility SPES (Selective Production of Exotic Species) and the upgrade of the accelerators complex at Istituto Nazionale di Fisica Nucleare – Legnaro National Laboratories (LNL) opening up new possibilities in the fields of nuclear structure, nuclear dynamics, nuclear astrophysics, and applications. The nuclear physics community has organised a workshop to discuss the new physics opportunities that will be possible in the near future by employing state-of-the-art detection systems. A detailed discussion of the outcome from the workshop is presented in this report.

[a] e-mail: daniele.mengoni@pd.infn.it (corresponding author)
[b] e-mail: javier.valiente@lnl.infn.it (corresponding author)

1 Executive summary

The Legnaro National Laboratories (LNL) of the Istituto Nazionale di Fisica Nucleare (INFN) are an user-oriented large-scale facility mainly dedicated to research programs in nuclear physics and nuclear astrophysics, and to high-level technology developments relevant to several disciplines [1]. The LNL accelerator complex consists in two smaller electrostatic accelerators (the 2 MV AN2000 and the 7 MV CN) and the Tandem-ALPI-PIAVE complex (TAP), with a 15 MV Tandem XTU and the superconducting RFQ PIAVE [2], equipped with a ECR source, acting as injectors of the superconducting Linac ALPI [3]. In addition, the SPES (Selective Production of Exotic Species) project will provide second-generation ISOL (Isotope Separation On-Line) beams. The SPES project is based on a dual-exit cyclotron B70 providing proton beams with energies ranging between 35 MeV and 70 MeV and a maximum beam intensity of 0.75 mA. This is the primary accelerator of the ISOL system, based on a UCx target, for the production of neutron-rich unstable ion beams. The cyclotron will be also used for applied physics activities. The available facilities at LNL together with the state-of-the-art instrumentation are discussed in Sect. 2. The SPES facility will provide ion beams that are complementary to the fragmentation beams which will be produced by FraISe (FRAgment Ion Separator) [4] at LNS. These two main laboratories of INFN devoted to nuclear physics are, and will be even more in the near future, attractive poles for worldwide users. The SPES facility will operate in a very competitive international environment with other facilities such as: HIE-ISOLDE, GANIL-SPIRAL, TRIUMF, etc. In this manuscript, many cases where SPES can coherently contribute to the the international endeavour will be presented.

The Nuclear Physics Mid Term Plan in Italy (https://web.infn.it/nucphys-plan-italy/) made possible to trigger and coordinate new ideas from the whole international community, in particular from the new generation of nuclear physics researchers that will be the leading forces in the exploitation of the new facilities. The LNL session of the workshop (https://agenda.infn.it/event/28738/) comprised four working groups on Nuclear Astrophysics, Nuclear Structure, Nuclear Dynamics and Applications, involving experimental and theoretical physicists.

This initiative follows the previous INFN Nuclear Physics Division joint initiatives on nuclear astrophysics [5] and on particle identification [6].

1.1 Nuclear astrophysics

A large variety of opportunities to be explored at LNL in the future have been highlighted. Two big topics have been discussed, the nucleosynthesis up to the iron peak (Sect. 3.1) and the nucleosynthesis of trans-iron elements (Sect. 3.2). The variety of accelerator facilities, innovative targets and state-of-the-art detection systems will allow the community to measure nuclear cross sections of astrophysical interest using both direct and indirect techniques. This will open a window on a wide range of astrophysical scenarios, including Big Bang Nucleosynthesis, quiescent stellar burning and explosive stellar burning. Radioactive beams from SPES will be used to investigate the properties of unstable nuclei and study nuclear reactions which are essential to explain the presence of radioactive elements in our Galaxy, as well as the synthesis of heavy elements through the s-, i- and r- processes.

1.2 Nuclear structure

An ample range of open problems and challenges in nuclear structure and astrophysical processes have been highlighted as explorable at LNL in the near and medium future using stable and radioactive beams from SPES. The interest of the community spans from light stable and near stable nuclei (Sect. 4.2) to neutron-rich ISOL beams from SPES to tackle subjects such as 3-body forces, mirror-symmetry breaking (Sect. 4.3), shell evolution (Sect. 4.4) and collective and resonant states (Sect. 4.5). The working group has also encouraged theoretical discussions on models that, by solving the many-body problem using either recent ab-initio theories, interacting shell model approaches or energy density functional theories (Sect. 4.1), could stimulate future experimental initiatives.

1.3 Nuclear dynamics

The attention was put on the several processes that drive the evolution of a nuclear reaction between heavy nuclei, considering its interplay with the structure. In fusion reactions, deviations from a purely statistical model in the evaporation channel have been observed. Their explanation require a detailed investigation of competing mechanisms (e.g. out-of-equilibrium emissions) and a better understanding of the role of nuclear clusters (Sect. 5.1). The study of more peripheral collisions allows to constrain shell model approaches and it is a powerful indirect method to probe reactions relevant in astrophysics. Moreover, multinucleon transfer processes close to the Coulomb barrier can be used to investigate nucleon–nucleon correlations and the population of neutron-rich heavy nuclei (Sect. 5.2). The upcoming availability of ^{238}U beams at energies around the Coulomb barrier opens up the possibility of using transfer and inelastic reactions to populate and study a wide variety of fissioning systems along the nuclear chart. At lower energies, sub-barrier fusion allows to probe the quantum behaviour of nuclear systems (Sect. 5.3).

Fig. 1 Aereal view of the Laboratori Nazionali di Legnaro

1.4 Nuclear physics applications

A wide range of fields were covered, ranging from medicine to material science, from nuclear waste management up to targets and detector development and characterization, radiation damage, etc. Thanks to the SPES facility, LNL will be a unique center in Europe for the production of novel medical radionuclides, able to exploit both the direct activation method (Sect. 6.1) with the LARAMED project and the ISOL-technique (Sect. 6.2) with the ISOLPHARM project. Considering the SPES cyclotron and the future beamlines, the refurbished XTU-Tandem and the upgrades at the CN, LNL will be able to offer a suite of neutron beams (En $\geq$ thermal) capable of serving a worldwide community, spread over a broad range of physics subjects, from basic to applied research (Sect. 6.1). The development, characterization and modification of material for nuclear physics applications have a consolidated background at LNL and a bright future, that range from micro beam analysis to detector development (Sect. 6.3).

For each working group, a dedicated chapter will describe the outcome of the discussions among the participants. The introduction of each chapter will contain a schematic view and a table with the main measurements and their tentative time-sequence (Phase A at the start of operations, which include the activities that can be performed as soon as the facilities will be ready, Phase B activities that can be performed with some minor upgrades, Phase C a longer Research and Development work is requested).

2 Introduction

The Legnaro National Laboratoires (LNL) [1] of the Istituto Nazionale di Fisica Nucleare (INFN) are a user-oriented large-scale facility mainly dedicated to research programs in nuclear physics and nuclear astrophysics, and to high-level technology developments relevant to several disciplines (accelerator science, innovative detectors, material science and applications of nuclear techniques). Currently, nuclear physics and astrophysics experiments mainly benefit from the high-quality ion beams delivered by the Tandem-ALPI-PIAVE complex (TAP) which consists of the 15 MV Tandem XTU and the superconducting RFQ PIAVE [2], equipped with a ECR source, acting as injectors of the superconducting Linac ALPI [3]. In particular, ion beams from hydrogen to lead are currently provided with energies ranging from few to 20 MeV/u and intensities up to $\sim$ 20 pnA. The foreseen upgrade of ALPI cavities in 2023 will further increase the final energy. The complete list of the available ion beams, maximum energy and intensity can be found at: https://www.lnl.infn.it/wp-content/uploads/Fasci_TAP.pdf. On the basis of new requests triggered by the User Community, authorizations for the acceleration of ^{238}U beam and the use of ^{232}Th and ^{238}U radioactive targets have been submitted to the regulatory authority responsible for nuclear safety and radiation protection. The ^{238}U beam will be delivered by the PIAVE-ALPI complex at an energy of 7.2 MeV/u, allowing to carry out experiments in inverse kinematic addressed to both the study of nuclear structure of exotic neutron-rich fission fragments and a better understanding of the fission process.

The most important initiative of LNL is the SPES (Selective Production of Exotic Species) project aiming at the construction and operation of a second-generation ISOL (Isotope Separation On-Line) facility, on which the mid- and long-term strategy of the laboratory is centred. An aerial view of the LNL can be seen in Fig. 1.

The SPES facility [7] will provide both low-energy (about 40 keV) and re-accelerated radioactive ion beams (10 *A*MeV for masses around A = 130) to carry out forefront research in nuclear physics and nuclear astrophysics. The facility, currently under construction, is based on a dual-exit cyclotron B70 providing proton beams with energies ranging between 35 MeV and 70 MeV and a maximum beam intensity of 0.75 mA. The cyclotron acts as driver accelerator for the ISOL system based on a UCx target

able to sustain a power of 10 kW. The fission mechanism induced by protons (40 MeV, 200 μA) inside the UCx target produces more than 10^{13} fissions/s, allowing the production of neutron-rich unstable ion beams with intensities one order of magnitude higher than in existing facilities. The second exit of the cyclotron will be used for applied physics activities such as the development and the production of innovative radionuclides for medicine, and neutron sources for material science study. SPES is included in the NuPECC Road map (https://www.nupecc.org/?display=front), together with HIE-ISOLDE at CERN (Switzerland) and SPIRAL2 at GANIL (France).

Depending on the needed efficiency and selectivity, different methods will be used for the extraction and selection of the fission products. In particular, three kinds of sources have been developed at SPES: the surface ionization source (SIS), the plasma ion source (PIS) and the Laser Ionization Source (LIS). The latter provides the most selective ionization process with inherent suppression of unwanted isobaric contaminations at the ion source. In addition, a High-Resolution Mass Separator (HRMS), with a resolving power R∼1/20000, will allow to reach a degree of purity of the beam nowadays not available.

The primary accelerator of SPES has already been installed and commissioned. First exotic beams re-accelerated with the Linac ALPI are expected to be available in 2026, allowing to perform experiments initially with Medium-Resolution Mass Separator (MRMS), and, subsequently, with full performance using the High-Resolution Mass Separator (HRMS). The schematic layouts of the SPES facility and the TAP complex are shown in Fig. 2. A complete list of the SPES beams and the foreseen intensities is available at the link https://web.infn.it/spes/index.php/characteristics/spes-beams-7037/spesbeamstable.

A schedule has been planned according to the main requests from the users, on the basis of the Letters of Intent (LOI) presented during the Third International SPES Workshop [8], and to the best compromise for the first operation of the SPES Target-Ion-Source (TIS) system.

For a safer commissioning of the ISOL system, at the beginning ^{26}Al and ^{26}Si beams will be produced with a SiC target. After these first experimental tests, a selection of beams produced with a reduced current (20 μA) on the UCx target, will be commissioned and provided, according to the feasibility and the user requests, also in terms of purity, for experiments to be performed with and without re-acceleration. In particular, the re-accelerated ^{132}Sn beam represents a benchmark for the nuclear physics community being requested by a large number of LoIs and involving all experimental setups installed at LNL and the itinerant ones such as AGATA [9], NEDA [10], PARIS [11] and FAZIA [12].

The current main research programs for nuclear physics and astrophysics concern studies on:

- Structure of neutron-rich nuclei populated by binary reactions
- Shell and shape evolution in different mass regions
- Nuclear structure at high spins, neutron-deficient nuclei and superdeformation
- Fusion and grazing collisions around and below the Coulomb barrier
- Fission and quasi-fission dynamics with heavy-ion beams
- Nuclear structure at high excitation energy (giant resonances)
- Nuclear reactions of astrophysical interest induced by light ions and neutrons
- Clustering processes in light nuclei

The forthcoming operation of the SPES facility will allow to extend those research line to unexplored regions of the nuclide chart.

2.1 Resident instrumentation for nuclear physics

Nuclear structure and reaction dynamics studies at bombarding energies above as well as well below the Coulomb barrier are based on dedicated instrumentation for γ-rays, light particles and complex fragments. Some of the techniques used in these dedicated instrumentation are discussed in Ref. [6].

Major experimental instrumentation resident at Tandem-ALPI-PIAVE accelerator complex consists of:

- PRISMA [13]: a large acceptance magnetic spectrometer devoted to the study of quasi-elastic processes, nucleon–nucleon correlations, and population of neutron-rich nuclei in heavy-ion collisions. It is based on the trajectory reconstruction [14] of the ions travelling through the magnetic elements (a quadrupole singlet magnet followed by a dipole magnet) via the information provided by position-sensitive detectors at the entrance [15] and the focal plane [16] of the spectrometer. Thanks to its high-performance in terms of cross section sensitivity and resolving power of experimental observables (such as nuclear charge, mass and Q-values), PRISMA was successfully used, during the 20 years of operation at LNL, for specific experimental campaigns in conjunction with several γ-ray arrays, such as CLARA [17] and AGATA Demonstrator [18]. Currently, PRISMA is being coupled to the γ-ray spectrometer AGATA in the 1π configuration for a first experimental campaign with stable ion beams. Several upgrades, aiming at improving the charge resolution and the efficiency for light ions, are under development in view of the exotic beams of SPES.
- GALILEO [19]: a γ-ray spectrometer composed of 25 Compton-suppressed tapered HPGe detectors at 90° and forward angles, and 10 triple clusters Ge detectors, mounted at backward angles. This compact array allows for high detection efficiency and energy resolution. The spectrometer is equipped with digital electronics with high-rate capabilities. It can be used together with several complementary detectors for light particles and fragments [20–22], $LaBr_3$(Ce) for the detection of high-energy γ-rays, and a plunger device for lifetime measurements. GALILEO is a competitive device for γ-ray spectroscopy fully dedicated to the SPES radioactive nuclear beams.

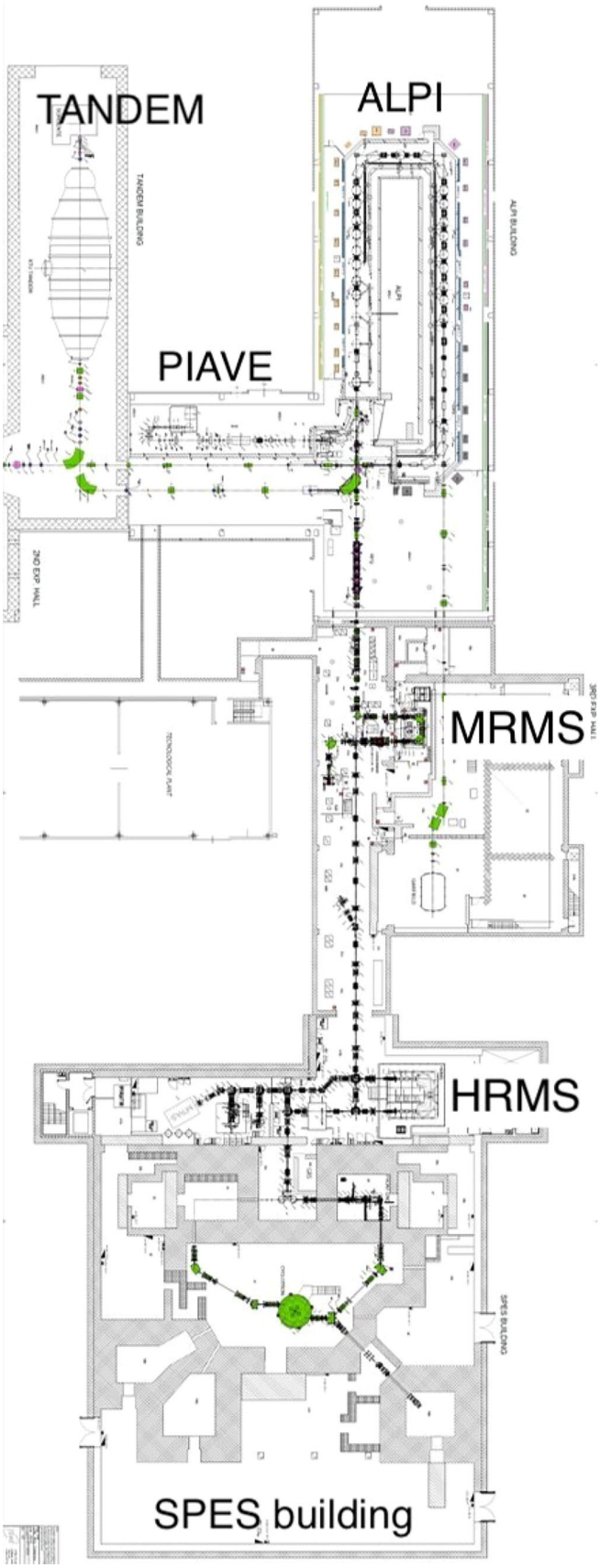

Fig. 2 Layouts of the SPES facility and the TAP complex

- GARFIELD [23]: a large solid angle multi-detector array devoted to studies of both direct, clustering and fusion–evaporation processes in the light-ion region and fusion–evaporation and fusion–fission reactions in the medium-mass region. The apparatus consists of two large volume gas detectors employing micro-strip gas chambers (MSGC) as ΔE stage, followed by CsI(Tl) scintillators as residual energy detectors. This allows to achieve low identification thresholds (0.8–1 *A*MeV) using the ΔE-E technique. The detector is also equipped with a Ring Counter, an annular three-stage telescope array (Ionization chamber-Si-CsI) at forward angles, and full digital electronics. An upgrade of the GARFIELD electronics is in progress in view of the first exotic beams of SPES.
- ATS (Active Target for SPES): an active target to study elastic and inelastic scattering, and few nucleons transfer reactions with low-intensity and low-energy exotic beams delivered by SPES. It is based on the design of the ACTAR TPC project [24] and makes use of the Micromegas technology in the amplification region and can be equipped with ancillary detectors such as Si-Si or Si-CsI(Tl) telescopes for escaping particles, to have a better reconstruction of the reactions of interest, and $LaBr_3$ or HPGe for γ-particle coincidences. The OSCAR hodoscope [25], developed by the NUCLEX collaboration, is an example of a complementary detector for the ATS. It is a modular detector made by two detection stages (SSSSD and silicon pads) allowing to identify low energy (about 1 *A*MeV) particles. It can be used standalone or as an ancillary detector.
- PISOLO [26]: a set-up composed of an electrostatic deflector followed by a time-of-flight spectrometer (two micro-channel plate detectors in transmission configuration followed by a transverse-field ionization chamber and a large area Si detector) used for fusion cross section measurements around and below the Coulomb barrier. A fast multi-electrode ionization chamber has been designed to be used with re-accelerated SPES beams. Preliminary in-beam tests proved that the detector can be operated at rates of the order of 100 kHz.
- EXOTIC [27]: a facility devoted to the in-flight production of low-energy light exotic beams (such as ^{7}Be, ^{8}B, ^{17}F, ^{15}O, ^{8}Li, ^{10}C and ^{11}C with intensities ranging from 10^3 to 10^6 pps) by inverse kinematics reactions. It is composed of: (i) a production gas target (H_2, D_2, ^{3}He and ^{4}He); (ii) a beam selection and transport system (a quadrupole triplet, a 30° bending magnet, a Wien filter and a second quadrupole triplet before the reaction chamber). EXOTIC is equipped with a detection system for reaction mechanism studies consisting of a radioactive ion beam (RIB) tracking system, based on position-sensitive Parallel Plate Avalanche Counters, and the charged-particle array EXPADES [28]. A Technical Design Report, concerning the coupling of EXOTIC to AGATA for nuclear structure studies with light radioactive beams, has been finalized in view of a future experimental campaign.

2.2 Itinerant instrumentation for nuclear physics

Existing collaborations between different European Research infrastructures allows at present and in the forthcoming years to share dedicated detection systems and electronics, designed and constructed to be used at RIB facilities under construction, among which SPES. Major itinerant European detectors which expressed the intent to perform experimental campaigns at LNL with stable and radioactive ion beams are the following:

- AGATA [9]: a γ-ray spectrometer based on the principle of γ-ray tracking through segmented high-purity germanium crystals, advanced digital electronics, and pulse-shape analysis [29]. It is the result of a combined effort of many different countries and institutions aimed at providing a new generation γ-ray array optimized for the new research challenges. The high energy resolution, coupled to the unprecedented position resolution, makes AGATA the best suitable array to study weak transitions or reactions involving large Doppler displacements. It is one of the major instruments foreseen to be used with re-accelerated RIBs of SPES allowing to access information on very exotic nuclei involved in the processes which govern the element formation in the universe. The spectrometer will be equipped with several complementary detectors for light particles and fragments, high-energy γ-rays ($LaBr_3$:Ce), and a plunger device [30], among which:
  - NEDA [10]: a NEutron Detector Array with a large efficiency and a good neutron-gamma discrimination, for nuclear structure studies with stable and radioactive ion beams. It allows the selection of neutron decay channels in nuclear reactions, providing multiplicity and energy information. NEDA turned out to be a very efficient set-up for the study of neutron-deficient nuclei, populated through fusion–evaporation reactions, and a well-suited device for the investigation of exotic nuclei populated with transfer reactions, where the emitted particle is a neutron. NEDA is equipped with full digital electronics and will be coupled to AGATA to perform measurements both with stable and radioactive ion beams.
  - DANTE [31]: a heavy-ion position-sensitive array, based on Micro-channel Plates (MCP) detectors of the CORSET type, suited to be installed in small reaction chamber like those used by γ-ray arrays. The main features are good position and timing resolutions, of the order of a few mm and hundred ps, respectively. DANTE allows to perform γ–γ coincidences, for the events outside the acceptance of PRISMA. The Doppler correction is performed using the position given by DANTE detectors and a velocity estimated by using the binary kinematics of the reaction leading to the product of interest.
  - SPIDER [20]: a modular array of segmented Si detectors for low-energy Coulomb-excitation experiments, to be used as an ancillary device for modern γ-ray spectrometers such as GALILEO and AGATA. Every module has a trapezoidal shape and is segmented on the junction side into eight annular strips. Each detector (300 μm thick) covers one-eighth of 2π in the azimuthal angle. It is possible to arrange SPIDER into different configurations, allowing for the array to be adapted to scattering chambers of different dimensions.

  - EUCLIDES [21]: a light charged particle array made up of 40 Si telescopes ΔE-E (130 μm and ∼1000 μm thick). In such configuration EUCLIDES can be inserted in the reaction chamber of γ-ray arrays. The EUCLIDES electronics is fully digital and it is synchronized by a distributed clock delivered by the GTS (Global Trigger and Synchronization) system, which enables the time synchronization between the γ-ray array spectrometer and all other ancillary detectors.

- GRIT [32]: a charged particle detector array consists in a new type of compact, high granularity, $\sim 4\pi$ acceptance Si array, with a new electronics read-out, allowing integration inside the AGATA array, as well as with the PARIS scintillator array. It is composed of a conical-shaped set of 8 trapezoidal telescopes in both the forward and backward hemisphere with respect to the beam direction, assembled together with a ring of squared-shape silicon telescopes around 90°. The first layer, made of small-pitch DSSD for position measurement, is also meant to perform Pulse Shape Discrimination (PSD) of low energy particles. The second layer is dedicated to residual energy measurements. Very forward/backward angles will be covered by annular type detectors. It will be used at LNL in conjunction with AGATA or FAZIA in experiments with RIBs, with the possibility to couple it also to cryogenic targets. Partial implementations of GRIT, such as the MUGAST [33] and TRACE [34] arrays, will also be available at LNL.
- PARIS [11]: a novel large solid angle γ-ray calorimeter for high-energy photons and medium-resolution γ-ray detection, to be used for the study of Giant Dipole Resonances, near barrier resonances, Pigmy Dipole Resonances and shell structure of light-mass nuclei. The device is composed of phoswich detectors: $LaBr_3$:Ce or $CeBr_3$ scintillators for the inner volume (high efficiency, excellent time resolution and relatively good energy resolution in a large energy range) and NaI(Tl) scintillators for the outer shell. The array can be used standalone or in different configurations (spherical or cubic) when coupled with other detection systems, like HPGe arrays (e.g., AGATA, GALILEO), particle detectors (e.g., MUGAST, NEDA, FAZIA, ATS) or heavy-ion magnetic spectrometers (e.g., PRISMA). It is planned to be used at LNL in experiments with both intense stable and radioactive ion beams.
- FAZIA [12]: a multi-detector array for charged particles and complex fragments, mainly devoted to the study of the thermodynamics and the dynamics of the exotic nuclei, to explore the isospin degrees of freedom of the nuclear matter. It is a modular detection system with high granularity and very good energy resolution, with A and Z identification capability and low-energy thresholds. A module of FAZIA consists of 16 three-stage telescopes Si-Si-CsI(Tl). It uses up-to-date techniques concerning detection, signal processing and data flow, with full digital electronics. It is foreseen to be used, coupled to GARFIELD or PARIS, in experiments with both intense stable and radioactive ion beams at LNL.
- CTADIR (Cryogenic TArget for DIrect Reactions) [35]: a cryogenic ^{3,4}He target developed by INFN LNL, financed by the PRIN2017 call for funding. The He gas will be kept at a pressure of 1 atm and a temperature of 8K, reaching a thicknesses of around 4×10^{20} atoms/cm^2. The cryogenic source of the CTADIR target is a Gifford-McMahon device, with a cooling power of 2 W at 4 K. A cold finger connects the second stage of the device to the target itself. This is made of a cylindrical aluminium body to minimize γ-ray absorption, with a diameter of about 6 cm. The gas chamber has a thickness of 4 mm, a diameter of 1 cm, and it is closed by 2 μm-thick Havar windows. The target is foreseen to be used during campaign of measurements using GRIT coupled to AGATA and other arrays to perform direct reactions like the proton transfer (^{3}He, d), the neutron transfer (^{4}He, ^{3}He) or inelastic (^{4}He, ^{4}He') scattering.
- SUGAR (SUpersonic GAs Jet TaRget) [36]: a device developed by Instituto de FÌsica, UNAM (IF-UNAM), Mexico, to produce gas-jet targets for nuclear reactions studies, where the purity and thickness of targets are crucial. Pure targets in gas state may be produced with SUGAR, reaching thicknesses around 1×10^{18} particles/cm^2. SUGAR is essentially composed of three main parts: a differential vacuum system, a jet chamber, and a pumping jet system. The differential pumping system prevents the need of entrance windows making SUGAR an ideal instrument for nuclear astrophysics experiments where an accurate knowledge of the beam energy is paramount. A campaign of measurements using SUGAR coupled to AGATA and NEDA arrays is planned, searching the simultaneous detection of charge particles, γ rays and neutrons from reactions involving pure gas targets.

2.3 New instrumentation for nuclear physics

It is worthwhile to mention that, according to the present time schedule, the first nuclear physics experiments at SPES will be performed by using low-energy RIBs. Major instrumentation is being developed at INFN for this as follows:

- A Tape Station (b-DS, Beta-decay station) equipped with plastic detectors at the implantation point for the identification of the emitted electron/positron and HPGe detectors (coaxial Ge detectors or Triple clusters of the GALILEO γ-ray spectrometer) to define the de-excitation scheme following the parent's decay. The b-DS stati will allow to study decay processes in a large range of lifetimes (few tens of ms up to hours) and is planned to be flexible in order to host detectors for lifetime measurements and high-energy gamma rays ($LaBr_3$:Ce scintillators), conversion electrons (Si(Li) detectors), beta-delayed neutrons (NEDA detectors).
- SLICES [37]: an off-line decay chamber coupled to the tape station will be used as a second measuring point hosting an electron spectrometer. The main components of SLICES are a magnetic transport system and a segmented, large-area lithium-drifted silicon Si(Li) detector. The magnetic lens, made of a set of permanent NdFeB N52 magnets, guides the electrons around a central photon shield towards the Si(Li) detector.

2.4 Instrumentation for applied physics

Applied and interdisciplinary projects make use of beams delivered by the TAP complex as well as the CN and AN2000 Van de Graaf accelerators. The main activities related to nuclear physics and SPES applications concern: the characterization of targets for precision cross section measurements; elemental microanalysis of targets for radionuclide production; in-beam tests and characterization of detectors; radiation damage of materials and devices. Available major experimental instrumentation for interdisciplinary and biomedical physics are the following:

- SIRAD: an irradiation facility, located at the TAP complex, for radiation damage studies equipped with a general-purpose irradiation chamber and an ion electron microscope.
- STARTRACK: detector for the measurement of the ionization-cluster-size distributions produced by protons and carbon ions in gas-filled cylindrical volumes. It uses stable beams from the TAP complex.
- BELINA: neutron time-of-flight system at CN, used both for the study of nuclear reactions of astrophysical interest and interdisciplinary activities.
- TOTAL-IBA: a facility to perform Ion Beam Analysis at CN comprising simultaneous PIXE, PIGE, prompt NRA and elastic back-scattering.
- Scattering chambers dedicated to Ion Beam Analysis with Rutherford and not-Rutherford Backscattering, Elastic Recoil Detection Analysis, prompt Nuclear Reaction Analysis, RBS-Channeling, in combination with Ion Beam Induced Luminescence (IBIL) and PIXE at AN2000.
- MICRO-BEAM: beamline equipped with the instrumentation for micro-PIXE analysis with a dedicated HPGe detector. Proton beams with typical size of 2–3 micrometers can be used at rated current of 500 pA. The beam line is also used for rarefied beam (10^2-10^3 protons/s) irradiation of detectors and IBIL and Ion Beam Induced Charge (IBIC) recording.
- LOW ENERGY IRRADIATION: a facility to irradiate with low energy protons (0.4–2.2 MeV) large area (up to 20 cm x 20 cm) spacecraft optical and optoelectronic materials and components. Also usable at CN accelerator for higher energy irradiation.

2.5 Infrastructures for applied physics

The forthcoming operation of SPES will allow to study and develop innovative radionuclides for medicine within the LARAMED (LAboratory for RAdioisotopes of MEDical interest) and ISOLPHARM projects, and to develop a neutron and proton irradiation facility (NEPIR) in the 20–70 MeV energy range, see Sect. 6.

The proposed fast neutron and proton irradiation facility NEPIR [38] will be constructed in phases: a first -minimal but effective- configuration, NEPIR-0, and a final configuration, NEPIR-1. With this project, LNL and Italy will have, for the first time, high-level neutron beams. For this reason, the NEPIR facility is part of the CANS [39] and the ELENA associations [40].

The NEPIR-0 is almost completely funded by the Italian Ministry for University Research (MUR), within the Italian SPARE (Space Radiation Shielding) project that deals with health risks due to cosmic radiation. In this phase the neutron source is a relatively simple, thick, low power (100 W) beryllium target located inside the conduit between the cyclotron hall and experimental hall of the SPES building [41]. The 3 m thick wall of the cyclotron cave provides shielding and the conduit acts as a collimator for the neutron beam directed to the neutron's experimental area. The expected neutron beam has a continuum spectrum with a different cut-off according to different proton energies. In this phase, a low proton current will be used ($\sim 1\ \mu$A) to reduce the radiation protection problems. The phase-0 facility will be open to academic and industrial users, to test microelectronic components and devices, for neutron detector characterization, and neutron shielding materials for space missions, in partnership with ASI.

In the final NEPIR-1 phase [42], the facility will be significantly extended: a dedicated bunker will be constructed, the proton beam current will be raised to $\sim 10\ \mu$A, and two neutron production targets will be used to generate high-flux neutron beams for different applications:

- thin (few mm) lithium and beryllium targets to produce Quasi Mono-energetic Neutron (QMN) beams [43] with a controllable energy peak in the 20–70 MeV energy range;
- Atmospheric Neutron Emulator (ANEM) system, a rotating composite target made of a beryllium sector and a tungsten disk, to produce an intense beam of fast neutrons with an atmospheric-like energy distribution in the 1–70 MeV energy range.

An independent, low intensity direct proton beam line is also foreseen.

3 Nuclear astrophysics

Nuclear astrophysics is an interdisciplinary field, characterized by a strong interplay of nuclear physics, astronomy and stellar modelling. The ambitious goal of nuclear astrophysics is to understand where and how all elements in the Universe are formed, and how nuclear reactions influence stellar evolution.

It is currently widely acknowledged that the first nucleosynthesis event happened a few minutes after the Big Bang [44]. Such event, called Big Bang Nucleosynthesis, left the Universe made of hydrogen, helium and traces of lithium. The vast majority of

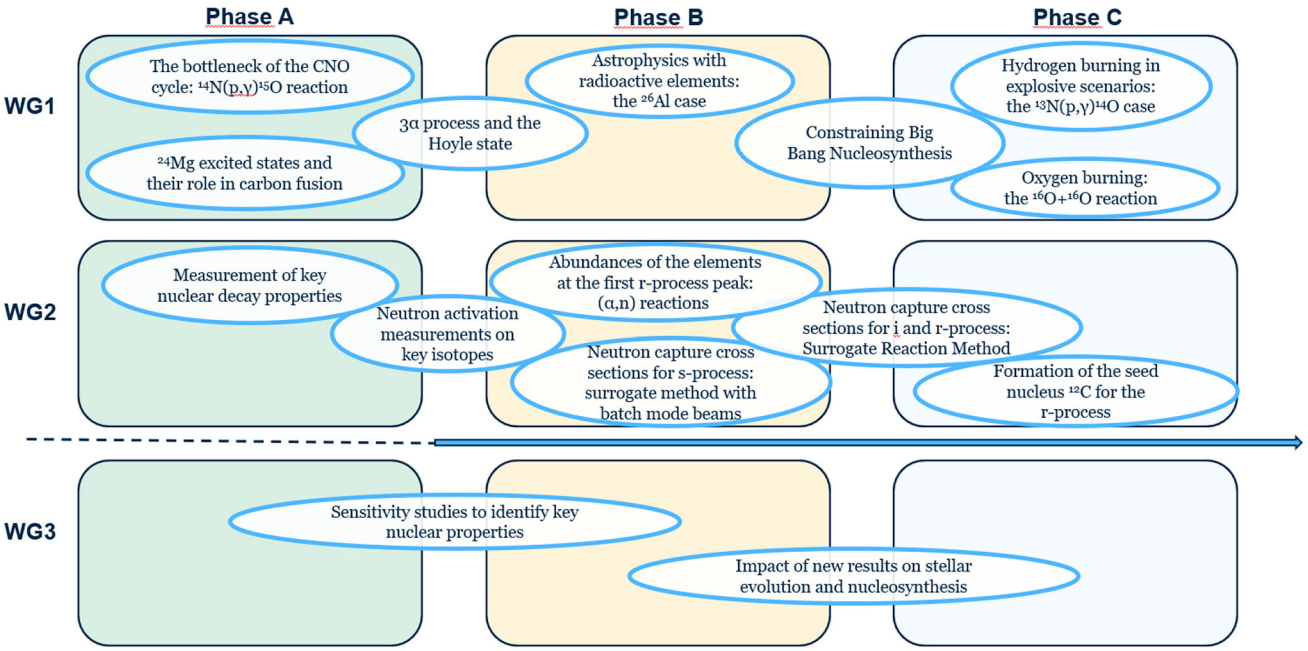

Fig. 3 Summary of nuclear astrophysics activities that could be performed at LNL in the next future, sorted according to the time phase

the other elements was produced (and is still being produced) in stars, through a complex network of nuclear reactions. Nuclear reactions are also a major source of energy for stars, and hence have a strong influence on stellar evolution. Nowadays, astronomical observations and analyses of meteorites provide very precise measurements of the abundances of the elements, and in many cases even isotopic abundances. On the other hand, stellar models aim at reproducing the observed abundances, exploiting increasingly high computational power to develop more and more realistic simulations. Stellar models rely on a number of parameters, including the cross sections of all nuclear processes involved in a given astrophysical scenario.

Italian nuclear astrophysics groups and laboratories have contributed significantly to the field for many years [5]. In the near future Legnaro National Laboratories will offer a variety of accelerator facilities and state-of-the-art detection systems, opening the possibility to explore a wide range of astrophysical processes. Figure 3 and Table 1 provide a snapshot of possible activities which could take place at LNL over the next years. Such activities entail the use of a number of different, and sometimes complementary, experimental techniques. Moreover, many nuclear astrophysics cases will benefit from advances in our knowledge of nuclear structure and nuclear reaction dynamics, as detailed in Sects. 4 and 5. Therefore, it is crucial to keep an active communication between the different groups.

The discussion on possible projects was carried out within heterogeneous working groups, each tackling a different topic: Nucleosynthesis up to the iron peak (WG1), nucleosynthesis of trans-iron elements (WG2) and nuclear astrophysics theory (WG3). A more detailed description of future possibilities at LNL is discussed in the next sections.

3.1 Nucleosynthesis up to the iron peak

In this section, we focus on all astrophysical environments contributing to the production of the elements up to the iron peak, starting from Big Bang Nucleosynthesis and proceeding through increasingly more advanced stellar burning phases.

3.1.1 Constraining big bang nucleosynthesis

Primordial abundances of light elements, produced during the so-called Big Bang Nucleosynthesis (BBN), can be used to probe the physics of the Universe a few minutes after its birth (for reviews see [44, 45]). The theoretical description of BBN is based on the standard cosmological model and predicts the abundances of primordial nuclides, as a function of the density of ordinary matter, or baryon density. Therefore, a comparison between the observed primordial abundances and those predicted by the BBN can be used to constrain this fundamental quantity. BBN probes the Universe during the first ≈10 min, in an epoch when observable quantities of ^{2}H, ^{3,4}He and ^{7}Li were produced. At that epoch, the temperature and the density were large enough for nuclear reactions to take place. Considering the limited number of isotopes involved in the BBN, the network of active nuclear reactions is relatively small (less than 15 reactions), but not yet known to the level of precision required by modern cosmology.

Table 1 Summary of key nuclear astrophysics topics and reactions that could be addressed at LNL in the next years. The activities are sorted according to the working group discussing the proposal and the time phase

Tag	Description	Reaction	Phase
LNL-NA-LE-a0	The bottleneck of the CNO cycle: ^{14}N(p, γ)^{15}O	^{16}O(^{3}He,^{4}He)^{15}O	A
LNL-NA-LE-a1	3α process and the Hoyle state	^{14}N(d,α)^{12}C	A
LNL-NA-LE-a2	^{24}Mg excited states and their role in carbon fusion	^{20}Ne(α,α')^{20}Ne	A
LNL-NA-LE-b0	Astrophysics with radioactive elements: the ^{26}Al case	^{26}Al^{m}(n,p)^{26}Mg	B
LNL-NA-LE-b1	Astrophysics with radioactive elements: the ^{26}Al case	^{26}Al^{m}(n,α)^{23}Na	B
LNL-NA-LE-b2	Astrophysics with radioactive elements: the ^{26}Al case	^{26}Al^{m}(p,γ)^{27}Si	B
LNL-NA-LE-b3	Constraining Big Bang Nucleosynthesis: Primordial deuterium abundance	^{2}H(p,γ)^{3}He	B
LNL-NA-LE-b4	3α process and the Hoyle state	^{4}He(^{12}C,^{12}C*)^{4}He	B
LNL-NA-LE-c0	Constraining Big Bang Nucleosynthesis: Primordial deuterium abundance	d+d	C
LNL-NA-LE-c1	Constraining Big Bang Nucleosynthesis: Primordial ^{7}Li abundance	^{7}Be(d,α)^{5}Li	C
LNL-NA-LE-c2	Hydrogen burning in explosive scenarios: the ^{13}N(p,γ)^{14}O case	^{13}N(d,n)^{14}O	C
LNL-NA-LE-c3	Oxygen burning: the ^{16}O+^{16}O reaction	^{16}O+^{16}O	C
LNL-NA-HE-a0	Measurement of key nuclear decay properties		A
LNL-NA-HE-a1	Neutron activation measurements on key isotopes		A+B
LNL-NA-HE-b0	Abundances of the elements at the first r-process peak: (α,n) reactions		B
LNL-NA-HE-b1	Neutron capture cross sections s-process: surrogate method with batch mode beams		B
LNL-NA-HE-b2	Neutron capture cross sections for i- and r-process: Surrogate Reaction Method		B+C
LNL-NA-HE-c0	Formation of the seed nucleus ^{12}C for the r-process	^{9}Be(α,n)^{12}C	C
LNL-NA-HE-c1	Formation of the seed nucleus ^{12}C for the r-process	^{4}He(nn,γ)^{6}He	C
LNL-NA-TH-a0	Sensitivity study		A+B
LNL-NA-TH-b0	Impact of new results on stellar evolution and nucleosynthesis		B+C

Primordial deuterium abundance

The observed primordial abundances are usually provided by spectroscopic observations of ancient astrophysical objects. The value of deuterium abundance relative to hydrogen has now reached percent accuracy, D/H $= (2.527 \pm 0.030) \times 10^{-5}$ at 68% confidence level [46]. Moreover, this precision is expected to increase by nearly an order of magnitude using new 30 m-class telescopes [47]. The reactions involved in the synthesis of deuterium are: production via the well known p(n,γ)d process and destruction via the d(d,n)^{3}He d(d,p)^{3}H and d(p,γ)^{3}He reactions. At present, several groups [48–51] have calculated the primordial deuterium abundance, obtaining different results depending on the adopted rate for deuterium burning reactions. As a consequence, cosmological predictions are also in disagreement.

A very recent breakthrough in BBN has been the new underground measurement of the d(p,γ)^{3}He reaction by the LUNA Collaboration [52] at the Gran Sasso National Laboratory in Italy, providing a reaction rate with unprecedented precision [53]. After the LUNA measurement, all most recent BBN analyses [48–50] agree that the largest contribution to the error on primordial deuterium from theoretical predictions comes from the uncertainty on two destruction process rates: d(d,n)^{3}He and d(d,p)^{3}H.

As a matter of fact, the study of the d(d,n)^{3}He, d(d,p)^{3}H and d(p,γ)^{3}He reactions with percent-level accuracy is extremely challenging. The measurement of the first two is crucial to match the precision of astronomical observation on the primordial deuterium abundance. The d(p,γ)^{3}He reaction is now well known at energies up to 400 keV, but in the energy range 400–800 keV there are still extrapolations in disagreement with each other [53, 54]. At LNL there are two accelerators potentially able to provide deuterium beam: the AN2000 and CN. The first one can reach the BBN relevant energies. The measurement can be performed delivering the deuterium beam to different types of solid deuterium targets, such as ZrD_2 or CD_2, both under development at LNL. The charged particles emitted by both reactions can be detected by an array of silicon detectors placed in close geometry at different angles to measure not only the total cross section, but also the angular distribution. To study the d(p,γ)^{3}He reaction, two CeBr3 detectors can be used. In this way it will be possible to measure all three deuterium-destruction channels in a broad energy range, and possibly with a very high accuracy and precision.

Primordial ^{7}Li abundance

While predicted and observed deuterium and helium abundances are overall in good agreement, the ^{7}Li-problem still remains largely debated in the scientific community because of the factor ∼2–3 discrepancy between the theoretical BBN abundances and the observed ones in halo stars [55]. Primordial ^{7}Li is mostly produced by the decay of radioactive ^{7}Be. From a purely nuclear point of view, several studies have been proposed in the last years in order to achieve a better understanding of the processes affecting the production and destruction of ^{7}Be and ^{7}Li (see, e.g., [56–58]). In this view, the Trojan Horse Method (THM) [59] has been recently exploited to study the ^{7}Be+n induced reactions, opening the new frontier of applying THM to reactions involving unstable nuclei and neutrons. Recent works [60–62] lead to a mitigation of the cosmological ^{7}Li-problem, reducing the theoretical BBN abundances by ∼10%. Measurements have also been carried out at the 7 MV CN accelerator, indicating that the ^{7}Be(n,p)^{7}Li reaction cross section is not large enough to guarantee a higher ^{7}Be burning rate during Big Bang Nucleosynthesis [63]. In order to further study the impact of nuclear reactions involving the unstable ^{7}Be isotope, a further channel to be investigated is the ^{7}Be(d,α)^{5}Li: a recent debate in the scientific community [64, 65] has been triggered by the direct measurements of Rijal et al., in 2019 [66]. A THM experiment could reach BBN energies, where resonant states of the intermediate ^{9}B nucleus could play an important role. For this purpose, THM could be applied to the quasi-free ^{6}Li(^{7}Be,α ^{5}Li)^{4}He break-up reaction by using a ^{7}Be beam impinging on a ^{6}LiF target, evaporated on a C backing. Indeed, ^{6}Li represents a suitable TH-nucleus because of its α+d structure, its relative low binding energy (∼1.47 MeV), and its well known momentum distribution for the α-d intercluster motion occurring in s-wave [59]. Moreover, the same approach could be also used to investigate the ^{7}Be(d,p)^{8}Be reaction, representing a further deuteron-induced destruction channel for ^{7}Be in primordial nucleosynthesis. This future experiments can be performed at the EXOTIC facility at LNL, with a detection system similar to the one used in [60], derived from the EXPADES detection setup [67].

3.1.2 Stellar hydrogen burning

H-burning is the nuclear engine which allows stars to shine for billions of years, balancing gravitational contraction. For stars belonging to the Upper Main Sequence (M> 1.5 $M_{\odot}$), the dominating process is the CNO cycle. The latter requires the presence of catalysts (carbon, nitrogen and oxygen isotopes), which allow the conversion of H into He. Although our understanding of stellar hydrogen burning has greatly improved in the last century, there are still open questions that could be addressed at LNL in the upcoming years.

The bottleneck of the CNO cycle: $^{14}N(p,\gamma)^{15}O$ reaction

The ^{14}N(p, γ)^{15}O is the slowest reaction in the CNO cycle. Hence, it regulates the rate of energy generation and impacts several areas of stellar structure and evolution. Its reaction rate at astrophysical energies is highly affected by a sub-threshold resonance located at $E_{cm} = -504$ keV, corresponding to the $E_x = 6.793$ MeV state in ^{15}O. The sub-threshold resonance greatly affects the cross section of the ground state transition at the typical energies of solar hydrogen burning (∼30 keV), where no direct cross section measurements are available. A precise extrapolation at solar energies is necessary to solve the so called solar composition problem [68], and to explain the observed flux of CNO neutrinos [69].

One of the methods to constrain the contribution of the sub-threshold resonance is the measurement of the lifetime of the corresponding excited state. The values for this lifetime, reported in literature, range from 0.6 fs [70] to 1.6 fs [71]. Other studies have reported only upper limits, which agree with a lifetime of the order of 1 fs [72, 73]. A promising technique to measure such a short lifetime is the Doppler Shift Attenuation Method (DSAM), applicable when γ emission occurs while the nucleus is slowing down inside the target.

Nevertheless, the expected lifetime of the 6.793 MeV state lies at the edge of DSAM sensibility. The AGATA array makes it possible to track the detected γ-rays, and thus to derive their direction of emission, with unprecedented resolution. Using the ^{3}He(^{16}O,^{15}O)^{4}He reaction to populate the 6.793 MeV state and coupling AGATA to the SPIDER silicon detector array, it is possible to derive the energy and direction of the ^{15}O particles and thus to reconstruct the real energy of the photon, pushing the sensitivity of the DSAM method to extremely short lifetimes. Preliminary simulations show that, thanks to the high angular resolution of the AGATA detector, the lifetime of the 6.793 MeV state can be determined at LNL with the precision required by R-Matrix models.

Hydrogen burning in explosive scenarios: the $^{13}N(p,\gamma)^{14}O$ case

The hot-CNO cycle heavily affects the nucleosynthesis in classical novae explosions. In this framework, several reactions induced by radioactive ions become important and their reaction rates provide necessary nuclear inputs for novae modeling, as well as novae nucleosynthesis [74]. The ^{13}N(p,γ)^{14}O reaction can be studied at LNL in the energy range of astrophysical interest by means of the Asymptotic Normalization Coefficients (ANCs) indirect method, explained in more details in Sect. 5.2.4, applied to the ^{13}N(d,n)^{14}O reaction in inverse kinematics, at a ^{13}N beam energy of 50 MeV. Simultaneously, the d + ^{13}N elastic scattering could also be studied in a proper angular range with expected statistical uncertainties around 10–15%. The experiment will be performed with an array of silicon detectors, allowing the required angular resolution, or with standard PSD, as performed in recent ANC applications [75, 76]. The experimental differential cross sections will be analyzed in order to compute the optical model parameters for the d + ^{13}N elastic scattering and the ANC for the reaction ^{13}N(d,n)^{14}O. It will be then possible to extract the ANC for the ^{13}N(p,γ)^{14}O reaction g.s. transition, and to obtain a more reliable estimate of its astrophysical S-factor at extremely low energies as well as its rate

within the novae temperature region. As a first step, we propose the development of a ^{13}N Radioactive Ion Beam (RIB) by means of the facility EXOTIC [77]. The RIB production technique will employ the two-body charge-exchange reaction p(^{13}C,^{13}N)n and the ^{13}N secondary beam will be selected and purified using the double filter on magnetic rigidity and velocity provided by the facility EXOTIC.

3.1.3 Advanced stellar burning stages

After the long-lasting H-burning phase, stars experience further nuclear burning stages. Low-mass stars (M<8 $M_\odot$) are only able to trigger He-burning. The latter occurs through two key reactions: the 3α process and the ^{12}C(α,γ)^{16}O reaction. The interplay between these two reactions determines the final carbon and oxygen budget of the star. More massive stars, on the other hand, are able to trigger advanced burnings up to the formation of an iron-rich core. Two key processes, characterizing the C-burning and the O-burning phases, are the ^{12}C+^{12}C and the ^{16}O+^{16}O fusion reactions, respectively. Both reactions are characterized by an extremely low cross section at astrophysical energies and multiple exit channels, making their experimental measurement very difficult.

3α *process and the Hoyle state*

Carbon is one of the fundamental elements for the existence of life on Earth, and it is most effectively produced in stars through the so-called 3α process, which occurs during helium burning. Helium burning proceeds predominantly through the formation of the unbound ^{8}Be nucleus and the subsequent radiative capture of a ^{4}He nucleus. The rate of the 3α process is enhanced by the so-called Hoyle state, i.e. the 7.654 MeV state in ^{12}C.

The reaction rate of the 3α process depends crucially on the energy and radiative decay partial width Γ_{rad} of the Hoyle state. An accurate knowledge of Γ_{rad} is therefore crucial to describe the production rate of ^{12}C. Literature data on the branching ratio for the radiative decay of the Hoyle state are conflicting [78, 79]. Recently, new measurements were performed at LNS for the γ decay of excited states of ^{12}C [80]. For the first time the two-γ-decay cascade to the ground state from the 9.64 MeV level was directly observed. The same level was also studied at RCPN Osaka laboratory [81], finding a γ-decay yield larger than the previously accepted lower limit [82]. In addition, the γ decay of the Hoyle state was measured finding an exceedingly large decay width, suggesting the possible presence of an Efimov state near the Hoyle level [83]. The radiative branching ratio Γ_{rad}/Γ of the Hoyle state in ^{12}C can be measured at LNL exploiting high-sensitivity charged-particle spectroscopy techniques and the CN accelerator beams. The proposed experiment uses the ^{14}N(d,α)^{12}C reaction, at about 2.7 MeV incident energy, to populate the Hoyle state (7.654 MeV,0$^+$) in the residual ^{12}C nucleus. The excitation energy and the emission direction of the residual nucleus are determined by measuring the light ejectile α, as done in a previous investigation [84]. A pair of detectors will be used, one placed at backward angles and one positioned at forward angles, allowing the study of coincidences between α particles and ^{12}C.

The experiment will be designed in a way that measured coincidences will be directly related to the decay branching ratio without the need to model the detection efficiency. A first test performed in October 2021 at the CN accelerator highlighted some issues concerning the beam spot, beam intensity and beam positioning, which will hopefully be solved in view of future experiments.

In addition to the Hoyle state, new states belonging to the ground state rotational band have been recently observed for the first time [85, 86]. On the theoretical side, the Algebraic Cluster Model and the Semimicroscopic Algebraic Cluster Model [87] do predict such states, and others that haven't been observed yet. An experiment could be performed at LNL to detect and identify some of the predicted states that remain unobserved, and confirm the existence of a rotational band built on the Hoyle state. The ^{4}He(^{12}C,^{12}C*)^{4}He break-up reaction is the best option to look for cluster-like states. The measurement will be performed using a ^{12}C beam from the TAP complex and a windowless Helium target, SUGAR. Charged reaction products will be detected by a silicon detector array (approximately 1500 μm thick). AGATA will detect coincident γ-rays.

^{24}*Mg excited states and their role in carbon fusion*

^{12}C+^{12}C fusion is responsible for the ignition of carbon burning in stars, and its cross section is a crucial parameter in modern astrophysics. The evolution and final fate of a star are closely related to the astrophysical reaction rate of the ^{12}C+^{12}C reaction. Indeed, only stars with mass higher than a critical value, M_{up}, can reach high-enough temperatures to ignite quiescent carbon burning. Those stars are believed to end their life as core-collapse supernovae, neutron stars or black holes. On the other hand, stars with mass lower than M_{up} become electron-degenerate before reaching the temperature needed for the ignition of the ^{12}C+^{12}C reaction, and end their life as C-O white dwarfs. Recently, an indirect study using the Trojan Horse Method (THM) has been published in Nature [88]. The authors reported results for proton and alpha channels down to 800 keV in the center of mass. The authors have observed several resonances, corresponding to excited states of the ^{24}Mg at energies between 14 and 17 MeV. As a result, the astrophysical reaction rate of ^{12}C+^{12}C fusion is increased by one order of magnitude. The observed ^{24}Mg levels are known from the literature, but their characterization is still poor. Therefore, a detailed study of those excited states may provide valuable information for the reaction rate calculation (i.e. precise resonance energies, spin, parities and partial widths of the states). Such a study could be performed at LNL using the resonant scattering technique, which allows to access multiple resonant states in the "compound" nucleus by measuring an increased cross section with respect to the nuclear elastic scattering. The ^{24}Mg excited states relevant to carbon burning can be investigated through ^{20}Ne+α resonant scattering using the ACTAR active-target demonstrator. Exploiting the

TPC that constitutes also the target for the experiment, it will be possible to reconstruct the trajectories and energies of the reaction products, and to separate the elastic events, thanks to the improved energy resolution.

Oxygen burning: the ^{16}O+^{16}O reaction

In massive stars, during the oxygen burning phase, the nucleosynthesis depends not only on the ^{16}O+^{16}O reaction rate, but also on the branching between proton-, neutron-, or α-decay channels of the compound nucleus. The oxygen fusion reaction produces compound nuclear states of ^{32}S that may decay by any of these four channels: i) ^{31}S+n (Q = 1.45 MeV); ii) ^{31}P+p (Q = 7.68 MeV); iii) ^{30}P+d (Q = 2.41 MeV); iv) ^{28}Si+α (Q = 9.59 MeV) [89]. At present, these reactions have only been measured at energies that are much higher than those of astrophysical interest. The main reasons for this are limitations in detector efficiencies, background reduction, and reaction yields. Therefore, the cross section at astrophysical energies can only be derived through extrapolations of existing experimental data. Unfortunately, discrepancies exist both between literature data sets [90] and theoretical predictions at energies below 5 MeV [91]. These facts clearly show the need of new experimental studies on this reaction. In the next years, the ^{16}O+^{16}O reaction could be studied using a gaseous target, like SUGAR, and detecting the light fragments in the exit channels. Although it is a challenge for the Tandem at LNL to accelerate ^{16}O beam in the energy window from 4 up to 8 MeV, counting on the forefront detector systems AGATA, NEDA and GRIT to detect γ rays, neutrons and charged particles, respectively, it will be possible to study simultaneously different reaction channels with high energy and angular resolution, as well as high detection efficiency. Moreover, the use of particle-gamma coincidences would also allow to reduce the background.

When assessing the behavior of the ^{12}C+^{12}C and ^{16}O+^{16}O fusion cross sections at very low energies, a major unknown is the existence and the entity of the hindrance phenomenon, so far only observed in slightly heavier systems. In this respect, the collaboration with the reaction dynamics working group is key, since they will try to extend systematic studies of the hindrance phenomenon to increasingly lighter systems, as explained in Sect. 5.3.2.

3.1.4 Astrophysics with radioactive elements: the ^{26}Al case

^{26}Al nucleosynthesis has recently been in the spotlight to understand the formation of the Solar System and assess the formation rate of neutron stars (which is a key parameter for Multimessenger Astronomy). Thanks to its powerful γ-emission, the observation of its radioactive decay is a direct evidence of the on-going nucleosynthesis in our Galaxy. Different ^{26}Al sources have been suggested over the years, such as Asymptotic Giant Branch (AGB) stars, classical novae, Wolf-Rayet stars, core-collapse supernovae and cosmic ray radiation in protostellar nebulae. To ascertain the most likely nucleosynthesis scenario, the ^{26}Al production and destruction mechanisms have to be investigated and the cross section of the reactions producing and destroying ^{26}Al need to be measured with adequate precision (better than 20%). Unfortunately, at the moment, the rate of ^{26}Al(n,p)^{26}Mg is trustworthy only for $T < 3\times10^8$ K and for ^{26}Al(n,α)^{23}Na, while the temperatures of interest are not covered at all by existing data. To this aim it is possible to study ^{26}Al(n,p)^{26}Mg and ^{26}Al(n,α)^{23}Na reactions via the THM, using ^{26}Al^m beam from SPES. It is worth noting that these measurements will be performed in synergy with LNS, where the same reactions on ^{26}Al in the ground state will be measured. Proceeding with the ^{25}Al nucleosynthesis, ^{26}Al(n,γ)^{27}Al, ^{25}Al(p,γ)^{26}Si and ^{26}Al(p,γ)^{27}Si (this last one influential in convective core H-burning for $T < 10^8$ K) can be studied with the indirect ANC method using an array of silicon detectors placed at backward angles, both using g.s. and isomeric ^{26}Al beams. Possible targets to study the neutron capture are d or ^{13}C, while for the proton capture ^{3}He or ^{10}B could be used. For these THM and ANC measurements, SPES beams at energies of the order of 3–5 AMeV for ^{26}Al are required, which can be easily obtained by the ALPI post-acceleration system.

3.2 Nucleosynthesis of trans-iron elements

Charged particle reactions in massive stars lead to the formation of iron-rich cores. The production of isotopes heavier than ^{56}Fe through charged particles (as those described in previous sections) requires energy input, instead of releasing it. Moreover, the Coulomb repulsion increases with the atomic number of reactants. Therefore, elements heavier than iron cannot be produced via charged particle reactions. Such a problem is avoided if one of the reactant is a neutron. Observed stellar abundances can be roughly reproduced by postulating the existence of two main neutron capture processes: the slow neutron capture process (s process) and the rapid neutron capture process (r process). Their typical neutron fluxes are 10^7 neutrons/cm^3 and $> 10^{20}$ neutrons/cm^3, respectively. The s process always proceeds close to the β stability valley. Each time an unstable nucleus is created by a neutron capture on a stable one, it has time to decay to its stable isobar, before capturing another neutron.

In the case of the r-process, instead, isotopes very far from the β stability valley can be produced via a series of multiple neutron captures starting from a single stable isotope. Such a sequence proceeds until isotopes with very short lifetimes are created. Once the neutron flux comes to an end, those isotopes can decay to their relative stable isobars along the β stability valley. The stellar environments of interest are two: low mass stars during their Asymptotic Giant Branch phase, for the s process, and the evolution of single or binary massive stars, for the r process. In the last years, a third neutron capture process, the intermediate process (i-process; [92]) received particular attention, due to its capability to reproduce observational data that can be hardly matched by other n-capture processes.

3.2.1 The slow neutron capture process

The facilities at LNL will allow to determine neutron-capture rates and relevant nuclear properties of interest for the nucleosynthesis of heavy elements, applying a variety of experimental techniques, as described in more details in the following sections.

Neutron-capture cross sections for s-process: surrogate reaction method

Neutron capture reactions on unstable targets are of high interest for astrophysical models since the knowledge of their cross sections, combined with the experimental knowledge of β-decay rates and of isotopic abundances, allows probing the neutron flux and, therefore, the environmental conditions of s-process nucleosynthesis. At LNL, it will be possible to determine neutron-capture cross sections on a number of key radioactive isotopes using the Surrogate Reaction Method (SRM). This indirect technique is based on the use of a (d,pγ) reaction as a surrogate for the (n,γ). The theory behind the SRM was recently developed by G. Potel and collaborators [93]. The method uses the fact that the neutron-induced reaction of interest proceeds through the formation of an intermediate compound nucleus (CN), which subsequently decays. In a surrogate-reaction experiment, a target-projectile pair is chosen to form a CN that has the same excitation energy and neutron and proton numbers as the one produced in the desired reaction.

At LNL, SRM experiments will be performed in inverse kinematics, delivering radioactive beams to a CD_2 target. Scattered light particles will be detected in a segmented Si array, while de-exciting γ-rays will be observed with a γ detector array.

A notable example is the neutron capture cross section in ^{85}Kr, competing with the β decay of this unstable isotope with $T_{1/2} \approx$ 11 year. Neutron capture on ^{84}Kr leads to both the ^{85}Kr ground state ($T_{1/2} = 10.7$ year) and the isomeric state at 350 keV ($T_{1/2} =$ 4.5 s) [94]. Because of its comparably short half-life, 80% of the isomer undergoes β decay to ^{85}Rb, and the remaining 20% decays to the ^{85}Kr g.s., whose half-life is long enough for the s-process flow to proceed further to ^{86}Kr, and then to ^{87}Rb, in competition with the β decay to ^{85}Rb. At low neutron density, the β-decay process dominates over the neutron capture and the s-process path runs from ^{84}Kr to ^{85}Rb to ^{86}Sr. When the neutron density is larger than a few times 10 cm^{-3} the neutron capture chain runs from ^{84}Kr to ^{86}Kr and on to ^{87}Rb.

Therefore, the relative abundances of Rb, Sr, Y, and Zr observed in AGB stars depend on the peculiarities of the neutron flow near the magic neutron number N = 50, and can be used to estimate the physical condition of the inner stellar layers [95].

Both, direct and indirect measurements of ^{85}Kr(n,γ) have been performed recently [96, 97], and a new experiment is ongoing at Argonne National Laboratories, but no conclusive results have yet been drawn. Future investigations at LNL could represent an important step forward in our knowledge of this branching point. Because radioactive ^{85}Kr is abundantly available commercially, this measurement can be performed simply connecting a bottle of ^{85}Kr directly to the ion source and accelerating it.

Another s-process branching point isotope, ^{79}Se, is located in a region where two scenarios may contribute, massive stars (weak s-process component) and AGB stars (main s-process component). The knowledge of the neutron-capture cross section of ^{79}Se provides a crucial test to assess the thermal conditions and, therefore, the role of the weak and main s-process components. The isotope ^{79}Se could be produced using irradiations at a fast reactor. The material could then be inserted in the SPES ECRIS ion source for further acceleration.

Neutron activation measurements on key isotopes

In stars, the energy distribution of neutrons follows a Maxwell-Boltzmann distribution. Therefore, the quantity needed for the calculation of the stellar reaction rate of neutron-capture reactions is the Maxwellian-Averaged Cross-Section (MACS). For many isotopes, the calculated MACS uncertainties are higher than the requested accuracy, being 3–5% for the s-process. To have a precise measurement with a reliable uncertainty estimation, the neutron spectrum should follow as much as possible the Maxwell-Boltzmann neutron spectrum (MBNS). Discrepancies between the experimental spectrum and the real MBNS complicate the determination of the uncertainties. A solution was proposed in [98], where a method to obtain experimentally a MBNS at kT = 30 keV was proposed, using the ^{7}Li(p,n)^{7}Be reaction. This method proposes to shape the neutron energy spectrum by shaping the projectile energy distribution in MBNS. Among different ways of shaping the proton beam, the easiest is to use a foil placed before the neutron-producing target: by choosing different materials of the shaper, beam energy, and integration angle, MBNS at different kT can be obtained. This method has been already validated at the CN accelerator, where a neutron beam line, called BELINA, has been developed. So far, a well-reproduced MBNS with 28 keV thermal temperature was measured.

In the next years, neutron beams with MBNS at different temperatures will be developed. This will open the possibility to perform activation measurements and determine the MACS at different kT. Since the MBNS at 28 keV was already measured, a first experiment to measure the MACS on two isotopes is planned. The proposal includes not only measuring the MACS on Au, as a reference measurement, but also measuring the MACS on Y and Zr as benchmark measurements. Then a long campaign of MACS measurement for s-process will start at BELINA. The results of the activation measurements will be directly compared with those obtained in the new NEAR station facility [99] at CERN (n_TOF collaboration; [100]). Once available, SPES RIBS can be implanted on a thin target, and the MACS measured at the BELINA beamline at CN. Because of the presence of both lines in situ, samples with very short lifetime can be measured.

3.2.2 The rapid neutron capture process

Determining the site (or sites) for the occurrence of the r-process is one of the main challenges for modern nuclear physics and astrophysics. The most natural candidates are explosive astrophysical scenarios, such as the collapse of a massive star or a merger of two neutron stars, or of a neutron star and a black hole. Obtaining a piece of direct observational evidence for one of these scenarios is a difficult task. However, following the detection of the kilonova A72017gfo as the electromagnetic counterpart of the gravitational-wave signal GW170817, it became clear that binary neutron-star mergers represent one of the main r-process sites in the Universe.

The high-temperature and density conditions of matter ejected from a binary neutron-star (BNS) merger allow neutron capture on heavy nuclei to proceed much faster than β decay. Thus, during the r-process, highly unstable neutron-rich nuclei close to the neutron-drip line are produced. In this view, radioactive ion beam facilities like SPES will allow us to investigate the properties of unstable neutron-rich nuclei and perform more accurate astrophysical simulations to quantitatively predict elemental abundances and the electromagnetic radiation emitted from these environments.

Sensitivity studies to identify key nuclear properties

Among the most important and uncertain nuclear inputs, there are neutron-capture rates on unstable nuclei with short lifetimes. Their direct measurements are hardly feasible, so one can only rely on theoretical rates computed via the Hauser–Feshbach (HF) statistical approach. However, depending on the different choices for experimentally-unknown nuclear structure properties, optical potentials, level densities, and γ-ray strengths of nuclei located far from stability, large variations, by over three orders of magnitude, in the capture rates are predicted [101, 102].

The r-process is normally characterized by a huge amount of free neutrons. However, when the availability of free neutrons drastically reduces, the so-called freeze-out phase takes place. At that point, the equilibrium between neutron captures and photo-disintegrations is no longer maintained and a deep knowledge of neutron capture cross sections is needed to properly shape the final heavy element abundance distribution. Sensitivity studies on outflows from BNS mergers, adopting a typical factor of 100 for the n-capture rate uncertainty [103], have shown that those rates have a large global effect on the predicted r-process abundance distribution. These studies pointed out that major relevant neutron capture rates include those on Cu, Zn, Ga, Se, Br, In, Sn isotopes and neutron-rich closed-shell nuclei ($N = 126$) with low neutron binding energies. Nuclear properties measurements for these nuclei are therefore highly demanded (see Sect. 4) and future experiments performed at next-generation radioactive ion-beam facilities like SPES will better constrain r-process yields calculations of BNS mergers and their contribution to the production of heavy elements in Universe. Recently, r-process calculations were performed for a Neutron Star Merger (NSM) scenario by considering 5 trajectories chosen as representative of various conditions in initial electron fraction (Ye), entropy and expansion timescale [104]. Each set has been explored for the different NSM components. Figure 4 shows the various final patterns obtained by varying single (n,γ) rates (multiplied or divided by a factor of 100). This sensitivity study focused on those rates with the greatest impact on the final r-process abundance pattern, having also a good chance to be measured by future experimental campaignes at SPES. We refer to [104] for more details.

Another predominant role during the r-process nucleosynthesis is played by β decays, which determine the speed at which heavy elements are synthesised, shaping the r-process abundances and, in the case of NSM, powering the electromagnetic transient known as kilonova [105, 106]. β-decay experimental campaigns, like the one planned at SPES, are thus crucial for a proper understanding of the r-process nucleosynthesis. Furthermore, these experimental efforts provide important feedback to nuclear models employed in network calculations and in the estimation of other observables. Finally, as revealed by previous campaigns at the RIB facilities, cross-checking previous measurements is vital to ensure the validity of experimental data employed in nuclear network calculations [105].

In order to assess the relevance of the planned β-decay experimental campaign at SPES in the context of the r process, we carried out a sensitivity study exploring the impact of β decays on r-process abundances. Starting from a baseline network calculation where β-decay half-lives (t_β) and β-delayed neutron-emission probabilities (P_n) were taken from the FRDM predictions [107], we varied the t_β and P_n of nuclei accessible at the SPES facility according to the predictions given by two other models: D3C* [108] and SkO' [109]. As for the astrophysical scenario, we employ four trajectories representative of different ejecta in NSM. The first two trajectories trace the baryonic wind produced by neutrino absorptions in NSM remnants [110] at different polar angles (along the polar axis, less neutron-rich, and at lower latitudes, more neutron-rich). The other two trajectories correspond to tidal dynamical ejecta in a 1.35–1.35 $M_\odot$ symmetric NSM system and shock-heated ejecta in a 1.4–1.2 $M_\odot$ asymmetric merger [111, 112].

Figure 5 shows the sensitivity of the final abundances when β-decay half-lives and β-delayed neutron emission probabilities of nuclei in the SPES region are varied. We find the largest differences around $95 \leq A \leq 115$ and above the second peak ($140 \leq A \leq 155$), where in some cases the variations on the predicted abundances are larger than 100%. These results suggest that future measurements of β-decay half-lives at the SPES facility around the neutron shell closures $N = 50$ and $N = 82$ could reduce the impact of nuclear uncertainties on network calculations estimating the production of lighter heavy elements and lanthanides in NSM, providing constraints regarding the existence of a light element primary process and the modelling of kilonova light curves.

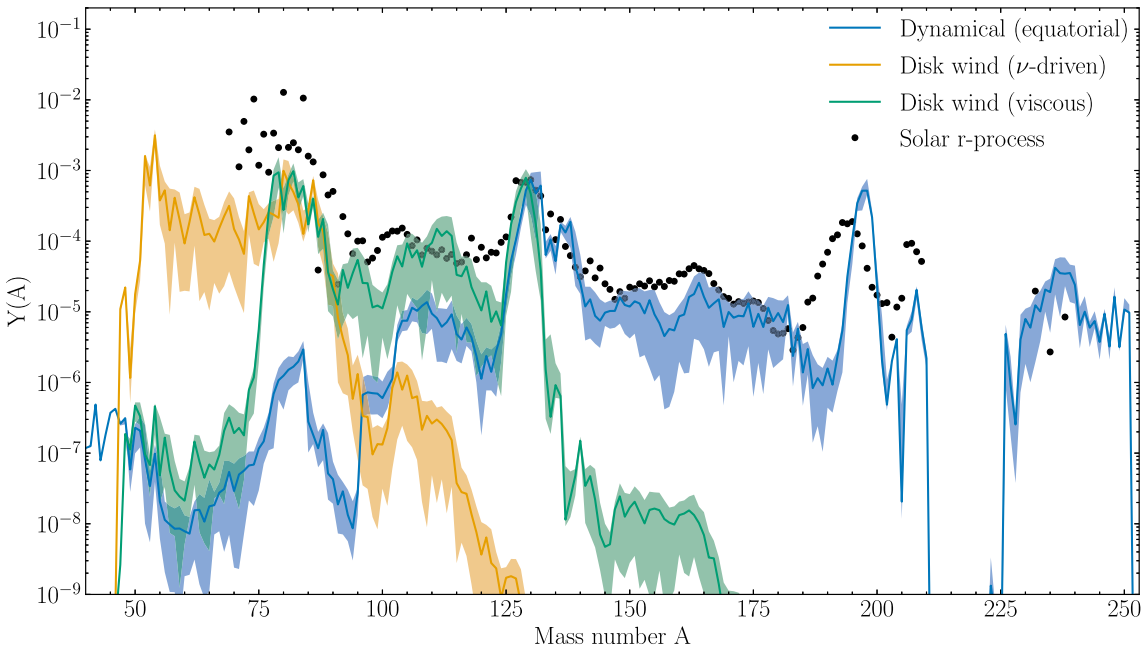

Fig. 4 Impact of n-captures rates uncertainties of nuclei in the SPES region on r-process abundances for three different trajectories. Final abundances as a function of mass number A are reported; bands represent variations obtained when different n-capture rates are employed. See [104] for further details and additional plots

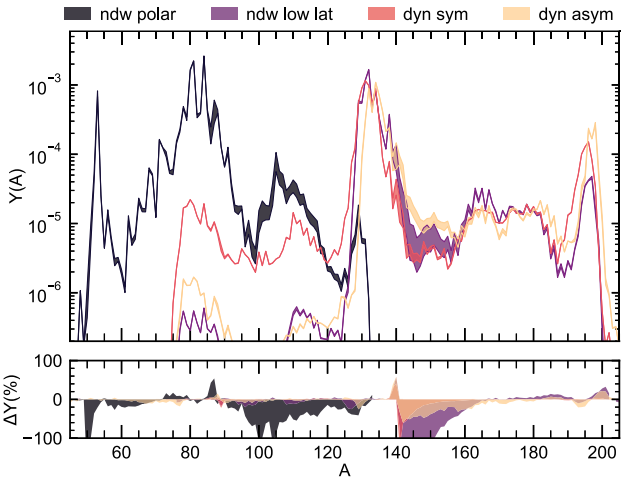

Fig. 5 Impact of β-decay rates uncertainties of nuclei in the SPES region on r-process abundances for four different trajectories. Upper panel: final abundances as a function of mass number A. Bands represent variations obtained when different β-decay rates and β-delayed neutron probabilities are employed. Lower panel: relative difference of final abundances respect to the predicted FRDM baseline calculations

Neutron capture cross sections for r-process: surrogate reaction method

As stressed in the previous section, any nuclear study aiming at extending the spectroscopic information, and providing the extraction of spectroscopic factors for n-rich unstable isotopes, is welcome. This is in particular true for the neutron-rich region around ^{132}Sn. The evolution of the shell structure, especially in the vicinity of nuclei having a more stable configuration with respect to nearby isotopes (for instance nuclei with a magic number of protons or neutrons), but far-away from the valley of β stability, is of paramount importance to investigate the nature of the nuclear mesoscopic system and the limit of nuclear existence. It is important to stress that the direct study of n-capture processes on nuclei far from the β stability valley is extremely challenging. However, as for the s-process, the surrogate technique is a valid alternative method. A possible experimental campaign involves the measurement, via SRM, of the partial cross sections for the population of the final states of the residues formed in light-ion direct reactions in inverse kinematics, using SPES re-accelerated beams. A day-one experiment can be pursued on a plastic CD2 target or a thick cryo-target, as for example CTADIR [113]. The production rate of the secondary beams at the target position are expected to be of the order of $\sim 10^{5\div 8}$ atoms/s, being the species of interest located only few nucleons away from the nearest stable nucleus. The expected yield, considering the lower and upper limits for the beam intensity, a target of 500 μg/cm^2 thickness, and an inclusive cross section of 10 mb for a typical direct reaction, will give from 0.01 to 10 ions/s of the final species. This will be reduced by the efficiency of the detection setup, which, for a direct reaction in inverse kinematics, consists in a γ detector complemented by a silicon detector.

Therefore the use of new-generation detection system, like γ tracking array (AGATA [9]) and silicon detector with embedded PSA (TRACE/MUGAST/GRIT [22, 33, 114]), is strongly envisaged.

Measurement of key nuclear decay properties

As previously stated, the knowledge of nuclear properties such as β-decay half-lives, as well as β-delayed neutron emission probabilities P_n, are critical inputs that go into calculations of r-process nucleosynthesis. However, also the measurement of the decay schemes of neutron-rich nuclei is important because they provide γ-ray strengths, which are key inputs for neutron capture theoretical rates computed via the HF statistical approach. Decay schemes can be measured at SPES, by profiting of the isobar beam purification of the HRMS and the β-DS tape station surrounded by γ detectors. In addition E_0 and EC transitions will be also at reach by profiting of the SLICES MOS/Si(Li) linked to the β-DS tape station. P_n values of the nuclei of interest, as well as neutron-gated γ-ray spectra, can be obtained by coupling the β-DS array to neutron detectors such as NEDA [10]. We would like to stress the importance of measuring nuclear properties not only for the nuclei with strong direct impact on the r process, namely around the closed shells 50, 82 and 126, but also for those with small impact, because they provide nuclear structure trends far away from stability, which can be important for building realistic nuclear models to be used in nucleosynthesis calculations.

Abundances of the elements at the first r-process peak: (α,n) reactions

The first r-process peak has been overlooked in the past and most of the works concentrate on the second and third r-process peaks. An interesting case is the nucleosynthesis of Molybdenum (Mo, Z = 42) which is not yet fully understood. Galactic chemical evolution (GCE) simulations estimated that about 40% of the solar Mo is made by the s-process while the r-process contribution is uncertain (e.g., Ref. [115]). Mo is most likely characterized also by a contribution from different explosive nucleosynthesis processes in collapsing supernovae (CCSNe) that is not associated to the r-process (see below Sect. 3.2.3). Therefore, the study of Mo abundance observed in the Galactic disc is a challenging task for current GCE simulations [116]. In a high-temperature, high-entropy and relatively high-Ye astrophysical scenario, nuclear statistical equilibrium is achieved and is dominated by α particles and neutrons. A large neutron-to-seed ratio could be achieved at the time of the α freeze-out, without requiring a large neutron-to-proton ratio. This results in an enhancement of "α-elements" and an extension of the Fe group to higher masses up to A $\approx$ 90. Recent studies have shown the influence on the abundance patterns of different (α,n) reactions. During the α-freeze-out, (α,n) reactions gradually lead to the accumulation of certain elements, and are a source of additional neutrons during the collapse of the star's core. Recent sensitivity studies include the neutrino-driven winds scenario [117], as well as the magneto-hydrodynamically driven supernovae [118] scenario. These studies have shown that (α,n) reactions most influence the nucleosynthesis while the reaction flow reaches the zone of Z = 26–45. Major relevant (α,n) rates include those on Cu, Zn, Ga, Ge, As, Se, Br, Kr, Rb, Sr, Y, and Zr. These elements will be available at SPES as post-accelerated beams, so that we can study (α,n) reactions in inverse kinematics on a ^{4}He gas jet target, like SUGAR, and detecting neutrons with NEDA.

Formation of the seed nucleus ^{12}C, for the r-process

The occurrence of the r-process in NSMs has been recently confirmed [119, 120]. In this context, two potential paths to the formation of the seed nucleus ^{12}C, for the r-process, to reach elements with mass number A = 50–80 are: (a) $\alpha(\alpha n,\gamma)^9\mathrm{Be}(\alpha,n)^{12}\mathrm{C}$; (b) $\alpha(nn,\gamma)^6\mathrm{He}(\alpha,n)^9\mathrm{Be}(\alpha,n)^{12}\mathrm{C}$. The relative weight of these two paths depends upon the reaction rates of all reactions involved, some of which are currently unexplored experimentally. In a neutron-rich environment, the formation of ^{12}C through the reaction $^9\mathrm{Be}(\alpha,n)^{12}\mathrm{C}$ can compete with the triple-α reaction and even dominate. Therefore, we propose to study $^9\mathrm{Be}(\alpha,n)^{12}\mathrm{C}$ reaction, in inverse kinematic with a ^{4}He gas target like SUGAR or CTADIR and/or in direct kinematics with a ^{9}Be solid target, counting on AGATA, NEDA, and GRIT experimental arrays. We underline that, for the case of direct kinematics, a ^{9}Be beam should be developed at LNL. The fusion of ^{9}Be and one α particle can result in different output channels, namely: complete fusion $^9\mathrm{Be}+\alpha \rightarrow {}^{13}\mathrm{C}+\gamma$ (Q = 10648 keV); $^9\mathrm{Be}+\alpha \rightarrow {}^{12}\mathrm{C}+n$ (Q = 5702 keV); $^9\mathrm{Be}+\alpha \rightarrow \alpha+\alpha+\alpha+n$ (Q = −1572 keV); $^9\mathrm{Be}+\alpha \rightarrow {}^8\mathrm{Be}+\alpha+n$ (Q = −1664 keV); $^9\mathrm{Be}+\alpha \rightarrow {}^5\mathrm{He}+\alpha+\alpha$ (Q = −2308 keV); $^9\mathrm{Be}+\alpha \rightarrow {}^5\mathrm{He}+{}^8\mathrm{Be}+\gamma$ (Q = −2400 keV). Quantifying the cross section for all exit channels, exploiting coincidence measurements, should be of value to study ^{9}Be nuclear structure, besides shading some light on the formation of ^{12}C.

Moreover, using a $^6\mathrm{He}^{2+}$ beam, and the AGATA and NEDA multi-detectors, it would be possible to study the reactions $^6\mathrm{He}(\alpha,\gamma)^{10}\mathrm{Be}$ (Q = 7409 keV) and $^6\mathrm{He}(\alpha,n)^9\mathrm{Be}$ (Q = 597 keV). This allows not only to analyze the ^{6}He-α structure of ^{10}Be, but also to improve the current knowledge on the reaction rates of the two different paths to ^{12}C formation.

3.2.3 The intermediate neutron capture processes

As already remarked, a well established nuclear astrophysics paradigm is that elements beyond iron are made by the s-process and by the r-process, with a comparable contribution to the solar abundances [121, 122]. On the other hand, other neutron-capture processes do happen in stars with intermediate neutron densities between the s-process and the r-process. The intermediate neutron-capture process (i-process, [92]) is defined by neutron densities in the order of 10^{14-16} neutrons cm^{-3}, and it can be activated by the $^{13}\mathrm{C}(\alpha,n)^{16}\mathrm{O}$ following the ingestion of hydrogen in convective He-burning environments. Different types of stars are potential stellar hosts of the *i*-process: low-mass AGB stars [e.g. 123, 124, 125, 126], post-AGB stars [127], super-AGB stars [128], massive stars [129–131], and rapidly-accreting white dwarfs within binary stellar systems [e.g. 132, 133, 134].

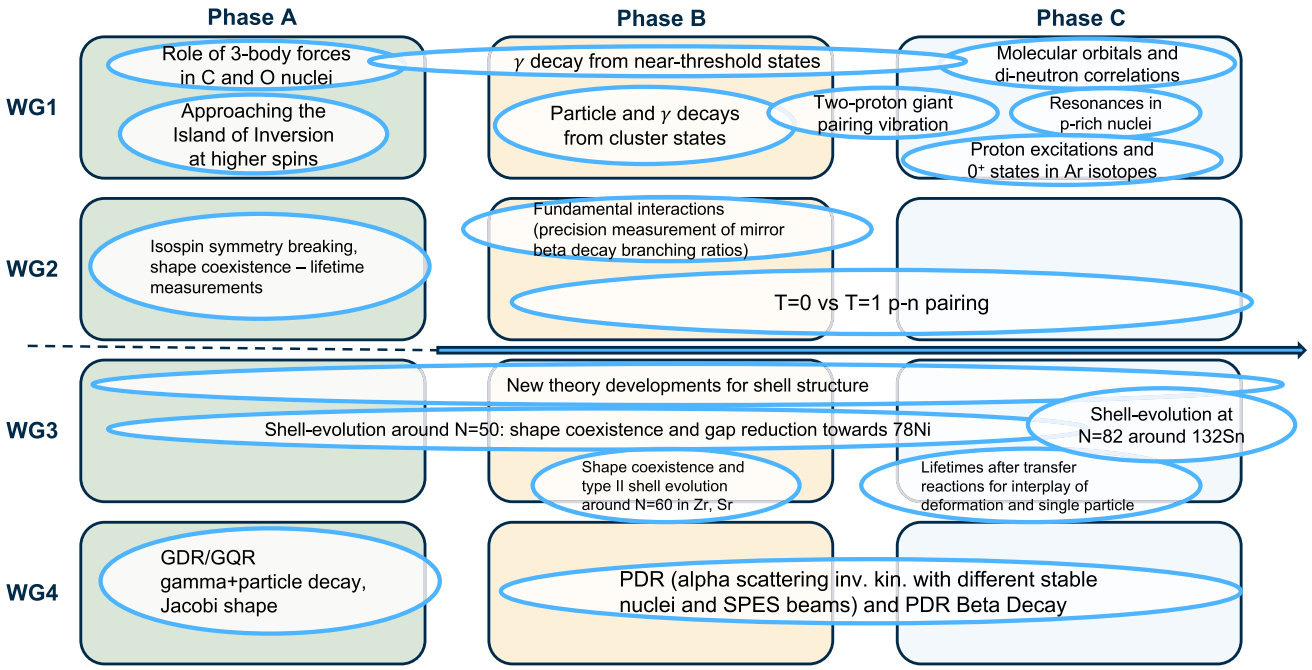

Fig. 6 Summary of nuclear structure activities that could be performed at LNL in the next future, sorted according to the time phase. See text for details

Along the nucleosynthesis path of the i-process, unstable isotopes are made up to 8–10 neutron-rich nuclides far from the valley of stability. Neutron-capture rates of these unstable isotopes are crucial sources of uncertainty, and may be studied at LNL through the surrogate method discussed in previous sections. First specific nuclear sensitivity studies have been made for the i-process: at low metallicities, ref. [135] studied the Ba region and ref. [136] analyzed the abundance distribution for AGB stars. Ref. [137] studied the Sr-Y-Zr region for post AGB stars, ref. [138] studied the mass region $32 < Z < 48$ and ref. [139] the mass region $56 < Z < 74$. From these studies, depending on the stellar site and on the observation, the authors have indicated as different relevant nuclear reaction rates to measure the ^{75}Ga(n,γ) and ^{66}Ni(n,γ) [138]; ^{87}Kr(n,γ), ^{88}Kr(n,γ), ^{89}Rb(n,γ) [137], the ^{135}I(n,γ) [135], the ^{137}Cs(n,γ), ^{141}Ba(n,γ) and ^{141}La(n,γ) [139].

4 Nuclear structure

The knowledge of the nuclear structure is a key ingredient to build a comprehensive microscopic understanding of nuclei, extended nuclear matter and astrophysical phenomena [3], nuclear reactions and decays [5]. Breakthroughs in the experimentation with exotic isotopes, novel theoretical concepts, cross-fertilization in different research areas, and the progress in computer technologies and numerical algorithms, make nuclear structure a modern and lively research field, with exciting prospects spanning from fundamental physics to applications.

In the coming years, Legnaro National Laboratories (LNL) will offer a variety of accelerator facilities and state-of-the-art detection systems, opening the possibility to explore a wide range of nuclear physics and astrophysics processes. Figure 6 and Table 2 provide a view of the possible nuclear structure topics (working groups in Sects. 4.2, 4.3, 4.4, 4.5) which could be explored at LNL in the near, medium and further future (phases A,B and C) using stable and radioactive ion beams. The experimental studies will profit of different, and sometimes complementary, approaches. A detailed description of the future possibilities at LNL is reported in the four following sections, preceded by a theoretical address: Light to medium-mass exotic nuclei (WG1), N∼Z nuclei and isospin symmetry breaking (WG2), Shell evolution (WG3) and Shape coexistence (WG4). The topics have been selected to strengthen existing research ambits and open new scenarios, in line with the facility development at LNL.

4.1 Nuclear structure theory of relevance to the experimental program

Nowadays, Interacting Shell Models (SM) [140], Energy Density Functional (EDF) theories [141], and ab initio methods [142] can provide complementary microscopic descriptions of nuclear properties in a broad range of masses. Yet, the growing quality of data expected from future campaigns will require sufficiently accurate theoretical predictions to facilitate the interpretation of experimental results. Systematic advances in accuracy and precision are being obtained within ab initio theory, with community efforts going into developing appropriate effective theories of two-, three-, and many-nucleon interactions [143], as well as theory

Table 2 Summary of key nuclear physics topics and reactions that could be addressed at LNL in the next years. The activities are sorted according to the working group discussing the proposal and the time phase

Tag	Description	Reaction	Phase
LNL-NS-LMN-a,b,c	γ decay from near threshold states	^{6}Li(^{6}Li,p)^{11}B, ^{13}C(^{7}Li,p)^{19}O, ^{7}Li(^{14}C,p)^{20}O	A,B,C
LNL-NS-LMN-b	Particle and γ decay from cluster states	^{11}C(α,α'), ^{15}O(α,α'), ^{21}Ne inelastic	B
LNL-NS-LMN-a0	Role of 3-body forces in C and O nuclei	^{18}O deep inelastic	A
LNL-NS-LMN-c0	Molecular orbitals and di-nucleon correlations	^{10}Be(α,α'), ^{10}Be(p,p')	C
LNL-NS-LMN-b,c	Two-proton giant pairing vibrations	^{A}C(^{3}He,n)	B,C
LNL-NS-LMN-c1	Resonance in proton-rich nuclei	^{26}Si(α,α'), ^{24,25}Al(p,p')	C
LNL-NS-LMN-a1	Approaching the Island of Inversion at higher spins	Multi-Nucleon Transfer ^{22}Ne, ^{26}Mg, ^{30}Si	A
LNL-NS-LMN-c2	Proton excitations and 0^{+} states in Ar isotopes	Two-proton transfer ^{A}Ca(^{14}C,^{16}O)	C
LNL-NS-NZ-a,c	Isospin-symmetry breaking, shape coexistence		A
LNL-NS-NZ-b	Fundamental Int. (precision measurement of mirror BR)	^{21}Na, ^{23}Mg, ^{45}V	B
LNL-NS-NZ-c	T = 0 versus T = 1 proton–neutron pairing	^{36}Ar(p,^{3}He) and (^{3}He,p), ^{46}V, ^{50}Mn	B,C
LNL-NS-SE-a	New theory development for shell structure		A,B,C
LNL-NS-SE-b0	Shell evolution around N = 50: shape coexistence and gap reduction towards ^{78}Ni	^{238}U+^{9}Be $^{78\div82}$Zn β decay	A,B
LNL-NS-SE-b1	Shape coexistence and type II shell evolution around N = 60	Sr, Zr β decay	B
LNL-NS-SE-c0	Shell evolution at N = 82 around ^{132}Sn	^{132}Sn(d,p), (^{3}He,d), (^{3}H,^{4}He)	C
LNL-NS-SE-c1	Lifetimes after transfer for interplay of deformation and single-particle states		C
LNL-NS-DEF-a0	Jacobi shape	^{48}Ca+^{48}Ti	A
LNL-NS-DEF-a1	Giant Quadrupole Resonance	^{17}O+^{40}Ca	A
LNL-NS-DEF-b0	Pygmy Dipole Resonance	noble gas +^{4}He	B
LNL-NS-DEF-b1	Pygmy Dipole Resonance	^{142}Cs β decay	B
LNL-NS-DEF-c	Pygmy Dipole Resonance	^{94}Sr + ^{4}He	C

and methods to solve the nuclear many-body problem [142]. In the first case, Effective Field Theories (EFT) allow to link the nuclear forces directly to the underlying QCD theory, with the aim of minimising modelization and phenomenological contents. Advances in terms of mass number reached over the past few decades by ab initio approaches are shown in Fig. 7. Methods based on handling directly all nucleon degrees of freedom offer, virtually, exact results, but are mostly limited to few-nucleon isotopes. Novel many-body approaches that offer polynomial scaling, by selecting computational degrees of freedom, have quickly extended near the heavy-mass regions, with supercomputing facilities. Full-space computations that need to explicitly account for correlations at play in complex nuclei (superfluidity, deformation, clustering, etc.) have explored the region around the calcium chain [144–149], and are now extending their reach to heavier and doubly open-shell nuclei. Valence-space methods built on the know-how of the empirical shell model have recently completed systematic calculations of the nucleon drip lines up to the iron chain [150].

The frontiers in advancing the above microscopic theory are directly lined to the opportunities that they present in conjunction with experimental programs. Perspectives for ab initio applications from light- to medium-mass nuclei can be identified along three directions:

1. Precision calculations around Z = 20. Progress in the modelling of two- and three-nucleon interactions is providing ab initio calculations with an ever-increasing accuracy, comparable to that of empirical calculations, or even higher. Tools like emulators or Bayesian analysis [153] allow to get systematic feedback from new measurements. Data beyond ground state properties, such as deformation, collective response and electroweak decays, will contribute to assessing theoretical uncertainties stemming from

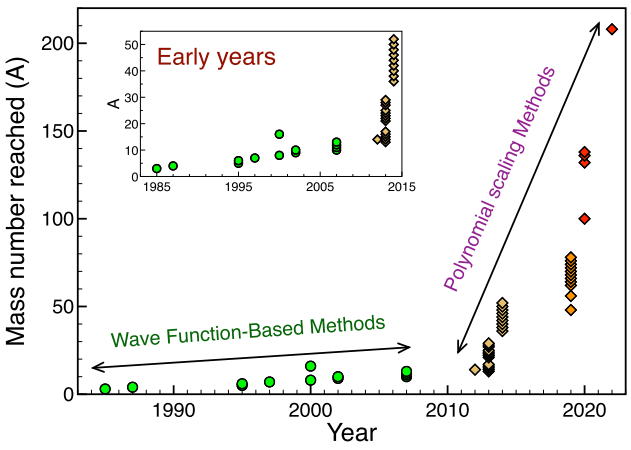

Fig. 7 Advances in terms of mass number reached over the past few decades (1980–2022) by ab initio theory. The different classes of methods used to solve the nuclear many-body problem are also displayed, as green dots for wave function-based methods and as yellow and red diamonds for polynomial scaling methods. (Inset) zoom on the early years (1985–2015). Data from Refs. [142, 151–153] and references therein

the nuclear Hamiltonian. New methods that exploit neural networks and Machine Learning techniques are now being pioneered for light nuclei [154, 155].

2. Discovery calculations around N = 50. Ab initio applications in the region N ≈ 50 will be challenging for two reasons. First, while many systems around calcium remain semi-magic, and can be approximately treated as spherical, the recourse to deformation will be crucial in this mass region. Methods that can explicitly handle deformation are being developed [156–159], together with the associated machinery to describe low-energy spectroscopy. Second, ab initio methods have been used to evaluate optical potentials at low scattering energies, along with structure information. Recent computations up to masses A = 40 [160–162] are improving in accuracy and becoming closer to the quality of standard phenomenological scattering. The opportunity to resolve the long-standing issue of consistency between structure and reactions will directly impact the quality of the analysis of experiments at LNL and at similar facilities worldwide.
3. Exploratory calculations around N = 82. Only few ab initio calculations have been attempted around ^{132}Sn, so far [152, 163]. Arguably, this region will constitute the ab initio frontier in the decade to come. Innovative computational techniques, including the exploitation of GPU accelerators, will have to be devised to tackle the increasing number of nucleons or valence space dimensions.

Experimental data in light and medium-mass nuclei, where high-precision ab initio calculations are possible, are then crucial to benchmark more challenging systems, and to improve on the interpretation of structure and reactions. Standard phenomenological mean-field approaches based on EDFs remain the best choice to understand several heavy and deformed systems, as discussed in the following sections for specific cases. Currently, advances are being made in Density Functional Theory with the aim of determining the energy-density functionals directly from ab initio theory, allowing for a similarly solid link with the underlying theory of QCD [164, 165].

4.2 Light to medium-mass exotic nuclei

A unified description of the structure of atomic nuclei, from deuteron to superheavy elements, still remains one of the greatest challenges of modern nuclear physics. Light nuclei, with a limited number of protons and neutrons, already provide a unique playground in which to investigate a variety of phenomena appearing in the first portion of the nuclide chart, up to $Z \sim 20$. Among them, the clusterization of nucleons, leading to molecular-like structures, is pivotal for the study of light systems such as Be, C, O, and Ne isotopes [166]. In this context, nuclear excitations in the continuum, in the proximity of particle-emission thresholds, as well as resonances at higher energies, are of particular interest [167, 168]. These states play a major role in nuclear astrophysics [169], as they influence the capture rates of reactions occurring in stars, and hence the abundance of elements in the Universe. The relevant nuclear structure properties may change when heavier systems are considered. Between Mg to Ca isotopes, the study of the interplay between single-particle motion and collective excitations is crucial to pin down the underlying shell structure. The latter is at the basis of the microscopic description of peculiar phenomena, such as the coexistence of different nuclear shapes at similar energies [170]. Overall, the different facets of atomic nuclei can be traced back to the complex nature of nuclear forces and nucleon correlations and interactions. These can be studied at best in light and medium-mass nuclei, with a limited number of degrees of freedom, providing stringent tests for the most advanced nuclear models (see Sect. 4.1).

In the coming years, a large part of the experimental activity at LNL will be devoted to the study of nuclear structure moving away from the valley of stability by employing state-of-the-art γ-ray and particle detectors, such as AGATA, GRIT, TPCs, etc. Superior sensitivity will be achieved compared to conventional spectrometers, boosting the study of even rarer nuclear phenomena. In this section, selected topics on light and medium-mass nuclei are presented. Possible experiments are discussed combining γ-ray and particle spectroscopy techniques and exploiting both stable and radioactive beams.

4.2.1 Weak gamma-decay branches and particle decays

γ decay from near-threshold states

In light neutron-rich nuclei, the investigations of γ decays from unbound near-threshold states is a very relevant topic. Such states are of great importance for the understanding of the onset of clusterization phenomena in molecular-like nuclei and play a key role in nucleosynthesis reactions in star. The most famous example is the Hoyle state in ^{12}C, lying only 287 keV above the α-decay threshold. The γ decay from near-threshold states is an almost unexplored territory, and AGATA will allow to access electromagnetic decays in neutron-rich B, C, O and N nuclei, with decay branches of the order of $10^{-3} - 10^{-5}$. Fusion reactions induced by intense ^{14}C and ^{6,7}Li beams on Be, C, Li and B targets, followed by the evaporation of a single charged particle, detected in the TRACE or GRIT systems, will be exploited. In this context, a very peculiar case is ^{11}B, where the existence of a narrow near-proton-threshold resonance was proposed on the basis of an unexpectedly high branch (two orders of magnitudes higher than predictions) of the extremely rare process of β-delayed proton emission starting from ^{11}Be [167, 171, 172]. A preliminary experiment with GALILEO points to a gamma-decay branch of $\sim 10^{-3}$ which can be further constrained with the AGATA setup, providing a strong benchmark to theory predictions [173, 174].

Particle and γ decays from cluster states

The range of light beams produced by the EXOTIC facility is under continuous development, and ideally suited to study near-threshold resonances in compound systems of the type beam+α, when using a helium gas-filled TPC target. These near threshold states are important to understanding the details driving nucleosynthesis processes that take place in stars. One such example is in the ^{15}O+α reaction that leads to X-ray bursts, some of the most energetic events in the Universe. This process is caused by breakout from the hot-CNO cycle leading to the onset of the rapid-proton capture (rp) process [169] and is thought to be dominated by a single α-clustered state in the ^{19}Ne compound nucleus [175]. Also possibly on the path of the rp-process are the states in ^{25,26}Si that can be studied through proton scattering of ^{24,25}Al SPES beams. Active targets are particularly well adapted to measuring elastic and inelastic resonant scattering: the large target thickness compensates the low intensity of radioactive ion beams, and the tracking of charged particles provides information to determine energies, cross sections and decay channels of the resonant states [176]. Coupling with γ-ray detection is also envisaged, using arrays of high-efficiency scintillators such as $LaBr_3$(Ce) or $CeBr_3$ [177]. Another development that offers significant new opportunities to explore near-threshold states is represented by thin solid noble gas targets that can now be produced [178]. This new technique leads to high-atom ratio 'gas' targets on a variety of substrates, such as silicon, aluminium or nitrides, suitable for low-abundance nuclei such as ^{3}He and ^{21}Ne. Such targets make novel inelastic and transfer reactions feasible, and, being thin, allow studies with highly segmented germanium detector arrays such as AGATA. This experimental approach opens up investigations of weak γ-decay branches from near-threshold states in both the target and reaction products by distinguishing between collective levels in cluster bands and single-particle states. A deeper understanding of the extent and impact of nuclear clustering in these systems will be obtained [179]. The advantages offered by thin solid noble gas targets to access light nuclei and the high precision achievable in such measurements are expected to challenge advanced theoretical approaches based on ab initio nucleon–nucleon interactions, including also continuum effects [173, 174].

4.2.2 Nuclear correlations and nuclear forces

Role of 3-body forces in light neutron-rich nuclei

The structural properties of light neutron-rich nuclei have significant impact on nuclear astrophysics and can be used to test the details of the nuclear force, including the three-body term (NNN) of the nucleon–nucleon interaction [180, 181]. In this context, ideal cases are neutron-rich O and C isotopes which can be reached by using deep-inelastic reactions with intense ^{18}O beams on heavy targets (e.g., ^{238}U, ^{208}Pb or ^{198}Pt) [182]. Here, ab initio calculations have shown a strong sensitivity to electromagnetic properties to NNN forces. By including the NNN term in the calculation the wave function composition can significantly change, thus affecting the lifetime of the excited states [183]. Among the most interesting cases are ^{16}C and ^{18}C. In ^{16}C, the lifetime of the second 2^+ state, calculated incuding two-body (NN) forces only, is equal to 230 fs versus 80 fs found including NNN forces. Similar calculations for ^{18}C provide a lifetime of $\sim$1 ps versus $\sim$2 ps, respectively. Precise lifetimes measurements are therefore needed, which require techniques able to extract information in the time intervals from one hundred femtoseconds to a few picoseconds, based on a detailed study of Doppler broadened γ-peak line shapes. A first experiment of this type was performed at GANIL in 2017, with the AGATA+VAMOS+PARIS setup [181]. The results for ^{20}O are presented in Fig. 8 (a further support to the need of three-body forces comes from an experiment with AGATA+MUGAST performed at GANIL [184]). At LNL, the larger angular coverage of AGATA, coupled to the PRISMA magnetic spectrometer positioned at forward angle to best profit of enhanced cross sections from deep inelastic processes, will provide a significantly improved sensitivity, crucial for accessing the most exotic cases [185].

Molecular orbitals and di-neutron correlations

The ^{8}Be nucleus is well known for its two-α cluster structure. The neutron-rich ^{10}Be with two neutrons added to ^{8}Be is predicted to form neutron molecular orbitals around the two α clusters. According to the molecular orbital model, there are two types of orbitals near the Fermi surface of ^{10}Be: the bonding π-orbital and the anti-bonding σ-orbital. According to theoretical calculations,

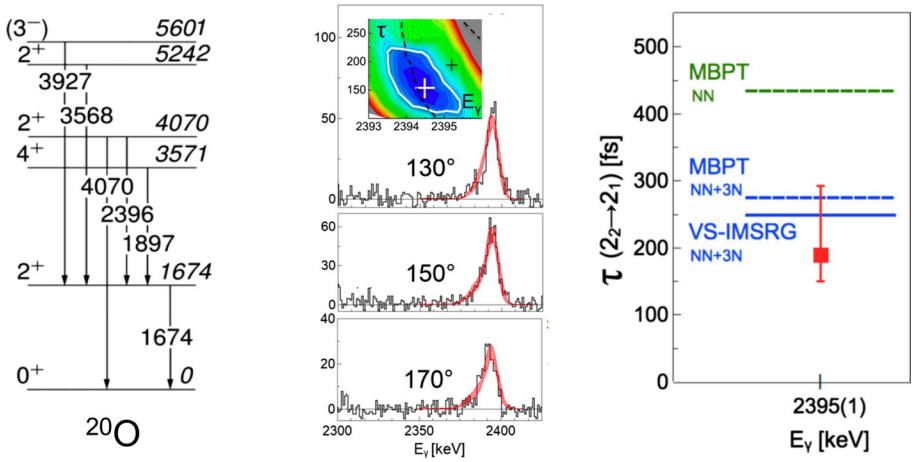

Fig. 8 Results for ^{20}O taken from the AGATA+VAMOS+PARIS experiment of Ref. [181]. (Left) Level and decay scheme of ^{20}O. (Center) Line shape of the 2396-keV γ ray de-exciting the 2^+_2 state in ^{20}O. The χ^2 lifetime-energy surface is also shown. (Right) Experimental partial lifetime (red) for the $2^+_2 \rightarrow 2^+_1$ decay in ^{20}O compared with ab initio predictions using different NN and NNN forces (see references in [181])

the latter is characterized by spatially extended neutron wave functions that stabilizes the two α clusters at a larger distance [186]. The π-type orbital generates the ground 0^+ band, whereas the second 0^+ state at 6.18 MeV is predicted to be the band head of the σ-type orbital configuration. The experimental data currently available for this latter state are too limited to support or dismiss the enhanced cluster configuration prediction. In addition, a recent theoretical study [187] of the inelastic scattering to the 2^+_2 state has shown a strong sensitivity to the di-neutron correlation. A very exciting possibility offered by light beams from SPES would be the study of the ^{10}Be(p,pγ) inelastic scattering reaction, using the GRIT-AGATA set-up to extract the transition strengths from the two types of molecular orbitals and the cross-section to the 2^+_2 state.

Two-proton Giant Pairing Vibrations

Pair correlations are known to provide an enhancement in the magnitude of the ground-state to ground-state transition matrix elements between systems that differ by two nucleons [188]. An analogous enhancement is expected from particle–particle correlations involving transitions to higher-lying single-particle shells. A particular mode, the Giant Pairing Vibration (GPV), predicted in the 1970s [189], is described as to the collective superposition of many particle–particle states. The GPV has been searched for in heavy nuclei in the last decades with no success [190]. Its search regained interest with the measurement of a compatible signal in the light carbon isotopes [191]. It was suggested [192] that the GPV is embedded in the continuum and the large background produced by other states makes its identification an experimental challenge. However, a two-proton GPV would be narrower than other nucleon–nucleon modes due to the Coulomb barrier. This offers the possibility to investigate the two-proton GPV in the carbon isotopes, for example, through the (^{3}He,n) reaction in reverse kinematics using NEDA and GRIT to measure their two-proton decay.

Giant resonances and deformations in light nuclei

The energy of giant isoscalar modes is closely related to the incompressibility of nuclear matter, a fundamental parameter of the nuclear equation of state [193]. It is thus essential to correctly determine the strength distribution of those modes. Because of the highly collective character of giant resonances (GRs), their strength distributions are strongly dependent on the nuclear shape: a ground-state deformation causes a splitting of the GR line shape. This has been observed for the well-studied isovector giant dipole resonance [194] and for isoscalar modes in medium-mass to heavy nuclei [195]. The unexpected splitting of the isoscalar monopole mode (ISGMR) in ^{154}Sm was explained as due to the coupling between the $K = 0$ components of the monopole and quadrupole resonances. Only recently, this effect has been observed in the deformed light nuclei of ^{24}Mg [196] and ^{28}Si [197]. Measurements in inverse kinematics have become possible with the use of active targets [198]. At LNL the method could be used with a stable ^{20}Ne beam or the radioactive ^{26}Si beam at SPES. Significant cross sections, however, are only expected for beam energies beyond 50 AMeV.

4.2.3 Structure of neutron-rich medium-mass nuclei

Approaching the Island of Inversion at higher spins

In Islands of Inversion, across the nuclear chart, ground states of magic nuclei exhibit strong admixtures of intruder configurations from the next higher-lying shell. This results in deformed ground states and in the disappearance of canonical magic numbers. In the original Island of Inversion centered on ^{32}Mg, the origin of collectivity can be traced back to the mixing of multi-particle-multi-hole configurations with excitations of neutrons from the *sd*-shell orbitals to the *fp* shell [199–201]. Nuclei in the Island of Inversion are characterized by deformation as well as configuration mixing and thus the evolution of the single-particle properties is best studied outside of the Island of Inversion. Fusion–evaporation reactions are not ideal to populate neutron-rich nuclei with sizable cross sections, yet allow for the population of high-spin states [202]. A powerful alternative are multi-nucleon transfer reactions which can populate medium-high spin states. Beams of ^{22}Ne, ^{26}Mg, and ^{30}Si are ideally suited to probe the region from O to Si using the

AGATA γ-ray spectrometer, and PRISMA for channel selection and Q-value measurements. Gamma-ray angular distributions and correlations as well as lifetime measurements using Doppler-shift methods can be employed to extract angular momenta, branching ratios, and reduced transition probabilities. A large and consistent data set, spanning from stability to the borders of the Island of Inversion, and comparisons with state-of-the-art theoretical calculations will be used to track shape change, intruder orbitals, and multi-particle-multi-hole configurations and, thus, infer the underlying structures in the Island of Inversion itself.

Proton excitations and excited 0^+ states

Excited 0^+ states in nuclei are critical signatures indicating shape coexistence. Such 0^+ states are effectively populated and studied using two-particle transfer reactions such as (t, p) or (^{3}He,n). An alternative and very powerful probes are the (^{18}O,^{16}O) and (^{14}C,^{16}O), two-neutron (2n) [203, 204] two-proton (2p) [205] transfer reactions, respectively. Pioneering studies at Orsay employed this reaction to discover the first excited 0^+ state in ^{68}Ni through the selectivity of the reaction and the measured angular distributions of ^{16}O ejectiles, allowing the identification of the momentum transfer [205]. A key nucleus in the understanding of the interplay of spin-orbit, tensor, and central forces and the development of complex shape evolution at $N = 28$ is ^{46}Ar. While its level structure and neutron properties are well-described by shell-model calculations [206] the B(E2) value is not [207]. The (^{14}C,^{16}O) two-proton transfer reaction on a stable Ca targets is ideally suited to probe the proton hole structure of the Ar isotopes, discover unknown excited 0^+ states, and resolve the controversy around the structure of ^{46}Ar. At LNL, the development of a radioactive ^{14}C beam is planned, and the detector setups of AGATA and GRIT will be available in the coming years. With these, it will become possible to study the $2p - 2h$ proton states, search for shape coexisting 0^+ states and probe their structure through γ and conversion-electron spectroscopy, determine branching ratios and lifetimes, and thus extract E2 and E0 reduced transition strengths. The experimental technique is applicable to many cases across the nuclear chart and has a high potential to investigate elusive excited 0^+ states, also, for example, in ^{34}Si, ^{62}Fe, ^{74}Zn, or ^{80}Ge.

4.3 $N \sim Z$ nuclei and isospin symmetry breaking

$N \sim Z$ nuclei offer a richness of unique phenomena that allows understanding of specific properties of the nuclear interaction. With protons and neutrons occupying the same orbitals, proton–neutron correlations are enhanced, favouring the development of quadrupole deformation. Regarding pairing correlations, while like-nucleon pairing is of $T = 1$ character, proton–neutron pairs can be coupled to $T = 0$ and $T = 1$. The contribution of both modes of *np* pairing decreases rapidly moving away from the $N = Z$ line [208]. With exchanged numbers of protons and neutrons, mirror nuclei offer the possibility to extract information about nuclear structure properties and isospin symmetry breaking terms of the nuclear interaction. At LNL, with the advent of the GASP [209] γ-ray array in the early 90's, nuclei along the $N = Z$ line have been studied up to high spin. These studies continued with EUROBALL [210] and more recently with GALILEO [19]. The main properties studied along the $N = Z$ line have been the high-spin phenomena such as backbending, band termination, and shape coexistence in deformed nuclei, as well as isospin symmetry breaking through the measurement of excited states in mirror nuclei.

In this Chapter we discuss open questions that can be explored in the short and midterm at LNL. The first two regard nuclear collective properties, the third concerns tests of the isospin symmetry of the nuclear interaction, followed by a glance on the search of new physics.

4.3.1 Neutron-proton pairing

The nuclear pairing mechanism is a central topic in low-energy nuclear physics [211]. The dominant pairing in almost all known nuclei with $N > Z$ is that in which "superconducting" pairs of neutrons (*nn*) and protons (*pp*) couple to a state with angular momentum zero and isospin $T = 1$, known as isovector pairing. However, for nuclei with $N \sim Z$, neutrons and protons occupy the same single-particle orbits at their respective Fermi surfaces and Cooper pairs, consisting of a neutron and a proton (*np*), may form. These pairs may couple in either isovector ($T = 1$) or isoscalar ($T = 0$) modes, the latter being expected to dominate in $N \sim Z$ nuclei. In spite of the fact that there are convincing arguments for the existence of isovector *np* pairs, the existence of a correlated isoscalar *np* pair in condensate form, and the magnitude of such collective pairing remains a controversial and fascinating topic in nuclear structure physics [212].

The lack of experimental confirmation [212, 213] is mainly because the region of the nuclear landscape near the proton drip line, where such phenomena are expected to appear, is largely unreachable, and because the experimental observables are either inconclusive and/or complicated to interpret.

Two-neutron transfer reactions such as (p, t) and (t, p) have provided a unique tool to understand neutron pairing correlations in nuclei [189, 214]. Similarly, the transfer of an *np* pair from even–even to odd–odd self-conjugate nuclei provides a powerful tool to study *np* correlations in $N = Z$ nuclei [215, 216]. Some possible reactions are listed in Table 3. Among these the (p,^{3}He) or (^{3}He,p) reactions offer the advantage to study, in the same experiment, exclusive cross sections populating the lowest $T = 0$ and $T = 1$ states in the final nucleus. The corresponding ratio $\sigma(0^+)/\sigma(1^+)$ can provide a model-independent approach to quantify the nature of and interplay between isovector and isoscalar pairing [217]. This ratio plays the role of a Weisskopf unit for *np* pair transfers.

At LNL, on the short term, high-intensity $N = Z$ stable beams could be used to study the ^{36}Ar(p,^{3}He) and (^{3}He,p) reactions to complete the systematics of the *sd* shell. In the mid-term, radioactive beams of ^{46}V and ^{50}Mn, that could be produced at SPES

Table 3 Possible pair addition and removal reactions to study *np* correlations along the $N = Z$ line

Reaction	Change in isospin
(p,^{3}He); (^{3}He,p)	0, 1
(d,α); (α,d)	0
(α,^{6}Li); (^{6}Li,α)	0

from primary non-fissile targets (TiC, ZrGe,..), will provide a complementary probe as in these cases we start from odd–odd $T = 1$ ground states and populate $T = 0,\ 1$ final states in the even–even $N = Z$ nucleus.

Neutron-proton pairing is also related to α-like quartets in nuclei. Indeed, it was suggested [218, 219] that these can be described as bi-pairs of neutrons-protons. Up to now, the experimental investigation of α clusters in nuclei has mostly focused on excited states of α-conjugate nuclei close to the α thresholds. The α-like quartets, instead, would appear in the ground state of α-conjugate nuclei as a collective state. In the same line as for pairing, the cross-sections for α transfer from α-conjugate nuclei to the 0^+ ground state should be enhanced with respect to the ones to the first 0^+ state. The systematic for the α-transfer reaction (^{6}Li,d) over the *sd* shell shows an enhancement very similar to what is obtained from the two-nucleon transfer reaction (t,p). However, existing measurements are not consistent in terms of energy and reaction conditions calling for consistent re-measurements. At LNL, there is the opportunity to revisit the (^{6}Li,d) reaction to re-assess the quartet structure of nuclei in the *sd* shell as a reference baseline to understand this phenomenon beyond ^{40}Ca. Further studies with ^{56}Ni and ^{58}Cu radioactive beams delivered by SPES might be possible.

4.3.2 Quadrupole collectivity in $N \sim Z$ nuclei

The development of nuclear deformation is a key property, central to our understanding of the nuclear force. Along the $N = Z$ line quadrupole correlations are quite strong and, in most of the cases, govern the nuclear structure features. This gives rise to different nuclear shapes and their coexistence at similar excitation energies. The study of these properties in medium-mass $N = Z$ nuclei is not straightforward from both theoretical and experimental aspects. It has been shown that the development of quadrupole deformation in nuclei above ^{56}Ni involves multi-particle multi-hole excitations across the energy gaps determined by the magic numbers [220, 221]. This is the same mechanism at the origin of the so-called Islands of Inversion. Shell-model calculations are so far the most precise methods to describe spectroscopic properties. Their limitations arise when the model space and the number of valence nucleons to deal with become too large. While new methods are being developed to overcome these limitations [222], we can rely on the predictions based on symmetries, variants of the SU(3) [221]. Large deformation in $N = Z$ nuclei above ^{56}Ni develop between ^{72}Kr and ^{80}Zr, shape coexistence is predicted in ^{84}Mo, and prolate-oblate competition in ^{88}Ru and ^{92}Pd. With the exception of ^{72}Kr, in $N = Z$ nuclei with $64 < A < 80$ only the $B(E2 : 2^+ \rightarrow 0^+)$ has been measured so far. Lifetimes of excited states in $N \sim Z$ nuclei can be measured at LNL using stable beams in fusion–evaporation and multi-nucleon transfer reactions combining AGATA with NEDA or PRISMA with a plunger device, to access levels lifetimes.

4.3.3 Isospin-symmetry in isobaric multiplets: transition matrix elements

Isospin symmetry is one of the key concepts in modern nuclear physics [223] and tests of its predictions form an important part of the nuclear-structure programmes at the current and emerging accelerator facilities.

To date, most of these studies have largely focused on measuring the energy differences between analogue states in mirror nuclei and isobaric multiplets. These differences arising from electromagnetic and isospin-non conserving interactions [224–229]. A crucial next phase in the study of isospin physics in nuclei would be to move to precision tests of the isospin symmetry through spectroscopic methods that probe the isospin purity of *wave functions* across isobaric multiplets. For a set of $T \rightarrow T$ analogue EM transitions, a similar linear dependence on T_z is expected for the proton matrix element (proportional to the square root of the reduced EM transition probability):

$$M(T_z)_p = a + bT_z \tag{1}$$

Here, a and b contain the isoscalar and isovector matrix elements for that specific transition as well as coefficients that depend on T but not on T_z. Again, deviations from the linear behavior may indicate isospin-symmetry breaking and/or isospin mixing. This rule is difficult to test precisely due to the experimental challenges in performing such measurements in neutron-deficient nuclei. Hence, this presents a major challenge for the next decade. The most straightforward way to test this rule is through the study of a $T = 1$ triplet of nuclei, measuring the analogue $B(E2)$ strengths between the $T = 1, 0^+$ ground state and the $T = 1, 2^+$ first excited state. The linearity rule can be tested by fitting a quadratic expression of the form $M(T_z)_p = a + bT_z + cT_z^2$ and extracting the c coefficient, which should be zero in the limit of exact isospin symmetry. Analysis using all available current data (from ref. [230], updated) is shown in Fig. 9, where the ratio $c/|a|$ is plotted. There are two observations from this data. Firstly, the error bars are large (mostly $> 10\%$ of the total matrix element), hence, the test of the isospin rule is not, generally, very precise. Secondly, in the case

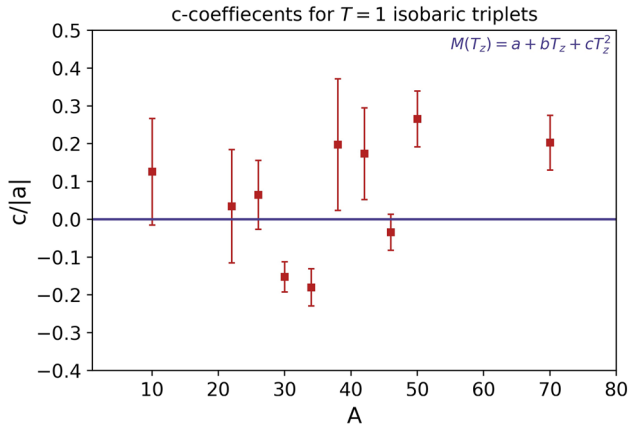

Fig. 9 The results of fitting a quadratic expression of the form $M(T_z) = a + bT_z + cT_z^2$ to the transition matrix elements measured in all three members of a $T = 1$ triplet. The measurement corresponds to the analogue $B(E2) \uparrow$ strengths between the $T = 1, 0^+$ ground state and the $T = 1, 2^+$ first excited state. A number of outlier cases are visible for which a non-null c parameter is estimated

of $A = 30$, 34, 50, 70, the deviation from the linearity rule appears to be significant. These await clarification from more precise spectroscopy that could be studied in LNL. In Fig. 9, the large error bars originate from uncertainties in the transition strengths for the $T_z = -1$, 0 members of the triplet and branching-ratio uncertainties in the odd–odd $N = Z$, $T_z = 0$ cases.

Specific isospin selection rules exist as well for electric dipole transitions, for which there is no isoscalar component. This implies that $T \rightarrow T$ $E1$ transitions in $N = Z$ nuclei should be forbidden, and also that $E1$ transitions should have identical strength in mirror nuclei. Again, deviations from these rules probe isospin mixing. These measurements are hampered by the potential for magnetic quadrupole $M2$ admixtures in the transitions in question. Precision lifetime measurements are required as well. The excellent in-beam γ-ray resolution of AGATA, in combination with enhanced $\gamma\gamma$ coincidence efficiency, and ability for angular distribution and polarisation measurements, represents an excellent opportunity to address 'isospin physics'. To keep systematic errors at a minimum, experiments should aim at measuring the relevant observables simultaneously across the full isospin multiplet of interest. They should be embedded in experimental campaigns with well-characterized set-ups, ensuring stable conditions for sufficiently long measurements. For most cases considered, combining AGATA with NEDA and a charged-particle array serves channel selection as well as event-by-event determination of recoil vectors. This knowledge can help to further reduce uncertainties in slowing down processes, when applying Doppler-shift based lifetime measurement techniques. Here, statistics should allow for $\gamma\gamma$ coincidences to avoid uncertainties from side-feeding. For a given case, AGATA plus PRISMA, including total kinetic energy cuts, might be a suitable alternative set-up.

4.3.4 Fundamental interactions in β decay around $N = Z$

The Standard Model (SM) has been a stronghold of particle physics for decades. It shows great success in the prediction of properties on the elementary particles and the mediators of the electroweak interaction. A crucial SM test using β decay is the unitarity test of the Cabibbo-Kobayashi-Maskawa (CKM) matrix. A non-unitarity of the matrix would imply the existence of hidden physics such as the existence of the fourth-generation quarks [231]. The unitarity can be tested through the examination of the square sum of the first column elements: ${V_{ud}}^2 + {V_{us}}^2 + {V_{ub}}^2$. Among the matrix elements, the up-down mixing element V_{ud} is critical, because the value and its uncertainty dominate the sum ($\mid V_{ud} \mid = 0.97370(25)$ [232]). Presently, the most precise value for V_{ud} comes from superallowed $0^+ \rightarrow 0^+$ nuclear β transitions for which the experimental parameters have been measured with increasing precision for many years. It was possible to reach a precision of few parts per 10^4 for the most favourite cases of superallowed decay from $T_z = -1$ isotopes (see, e.g., fig. 3 in [233]). Improving such high-precision measurements is very challenging and an alternative to the study of the superallowed decay of $T_z = -1$ nuclei is the measurement of the so-called 'mirror' β decay, between $T = 1/2$ states in mirror nuclei that can be used to extract another value for V_{ud}. These decays include both Gamow-Teller and Fermi transitions, and the measurement of the branching ratios with high precision is needed. A recent publication [234] reports the state-of-the-art, pointing to cases where the uncertainty in the branching ratios ranges from 0.1 to 1.2% (see figs. 2 and 3 in [234]). There will be the possibility for LNL to prepare the setup needed to improve the precision of the branching-ratio measurements for some key cases, exploiting synergies with the β-decay station in preparation for the SPES facility. With this facility it will be possible to measure the branching ratios in the decay of the isotopes ^{21}Na, ^{23}Mg, and ^{45}V, and the measurement of the lifetime of ^{25}Al, ^{29}P, and ^{41}Sc.

4.4 Shell evolution

The present mid-term plan for the study of shell evolution at LNL concentrates at first on the need to precisely define the observables linked to the concept of single-particle shell. The expected evolution of nuclear models in the next years is then presented, in particular pointing out the developments relevant to the future experimental studies with stable and exotic beams at LNL. The plan

then describes the measurements that are envisaged to build a comprehensive picture of shell evolution in exotic neutron-rich nuclei from mass A∼70 to mass A∼140, highlighting the beams required as well as the experimental setups needed.

4.4.1 Observables in shell evolution

Atomic nuclei are strongly-interacting two-components quantum mesoscopic systems whose complexity manifests itself through a rich phenomenology and the non-trivial way A-body observables evolve as a function of, e.g., the number of their constituents.

In this context, the role of any given theoretical scheme is to define and correlate, a priori, disparate experimental observables via a reduced set of building principles: a choice of appropriate effective degrees of freedom (e.g. point-like nucleons in so-called ab initio methods), evolving in a dedicated kinematical space (e.g. tensor product of reduced one-nucleon Hilbert spaces in the so-called valence-space shell model), on the basis of an appropriate kinematical or dynamical laws (time-independent or time-dependent Schrödinger's equations in quantal schemes), governed by their appropriate interactions (e.g. a Hamiltonian rooted into QCD through a specific power counting, in ab initio methods). By construction, any given theoretical scheme attempts to correctly correlate nuclear observables over a limited range of energies and nuclear systems, that shall not be necessarily the same for the various schemes under consideration in low-energy nuclear physics; i.e. each postulated theoretical scheme comes with its own intrinsic limited applicability domain. In this process, one wishes to further correlate the behaviour of *experimentally measurable observables* to a common theoretical construct denoted as *the nuclear shell structure*, the goal being to use a simple one-body quantity to provide a simplified picture of the inherent complexity displayed by actual A-body observables. While this makes the nuclear shell structure and its evolution, e.g., away from β stability, a topic of great current interest, two crucial features must be kept in mind when referring to it:

1. While effective single-particle energies (ESPE) making up the nuclear shell structure are unambiguously defined mathematically [235, 236], they constitute a purely theoretical construct and are thus not observable [237, 238], i.e. they only exist within the theory such that their actual values depend on characteristics of the theoretical scheme under consideration that do not however impact actual observables computed within that scheme. Whereas one must expect two different theoretical schemes to reproduce equally well experimental observables (as long as they fall within their respective applicability domains), one must not expect that the shell structure one wishes to correlate them with is the same within the two theoretical schemes. In other words, the simplified picture associated with the shell structure depends on the theoretical scheme used (even if it shall bare qualitative resemblance whenever the theoretical schemes are intrinsically close). This further implies that the evolution of the nuclear shell structure delivered through the study of various nuclei must, in principle, be based on the same, coherent, theoretical scheme.
2. Observables that most strongly correlate with ESPEs, within any given scheme, are cross sections and separation energies associated with one-nucleon addition and removal processes. Given that such spectroscopic data have seldom been accessed in stable nuclei (i) in both the addition and removal channels, (ii) over a large range of excitation energies and (iii) for states characterized by small cross sections [239], reaching more than a few final states via addition and removal experiments on unstable and very exotic nuclei constitutes a tremendous challenge. Because the computation of the nuclear shell structure within standard theoretical schemes (e.g. valence-space shell model, ab initio methods) can however be shown [240] to be sensitive, even in doubly closed-shell nuclei, (a) to states up to more than 10 MeV excitation energies in the main channel, (b) to (at least) the main state in the secondary channel and to states down to 1% spectroscopic strength, taking up this experimental challenge in the years to come is of prime importance to deliver the nuclear shell structure with a small enough theoretical uncertainty.

In conclusion, the study of shell evolution bears some interlaced experimental and theoretical caveats. One the one hand, the determination of energy centroids of effective single-particle energy distribution requires to measure even small nucleon pick-up and stripping cross sections to identify fragments which may imply non negligible shifts on the final energy centroid. On the other hand, ESPE are not an observable, but they acquire a quasi-observable within a given coherent theoretical framework for structure and reaction models. This coherence of the theoretical models employed is particularly relevant for the study of shell evolution on a range of nuclei.

In the following, the opportunites and plans for such detailed measurement at the stable and radioactive ion-beam facilities at LNL will be outlined.

4.4.2 Shell evolution with energy density functionals and related techniques

The underlying shell structure obtained from the nuclear interaction is clearly manifested in the properties of nuclei with an odd number of protons and/or neutrons. Therefore, the experimental study of these nuclei will help to determine how shells evolve in different regions of the nuclear chart. Nuclear energy density functionals (EDFs) such as Skyrme, Gogny and/or relativistic Lagrangians [241–244] have been designed to be universally applied once the specific form and parameters of the interaction are fixed. However, the study of bulk and spectroscopic nuclear properties at low excitation energy such as binding energies, radii, excitation energies and transition probabilities with EDFs is scarce for odd nuclei [245–249] or approximations like the equal filling

approximation (EFA) are routinely used [250–252]. The situation is even worse for EDFs that include beyond-mean-field (BMF) effects such as symmetry restoration and configuration mixing [253–255].

There are several technical problems that make these calculations more difficult and time-consuming than those for even–even systems. On the one hand, the most general mean-field transformation must be built with one-quasiparticle intrinsic states (blocking) that breaks the time-reversal symmetry. That means that the EDF solvers have to include time-odd fields [245, 248, 249, 256, 257]. On the other hand, this symmetry breaking normally implies the use of triaxial angular momentum restoration that is involved and computing-demanding [253–255, 258]. Finally, pathologies that may appear in the definition of BMF-EDFs constitute an additional difficulty [259–261].

Currently there are several codes that allow the study of properties of odd nuclei with mean-field EDFs with full blocking although their use has not been very extensive so far and their predictive power is limited. A first mean-field approach to the ground-state of odd-systems can be obtained with self-consistent blocking axial calculations. In such a case, the angular momentum of the state is approximated by the K-quantum number (the projection of the angular momentum along the z-axis of the intrinsic reference frame) of the blocked quasiparticle state.

Even though these results could give a first attempt to the description of the spectrum of odd systems, this approach lacks for many relevant beyond-mean-field effects, such as symmetry restorations and shape mixing, and cannot provide a quantitative reliable comparison with experimental data. Amongst the beyond-mean-field extensions, one of the most promising techniques is the so-called projected generator coordinate method (PGCM) that is based on the mixing of particle-number and angular momentum restored mean-field wave functions using Hamiltonians instead of EDFs [222, 262–266]. PGCM can provide both observables to be directly compared with experimental data (energies, radii and transition probabilities) and non-observable quantities, e.g., collective wave functions or effective single-particle energies. A lot of work is in progress to extend the applications of mean-field EDFs and PGCM techniques to odd-nuclei. Therefore, the experimental study of such systems will be a very suitable playground to validate these developments and a key tool to study the shell evolution.

4.4.3 Shell-evolution around the doubly-magic ^{78}Ni

Isotopes around ^{78}Ni are at the very edge of the present knowledge in nuclear shell structure. The $N = 50$ region has been the object of an intense research in the last years, with the first spectroscopic study of ^{78}Ni having been published recently [267]. The development of deformation around the $N = 50$ shell closure [267–269] as well as the reduction of the $N = 50$ shell gap [270, 271] when approaching ^{78}Ni have been studied with complementary experimental approaches. Indeed, the first spectroscopy of ^{78}Ni and ^{79}Cu has opened some questions. In ^{78}Ni, recent large-scale shell-model calculations predict an intruder structure close to and even lower than the first 2^+ state, which is already lying at a somehow low energy of 2.6 MeV [267]. Gamma-ray spectroscopy of ^{78}Ni has provided tentative evidence of intruder states [267]. In ^{79}Cu the first spectroscopy via proton-knockout has revealed a plethora of states around the ^{78}Ni 2^+ energy quite difficult to disentangle [272]. There was no sign of a low-lying proton $f_{7/2}$ strength coming from a $Z = 28$ core break, which is important for the ^{78}Ni 2^+ level energy [267, 269].

A first experimental approach would be the spectroscopy of the yrast states in $N = 50$ isotones. States up to 7–8 units of angular momentum can be populated with ^{208}Pb,^{238}U+^{9}Be fusion–fission reactions. Stable lead or uranium ALPI beams at 6–7 AMeV will impinge on a Be target at the centre of the AGATA-PRISMA setup, to measure the γ-ray decay of fission fragments identified event by event. One could measure states, in ^{80}Zn, representing a core-breaking excitation which has been used to define a $N = 50$ "spectroscopic" gap size through shell-model calculations. On the other hand, also the spectroscopy of the first excited yrast states in ^{79}Cu should be accessible, making it possible to study states coupled to the ^{78}Ni core excitations.

With the advent of radioactive beams from the SPES facility, neutron-rich nuclei around $N = 50$ can also be studied by means of β decay studies. The large Q value ($\gtrapprox$ 8–10 MeV) available for β decay in nuclei produced by SPES like $^{78-80}$Cu, $^{78-82}$Zn, $^{80-87}$Ga, $^{83-87}$Ge, $^{84-89}$As, $^{94-102}$Rb makes it possible to observe a significant Gamow-Teller strength (GT) in the β decay. These allowed decay proceed through "doorway states". i.e. states coupled to particle-hole excitations across the $N = 50$ core. As a result, the GT strength distribution becomes a sensitive probe of the correlations arising from intruder states close to ^{78}Ni [273, 274]. The decay spectroscopy requires the SPES Decay Station coupled to a neutron time-of-flight detector for β-delayed neutron spectroscopy, since the decreasing neutron-separation threshold in exotic nuclei implies that a significant part of the GT strength could lead to neutron emission from highly excited states in the daughter nuclei.

4.4.4 Characterization of the $N = 50$ shell closure

Characterizing the evolution of the N = 50 shell closure towards ^{78}Ni and the possible appearance of unexpected intruder states at rather low energy is essential if one aims at predicting the structure of nuclei further away from stability, including those involved during nucleosynthesis processes. While transfer reactions, such as (d,p) nucleon addition, were largely used to quantify precisely how valence orbitals evolves along isotonic chain in lighter regions, the N = 50 chain towards ^{78}Ni remains poorly studied. The distribution of single-particle strength for valence orbitals ($2d_{5/2}$, $3s_{1/2}$, $2d_{3/2}$, $1g_{7/2}$) in N = 51 nuclei is only studied in details for ^{91}Zr, ^{89}Sr, ^{87}Kr [275] still far from Z = 28. For the more exotic ^{85}Se and ^{83}Ge, only the ground and first excited states were

populated, by nucleon addition, for the first time in Oak Ridge in a pioneering experiment with rather limited statistics and excitation energy resolution [276].

SPES high intensity beams of ^{84}Se of ^{82}Ge ($\sim 10^5$ to 10^6 pps), combined with the state-of-the-art particle-γ detection setup GRIT+AGATA, will be ideally suited to reach a considerably higher resolving power and statistics to precisely extract, for the first time, a large fraction of the single-particle strength distributions in ^{85}Se and ^{83}Ge.

4.4.5 Shape coexistence

Shape coexistence in nuclei is a widespread feature that may occur in nearly all nuclei. It is associated with the fundamental tendency of nuclei to deform, if not in their ground states, in their excited states. The distinctive character of shape coexistence lies in the interplay between two opposing trends: shell and subshell closures have a stabilizing effect leading to sphericity, while residual interactions between protons and neutrons outside closed shells drive the nucleus to deformation. Valuable data in support of this idea are available, for example, in the region Z $\sim$ 40, N $\sim$ 60 (see e.g. ref [277]), which show that nuclei at, and close, to double-subshell gaps can exhibit shape coexistence via the suppression of ground-state collectivity. The main observables related to shape coexistence are the strength of the electric monopole transitions (E0) and of electric quadrupole (E2) and magnetic dipole (M1) transitions.

An exclusive contribution to clarify the configuration of low-energy states can be obtained from the analysis of their electric monopole (E0) decay [278, 279]. Precise measurements of the E0 strength required the use of electron spectrometers, as the newly developed SLICE [37].

As an example of the investigation of nuclear shape coexistence that can be performed via measurements of the electric monopole strength, we refer to the Sr isotope case, which can be populated via β-decay of the father Rb nuclei, produced at the SPES facility.

Another key observable related to shape coexistence is provided by reduced transition probabilities, which give information on the shape of the nucleus, allowing to study phenomena such as nuclear deformation and shape coexistence [277, 280]. The fast-timing technique is a powerful tool that provides access to nuclear lifetimes spanning a range going from few picoseconds to nanoseconds [281–283]. In recent years, new technologies such as state-of-the-art fast scintillator materials ($LaBr_3$:Ce, $CeBr_3$) and digital electronics are being exploited to obtain improved time resolutions [281, 284–287]. Such improvements allowed precise lifetime measurements, for instance in the mass regions A $\simeq$ 70,100–110,180 [288–291].

SPES non post-accelerated beams will provide the possibility of accessing key regions of the nuclear chart where shape coexistence phenomena are predicted, such as the region comprising Kr, Zr, Mo, Pd and Cd isotopes around mass A = 100, exploiting the resident β-DS decay station array equipped with $LaBr_3$:Ce detectors. The possible coupling of these detectors to the resident γ spectrometer GALILEO will further expand the use of fast-timing techniques at LNL.

4.4.6 Coulomb excitation for deformation and shape coexistence

Low-energy Coulomb excitation is one of the most well established experimental techniques used for studying the nuclear structure and, still to this day, one of the most widely employed. By carefully choosing the beam energy to guarantee the so-called *safe* condition [292] (typically a few AMeV), the nuclear interactions become negligible in the Coulomb-excitation scattering process and the observables of interest can be extracted in a model-independent way. The technique allows for determining reduced transition probabilities and spectroscopic quadrupole moments. Also, it is the only experimental technique allowing for the model-independent extraction of relative signs of E2 matrix elements, needed to link transitional and diagonal E2 matrix elements to the Hill-Wheeler parameters (β_2, γ) [292, 293], which identify any quadrupole shape. These unique features make low-energy Coulomb excitation a powerful tool to investigate phenomena such as shape coexistence, shape transitions, superdeformation, and octupole collectivity (see, for instance, refs. [294–296]). Very interesting and well beyond the scope of nuclear physics, are transitional nuclei, for which the octupole-deformation parameter β_3 [297] is sizable [296, 298–300], and [301]. These nuclei are predicted to enhance a CP-violating nuclear Schiff moment, e.g., see ref. [302] and references therein. Due to the vanishing small intensities of $E3$ transitions, when compared to dominant fast $E1$-decay paths, in general, a direct experimental determination of the electric-octupole moment requires the measurement of excitation paths using the technique of safe Coulomb-excitation (Coulex).

SPES will offer advantages in terms of beam energy and intensity for Coulomb excitation in key nuclei with respect to previous experiments at other ISOL facilities. Examples of isotopes that could be further investigated with this technique in the near future at LNL are neutron-rich Zn and Sn isotopes previously studied at ISOLDE and HRIBF (see, for instance, refs. [303, 304]). In addition, the measurement of spectroscopic quadrupole moments and, possibly, Hill-Wheeler parameters would directly probe the collective character of these isotopes, which is also relevant for r-process calculations [305–307]. It is also clear that from the expected high-energy and high-intensity SPES beams close to ^{78}Ni and ^{132}Sn, several nuclei in these regions of the nuclide chart will be studied with Coulomb excitation for the very first time. Other region of interest for octupole deformation will be also accessible, for example the region of Ba nuclei, with much larger statistics than presently available [299].

4.4.7 Nuclear deformation around $N = 60$

When going to deformed or shape-coexisting systems, nucleon transfer reactions are still extremely useful, although more challenging to perform and interpret. A first illustration is a recent study of the ^{94,95,96}Sr(d,p) reactions [308, 309] before the N = 60 shape transition, in which nucleon transfer region provided additional insight on the microscopic nature of coexisting configurations. At SPES, beams of ^{94,95,96}Kr,^{96,97,98}Sr should be produced with high intensities and represent good candidates to investigate this transfer technique below Zr (Z = 40), in inverse kinematics. This would allow to better characterize how proton vacancies impact neutron configurations and consequently affect this transitional phenomenon. The combined use of direct nucleon transfer to study single-particle configurations and the above-mentioned Coulomb excitation studies to precisely characterize collectivity represents the optimal strategy to firmly enhance our microscopic understanding of the structural mechanism at play in this sudden phase/shape transition.

4.4.8 Shell-evolution around the doubly-magic ^{132}Sn

The region around the doubly-magic ^{132}Sn has been the object of many studies to probe both the neutron and proton shell structure at the $N = 82$ and $Z = 50$ shell closures. Generally, nuclei around doubly closed shells play a crucial role in establishing the two-body matrix elements of the effective nuclear interactions [310]. As described in Sect. 4.1, ab initio methods start to be applied also to this relatively heavy nuclei [152, 163], making it possible to compare such predictions to spectroscopic data from direct transfer reactions. The large angular momentum of the nuclear orbitals in this region ($\ell = 3, 5, 6$) suggests the use of neutron adding reactions with heavier target nuclei like (^{4}He,^{3}He), (^{13}C,^{12}C) and cluster transfer on weakly-bound ^{7}Li targets [311], together with the more standard (d,p) reactions [312, 313]. In this context, of particular interest are one-proton-valence nuclei of Sb, with A = 127–134, and two-proton-valence nuclei of Te, with A = 129–135. For example, in the case of the ^{132}Sb nucleus (one-proton-particle, one-neutron-hole with respect to the ^{132}Sn core), the level structure at low excitation energies arises from 1p-1 h couplings involving $1g_{7/2}$, $2d_{5/2}$, and 1 $h_{11/2}$ proton particles, and $3s_{1/2}$, $2d_{3/2}$, and $1h_{11/2}$ neutron holes. Most of the 1p-1 h states involving the $g_{7/2}$ proton and $d_{3/2}$ neutron hole have been tentatively located, while the information about other multiplets is largely missing. The one-proton, one-neutron nucleus ^{134}Sb is not well known either. We note that one-nucleon valence systems also play a key role in understanding complex excitations arising from the coupling to the excited ^{132}Sn core [314].

Considering the SPES beam intensities and energies of re-accelerated beams around ^{132}Sn, reactions envisaged are the neutron adding transfers $^{132-134}$Sn(d,p; ^{4}He,^{3}He;^{13}C,^{12}C)$^{133-135}$Sn. They can probe the neutron $1f_{7/2}$, $2p_{3/2}$, $2p_{1/2}$, $0h_{9/2}$, $1f_{5/2}$, $0i_{13/2}$ shells beyond $N = 82$. Proton stripping reactions, like ^{132}Sn(^{3}H,^{4}He)^{131}In, and proton adding transfers, like ^{132}Sn(^{3}He,d)^{133}Sb, can instead help to understand the shell evolution both below and above $Z = 82$. These reactions will exploit the unprecedented efficiency and granularity of the AGATA-GRIT setup. The use of exotic beams with intensities as low as 10^4pps implies the need of dense helium targets, at least 10^{20} at/cm^2, to have a sufficient luminosity for direct reactions with cross sections of $\sim$1 mbarn. The CTADIR cryogenic target, being built at LNL and financed by the PRIN2017 call for funding, will allow the use of a 4 mm thick ^{3,4}He target kept at a temperature of 9 K by a cryocooler with up to 10^{21} atoms/cm^2. The target is designed to be compatible with the AGATA-GRIT setup.

4.5 Deformation and collective modes

Studying the emergence of collective behaviour in atomic nuclei allows to address the more general investigation of complex many-body systems, that could manifest astonishing simplicities and regularities. One of the best examples of collective modes in nuclei is the Isovector Electric Giant Dipole Resonance (IVGDR), interpreted as an oscillation of all the neutrons against all the protons (see Fig. 10). This phenomenon, and its rather simple patterns, has been extensively used to extract valuable information focusing on both zero and finite temperature [194, 315]. However, there are aspects which are still subject of modern large-impact research. They concern, for example, the understanding of the IVGDR evolution as a function of Isospin (e.g. in exotic neutron-rich nuclei) and the study of the low-lying electric dipole strength (Pygmy Dipole Resonance) [316, 317]. An important feature of the IVGDR is also the dependence of its properties on the nuclear shape, which makes it a good tool for the studies of nuclear deformation [318–321]. In the following, a list of physics cases will be presented. They represent interesting possibilities to advance our understanding of nuclear structure by means of specific gamma-ray spectroscopy studies. These experiments can be performed using accelerator facilities and instruments that are presently available, or will be available in the mid-term, at LNL. Experiments to be performed with SPES radioactive neutron-rich beams are highlighted, while stressing the relevance that experiments using stable beams still have.

4.5.1 Selected theoretical methods

The random phase approximation (RPA) and the quasiparticle RPA (QRPA) are well known and largely applied microscopic methods to describe nuclear excitations [323]. Their main advantage, in comparison to other nuclear structure models, is that large single-particle spaces can be used, allowing thus for a full description of the total excitation strength and the corresponding energy

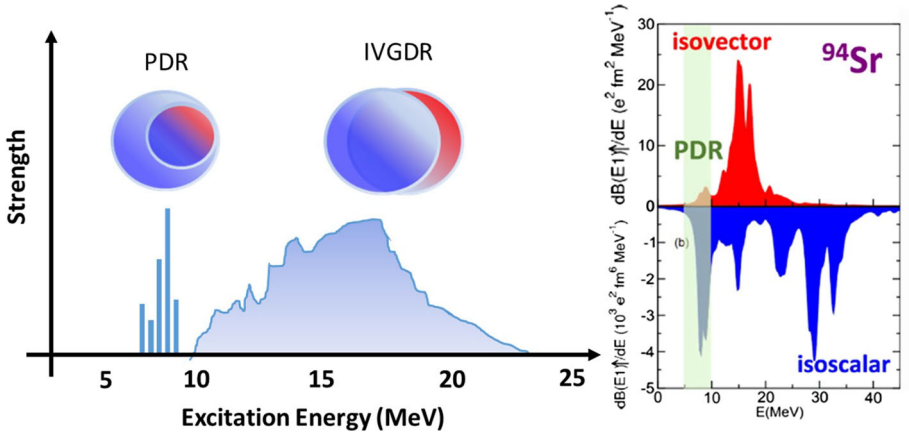

Fig. 10 Left panel: schematic drawing of the PDR and IVGDR modes overlaid in the electric-dipole excitation spectrum of a nucleus. Next to the peaks there are two sketches representing their associated macroscopic interpretations. Right panel: RPA calculations of the strength distributions of the unstable nucleus ^{94}Sr [322], showing the isovector (top) and isoscalar (bottom) responses. A clear increase is seen in the 5–10 MeV PDR energy region (marked in green)

weighted sum rules. In the RPA and QRPA, excited states are approximated by a linear superposition of one-particle one-hole and two-quasiparticle excitations, respectively, neglecting higher order configurations of the many-particle many-hole type. This picture has been shown to successfully describe the Giant Resonances. Extensions, such as the Particle Vibration Coupling (PVC) [324], the Second RPA (SRPA) [325], the Quasiparticle Time Blocking Approximation [326] or the Quasiparticle Phonon Model [327], aim at describing the spreading widths of collective excitations and their fragmentation, due to the coupling to more complex states, like 2p-2 h or 4-quasiparticle configurations. In order to support the experimental activities proposed in the present manuscript, a QRPA code based on the self-consistent solution of the Skyrme-Hartree-Fock plus BCS equations has become recently available to the community [328]. Further developments to improve the treatment of pairing within the Bogoliubov approximation are envisaged within the time scale of the mid term plan (see, e.g., ref. [329]). PVC codes could also become available [330].

4.5.2 Pygmy resonances

In recent years the study of the low-energy electric dipole response in nuclei attracted strong interest. This is mainly associated to the phenomenon of the Pygmy Dipole Resonance (PDR) [316, 317]: the observation of the systematic presence of resonance-like structures at energies around the nucleon emission threshold in the excitation spectra of neutron-rich nuclei. A simple interpretation describes this phenomenon as related to a new collective mode, originating from the oscillation of the N = Z core against the neutron skin of neutron-rich nuclei (see Fig. 10), but this is still under debate. Independently on the success of such particular description, these experimental studies are a very good testing ground for the problem of emergence of collectivity in nuclear structure. It was shown, in fact, already long time ago, that the inclusion of the PDR in the calculations of neutron-capture cross sections results in a better reproduction of the experimental data [331]. More recently, growing interest was prompted by theoretical works showing the possible impact of the PDR also beyond nuclear structure. For example, a collective mode involving the presence of the neutron skin, would allow to extract information on its thickness, which is determined by the symmetry energy of the equation of state (EOS) and directly linked to its parameters [332–334]. This has implications on the description of relevant astrophysics objects, like neutron stars. Experimental data on the PDR in neutron-rich exotic nuclei are still scarce. For this reason, measurements that can be performed with SPES radioactive beams are a great scientific opportunity to extend the systematics obtained with $(\alpha,\alpha'\gamma)$ reactions on stable target nuclei [316]. To study the PDR in radioactive nuclei, the experiments must be performed in inverse kinematics, requiring a target made of ^{4}He (or ^{3}He) with sufficiently high density. The CTADIR cryogenic target [113] will complement an experimental setup composed by AGATA [9] and the GRIT advanced silicon array [335], for the detection of the scattered particles. The additional presence of a highly efficient scintillator array (like PARIS [11, 336]) would allow to increase even further the experimental sensitivity of the setup for in-beam high-resolution γ spectroscopy studies. Inelastic scattering experiments can be realized in inverse kinematics to study the structure of unstable nuclei, such as ^{94}Sr and ^{132}Sn. In particular, for the case of ^{94}Sr, calculations [322] show that the cross section for the population of PDR states in these experimental conditions is sizable (see right panel of Fig. 10). It has to be said that for the case of ^{132}Sn, published data already exist [337]. However, the experimental conditions were completely different than those at SPES (i. e., relativistic Coulomb excitation with exotic beams at GSI). While the cross section for the population of the PDR states at these extremely high energies is much larger, the increased sensitivity brought to the LNL setup by the availability of AGATA, and the dominant role of the nuclear interaction at SPES energies, give the possibility to extract complementary nuclear structure information. We note that not only the 1^- PDR states will be populated, but also states of other multipolarity. This means that the same experiments would allow to study at the same time also the phenomenon of the Pygmy Quadrupole Resonance [338]. As stated in [339], one thing that became clear in the study of the phenomenon of the PDR is the need of a sort of "multimessanger approach", meaning that information on the structure of the PDR can be obtained populating the same states with different, complementary, nuclear reactions (thus having different population cross sections, see e.g. also [340]). In this view, for example, nucleon transfer reactions can be useful to probe the single particle nature of PDR states, as already demonstrated

in [341]. Some stable nuclei (noble gasses, for example), rarely studied in the past on this respect, can be accessed with experiments in inverse kinematics.

Another recent question around the PDR regards whether this type of excitation survives in nuclei at finite temperature. This issue is of basic relevance for astrophysical processes that mostly take place in a finite temperature environment. Predictions [342–345] indicate the presence of PDR states at finite temperature and even an increase in strength with temperature, but no measurements are available so far. In addition, no predictions combining thermal fluctuations and spin effects to the intrinsic dipole response at finite temperature are available. To search for an experimental signal of the PDR at finite temperature the predicted difference between a chain of nuclei should be measured as function of the increasing number of neutrons. In a first step one could use fusion evaporation reactions and observe the subsequent statistical γ-decay yield. Indeed, the comparison of different reactions could provide a way to entangle the features of the pygmy strength with temperature.

Finally, PDR states can be studied also in decay spectroscopy measurements [346]. SPES has a dedicated β-decay station that has been built to perform this kind of experiments, also using non re-accelerated beams [346, 347]. Beta decay represents a further experimental probe, which allows the population of two-particle two-hole configurations, not reached by inelastic scattering experiments. Examples of possible nuclei to be studied with this method can be found in [346].

4.5.3 Jacobi shape transition

The Jacobi shape transition is a phenomenon consisting in an abrupt change, as a function of angular momentum, of the nucleus shape from oblate, through tri-axial, to more and more elongated shapes. Its existence is predicted to occur for many nuclei at high angular momenta [318, 348, 349] in the region of highest possible deformations of the nucleus before it fissions. So far, this phenomenon was observed only in the light mass nuclei (A$\sim$40) [318–321]. Another region, where very extreme spins can be reached, corresponds to 90<A<140, as here the limiting angular momentum for fission process is very high. Stable beams at LNL can therefore be used to investigate the shape evolution of hot nuclei in the A$\sim$100 and A$\sim$130 mass regions, at extreme angular momenta, via the measurement of high-energy γ rays from the GDR decay in coincidence with light charged particles and discrete transitions in evaporation residues, using AGATA [9] coupled to PARIS [11, 336], and EUCLIDES [21] silicon particle detectors. The research on the Jacobi shape transition was proposed for nuclei selected on the basis of calculations of the total energy surfaces, as a function of quadrupole deformation parameters β and γ, for increasing spin with the Lublin-Strasbourg Drop (LSD) model [349]. In the mass region A$\sim$100, the Jacobi shape transition can be studied in the ^{96}Mo nucleus using a ^{48}Ca beam at 250 MeV energy impinging on a ^{48}Ti target, leading to the ^{96}Mo compound nucleus at 120 MeV excitation energy and with maximum angular momentum of 80 $\hbar$. Nuclei with heavier masses could also be populated in a similar manner, for example ^{130}Ba and ^{142}La. To study the Jacobi shape transition, the high-energy γ rays from the GDR decay will be measured with the use of PARIS detectors. The experimental selection of events corresponding to high angular momenta will be possible by gating on multiplicity, using PARIS as a multiplicity filter, or choosing particular decay channels, especially those with one alpha-particle emission (in case of ^{98}Mo) detected with use of EUCLIDES. The low spin gamma transitions in the final reaction products, measured in coincidence with AGATA, will help to determine the residue by the coincidence gating on discrete γ-ray transitions.

4.5.4 Gamma decay from Giant Quadrupole Resonance excitation

Despite the Giant Quadrupole Resonances (GQRs) have been widely studied in the past, experimental data on their gamma decay are extremely scarce. This is mainly due to the experimental difficulties originated by the small gamma branching, which is obscured by the strongly competing channel of neutron emission. However, performing such experiments is very appealing due to the unique features and illuminating features associated with the detection of the electromagnetic decay. Experiments of this kind were recently performed at CCB Krakow [350], following the pioneering work of J. Beene and collaborators [351] (done in this case with the ^{17}O nucleus as GR exciting probe). Recent theoretical work has also been done [352], showing the importance of obtaining these kind of experimental data. In the mid term it will be available at LNL an experimental setup made of the composite system of AGATA coupled with a scintillation detector array like PARIS [11, 336] or HECTOR+ [353], in order to guaranty the necessary efficiency at high energy. The reaction used would be inelastic scattering of ^{17}O at 20 AMeV bombarding energy to study the gamma decay of the GQR populated in stable nuclei of various masses (e.g. ^{40}Ca). In addition, a silicon detector array would be needed to detect the inelastically scattered ^{17}O ions and eventually also the charged particles emitted following the GR decay (allowing to study also other GR decays in addition to the gamma type). The proposed studies will be complementary to that carried out at CCB IFJ PAN with the use of proton beam [350].

4.5.5 Isospin mixing

The concept of Isospin was introduced by Heisenberg in 1932 and it is an extremely useful tool to describe and predict the structure of nuclei, exploiting the fact that the interactions among nucleons are to a large extent independent from the considered particles being protons or neutrons (see also Sect. 4.3). However, Isospin is not a perfect symmetry. It is broken, in the first instance, by

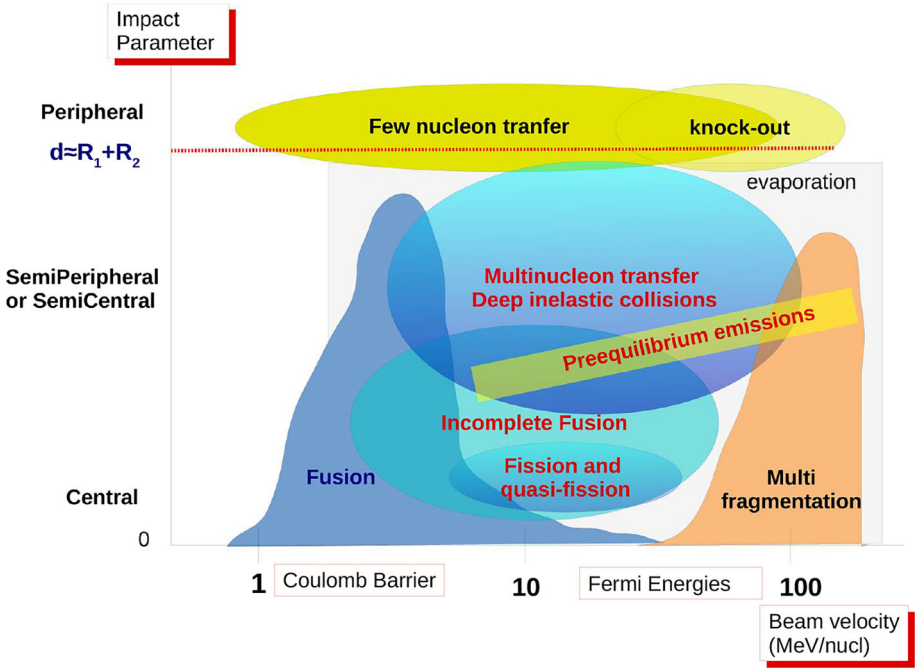

Fig. 11 Schematic view of reaction mechanism phenomenology at Coulomb and Fermi energies. The horizontal axis ideally represents the energy of the projectile, expressed in MeV/u, while the vertical axis indicates the semi-classical impact parameter. Each cloud schematically indicates the energy and impact parameter region where a given reaction mechanism dominates. Semi-transparent green and grey squares are unavoidable sources of background. LNL energies range from deep-sub-Coulomb energies up to the onset of multi-fragmentation phenomena

the Coulomb force. This causes the mixing. Significant effort was made to quantify the Isospin mixing for nuclei in different mass regions [225, 354, 355]. In particular, for studying Isospin symmetry breaking in electric dipole (E1) transitions, the giant dipole resonance mode (GDR), where approximately all the electric dipole harmonic oscillator strength is concentrated, is a favourable case for searching for small effects in the violation of the associated selection rule [356–358]. It was pointed out that these studies have also consequences that go beyond nuclear structure. In particular, one of the (small) corrections to the first term of the Cabibbo-Kobayshi-Maskawa (CKM) matrix V_{ud} value, actually depends on the Isospin mixing [359, 360]. These kind of experiments are performed using fusion evaporation reactions. The main requirement from the point of view of the experimental setup is to have a combination of an highly efficient system for the detection of gamma rays in the range up to 20 MeV and a high resolution gamma spectrometer to detect discrete, lower energy, lines (thus allowing to identify the residue nuclei of the fusion evaporation reactions). An array of large volume scintillators like PARIS or HECTOR+ [353], coupled with a high resolution spectrometer as AGATA would perfectly fit the experimental needs.

5 Nuclear reactions and dynamics

Section 4 has focused on experiments to probe the fine details of the nuclear structure which are related to the properties of a specific nuclear system. In this section we discuss the interaction between colliding nuclei by studying the dynamical evolution of nuclear reactions. The proper description of such evolving systems depends directly on our basic knowledge of the nuclear potential and it is linked to the nucleon–nucleon potential emerging from the residual strong interaction. A detailed knowledge of the reaction mechanisms is also necessary to correctly interpret the results in experiments attempting to probe nuclear structure aspects and vice-versa. Nuclear reactions, indeed, are a a powerful tool to produce nuclei in conditions away from the ground state, providing access to excited nuclear levels, and it is well known that the interplay between nuclear structure and reaction dynamics is a key ingredient for a proper interpretation of the experimental results. Moreover, at higher energies, the study of reaction dynamics and thermodynamics is crucial to constrain the Equation of State of nuclear matter.

In this framework, LNL is the ideal playground infrastructure to probe dynamical aspects of nuclear systems and nuclear reactions at low energies (i.e. $E_{beam} \leq 15 - 20$ MeV/u). In this energy regime, several dynamical processes can influence the outcome of a nuclear reaction, which is made more complex by the existence of a strong interplay with the structure of nuclei involved in the collision. Figure 11 schematically depicts the various reaction mechanisms that usually occur at low-to-medium incident energies. On a qualitative point of view, but useful to illustrate the main topics that are of interest for the investigations proposed in this section, the reaction mechanism is mainly affected by the velocity of the beam (i.e. its kinetic energy per unit mass) and the semi-classical centrality of the collision (i.e. its impact parameter). Figure 11 describes this point by using a centrality (vertical axis) and energy (horizontal axis) plane. In this schematic view, for the sake of clarity, we avoided representing other crucial parameters of the collision (such as size, charge and isospin of the entrance channel, as well as the structure of entrance and exit channels). Each cloud indicates the impact parameter and energy region where a given reaction mechanism dominates, while the green and grey squares

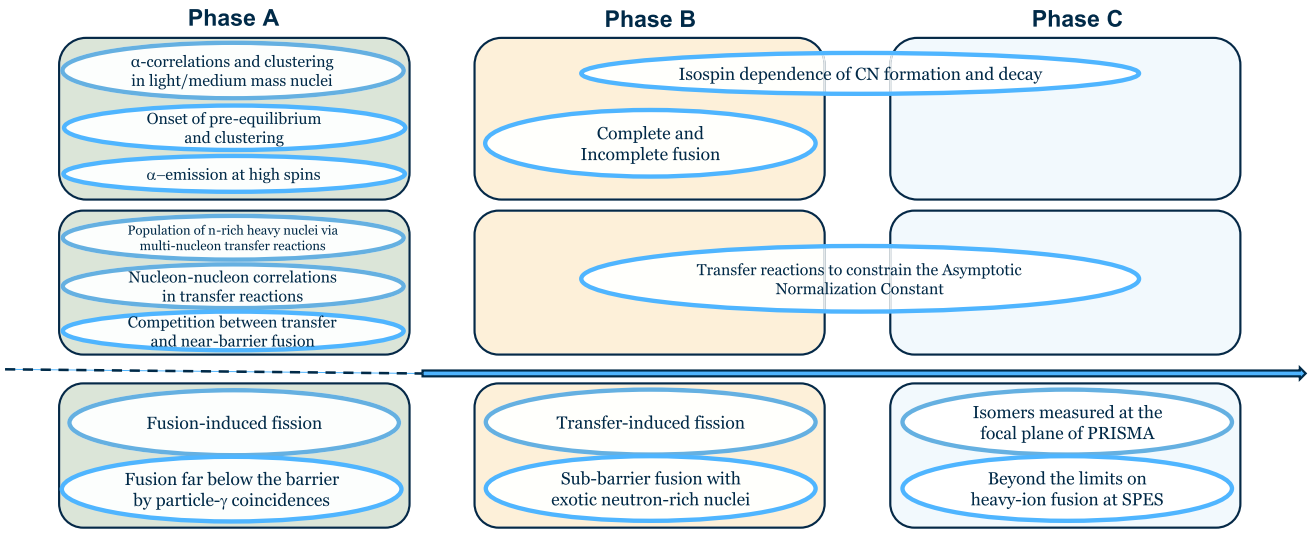

Fig. 12 Summary of the nuclear reactions studies that will be performed at LNL in the next future, sorted according to the time phase

Table 4 Summary of key topics on nuclear reactions and dynamics that will be addressed at LNL in the mid term future. The activities are sorted according to the working group discussing the proposal: (i) dissipative colisions and pre-equilibrium emissions; (ii) transfer reactions; (iii) fission and sub-barrier fusion. The three phases represent the readiness of the experimental campaigns

Tag	Description	Reactions/beams	Phase
LNL-RD-FU-a0	α-correlations and clustering in light/medium mass nuclei	$^{16-18}$O at 10 MeV/u	A
LNL-RD-FU-a1	Onset of pre-equilibrium and clustering	$^{16-18}$O, ^{22}Ne at 18–20 MeV/u, exotic Sn and Rb isotopes	A
LNL-RD-FU-a2	α emission at high spins	Ti, Ni at 10 MeV/u	A
LNL-RD-FU-b0	Complete and Incomplete Fusion		B
LNL-RD-FU-b1	Isospin dependence of CN formation and decay	^{88}Kr and ^{94}Kr at 10 MeV/u on $^{40-48}$Ca	B-C
LNL-RD-TR-a0	Population of n-rich heavy nuclei via multi-nucleon transfer reactions	Beams: ^{48}Ca, ^{94}Rb, $^{124-132}$Sn, $^{136-144}$Xe, ^{208}Pb. Targets: ^{48}Ca, ^{124}Sn, ^{208}Pb	A
LNL-RD-TR-a1	Nucleon–nucleon correlations in transfer reactions	^{88}Sr+^{144}Sm, ^{48}Ca+^{208}Pb, ^{40}Ca+^{132}Sn, ^{60}Ni+^{116}Sn	A
LNL-RD-TR-a2	Competition between transfer and near-barrier fusion	^{58,69,70}Ni+^{124}Sn	A
LNL-RD-TR-b0	Transfer reactions to constrain the Asymptotic Normalization Constant	^{7}Li(d,p)^{8}Li, ^{7}Be(d,n)^{8}B, ^{16}O(^{3}He,d)^{17}F @ 10 MeV/u	B-C
LNL-RD-FF-a0	Fusion-induced fission	Pb beam	A
LNL-RD-FF-b0	Transfer-induced fission	^{238}U beam	B
LNL-RD-FF-c0	Isomers measured at the focal plane of PRISMA		C
LNL-RD-FF-a1	Fusion far below the barrier by particle-γ coincidences	^{16}O, ^{19}F,^{12}C,^{13}C beams on light targets	A
LNL-RD-FF-b1	Sub-barrier fusion with exotic neutron-rich nuclei	^{96}Sr,^{94}Kr beams on ^{40}Ca,^{28}Si	B
LNL-RD-FF-c1	Beyond the limits on heavy-ion fusion at SPES	$^{24-26}$Al beams on ^{12}C,^{19}F,^{26}Mg	C

represent unavoidable competing processes. The following paragraphs describe the state of the art and the future plans for the study of these mechanisms. The topics have been mainly arranged according to the experimental techniques used and include the study of: dissipative collisions and pre-equilibrium emissions (WG1); transfer processes and particle spectroscopy (WG2); fission and sub-barrier fusion (WG3). The physics cases that are summarized in Table 4 and reported in Fig. 12.

5.1 Dissipative collisions and pre-equilibrium emissions

5.1.1 Fusion reactions and compound nucleus decay

Fusion reactions above the Coulomb barrier have been the subject of intense experimental campaigns, especially during the ′70s and the ′90s of the past century [361–365], providing data in hundreds of systems and collisions [366, 367]. A detailed analysis of the systematic trends shows that the fusion cross section has a different behaviour dependent on the energy regimes, which can be described by a number of models based on several phenomenological approaches [361, 368–373]. Those can be microscopical (as TDHF, see [374, 375]), molecular dynamics (see [376, 377]), or macroscopical (such as critical distance models, based on the occurrence of entrance channel effects [378, 379] or more basic approaches based on the liquid drop model [380]).

Recently, state-of-the-art artificial intelligence approaches based on a hybridization of genetic programming and artificial neural networks [381–383] have been successfully adopted to model the fusion cross section, exploiting a large number of collision systems [384]. These techniques are particularly interesting as they allow to derive, in a completely data-driven way, a mathematical expression for the description of experimental data, even in presence of particularly complicated problems. In addition to these aspects, the underlying methods also allow to suitably select the variables needed to predict the output (see e.g. [385–387]). This is extremely relevant for the modeling of nuclear physics data, as it allows to effectively probe correlations between nuclear variables and to drive theories towards the description of nuclear properties. The analytical model derived in Ref. [384] had a discrete success in predicting the cross section of the fusion between light-to-medium mass nuclei above the Coulomb barrier. A detailed analysis of the new model in the high energy region ($E_{beam} \approx 5 - 10$ MeV/u) shows the presence of large discrepancies for several collision systems, which were also evidenced in other recent studies [373].

The aforementioned discrepancies clearly demand for further experimental campaigns to investigate the complete fusion cross section at high energies. However, these investigations are made particularly complex by the underlying mechanisms. In fact, while at lower energy (for medium-mass systems, like those considered in ref. [373]) the dominant reaction mechanism is that of the complete fusion, at energies over a few MeV/u the complete fusion is hindered and incomplete processes become dominant. The emission of few particles before thermalization, known as out-of-equilibrium emission, for example, can contaminate fusion–evaporation data. These phenomena are possibly enhanced by the occurrence of clustering [388], which have a strong interplay with the formation and decay of hot nuclear states. On the other hand, quasi-fission mechanisms, in which few nucleons are exchanged between projectile and target without the formation of a thermally equilibrated compound nucleus, also gain importance at increasing energies, and increasing masses of the reaction partners. The latter are, moreover, particularly difficult to disentangle from fusion–fission mechanisms, which instead involve the formation and decay of a a fully equilibrated compound nucleus. It is therefore clear that a solid description of these competing mechanisms is mandatory to clarify the full picture. The following paragraphs summarize the open questions that will be subject of studies in the medium term future at LNL.

Complete and incomplete fusion (LNL-RD-FU-b0)

Absolute fusion cross-section measurements can be effectively exploited in the study of nuclear properties but particular care has to be put in understanding the reaction mechanism. Indeed, open questions on the correct values of the fusion cross sections close to its maximum are still present, even for reactions induced by stable nuclei. Moreover, measurements involving Radioactive Ion Beams (RIB) can highlight exotic nuclear properties, such as the presence of halo nuclei.

The collision of heavy ions can lead to incomplete fusion where projectile and target exchange few nucleons but never form a compound nucleus. This process, called *quasi-fission* is faster then the complete fusion leading to fission (fusion–fission), but final products are similar to the fission fragments. While fusion–fission is ruled by the thermodynamics of the compound system and by nuclear structure properties, quasi-fission is mainly a dynamical process that mixes with the complete fusion cross section, possibly altering the outcome of the measurement. A possible way to identify quasi-fission phenomena has been recently proposed [389]: the idea is based on the exchange of nucleons between the partners of a di-nuclear system, which tends to equalize their masses, and involves the measurement of the mass distribution for several angles. Mass-angle distributions should be linked to the lifetime of the process, which is rather short for quasi-fission mechanisms and longer for fully equilibrated systems.

Traditional fusion cross-section experiments are performed using thin targets and telescope detectors that cover only a limited portion of the full solid angle. As a consequence, to extract the fusion cross section the integration of the angle and energy distribution of the detected products is mandatory. Eventually, in order to build the excitation function the beam energy should be changed several times. Such issues can be overcome exploiting an active target for fusion cross section measurement [176]. Moreover, the isovector giant dipole resonance (IVGDR) represents a promising observable to describe the collective behavior of the composite system on its way to fusion. The IVGDR is, indeed, a collective excitation mode of the nucleus in which protons and neutrons are moving out of phase. According to the Brink-Axel hypothesis, the properties of the IVGDR are the same, whether the IVGDR is built on the ground state or on an excited state. Applying this hypothesis to highly excited compound nuclei formed in fusion reactions, the IVGDR could help answering questions related to the deformation and to the fission dynamics. In addition, this approach is particularly interesting for very high masses since nuclear structure data on super-heavy nuclei (SHN) are very scarce and generally limited to the low excitation energies due to the low production cross sections and to competing processes. To characterize the IVGDR in SHN and get hint on the temperature at which the CN is formed, we plan to extract the pre-fission γ-ray energy spectra

as well as the γ angular correlations with respect to the fission axis by applying the differential technique and two bombarding energies [390]. It is proposed to simultaneously measure the high-energy γ decay with the PARIS array [336] and, in coincidence, the fragments from binary reactions with the two-arm of a TOF spectrometer based on the CORSET project [391] already available at LNL. Such type of measurements recently proved to allow for a better understanding of the reaction mechanism [392, 393].

Isospin dependence of compound nucleus formation and decay (LNL-RD-FU-b1)

The isospin content of a compound nucleus is expected to play a crucial role in its formation and in the competition among the various de-excitation channels like Fusion–Evaporation and Fission-Like processes, thus providing information about fundamental nuclear quantities such as level density and fission barrier. For example, the level density parameter plays a key role in the thermal properties (entropy) of excited nuclei [394–396]. It is also related to the effective mass of nucleons in the nuclear medium, a property of the effective mean-field interaction that is sensitive to the neutron-proton composition of nuclei. In addition, the fission barriers depend clearly on the symmetry energy that is weakly constrained by existing data [397, 398], specifically in the nuclear surface region.

Novel information on these nuclear properties can be gained from the variation of the fusion cross section across long isotopic chains of compound nuclei, extending from the neutron-rich to neutron-poor side, all produced with comparable excitation energies and angular momenta. Examples of such experimental campaigns are available [399–401] and have shown that the neutron richness of the projectiles seems to discourage the formation of a compound nucleus.

The key observables are the reaction cross-sections as well as multiplicities, angular, mass, momentum distributions for the various emitted species (Light Charge Particles, Intermediate Mass Fragments, heavy products and Evaporation Residues). The choice of inverse kinematics can be advantageous in such measurements since the method boosts and concentrates reaction products in the forward direction.

At LNL, SPES will offer the opportunity to produce excited nuclei in unexplored regions of the nuclear landscape, allowing also to study spin and internal degrees of freedom; besides experiments with radioactive beams might provide additional constraints on the sophisticated models attempting to describe statistical and/or dynamical properties in the formation and decay of excited nuclei [402–409].

State-of-the-art isotopic resolution and broad angular acceptance with high angular resolution could be assured using the FARCOS or FAZIA particle detectors. Experiments in this framework will be realized by studying the reactions induced by ^{88}Kr and ^{94}Kr on ^{40}Ca and ^{48}Ca targets at 10 MeV/u.

5.1.2 α-Clusters in compound nucleus decay

α-correlations and clustering (LNL-RD-FU-a0)

Many recent works demonstrated the persistence, in light (and medium light) excited nuclei, of cluster structures like those predicted by the Ikeda diagram [410]. In particular, signals of an underlying α clustered structure have been put into evidence in fusion-like reactions especially between self-conjugate systems forming compound nuclei (CN), also well beyond the threshold for particle emission [411–415] and even at bombarding energy in the Fermi domain [416, 417] where the multifragmentation channel is open [418]. In some cases also the occurrence of molecular structures has been suggested [419]. These α-clustering effects have been shown by means of refined studies on the de-excitation chains of the CN. In particular, the branching ratios associated to evaporation residues reachable through the emission of (only) α particles have been compared to the prediction of the statistical model not containing specific refinements on nuclear structure; the experimental branching ratios for these channels are significantly higher than predicted ones. When the α-particle emission is accompanied by neutrons, favoured configurations with the α particles emitted one after the other have been found [411, 414, 415]. Despite the large amount of experimental data already available, some aspects still need elucidation. We mention here some examples: the role of cluster structures in compound nuclei close to the self-conjugate configuration and the persistence of such structures far from the N = Z line; the maximum spin and excitation energy achievable in compound systems; the role of molecular configurations and their trend with the angular momentum and, finally, the sequential or instantaneous nature of the multi-α emission from excited N = Z nuclei such as ^{12}C or ^{16}O [417].

The main experimental observables useful to investigate such topics are the branching ratios associated to the specific decay chains, in coincidence with the measurement of the charge and, possibly, of the mass of the evaporation residue, particle correlations and Jacobi coordinates to study the decay topology. Morevoer, Dalitz plots, built from the particle relative energies, can be used to investigate the nature (sequential or instantaneous) of the disintegration of light clusters into α particles. From the point of view of the experimental setup, the detection of complete (in charge) events for light and medium-mass systems (up to Z = 15–20, depending on the energy) is very useful to identify the involved configurations and decay chains. It is mandatory to tag and, at least partially, identify the evaporation residue; its mass identification, when possible, is very useful to estimate the free neutron multiplicity. Since particle correlations are extremely important to reconstruct the different steps of the decay chain, and to investigate the resonances associated to excited states of the nuclei (for example, the α-decaying levels of ^{12}C) a relatively high granularity is mandatory. At LNL there is an ongoing effort to continue the work reported in references [411, 414, 415]. The GARFIELD array will be used to extend the scope of exploration to more asymmetric and energetic systems like $^{16-17-18}$O+$^{12-13}$C up to 300 MeV incident energy.

Clearly, the availability of the future SPES n-rich beams of unstable isotopes will allow to extend the present studies on some of the previously mentioned physics cases, in the limit of the beam energies below 15 MeV/u.

5.1.3 Out-of-equilibrium processes

Onset of pre-equilibrium emission in medium mass systems. (LNL-RD-FU-a1)
The intermediate step of the fusion process is characterized by a rapid transfer of energy and angular momentum of the projectile and target relative motion into the internal degrees of freedom. Several models allow to describe the excited Compound Nucleus (CN) cooling mechanisms consisting, mainly, in light particle and γ-ray emission, in competition with fission for heavy systems. Pre-equilibrium emissions decrease the excitation energy and the angular momentum and must be determined precisely because these quantities have a major influence on the CN survival probability. This has a direct effect on the synthesis of very exotic systems such as the superheavy nuclei (SHN). For high beam energy, apart from quasifission, the pre-eqilibrium emission of the particles should be taken into consideration as it changes the mass-over-charge ratio of the CN and its excitation energy. The observation of relatively narrow resonances ($\Gamma \approx 100$–200 keV), in the elastic and inelastic channels of α-like nuclei, [363] inspired many studies on the formation of highly deformed excited systems, with lifetimes comparable to those of the compound nuclei. Although the nature of these states and the production reaction mechanisms involved are not yet completely understood, different interpretations, relying on the existence of largely-deformed intermediate dinuclear system, have been proposed. These states could act as doorway states to fusion with a strong memory of the entrance channel (see [420]). In this regard, the dependence on the entrance channel dynamics may affect the evaporative decay, if the dinuclear complex is formed in a highly deformed configuration. The phase-space may not be fully sampled or limited for the compound nucleus (CN) if formed from particular entrance channels. Resonances are indeed demonstrations of the production and the surviving of a particular nuclear state. Lately, the peculiar behavior of the branching ratio for the exit channels where only α-particles (and possibly neutrons) are emitted [388] was also observed and underlines the importance of nuclear structure effects in the decay of the compound nucleus. The idea is to set up an experimental campaign to scan the evolution of the non-equilibrium emissions from to 16 MeV/u. Such investigation will aim to study the out-of-equilibrium emissions from an energy region beyond the onset of the pre-equilibrium emission, to a region where it has the most important role. Studying $^{16-18}$O-induced reactions at the LNL highest available energies (16 MeV/u), where the pre-equilibrium part is well assessed can also be a way to reach the information about α-particles emitted before full equilibration of the projectile-target system into compound nucleus.

Pre-equilibrium emission of α-particles at highest spins (LNL-RD-FU-a2)
Since the α-particles are emitted from the hot CN in the beginning of the de-excitation cascade, they retain the information about the spin and the deformation of the equilibrated system. The measurements of the γ-decay yield at bombarding energies on- and off-resonance have allowed to enlighten a strong resonant effect in the inelastic channels and, to a minor extent, in certain fusion–evaporation channels, see for instance the measurements of the ^{48}Cr nuclei [421]. A deeper understanding of this mechanism requires the use of other probes: in fact various decay branches of the highly excited CN are energetically possible and, in particular at high spin, the α-particle evaporation is dominant with respect to the γ-ray emission. The search for extremely elongated configurations in rapidly rotating medium-mass nuclei, that has been pursued exclusively by using γ-ray spectroscopy, will indeed benefit of observables related to light charged particle emissions. This has been shown in previous experiments (see for instance [422–425]) where deformation effects in γ yields might be washed out by particle-decay evaporation. In those cases the α-particle energy spectra and correlations clearly indicate the presence of significantly large deformations. The analysis of light-particle energy spectra and angular correlations, in the framework of the statistical model (SM), indicates, for several nuclei [423, 424, 426], the onset of large nuclear deformations at high spin. In the rotating liquid-drop model (RLDM), these nuclei do not survive such high spins. A possible description can be provided by cranked cluster model predicting an axis ratio up to 3:1 at values of spin sustainable only assuming cluster structures. A similar outcome is provided by a new version of the Lublin-Strasbourg-drop (LSD) model [349] that predicts Jacobi transitions implying a dramatic shape instability consisting in the rapid increase in elongation for relatively small changes in the values of spin. More precisely, the LSD model indicates that nuclei change their shapes from oblate (with spin parallel to the symmetry axis) to elongated prolate or triaxial shapes at high spins. However, the α particles are not the solely probe indicating the presence of the Jacobi shape transitions: the Giant Dipole Resonance strength functions, measured in the ^{46}Ti [427] and ^{45}Sc [428] composite system decays and a number of superdeformed bands of discrete γ-ray transitions (e.g. [429–432]) support this hypothesis (see also 4.5.3).

Entrance channel mass asymmetry-deformation dependent pre-equilibrium emission
The evolution of the nuclear dynamics of hot rotating nuclei is one of the aspects that were explored through the study of the GDR γ decay, see for instance [315]. In addition to the thermally excited GDR described before, a pre-equilibrium GDR, liable to the charge equilibration process between the colliding nuclei, can take place during the dinucleus phase. Therefore this fast relaxation of the charge asymmetry degree of freedom occurring before complete damping of the kinetic energy, i.e. the formation of the CN, can be investigated. A comparative analysis of observables measured for the same composite system, populated using different projectile/target combinations, can elucidate on the emission from the pre-equilibrium phase and the connection with the mass asymmetry equilibration can be studied. Large γ-ray multiplicities are produced in reactions with stronger damping of the kinetic

energy and/or with more extensive mass transfer. Therefore, the γ-fold measurement can provide a tool to discriminate between faster (e.g. pre-equilibrium) and slower processes (like those originating from CN decays). Complementary information on the nature of the emission process can be obtained from the α-spectra and α-evaporation residue correlations over a wide angular range, being these observables, together with the more exclusive α–α and α–α–α correlations, dependent on both the nuclear temperature and the shape of the emitting nuclei. Different examples on how the high spin deformation can affect the α-particle spectra and correlations can be found in [433, 434]. Although the proton emission usually occurs at lower angular momenta with respect to the α-particle one, it should be taken into account as it represents the main competing mechanism in the CN decay. Therefore simultaneous measurements of charged particles, γ rays and evaporation residues are needed to undertake studies of the composite system shape evolution; the rich information on the detected events will allow stringent tests of model predictions. Several experimental studies, based on non-comprehensive data sets, seem to indicate the presence of doorway states for fusion at angular momenta higher than the critical ones in the mass region of A $\approx$ 40–50. A similar behaviour has been recently predicted even for larger mass nuclei A $\approx$ 60–70. The wide variety of beams delivered by the LNL accelerators allow to perform highly desirable systematic studies on nuclei at high spins, as well as to modify the neutron/proton ratios in the entrance channels to evaluate how they influence the reaction. As for experimental equipment, the hard γ emission and γ multiplicities can be efficiently measured with the powerful PARIS modules [11, 336].

5.2 Transfer processes and particle spectroscopy

The process of transferring one or more nucleons between colliding nuclei plays a critical role in heavy-ion reactions. In such process, mass, energy and angular momentum are exchanged by the projectile and target nuclei. Therefore, transfer reactions are generally highly selective and are very often used as a tool for studying the nuclear structure of light-to-medium mass nuclei. As an example, for relatively light systems, peripheral collisions lead to transfer reactions involving few nucleons. In these reactions the projectile exchanges some nucleons with the target through a fast and direct process, leaving the residual populated in excited states. From a measurement of charge, mass and momentum of the leftover, it is possible to reconstruct the excitation energy of the residual nucleus. This requires particle identification capabilities and good angular and energy resolution. Angular distributions of the differential cross section contain information on the reaction mechanism and, for direct processes, provide information on the angular momentum transfer. The comparison of the experimental distributions to DWBA calculations leads to the C^2S spectroscopic factors. The latter are phenomenological quantities used to estimate the single or multi-particle nature of the excited state under investigation (see, as an example, reference [435]). Another approach deals with the description of the asymptotic properties of the residual nucleus, assuming a single or multi-particle nature, in terms of the so-called Asymptotic Normalization Coefficient [436]. This information can be linked to direct radiative capture rates, useful in astrophysics, which cannot be easily constrained with direct laboratory experiments due to the low cross section, making transfer reactions particularly interesting as surrogate methods for astrophysics [437]. Another important application of transfer reactions is in indirect measurements, where an alternative projectile and target combination is used to extract relevant information of certain key reactions that, under particular conditions, present very low cross sections. Although being model dependent, this method is heavily exploited in studying reactions related to nuclear astrophysics.

5.2.1 Population of n-rich heavy nuclei via multi-nucleon transfer reactions

Multi-nucleon transfer reactions, characterized by the exchange of many nucleons at energies around the Coulomb barrier, have been extensively used in the last decades to populate mid-mass neutron-rich nuclei [438–440]. The use of light stable projectiles on heavy targets allows to populate in the quasi-elastic regime only proton stripping and neutron pick-up channels of the projectile-like fragments [438]. With neutron-rich projectiles the trend should turn and the proton pick-up and neutron stripping channels open up, leading to the population of neutron-rich heavy fragments [441–445]. However, secondary processes, such as neutron evaporation and fission, can significantly modify the final yield distribution of heavy primary nuclei.

Populating n-rich nuclei with stable and radioactive ion beams (LNL-RD-TR-a0)
New experiments will be proposed to continue and extend the research started with the large-acceptance magnetic spectrometer PRISMA [13, 446] coupled to a second arm detector NOSE [447, 448], DANTE [442] or a gamma array [13]. In this respect, several combinations of stable (^{48}Ca, ^{124}Sn, ^{136}Xe, ^{208}Pb, ^{238}U) and radioactive (^{94}Rb, ^{132}Sn, ^{140,144}Xe) projectiles and neutron-rich targets (^{48}Ca, ^{124}Sn, ^{208}Pb) offer great opportunity to study the production of neutron-rich nuclei. While stable beams are already employed at LNL, the radioactive projectiles will soon become available with the development of the SPES facility. In order to populate nuclei far from the stability it is also important to understand the evolution of quasi-elastic to deep-inelastic scattering and quasi-fission. Insight can be gained by identifying reaction products in mass and charge, and by measuring Q-value distributions, angular distributions and total cross sections, as well as by comparing these observables with theoretical calculations.

Table 5 Selected examples of reactions with SPES beams which are relevant for transfer studies at Coulomb energies. Neutron transfer Q-values given in units of MeV

System	Pickup			Stripping		
	+1n	+2n	+3n	−1n	−2n	−3n
^{58}Ni+^{124}Sn	0.510	5.952	4.952	− 6.483	− 8.540	− 19.656
^{69}Ni+^{124}Sn	− 1.183	− 2.865	− 4.789	1.147	1.545	1.265
^{70}Ni+^{124}Sn	− 4.225	− 3.280	− 8.142	− 1.573	2.031	− 0.234

5.2.2 Nucleon–nucleon correlations in transfer reactions

One of the still unanswered questions is whether and to which extent the transfer of a pair of nucleons affects the behaviour of the cross section. These measurements are best performed at the energies near and below the Coulomb barrier, where the conditions to study particle–particle correlations with two-nucleon transfer reactions are most suitable. The studies of the neutron–neutron correlations have shown significant progress in the past years where different systems have been measured using the PRISMA setup to measure reactions in inverse kinematics [449–453]. The experimental transfer probabilities for ^{116}Sn+^{60}Ni have been well reproduced, for the first time with heavy ions, in absolute values and in slope by microscopic calculations which incorporate nucleon–nucleon pairing correlations, microscopically calculated optical potentials and successive transfer processes [450, 451].

Transfer of n–n and p–p pairs to probe the pairing force (LNL-RD-TR-a1)

The role of the transfer of a pair should be better understood by using different superfluid combinations (for instance ^{208}Pb+^{144}Sm, ^{144}Sm+^{88}Sr which involve superfluid proton nuclei) or doubly-magic nuclei (for instance ^{208}Pb+^{48}Ca). The role of proton-proton correlations is here particularly interesting since it is even less understood and yet to be thoroughly investigated. Finally, the use of nuclei with an extended neutron distribution should allow the possibility to study the density dependence of the pairing force. The use of ^{132}Sn beam and different targets (^{40}Ca, ^{64}Ni, ^{208}Pb) and comparison of data with microscopic calculations, as well as cross comparison between reactions performed with stable and radioactive beams, will provide valuable insight into this topic. In recent years, microscopic theories have been extensively developed with the use of supercomputers. For instance, it is nowadays possible to take into account quantal fluctuations and correlations going beyond the time-dependent Hartree-Fock (TDHF) approach [454]. The stochastic mean-field (SMF) theory [455, 456] or time-dependent random phase approximation (TDRPA) [457] is one of those theories, which enables a quantitative comparison with experimental data, providing not only the mean values of observables, but also their distributions. Further, dynamic effects of pairing correlations can be studied within a fully microscopic framework, called time-dependent superfluid local density approximation (TDSLDA) [458]. New experiments in close collaborations with theoretical groups will certainly develop our understanding of low-energy heavy-ion reactions.

Moreover, the data of Ref. [450] were recently interpreted as a manifestation of a nuclear Josephson effect, where entangled neutron pairs play the role of Cooper pairs tunneling between the superfluid nuclei [459–461]. A gamma ray emission, associated with the oscillating motion of a neutron pair between the interacting binary partners, is expected to be centered at ∼4 MeV with a broad distribution. These predictions can be experimentally tested thanks to the powerful coupling of PRISMA and AGATA [9] by measuring the same system at an energy close to the Coulomb barrier in inverse kinematics.

5.2.3 Competition between transfer and near-barrier fusion

Despite the fact that the mechanisms of nuclear reactions and the properties of nuclear structure have been largely investigated, the interplay of multi-nucleon transfer and fusion reactions still represents an extremely complex problem both experimentally and theoretically. Since the neutron transfer process can act as a doorway to fusion [462], it is expected that such reactions with positive Q-values enhance the sub-barrier fusion cross sections [449, 463]. To validate this assumption, a considerable number of reactions involving different isotope combinations have been investigated in the last decades. The overall results have confirmed that, in fact, most positive Q-value neutron-transfer reactions enhance the fusion cross sections at energies below the Coulomb barrier. However, for few systems with positive Q-values for the neutron transfer channel, no enhancement has been observed [464]. This means that the role of neutron transfer on the sub-barrier fusion cross sections has not yet been completely explained from both macroscopic and microscopic aspects.

New systematic studies on transfer at the Coulomb barrier (LNL-RD-TR-a2)

To understand the dynamics of neutron transfer and its effect on the sub-barrier fusion reactions, a systematic investigation involving several different systems will be pursued.

The advent of high power accelerators producing intense radioactive ion beams paves a new road to explore the dynamics of nuclear reactions involving isotopes with exotic neutron to proton ratios, the bulk properties of such nuclear species and their interactions. Different combinations of stable and radioactive projectiles, impinging on the same targets, can shed some light on the role of positive Q-value neutron transfer on sub-barrier fusion reactions. As shown in Table 5, the ^{58,69,70}Ni + ^{124}Sn reactions are good candidates for a systematic study, since the pickup and stripping neutron transfer Q-values can be quite different. The

projectiles can be produced at SPES and all the relevant channels can be measured using the electrostatic deflector PISOLO installed at the LNL [465, 466]. With such apparatus, the fusion cross sections can be experimentally determined by directly detecting the corresponding evaporation residues. In addition, the other relevant reaction channels, such as the elastic scattering, the inelastic excitation of low-lying states, and the transfer of one or few neutrons, can be measured either by installing silicon surface barrier detectors around the ^{124}Sn target in the reaction chamber or by performing complementary experiments with magnetic spectrometers such as PRISMA. The new data will be valuable in the development of realistic models aiming to describe simultaneously all the relevant reaction channels [467].

5.2.4 Transfer reactions to constrain the asymptotic normalization constant (ANC)

Transfer reactions constitute a useful tool for studying the nuclear structure, especially of nuclei presenting a single-particle nature. These are for instance halo nuclei, composed of a compact core and one weakly-bound proton or neutron, such as the one-neutron halo nuclei ^{11}Be and ^{15}C, or the one-proton halo nucleus ^{8}B. Also nuclei described by a cluster structure with a compact core and a valence α particle, e.g. ^{16}O clusterised as ^{12}C + ^{4}He, present a single-particle nature. Following Ref. [468], it has been suggested to rely on the strong sensitivity of transfer reaction to the single-particle structure of the nucleus to measure the asymptotic normalization constant (ANC) of the wavefunction describing the valence particle. The idea would be to measure the transfer of the valence particle x to the target A, e.g. in a A(d,x)B reaction, where x is a neutron or a proton. A particularly precise estimate of the ANC would be obtained selecting transfer data at low beam energy and forward scattering angles, i.e. $E < 10$ MeV/u and $\theta < 12°-15°$. This method has been presented in [469] and recently applied to study the cases of ^{10}Be(d,p)^{11}Be and ^{14}C(d,p)^{15}C [470, 471]. In the case of ^{11}Be the obtained ANC was in agreement with ab initio predictions [472] and has been used to solve an apparent discrepancy in the ^{11}Be dB(E1)/dE estimate for this nucleus [473]. The ^{15}C structure has been used as the only input to the excellent description of Coulomb breakup at intermediate and high energies and radiative capture [471]. Such radiative capture theoretical prediction resulted to be the best prediction in comparison with the latest direct measurement of radiative capture from GSI [474]. The method to extract the ANC from peripheral transfer data is detailed in [469–471]. Besides precise models of reactions, it requires a description of the effective interaction V_{Ax} based on halo effective field theory (halo EFT) [475–477]. The ANC is one of the most relevant parameters for purely peripheral processes, like radiative capture [468]. Radiative capture reactions, e.g. (n,γ), (p,γ), or (α,γ) involving halo or clusterised nuclei, are considered crucial processes in nuclear astrophysics for the production of heavy elements in inhomogeneous big-bang nucleosynthesis and have been shown to be part of possible reaction routes in the nuclear chart during the r-process [478, 479] (see also chapter 3). Direct measurements of radiative capture cross section at astrophysical energies are possible yet challenging, and indirect methods are normally used to deduce the cross section of radiative capture at low energies. Therefore, transfer reactions is suited as surrogate method for radiative capture. In fact, from the analysis of the transfer differential cross section of A(d,x)B reaction one can constrain the ANC of the nucleus B ground state, and finally use this information to infer the radiative capture cross section A(x,γ)B.

ANCs of ^{8}B and ^{8}Li mirror nuclei (LNL-RD-TR-b0)

The Legnaro facilities are suited for this particular measurements, thanks to the low beam energy available and the excellent purity and intensity of the light radioactive ion beams that can be produced.

A possible case study that can be developed at LNL is the investigation of ^{8}Li and ^{8}B mirror nuclei. To extract ^{8}B and ^{8}Li ANC, these two nuclei could be measured through ^{7}Li(d,p)^{8}Li and ^{7}Be(d,n)^{8}B in inverse kinematics, using ^{7}Li and ^{7}Be from the EXOTIC facility. Measurements of ^{7}Li(d,p)^{8}Li are available in literature [480, 481], but there is a lack of data in the conditions for a peripheral reaction, i.e. low beam energy and forward scattering angles. To avoid the uncertainties in the scattering angle when detecting neutrons, (d,n) reactions could be substituted by (^{3}He,d), possibly measured in inverse kinematic using a ^{3}He cryogenic target. The theoretical model to extract the ANC in this case has not been tested, thus giving the opportunity to expand the applicability of this precise method. Direct measurements of the radiative capture process are available [482, 483] to compare the theoretical predictions extracted by peripheral transfer measurements. To have an idea of the magnitude of transfer cross section in these conditions, preliminary calculations for the differential cross section of such reactions at different low beam energies are shown in Fig. 13. These results are obtained using the computer code TWOFNR [484] in the adiabatic distorted wave approximation (ADWA), KD03 optical potential [485], selecting the simpler approximations (such as zero-range and non locality) and default options. Besides being a way to investigate indirectly two radiative capture reactions relevant for nuclear astrophysics, such a measurement could also be a good occasion to test the theory for mirror nuclei (e.g. [468]).

This theoretical method applied to (^{3}He,d) reactions could be tested also in the case of ^{16}O(^{3}He,d)^{17}F (see Fig. 13). Such a measurement at low energy and forward angles would allow us to extract precisely the ANC of ^{17}F, that together with its binding energy, would allow us to provide a precise ^{16}O$(p,\gamma)^{17}$F radiative capture estimate. This reaction is part of the CNO cycle, a series of reactions that is believed to take place in the hydrogen-burning shells of red giant stars [478]. The direct measurements available for this proton capture process [486–488], would provide a benchmark to consolidate the method.

Another interesting reaction is ^{12}C$(\alpha,\gamma)^{16}$O, part of the He burning reactions. When measured at low energy, it allows to extract the phase-shift of the continuum state from which the alpha is captured, a valuable information for ab initio theories. This reaction can

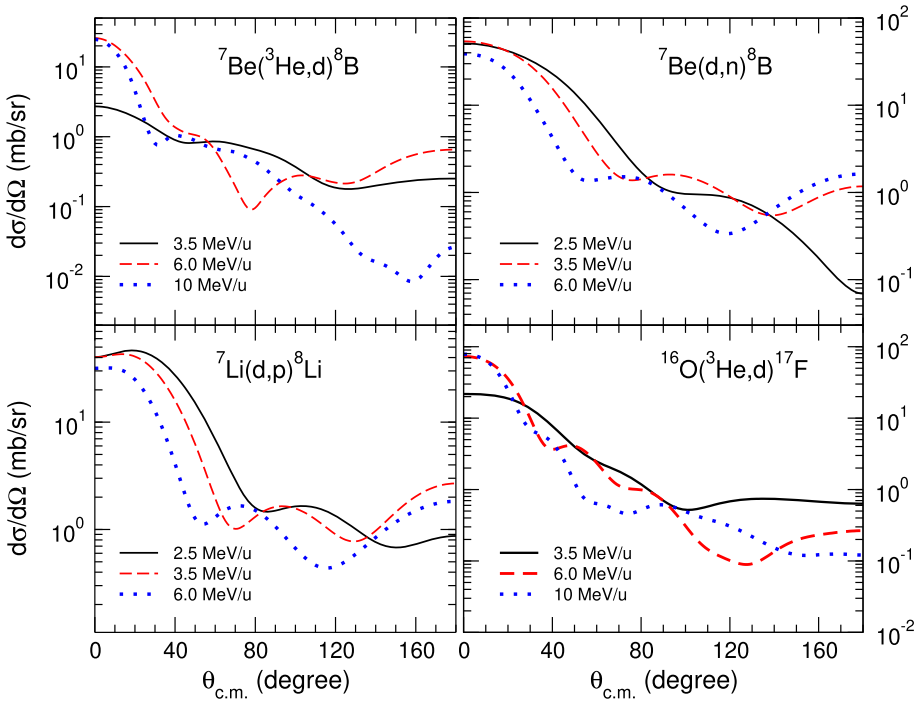

Fig. 13 Theoretical predictions of transfer cross sections for different reactions. The calculations were performed at 3 bombarding energies. The corresponding results are shown as solid black, dashed red and dotted blue curves

be investigated through indirect methods studying ^{12}C(^{6}Li,d)^{16}O and ^{12}C(^{7}Li,t)^{16}O transfer processes, updating the measurements obtained in [489].

5.3 Fission and sub-barrier fusion

5.3.1 Nuclear fission

A detailed investigation of fusion–fission is of paramount importance for the understanding of the dynamics of nuclear systems and quantum shell effects. Shell closures play a fundamental role in the mass splitting of thermally equilibrated compound systems [490], resulting usually in asymmetric decompositions, which reflect the shell structure of the nuclei populated in the exit channel. For example, recent fusion–fission studies succeeded in pointing out the existence of the $Z = 52$ and $Z = 56$ closed shells, associated with pear-like deformation in medium-mass systems [491]. In the last years, the study of nuclear fission is experiencing a certain revival thanks to the development of new experimental techniques and powerful and detailed models. Much of the attention is focused on the interplay between collective and intrinsic properties, such as the influence of nuclear structure and shells, and the study of fission dynamics, such as dissipative effects and energy balance.

Recent models profit from comprehensive descriptions of the system and high computational power in order to track the time evolution of the fission process along and reveal the dynamics involved. The application of energy density functionals in real-time frameworks are just one example of these new approaches [491, 492].

Experimentally, the use of inverse kinematics and magnetic spectrometers permits to access the neutron and proton content of the full distribution of fission fragments, together with a wealth of new observables that can be directly connected to theoretical descriptions. The most recent examples are the campaigns being carried out with Coulomb-induced fission at GSI with the ALADIN spectrometer, where neutron-deficient minor actinides are studied [493, 494], and with transfer- and fusion-induced fission at GANIL with the VAMOS spectrometer, where fission from a wide region between sub-lead neutron-deficient systems and trans-fermium isotopes can be accessed [495–500].

At LNL, the availability of the large-acceptance spectrometer PRISMA [15, 16, 501] and heavy-ion beams with energies around the Coulomb barrier and intensities of more than 10^9 particle per second offer the possibility of performing experimental fission studies with inverse kinematic and fully identified fragments, and contribute to the fission campaigns already in place at GSI and GANIL.

The layout of PRISMA is very similar to that of VAMOS, with a wide acceptance and the possibility of rotating the spectrometer axis in order to scan the angular distribution of the fragments. However, the maximum magnetic field is presently limited to somewhere below 1.2 Tm; a limitation that can effectively reduce the scan of the angle in c.m. and, for some systems, may represent a severe cut in the measured yields. Besides this limitation, PRISMA, and LNL in general, has an important asset in the ensemble of ancillary detectors available on-site that can complement the direct observables measured from the fragments. As discussed in

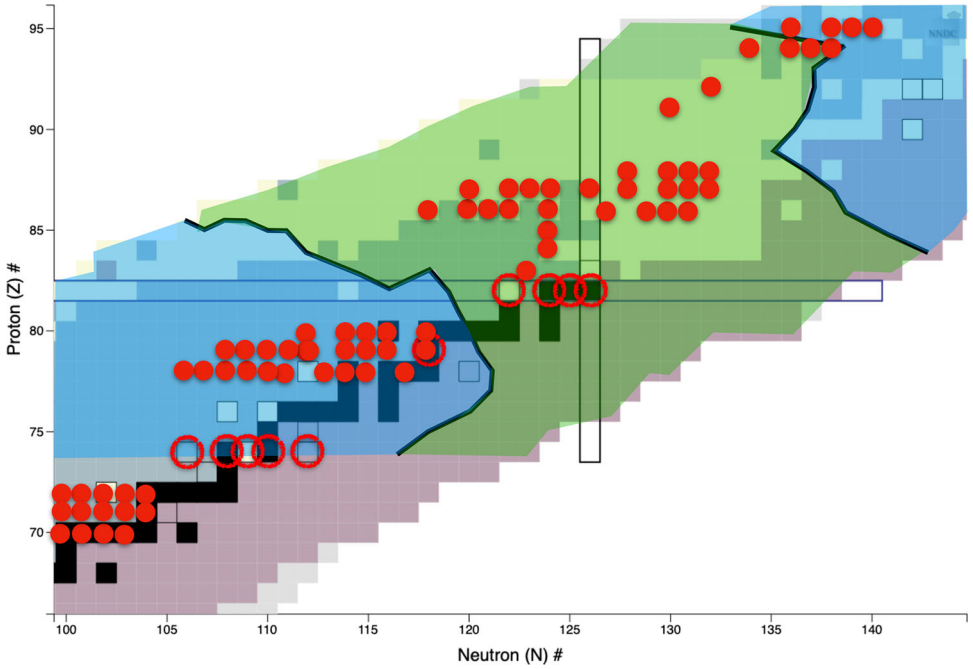

Fig. 14 A sample of compound systems (red dots) produced in fusion–fission reactions from beams around lead (red empty circles) and ^{9}Be, ^{10}B, ^{12}C, ^{24}Mg, and ^{27}Al targets. The blue-shaded regions correspond to expected asymmetric fission, while the green-shaded region shows expected symmetric fission [504]

chapter 4, high resolution gamma-ray spectroscopy of the fission fragments will be performed by coupling PRISMA with state of the art gamma-ray arrays such as AGATA.

In general, we can think of three main reaction channels related to fission that can be produced and studied in a setup like PRISMA: Fusion-induced fission, quasi-fission reactions, and transfer-induced fission (including inelastic channels). In the following sections, we address fusion-induced and transfer-induced fission.

Fusion-induced fission (LNL-RD-FF-a0)

Fusion-induced fission reactions produce a well-defined compound system, with a unique excitation energy that is directly determined by the participants and the c.m. energy. In addition, an angular momentum distribution that can easily reach tens of $\hbar$ is also induced in the compound system. These reactions provide a good setting to study the influence and resilience of nuclear structure in fission from hot systems. Traditionally, one would expect that a high excitation energy would wash out structure effects, but recent data suggest that this may not be the case and that nuclear structure still has an impact in particular aspects of the process such as the configuration at scission or the energy sharing between fragments [496]. Still open is also the question whether this is a consequence of a partial cooling down through neutron or γ evaporation before the process [502, 503].

Fusion-induced fission reactions can be studied with PRISMA at LNL right away. No major modifications of the setup are needed, and the available beams and energies provide a wide collection of systems to be produced. Figure 14 shows a sample of compound systems in the region around lead that can be populated with the present beams available at LNL and a collection of typical light targets. We can see how such a set of measurements would be able to track the evolution from asymmetric to symmetric fission for neutron-deficient systems.

Transfer-induced fission (LNL-RD-FF-b0)

The upcoming ^{238}U beam that is being expected at LNL with energies around the Coulomb barrier opens the possibility of using transfer and inelastic reactions to produce fissioning systems around the actinide region. The excitation energy gained in these binary reactions is enough to allow the beam-like heavy system to overcome the fission barrier. In addition, this excitation energy is produced following distributions that depend on the particular channel being populated and spanning tens of MeV. In this way, it is possible to study the properties of low-energy fission as a function of the excitation energy [505, 506].

At these relatively low energies, the effect of nuclear shells is particularly strong, and their impact on observables such as the fragments yields, the fragments kinetic and excitation energies, the neutron evaporation, or the neutron-to-proton content allows to obtain evidences on features like the scission configuration, the energy balance, or the dissipation for different initial excitation energies.

Isomers measured at the focal plane of PRISMA (LNL-RD-FF-c0)

As a future perspective, the equipment of the focal plane of PRISMA with an array of gamma-ray detectors could provide the possibility of studying the decay of implanted long lived isomers in the actinide region populated in fission reactions induced both by stable and radioactive ion beams.

5.3.2 Sub-barrier fusion

In recent years, the study of fusion cross sections well below the Coulomb barrier has seen a noticeable increase of interest, especially due to advancements in the experimental techniques needed to measure rare events (see e.g. [90, 364] and references therein). Close to the Coulomb barrier, couplings to collective excitations in the fusion participants seem to describe well the enhancement of the sub-barrier fusion cross section, which cannot be fully accounted for by simple Coulomb-penetrability arguments. At deep-sub-Coulomb energies, a damping of the coupling effect is observed, leading to the so-called fusion hindrance. A relevant theoretical effort has been recently done to understand the hindrance effect [507–513], but additional experimental data seem to be still required to fully constrain the models. The hindrance effect appears unavoidable for heavy systems with negative Q-values for the fusion. However, whether the hindrance effect might play a role in astrophysically relevant light systems (which have usually $Q > 0$) is still an open question. Some recent data, involving light-to-medium mass systems at deep-sub-Coulomb energies, have shown the evidence for the occurrence of hindrance of the fusion cross section in $Q > 0$ systems [514], but a direct observation of these effects in astrophysically important reactions is still missing. Similar investigations require high-purity targets and intense and high-quality beams at low energies, which are readily available at LNL.

Fusion far below the barrier by particle-γ coincidences (LNL-RD-FF-a1)

Fusion measurements far below the barrier using the combined set-up of AGATA [9] and silicon-array EUCLIDES [21] will be performed to identify and count the fusion events by coincidences between the prompt γ-rays and the light charged particles evaporated from the compound nucleus. This powerful method has been recently developed for the measurement of very small fusion cross sections in light systems of astrophysical interest. The first experiments of this type were performed at Argonne National Laboratory where the Gammasphere [515] array was used in coincidence with a compact set of three annular double-sided silicon strip detectors located inside the target chamber, to measure ^{12}C + ^{12}C fusion at very low energies [516]. Complementary to this technique, measurements at relatively larger cross sections will be performed using the electrostatic deflector set-up PISOLO [517] where the absolute cross sections scale can be fixed to within $\pm$7–8% even down to around 1 μb. In this way the results of the γ-particle coincidence experiments will be normalised to the higher energy cross sections. Far-reaching consequences in astrophysics may be envisaged, when very low energies and/or lighter systems are considered, which are known to be relevant for stellar evolution. In the system ^{12}C + ^{30}Si fusion hindrance was observed a few years ago at the level of $\sigma_{fus} \sim 90\,\mu$b [518]. This case will be used for a test of the method, to demonstrate the feasibility of fusion measurements in the nano-barn range. This will open the door to further experiments along this line, using intense beams like ^{16}O, ^{19}F, ^{12}C and ^{13}C and light targets.

Sub-barrier fusion with exotic neutron-rich nuclei (LNL-RD-FF-b1)

The use of extremely neutron-rich projectiles might give access to unexpected phenomena in the fusion process below the Coulomb barrier. In particular, systematic data on the role of transfer in fusion are required, as anticipated in Sect. 5.2.3. We would like to start an experimental activity in this field by exploiting selected beams that will be produced by the SPES facility. Starting from the two isotopes ^{96}Sr and ^{94}Kr (that will be provided with intensities in excess of 10^5 pps) on ^{40}Ca and ^{28}Si targets, we will continue along Se, Sr and Kr isotopic lines. For the mentioned systems, neutron transfer reactions with Q-values as large as +26 MeV are available. The low-energy structure of the involved nuclei is well known and can be reliably included in model calculations, so to clearly point out the effects of transfer. Heavier beams like ^{134}Sn, ^{136}Te will be produced with comparable intensities, and in a second step their fusion with lighter targets will be investigated. Our goal is to measure cross sections smaller than 1 mb, where transfer couplings effects show up more clearly. The beam quality (stability, energy definition and size of the spot on target) and its purity are essential for fusion experiments below the Coulomb barrier. This is not always the case with radioactive beams, therefore particular care will be put in the arrangement of the experimental setup. For low intensity beams, placing a detector right along the beam path and detecting the forward-peaked fusion–evaporation residues (ER) with almost 100% efficiency will be possible, provided the detectors can withstand high counting rates and one can filter out the overwhelming beam-like background. The electrostatic deflector set-up (PISOLO) we are using for the experiments near 0^o with stable beams has a very good beam rejection factor ($\simeq 10^8$) but a very low efficiency ($\simeq 10^{-3}$). A substantial upgrade will be needed, as recently done at Oak Ridge National Laboratory (ORNL) [519, 520]. Other exotic beams of interest will be ^{94}Sr, ^{92}Kr, ^{132}Sn, ^{134}Te and ^{140,142}Xe that are produced with higher intensities (ranging from 10^6 to 10^8 pps). In this case, the experiments will need a more standard approach using the electrostatic beam deflector PISOLO, possibly coupled to the innovative, multi-sampling ionization chamber mentioned in the next paragraph.

Beyond the limits in heavy-ion fusion and astrophysics with a multi-sampling ionization chamber and the exotic beams of the SPES facility (LNL-RD-FF-c1)

Fusion of light heavy-ions is known to be very relevant in the late evolution of massive stars, where their reaction rates determine the quantity of heavier elements produced. Concerning the very important case of ^{12}C + ^{12}C, recent data have been published [88, 516, 521]. Establishing the behaviour of the S-factor at the very low energies of interest for stellar fusion is very challenging and still much debated, due also to the many resonances observed.

Despite the efforts ongoing worldwide to perform direct measurements, astrophysicists still rely on model-based extrapolations of these cross sections. The existence of hindrance would lead to significant changes in the abundances of many isotopes. Moreover it would increase the estimated ignition temperature of ^{12}C + ^{12}C both for quiescent C burning in massive stars and for explosive

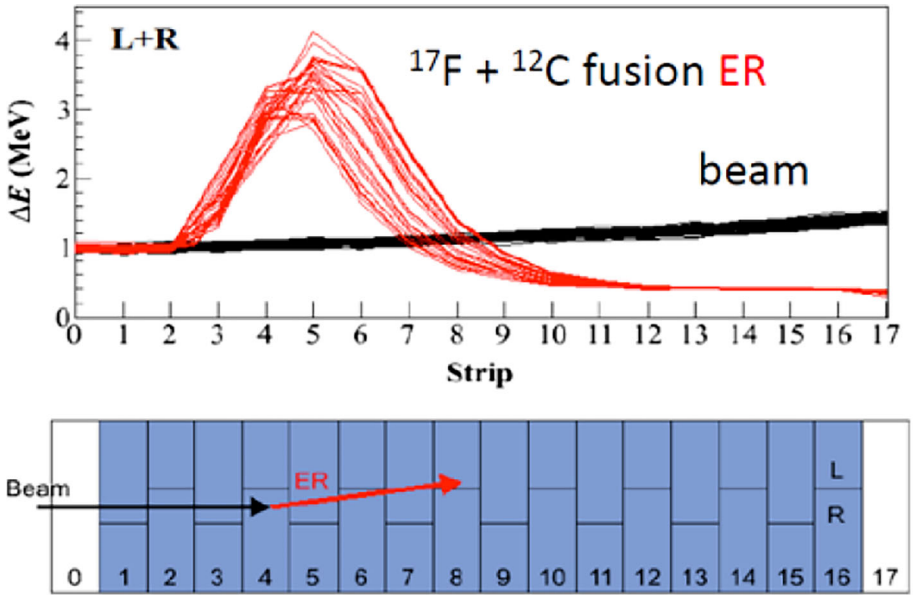

Fig. 15 (top) Typical signals for beam (in black) and for fusion events (in red), obtained in the recent experiment at Florida State University. See text for further details. (bottom) Scheme of the segmented anode for the new Ionization Chamber

C burning in accreting white dwarfs, eventually giving rise to thermonuclear supernovae (the standard candles of cosmology). The ^{12}C + ^{12}C reaction has also been proposed to be a trigger for the super-bursts at the surface of accreting neutron stars.

It appears then that the investigation of systems slightly heavier than ^{12}C + ^{12}C and ^{16}O + ^{16}O is of great interest since their behaviour at very low energy will give us reliable guidances for the low-energy extrapolation of the lighter systems. Therefore we propose to study the existence of the hindrance effect in ^{12}C + ^{19}F, ^{26}Mg with stable beams as a first step, by developing and constructing a multi-sampling ionization chamber (IC) with a segmented anode, getting inspiration from the design of the MUSIC detector [522, 523].

This chamber will work as an active target detector measuring energy losses of the beam ions and of the fusion–evaporation residues (ER) produced in the interaction of the beam with the nuclei of the filling gas (see Fig. 15, (up)). The ER will experience much higher energy loss inside the chamber gas. As a consequence, fusion events will produce a peaked signal in the detector, while beam particles will gradually lose energy throughout the chamber (see Fig. 15, (down, right)). Being segmented, the chamber will also allow to determine the position where the reaction takes place. Since the beam energy decreases moving forward in the chamber, fusion cross sections will be measured simultaneously at different energies in a single run.

The experience gained in the measurement of the systems ^{12}C+^{24}Mg and ^{30}Si [518, 524] will be exploited to test the set up with low-intensity beams. The SPES facility will be able to provide light exotic beams, such as proton rich isotopes of aluminium (^{24,25,26}Al), using silicon carbide (SiC) primary targets. Those beams will be used on ^{12}C and ^{19}F targets, filling the IC with CH_4, C_4H_{10} or CF_4. We point out that fusion reactions involving ^{26}Al may be influenced by the existence of an isomeric state 0^+ at 228 keV whose importance in astrophysics is well known [525].

6 Applications

Nuclear physics applications cover a wide range of fields, ranging from medicine to material science, from nuclear waste management up to targets and detector development and characterization, radiation damage, etc. In the next years LNL will offer a variety of accelerator facilities opening the possibility to perform a wide range of experiments for interdisciplinary and applied physics, considering proton, neutron and, in future, also deuteron and α beams. The SPES facility will enlarge the possibilities related not only to nuclear physics and astrophysics, but also to applied research, such as the production of novel medical radionuclides. In this framework, LNL will be a unique centre in Europe, able to exploit both the direct activation method with the LARAMED project [526] and the ISOL-technique with the ISOLPHARM project [527]. This emerging role of the LNL is already under the spotlight of the international community gathered in the PRISMAP consortium [528]. The recent *Radioisotope Service for Medicine and Applied Physics* of the LNL Research Division will coordinate these activities and will provide medical radionuclides for internal and external users, driving forward the development of new radiopharmaceuticals.

Considering the SPES cyclotron and the future beamlines in the A9 bunker (a. 17) [526], the refurbished XTU-Tandem, and the upgrades at the CN, LNL is in the position to offer a suite of neutron beams ($E_n \geq$ thermal) capable of serving a worldwide community, spread over a broad range of physics, from basic to applied research, presented in Sects. 6.1 and 6.3. It is also important to

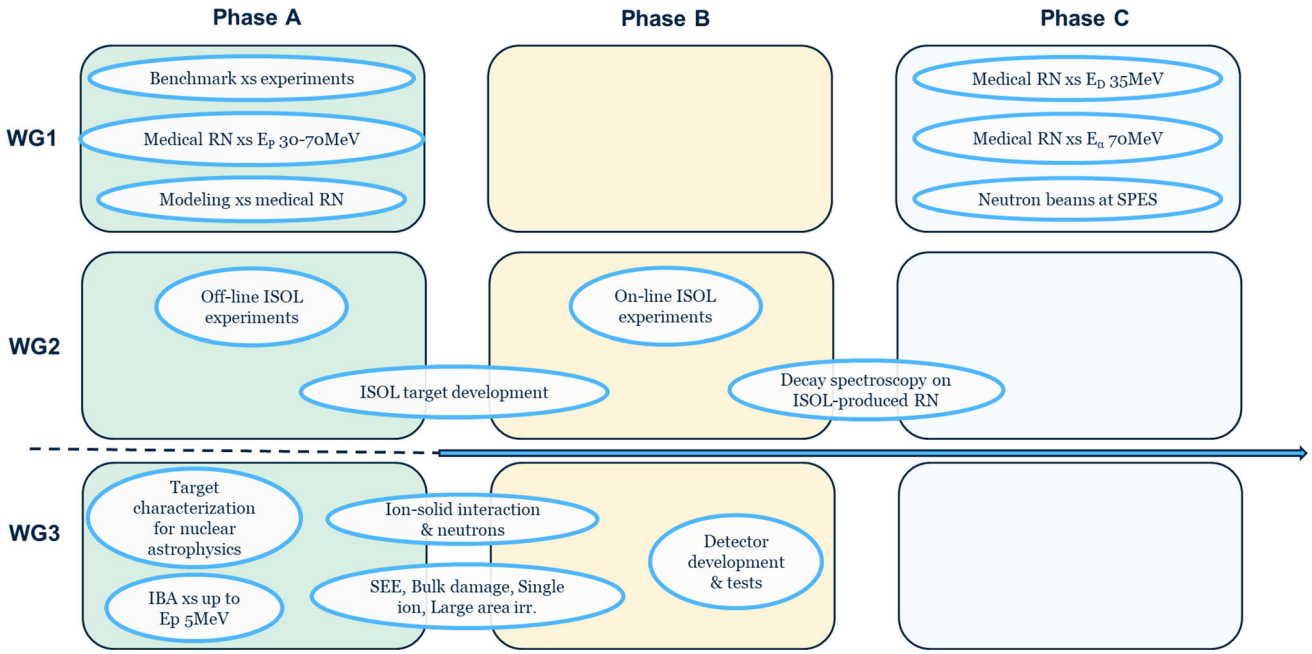

Fig. 16 Summary of nuclear physics application activities that could be performed at LNL in the next future, sorted according to the time phase

underline the role in the next years of several applied and interdisciplinary activities carried out at the AN2000, CN and Tandem-ALPI accelerators, that strongly support various experiments of the nuclear physics community, as described in Sect. 6.3.

Figure 16 provides a snapshot of possible activities: Nuclear cross sections measurements and modelling for direct radionuclide production and neutron beam lines at SPES (WG1), ISOL and laser applications at the SPES facility (WG2) and Development, characterization and modifications of materials for applied nuclear physics (WG3), which could take place at LNL over the next years, while Table 6 shows a selection of the nuclear reactions of interest for the community working in the applications of nuclear physics. The next sections provide a more detailed description of each activity.

6.1 Nuclear cross sections measurements and modelling for direct radionuclide production and neutron beam lines at SPES

The status of the SPES infrastructure devoted to applications, described in Sect. 2.5, is shown in Fig. 17, where the A9 bunker will be devoted to SPES-δ, exploiting high energy neutron beams as described in Sect. 6.1.3. The LARAMED bunkers will be devoted to the measurement of the excitation functions with low-intensity beams (100 nA, provided by the L3c beamline, expected to be installed in 2023) and to produce limited amounts of novel radioisotopes for research purposes by using high-current proton beams (bunker RI#3).

The selection of an appropriate radionuclide for medical use depends on several criteria and parameters [529]. The theranostic approach, that combines therapy and diagnostic using the same radiopharmaceutical, has been widely explored [530], since it allows the selection of the patients with a high chance to positively respond to the therapy, performing SPECT (Single Photon Emission Computed Tomography) or PET (Positron Emission Tomography) imaging prior the treatment. This goal can be achieved by using a "single" theranostic radionuclide (e.g., ^{67}Cu, ^{47}Sc, etc.), with decay characteristics suitable to perform both diagnosis (γ or β^+ emission) and therapy (β^-, Auger-e or α emission) with the same radiopharmaceutical. On the other hand, it is also possible to use the so-called "real theranostic pairs" (e.g., ^{64}Cu/^{67}Cu, $^{43/44\,g}$Sc/^{47}Sc, etc.), to label the same molecule with specific radioisotopes of the same element, to perform low-dose imaging prior therapy assuring also in this case an identical biodistribution. Currently, radionuclides of elements with similar chemistry are used worldwide to label the same molecule to have the essential information to tailor patient' dosimetry (e.g., $^{99\,m}$Tc/^{188}Re, ^{68}Ga/^{177}Lu, etc.).

In general, an ideal radiotracer must be characterized by (i) high specific activity (i.e., activity/mass of isotopic carrier), (ii) high activity concentration (i.e., activity/volume or mass of substrate), (iii) high radionuclidic, radiochemical and chemical purities. Furthermore, to allow the use of these labelled compounds on living organisms, it is necessary to guarantee their biological compatibility with in vitro and in vivo experiments. High specific activity radionuclides can be obtained by either p, d or α irradiation, followed by selective radiochemical separation from the irradiated target in No Carrier Added (NCA) form, reaching specific activity values close to the theoretical "carrier-free" one.

Table 6 Summary of key applied nuclear physics topics and reactions that could be addressed at LNL in the next years. The activities are sorted according to the working group discussing the proposal and the time phase

Tag	Description	Reaction	Phase
LNL-APP-SPES-a0	Benchmark experiments for cross section (xs) beam line characterization	^{nat}Ni(p,x)^{57}Ni, ^{nat}Ti(p,x)^{46}Sc, etc	A
LNL-APP-SPES-a1	Proton-induced xs measurements for medical radionuclides (RN) production	^{70}Zn(p,x)^{67,64}Cu, ^{159}Tb(p,x)^{155}Dy/^{155}Tb, etc	A
LNL-APP-TH-a2	Modeling nuclear xs for medical RN production	^{159}Tb(p,x)^{155}Dy/^{155}Tb, ^{48,49,50}Ti(p,x)^{47}Sc, etc	A
LNL-APP-SPES-c0	Neutron beam lines at SPES for cross section of SEE	n–n scattering up to 70 MeV, ^{45}Sc(n,p)^{45}Ca, etc	C
LNL-APP-SPES-c1	Deuteron-induced xs measurements for medical RN production	^{48,49,50}Ti(d,x)^{47}Sc, ^{70}Zn(d,x)^{67,64}Cu, etc	C
LNL-APP-SPES-c2	Alpha-induced xs measurements for medical RN production	^{nat}Eu(α,x)^{xx}Tb, ^{44}Ca(α,p)^{47}Sc, etc	C
LNL-APP-ISOL-a0	ISOL experiments with off-line front-end		A
LNL-APP-ISOL-a1	ISOL targets development		A+B
LNL-APP-ISOL-b0	ISOL experiments with on-line front-end		B
LNL-APP-ISOL-b1	Decay spectroscopy on ISOL-produced RN		B+C
LNL-APP-LE-a0	Target characterization (IBA) for nuclear and astrophysics experiments	EBS, NRA, PIXE and PIGE	A
LNL-APP-LE-a1	xs measurements for IBA experiments	EBS xs (p,p') on ^{49,50}Ti, ^{30}Si, ^{15}N, ^{17}O	A
LNL-APP-LE-a2	Ion-solid interactions and neutron-damage experiments	^{51}V(n,p)^{51}Cr, ^{14}N(^{7}Li,x), ^{8}B(p,n), etc	A+B
LNL-APP-LE-a3	SEE, bulk damage, single ion and large area irradiation experiments	Light and heavy ions beams	A+B
LNL-APP-LE-b0	Detector development and tests, Quenching effects in scintillators	(n,p) reactions from thermal to 4 MeV, Neutron endurance tests	B

6.1.1 Cross section measurements for medical radionuclides production

To optimize the radionuclidic purity two main approaches must be considered: (i) an accurate knowledge of "experimental" cross sections of the reactions involved, as well as of the excitation functions of both stable and radioactive isotopes produced by side reactions; (ii) the optimization of very selective radiochemical separations for the produced radionuclide.

Nuclear cross sections measurements are thus key ingredients in the optimization of medical radionuclides production. The experiments rely on an activation process (i.e., the bombardment of thin targets, often assembled in the "stacked-foils" configuration) followed by γ-spectrometry to identify and to quantify the radionuclides produced. For this purpose it is necessary to have a precise knowledge of the energy, and of the energy spread, of the charged particle beam extracted and of the charge deposited in the targets, possibly with $< 1\%$ errors. Since the use of monitor reactions is useful in determining the energy and intensity of the bombarding beam [531], the firsts experiments at the L3c beamline will be devoted to benchmark measurements of the well-known reactions ^{27}Al(p,x)^{24}Na, ^{nat}Ni(p,x)^{57}Ni, ^{nat}Ti(p,x)^{46}Sc, ^{nat}Cu(p,x)^{56}Co and ^{nat}Cu(p,x)^{58}Co, available in the IAEA database [532].

Among the priority radionuclides for the LARAMED project, there are the theranostic ^{67}Cu, ^{47}Sc and the Tb-isotopes [526]. ^{67}Cu ($t_{1/2}$ 61.83 h) is a β^- and γ emitter and it is considered one of the most promising theranostic radionuclides [529, 533–536]. It can also be used as therapeutic counterpart of the PET ^{64}Cu ($t_{1/2}$ 12.7 h), already available. Currently, there is not a clear consensus about the best nuclear reaction to be used for ^{67}Cu massive production, due to the impact of the co-produced isotopic ^{64}Cu, occurring with some specific routes [533, 535, 536]. Nuclear data are therefore important to help defining benefits and drawbacks associated with specific production routes. Among the feasible ones are the ^{68}Zn(p,2p) and ^{70}Zn(p,x) nuclear reactions. The measurement of the ^{70}Zn(p,x)^{67,64}Cu cross sections in the 30–50 MeV range, where no data are available [535, 537], is therefore very interesting also in view of the dosimetric impact on Cu-labelled radiopharmaceuticals [538]. ^{47}Sc ($t_{1/2}$ 3.3492 d) is another example of theranostic radionuclide under the spotlight of the scientific community thanks to its β^- and γ-radiation (β^- mean energy 162 keV, 100% int.; E_γ =159.381 keV, 68.3% int.) [529, 534]. The interest in ^{47}Sc comes also from the possibility of pairing it with β^+ emitting isotopes (e.g., $^{44\,g}$Sc or ^{43}Sc) to perform PET with the same radiopharmaceutical. Among the possible proton-induced routes to produce ^{47}Sc, the most intriguing are with ^{nat}V and Ti targets [539–541]. In particular, considering the composition of ^{nat}Ti (^{50}Ti: 5.18%,

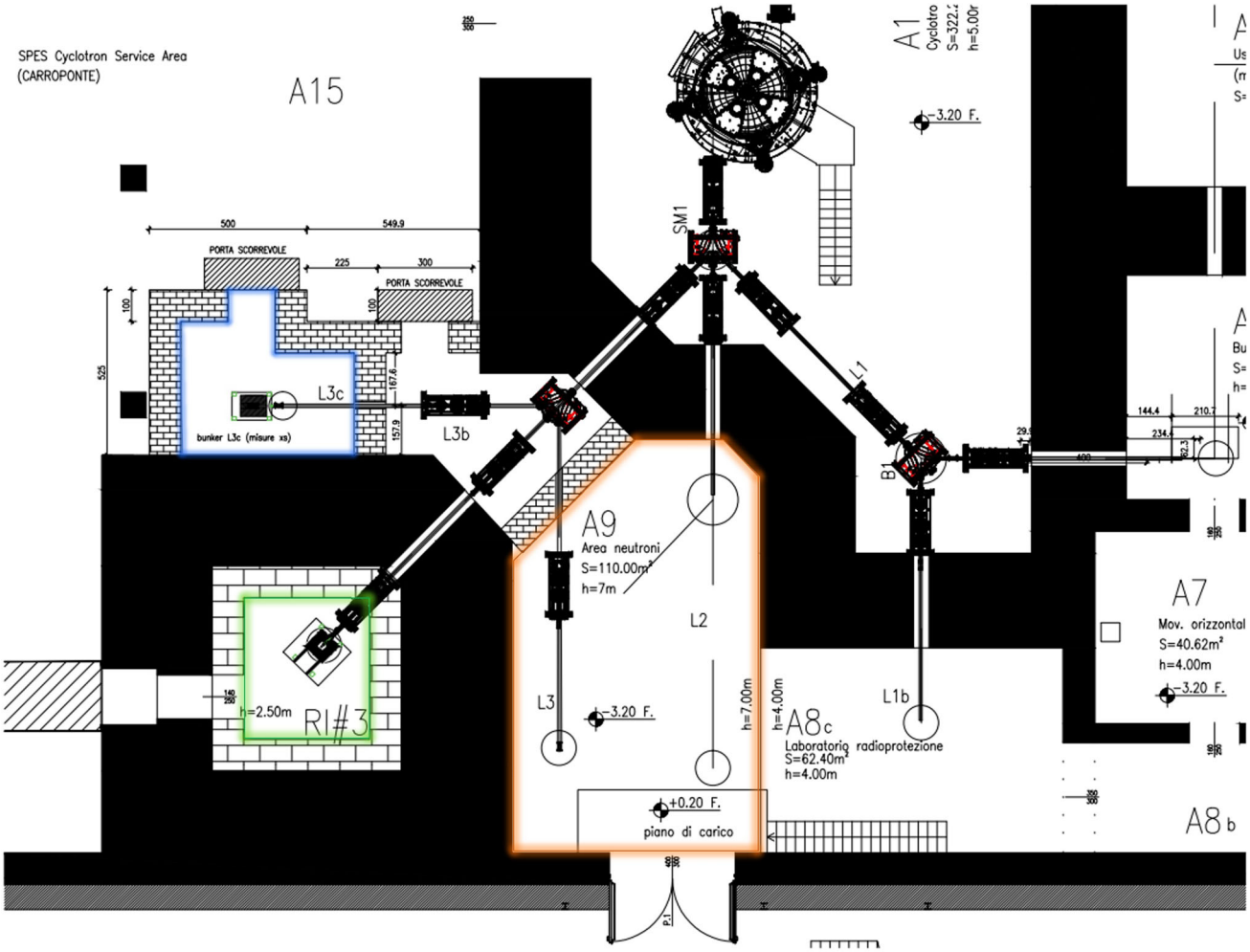

Fig. 17 A detailed layout of the underground level in the SPES building, showing the A1 bunker with the cyclotron, the LARAMED bunkers RI#3 (green lines) and A9c (blue lines), and the future neutron facilities in the A9 bunker (orange lines)

^{49}Ti: 5.41%, ^{48}Ti: 73.72%, ^{47}Ti: 7.44%, ^{46}Ti: 8.25%) it is not possible to extract the contribution of each titanium isotope to the production of the specific radionuclide of interest. Since no data are available for the ^{49}Ti(p,x)^{47}Sc reaction and only a limited set of data are published for ^{50}Ti(p,x)^{47}Sc and ^{48}Ti(p,2p)^{47}Sc cross sections, it will be desirable to add these experimental data points to evaluate which production routes can be competitive with the ^{nat}V(p,x)^{47}Sc reaction [542]. Terbium-isotopes have being named "Swiss knife of nuclear medicine" [543] because of their four valuable radioisotopes, ^{149}Tb, ^{152}Tb, ^{155}Tb, and ^{161}Tb. ^{149}Tb is the only Tb-radioisotope promising for targeted α-therapy, emitting α and β^+, with an additional γ-ray (E_γ =165 keV, I_γ = 26.4%), which helps its detection. ^{152}Tb is a multiple β^+ emitter with prominent end-point energies at 2.62 MeV (5.9%) and 2.97 MeV (8%) and it could be used for in-vivo PET dosimetry to monitor ^{149}Tb bio-distribution in radiotherapy; ^{152}Tb is also a potential SPECT candidate thanks to its multiple γ-lines. In the ^{155}Tb decay some X-ray and γ-ray are emitted in addition to Auger electrons, that having a high LET (Linear Energy Transfer) can be effective in reducing the survival capacity of cancer cells. However the most promising tool in nuclear oncology is ^{161}Tb, which mainly decays by release of Auger electrons and β^- particles. These terbium isotopes can be produced with several projectile/target/energy ranges, obtaining different yields and contaminant profiles [529]. For example, ^{155}Tb production is mainly relied on the ^{155}Gd(p,n) and ^{156}Gd(p,2n) reactions [544] but ^{155}Tb can be also produced with a ^{155}Dy$\rightarrow$^{155}Tb generator system, exploiting the ^{155}Dy decay. In this case, ^{155}Dy can be produced with high energy p-beams and natural Tb-targets, using the ^{159}Tb(p,5n)^{155}Dy reaction.

Additional examples of radionuclides with potential interest in the next years are also $^{117\,m}$Sn, ^{119}Sb and $^{133/135}$La. $^{117\,m}$Sn has theranostic decay emissions consisting in short-range conversion electrons and the main γ-ray (E = 158.56 keV, I = 86.4%) useful for SPECT imaging. Some applications of $^{117\,m}$Sn have been investigated already, including bone pain palliation treatment of oncological diseases [545]. A possible way to produce $^{117\,m}$Sn using a 70 MeV p beam is exploiting the ^{nat}Sb(p,x) reaction. The main co-produced contaminants are ^{113}Sn and $^{121\,g/m}$Sn that can be avoided using enriched ^{121}Sb targets; however, measurements to evaluate the ^{113}Sn co-production are still demanded. ^{nat}Sb targets can be also used to indirectly produce ^{119}Sb, a promising candidate

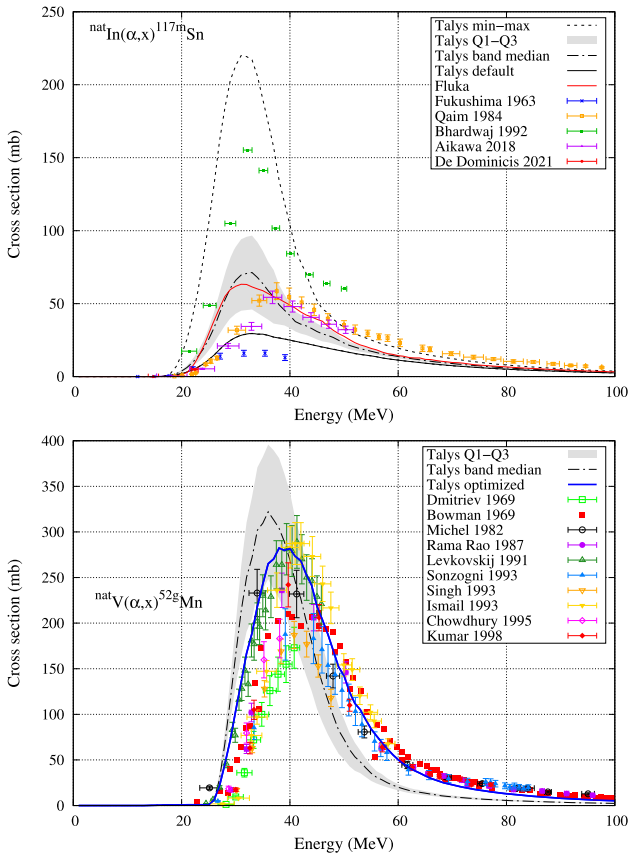

Fig. 18 *Top:* ^{nat}In(α,x)^{117m}Sn cross section. TALYS "min/max" refers to the minimum/ maximum values of cross section for the set of calculations, "Q1-Q3" denotes the interquartile band of the set, and "band median" indicates its center. *Bottom:* ^{nat}V(α,x)$^{52\,g}$Mn cross section. The band median is reported as dash-dot line and the gray area denotes the interquartile band. The newly TALYS optimized curve [559] is represented with the solid blue line

for targeted Auger therapy [546], via the precursor system $^{119/119\,m}$Te. Few ^{nat}Sb(p,x) cross section data are available in literature and they are often discordant from one another [547]: for this reason, a new set of measurements is advisable. It will be interesting to study also the ^{119}Sb production by using the enriched ^{121}Sb target as there are no literature data. Even if the $^{133/135}$La theranostic pair has been recently introduced [548, 549], it has already been successfully employed in animal trials [550]. The Auger electrons from ^{135}La have the potential for targeted Auger therapy [551], while ^{133}La has suitable characteristics for PET imaging ($E_{\beta^-,\,mean}$ = 460 keV, I = 7.2%). To achieve a high specific activity product, the ^{nat}Ba(p,xn) and ^{nat}Ce(p,2pxn) reactions can be studied, as few cross section data are available in literature in both cases [552, 553]. In particular, experimental data on ^{133}La production from ^{nat}Ba target and on ^{135}La production from ^{nat}Ce target are currently missing.

Considering the possible future developments of the SPES cyclotron, it is worth noting that some nuclear cross sections induced by *d* and *α* beams could also be studied for the production of medical radionuclides with potential impact in nuclear medicine [529, 554].

6.1.2 Modelling of nuclear cross sections for applications

Modern nuclear-reaction codes are openly available for modeling and simulating nuclear reactions at low (< 20 MeV), intermediate (< 70 MeV), and high energy (70–150 MeV) ranges. A not exhaustive list of known codes involves TALYS [555], EMPIRE [556], FLUKA [557], and PHITS [558], each one characterized by its specificity (Monte Carlo, deterministic, semi-classical, etc). These codes provide the fundamental reaction quantity, i.e., the cross section in both its angular dependence and integral form, generally for proton and neutron beams; *α* projectiles are included in their capabilities and so are the deuteron beams, in most cases. The upgrade of the FLUKA code including *d* as projectiles is almost ready to be released. Currently, photon beams are being upgraded in some of the codes, as well.

Open Source codes should be preferred, as well as codes with the possibility to select specific key theoretical ingredients, such as the optical models, level-density models, or different pre-equilibrium approaches. Not all the codes possess these features: TALYS, for example, provides several pre-equilibrium (PE) and level-density (LD) models (and so does EMPIRE), as described in [539, 559]. The combination of these possibilities leads to the calculation of up to 30 cross sections, as shown in Fig. 18 referring to the ^{nat}In(*α*,x)^{117m}Sn [559, 560] (top panel) and ^{nat}V(*α*,x)^{52g}Mn reactions [554] (bottom panel).

The variability of these models can be described statistically introducing an interquartile band (shown as a gray area in Fig. 18), measuring the model dispersion between the lower Q1 and the upper Q3 quartile. The median of the band provides an evaluation

of the cross section representative of all models; the corresponding half-band width indicates an evaluation of the theoretical indetermination. It is evident from Fig. 18 that a collective description, gathering most of the model combinations in the code within a statistical band, is much more informative with respect to a single model line as obtained with a FLUKA curve or the TALYS "default" one. In fact, this approach better shows the potential and the limitation of the cross sections modelling. Recently, few other analyses using this statistical band approach appeared in literature [554, 559]. Not in all cases the improvements achieved with the statistical band approach were sufficient for an accurate estimate of the radionuclide production cross section. This is the case of the ^{nat}V(α,x)^{52g}Mn reaction (Fig. 18 bottom panel), where the production cross section for the paramagnetic PET tracer ^{52g}Mn could not be reproduced in the peak region (dashed dotted line) [554]. To obtain a satisfactory cross section reproduction, as given by the blue solid line, one had to resort to an optimization technique for the level densities, explained in detail in Ref. [559]. In addition, optical model parameters could be varied, since they may not be well known close to the Coulomb barrier.

Another aspect that will become dominant in SPES physics is pre-equilibrium, since its overall effect in the cross section grows with energy. In the recent TALYS-1.95 GDH version [561], the Geometry Dependent Hybrid model [562, 563] has been added. It has been observed [559] that the calculated excitation function with the GDH model better reproduces the experimental data at higher energies. FLUKA [557] is another reaction code that gives good description at intermediate energy. This code couples a classical intranuclear cascade model, supplemented with quantum corrections, with a pre-equilibrium framework inspired by the GDH approach. The performance of FLUKA is not optimal at low energies, close to the reaction thresholds, but it generally provides better results at higher energies. Beyond 100 MeV, the difficulty of describing charged-particle nuclear reactions, relevant to the production of established and novel radioisotopes, has been addressed in a recent study, with the default code predictions largely failing to reproduce the measurements due to consistent underestimation of the pre-equilibrium emissions. A standardized procedure was developed to determine the best parametrization for the pre-equilibrium two-component exciton model, to improve the description of measured data [564].

In conclusion, it is clear, from this overview, that modeling accuracy is crucial in the development and optimization of the production routes. When nuclear data are missing, it is possible to introduce a statistical-band approach to predict cross sections and to quantify the theoretical indeterminacy due to model dependence (or variability). Instead, when some reliable nuclear data are present, it is possible to introduce an optimization of the parameters connected to the nuclear level densities, obtaining reliable cross section simulations to extract more accurate production quantities. In sum, nuclear reaction simulations can be performed in a completely global sense, where varying nuclear models gives an estimate on the uncertainty or, on the other hand, precisely fitted to experimental data. The latter may lead to trends in nuclear model parameters which then, in turn, can improve the global models, leading to better predictive power. An assessment of the global predictive power of a model code is important, since it may determine the priority list of the experimental measurements.

6.1.3 Neutron beam lines at SPES

There is growing interest in neutrons in the 1-to-tens of MeV energy range driven by nuclear astrophysics and material science, nuclear waste transmutation, generation-IV reactors, accelerator-driven-systems, fusion reactors, and decommissioning of first-generation fission reactors. Other important application fields are neutron detection, dosimetry, radiation protection, medical physics, and the study of neutron-induced radiation damage effects in electronics for very diverse applications such as high-energy physics, space, avionics, and information technology. In particular, for what concerns space, over the last few years neutrons are of particular concern because of health issues in manned missions to Mars. For all these fields, Quasi Mono-energetic Neutron (QMN) beams and suitable shaped neutron energy beams are mandatory. The high current variable energy SPES cyclotron open the possibility to build an irradiation facility with p and n in the 20–70 MeV energy range (beam intensity up to 1 mA). The description of the first (NEPIR-0) and the final configuration (NEPIR-1) of the future neutron facility in the SPES building can be found in Sect. 2.5. The Atmospheric Neutron EMulator (ANEM) target, whose facility layout is shown in Fig. 19, will be able to produce an intense beam of fast neutrons with an atmospheric-like energy distribution in the 1–70 MeV energy range. This neutron flux will be mainly devoted to study the low energy neutron effects in state-of-the-art digital electronics. Neutrons are the main threat, inducing Soft Errors (SE) in digital electronics [565–567] and ANEM can provide single event effect (SEE) tests, even of full devices (like a PC). Japanese private companies (NTT, for instance) already defined a protocol for testing telecommunication servers using a compact accelerator neutron source with beam energies up to 70 MeV.

Higher energy neutrons than those available at the CN at 4 MeV (as described in Sect. 6.3) are required to follow the energy dependence of the SE cross section curve from threshold to higher energies, towards the knee and onwards to the saturation value ($E_n \geq 20$ MeV). These measurements can be carried out at the QMN (quasi-monoenergetic) neutron beam line. QMN finds application in several fields, since it is possible to study excitation functions for different measurements, as for example fundamental physics, SEE, applied physics (energy and non energy applications, radiopharmaceutical production, dose effects). Within the SPARE project, selected materials suitable for space mission are planned to be tested at QMN at different neutron energies.

The REMO (Radiotrazadores para el estudio de Ecosistemas Marinos y Oceánicos) project shows how radiotracers play an essential role in monitoring biological processes of environmental interest [568]. As the release of carbon dioxide from humankind's industrial and agricultural activities has increased, the Ocean Acidification (OA) process has decreased the pH of seawater, making carbon ions less abundant [569]. As many marine shelled organisms need CO_3^{2-} to build the calcium carbonate ($CaCO_3$) shells and

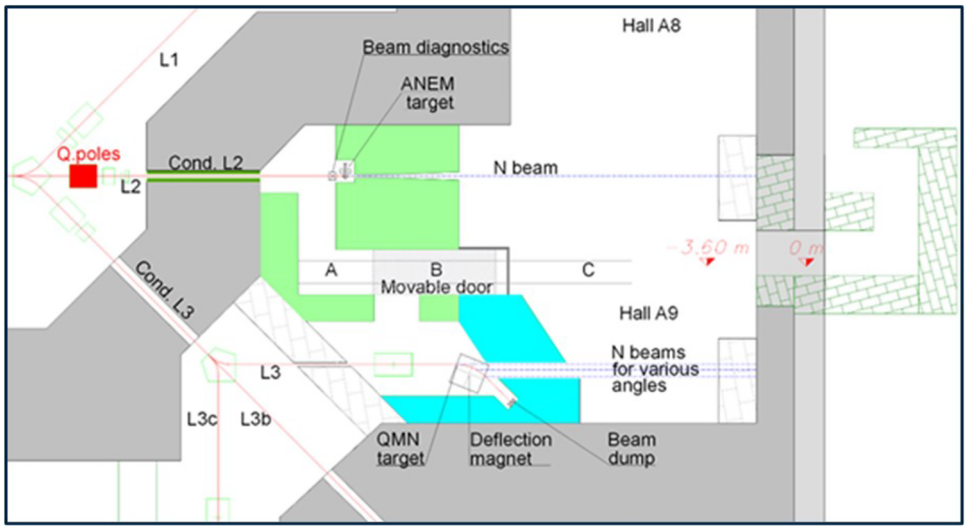

Fig. 19 Layout of the foreseen neutron-facilities at SPES

skeletons, the project aims at measuring the calcification rate at different water pH, using ^{45}Ca as radiotracer. Tests are performed placing the organisms in tanks filled with the same amount of ^{45}Ca but with water at different pH levels and then, at the end of the incubation period, the skeleton is dried to measure the ^{45}Ca activity with scintillator counters. In general, ^{45}Ca ($t_{1/2}$=163 d) is produced at reactors using ^{44}Ca targets and applying an isotopic separation from ^{41}Ca ($t_{1/2} = 10^5$ y). It is therefore interesting to investigate a new route based on the insertion of a ^{45}Sc target close to the SPES one, exploiting the ^{45}Sc(n,p)^{45}Ca nuclear reaction; in this case, only a chemical separation is required. To estimate the ^{45}Ca production it is necessary to know the cross section at neutron energies available at SPES (1–10 MeV) [570]: since there are no experimental data up to 6 MeV, it is proposed to measure the ^{45}Sc(n,p)^{45}Ca cross section up to 10 MeV.

6.2 ISOL and laser applications at the SPES facility

ISOL (Isotope Separation On-line) is regarded as one of the main method for the production of high intensity and high quality Radioactive Ion Beams (RIBs), to be employed in several fields of research, ranging from nuclear physics studies to technological applications [527, 571]. Typically, an ISOL system consists of a series of different steps: isotope production, thermalization of the produced nuclei, ionization and subsequently extraction, mass separation, eventually cooling and charge-state breeding, and acceleration. As these processes are governed by physical and chemical phenomena, both physical (e.g., production cross section, decay half life, ionization potential) and chemical (e.g., molecular formation probability, volatility) properties of the nuclei of interest and of the target material have to be taken into account. In such framework, the SPES facility (Selective Production of Exotic Species) represents the LNL declination of the ISOL technology and foresees the production of intense neutron-rich RIBs by impinging a multi-foil uranium carbide target with a 70 MeV proton beam. Details of such facility are provided in the previous sections. Among the applications of the SPES facility, ISOLPHARM is a collaborative experiment aimed at developing innovative radiopharmaceuticals starting from ISOL-produced nuclides, that are intrinsically of high purity. Such mission is accomplished by collecting SPES RIBs of medical interest on an appropriate implantation substrate, placed at the end of a dedicated beam line on the low-energy experimental area. After irradiation, the collection target are dissolved and the nuclides of interest are chemically harvested. The combination of chemical purification and mass separation, provided by the ISOL technique, ensures the high purity of the collected radionuclides, used to label No Carrier Added radiopharmaceuticals. One of the most promising nuclides in the ISOLPHARM program is ^{111}Ag, which was studied with the CSN5 experiments ISOLPHARM_Ag and ISOLPHARM-EIRA [572, 573].

6.2.1 Laser spectroscopy and applications

LIS (Laser Ion Source), the most effective ionization strategy to produce ion beams of high purity, is based on the photo-ionization principle and it is used in the SPES project to produce RIBs. Photo-ionization is the physical process in which an ion is formed from the interaction of a photon with an atom or molecule, and usually involves a photon absorption ladder within the electronic levels of the atom. Mainly three different routines can be adopted to provide to an electron of the neutral atom an amount of energy above the ionization threshold. The first one foresees the step-wise excitation of the electron directly to the continuum, with a precise combination of different photons, whose wavelengths are opportunely tuned according to the atomic levels of the element of interest. A second approach consists in exploiting an auto-ionizing state that allows the spontaneous emission of one of the outer-shell electrons. Indeed, the quantum emitted by the de-excitation of one electron provides the energy needed to remove another electron

on the same excited state. The third method exploits a ionization scheme including highly excited Rydberg states, that are a series of high-lying excited states with energy slightly below the ionization potential. Such states are very sensitive to external effects, and lead to the electron emission in presence of sufficiently intense electric fields of atomic collisions.

In the SPES project, the basic principle of LIS is to convert the neutral vaporised atoms to ions through interaction with laser light(s) of precise wavelength(s). If compared to other ionization methods, LIS provides several advantages, such as higher element selectivity and reduced isobaric contamination. In the specific case of SPES, the interaction region of the ionizing lasers with the effusing neutral atoms corresponds to the internal space of a tubular hot cavity, directly connected to the production target. The typical effusion time of the atoms through the hot cavity is of the order of 100 μs, therefore, in order to ensure at least one laser pulse-atom interaction, the minimum laser repetition rate must be around 10 kHz. The hot cavity for the LIS source shares its design with the one adopted for the SPES Surface Ion Source, and has to work at high temperature (above 2000°C) to avoid the sticking of the effusing atoms on its internal surfaces. However, such design solution comes with the clear disadvantage of contamination from the surface-ionized isobars (produced by thermal ionization of low-ionization potential species with the high temperature surface of the hot cavity). In the framework of the ISOL community the development of more effective ionization schemes for the widest variety of elements represents a challenge. Indeed, more than 50% of the elements for which photo-ionization has been currently realized rely on a last non-resonant ionization step. In this particular case, the last step which ionizes is not saturated, and the ionization efficiency is proportional to the available laser power for this step. In a different scenario the efficiency can be significantly improved if the final step populates an Auto-Ionizing State or a highly excited Rydberg state by exploiting the favourable cross section for these levels respect to a non resonant step. Another challenge is represented by the reduction of the surface-ionized contaminants, for which several techniques have been employed and other are being studied, with the aim to enhance the quality of the RIBs provided to the users. At SPES the laser spectroscopy activities are being performed in two different laboratories, equipped with different laser set-ups. In the new SPES building the online laser laboratory will be exploited for the actual production of RIBs, using three TiSa lasers which provide around 6–7 W power laser beam in the fundamental wavelength at repetition rate of 10 kHz. These lasers beams are further delivered to the ion source with the aid of position sensing closed loop mirrors setup, which ensure beam pointing stability. The SPES-laser group has also an offline laser lab where laser spectroscopy is performed with the use of low rep-rate dye lasers, Hollow Cathode Lamps (HCLs) and a Time-of-Flight Mass Separator. Several ionization schemes of several elements including Al, Sn, Mo have been successfully studied. At the moment, photo-ionization scheme of Ag is being studied and a two-step ionization scheme has been successfully identified. These schemes will be employed in the online laser lab once the SPES facility will be fully operative.

6.2.2 Nuclide production with ISOL for medicine and nuclear physics

One of the fundamental steps to evaluate the feasibility of an experiment with ISOL-produced RIBs is the identification of the most suitable target for the production of the desired nuclides, to be employed for both medicine and nuclear physics. Indeed, the achievable yield producible with ISOL depends on many target-related factors, from the atomic composition to its micro-structure. On one hand, the in-target nuclear reaction products are dependent only from the impinging beam energy and particle and target isotopic composition; on the other hand, the possibility of extracting them as a beam depends on many other phenomena, in particular their release from the target. The nuclide release is governed by the diffusion and effusion phenomena, that are activated and boosted if the target working temperature is maximized. For such reason, ISOL targets are normally designed to withstand temperature in the 1500–2000 °C range, implying that only material characterized by high melting point are usable. Additionally, it has been demonstrated that porous materials have enhanced release properties, as the atomic effusion through the target pores is much faster than the diffusion through the bulk material. The typical SPES ISOL target is a porous uranium carbide multi-foil target, designed for a 40 MeV 200 μA proton beam, made up of seven coaxial disks (40 mm diameter and 0.8 mm thickness), opportunely spaced and positioned inside a cylindrical graphite box, closed at its extremities by thin graphite disks. The main advantages of such target design are the increased acceptable proton beam intensity, since the beam power deposition is split between the seven disks, and the improved release capabilities, since the diffusion paths through the target are generally shorter. The 8 kW proton beams (40 MeV 200 μA) is completely absorbed by the 7 disks uranium carbide target, which, thanks to the sole contribute of the deposited power, is capable of reaching a temperature level generally above 2000°C. In addition, the target disks are opportunely spaced in order to guarantee a homogeneous temperature level in the target. Such target can be employed for producing a characteristic set of neutron-rich radionuclides, with mass ranging from 70 to 160 amu. However, the RIBs availability at SPES can be enlarged if other targets are developed, enabling for instance the production of lighter nuclei or neutron-deficient radionuclides. In particular, some aluminum RIBs can be produced with a Silicon Carbide target, currently under development, whereas the ongoing research on Titanium Carbide for ISOL could provide the possibility of producing Scandium isotopes of medical interest (^{43}Sc, ^{44}Sc and ^{47}Sc) in the framework of ISOLPHARM. Other possibilities could be provided by several other materials, such as Zirconium Carbide, Boron Carbide, Lanthanum Carbide, Zirconium Oxide, Hafnium Oxide, Cerium Oxide, Zirconium Germanide, Cerium Sulfide and many others. In case of SPES, target materials have to meet some specific mandatory requirements: they have to be solid (liquid targets are not yet foreseen at SPES); they have to be refractory (indeed the higher the working temperature the faster the release); they have to be porous (as the presence of open porosity enhances the releases of the produced nuclides). Additionally, they have to withstand extreme conditions, in terms of high power, thermal stresses, radiation damage. As a consequence, each new target

material requires efforts in its development and characterization before being ready for irradiation. Considering such requirements and the typical SPES multi-foil target architecture, ceramic materials are the most suitable for such application. The typical ceramic targets production methods are the dry method, which consists in cold pressing of pre-milled powders (with eventual organic binders) and sintering at high temperature and the Sol–gel method which foresees the addition of a gel solution to the powder. The latter, in particular, is used for the production of micro- or nano-structured materials with high porosity (usually 30–70%), that currently represent the state-of-the-art method to produce high performance carbide targets. Currently, in the framework of the INFN-E Project AM4INFN, in collaboration with INFN-PD and UNIPD, the possibility of producing such materials Additive Manufacturing (AM) is being explored [574]. AM of ceramic regular structures can provide several advantages, in particular, the maximization of radiative heat transfer, which can imply an increment of the sustainable proton beam intensity, and improved release properties thanks to the regularity of the micro-structure. In addition to the equipment and furnaces for the production of ceramic disk-shaped targets, in the framework of SPES specific test apparatuses were developed for the high temperature tests, thermal and structural characterization of the target material of interest. Several carbides such as Uranium Carbide, Lanthanum Carbide and Silicon Carbide were already characterized and tested. This is a fundamental step as it allows the identification of the limit working conditions for each material in terms of acceptable proton beam intensity and maximum temperature. Target material research would greatly benefit for a coordinated approach and a facilitated transnational access. Complementary laboratories including characterization techniques are present across all ISOL facilities, for instance, institutions like SCK CEN have very large service infrastructure for materials characterization (including nuclear materials and post-irradiation examination) whereas LNL has a consolidated expertise of thermal and structural characterization of multi-foil target. The collaboration with the ISOL community could also allow the development of consistent characterization and material production protocols making possible state-of-the-art operation at all involved facilities.

6.2.3 Decay spectroscopy of nuclide of medical interest

ISOLPHARM required the development of a device able to handle the collection targets and perform spectroscopic analysis for the quality control of the collected radionuclides that will be located in the SPES low energy experimental hall. Indeed, precise quantification of the radionuclide yields is of fundamental importance for assessing the final product quality and performing the subsequent labeling process; moreover, the spectroscopic characterization of irradiated targets will allow the efficiency quantification of the whole production process. For this reason, a dedicated spectroscopy system will be designed and characterized at LNL; preliminary studies will focus on the selection of the most suitable detection strategy: for γ-counting, High-Purity Germanium detectors represent the gold standard in γ-spectroscopy, ensuring energy resolution as good as 1.5 keV at 1.1 MeV, allowing for high-resolution energy spectra acquisition. The overall energy spectra should not present many peaks, since the radioactive ion beam deposited onto the target is expected to be isobaric; for this reason, the use of inorganic scintillators can be a viable alternative. Nowadays, there are some appealing choices for inorganic scintillators with good energy resolution, such as LaBr3 and LBC crystals, which can reach 2.5% at 1.3 MeV. Different detectors will be evaluated not only in terms of their performance (efficiency, energy resolution, noise rate) but also by their ease of operations and the need for dedicated infrastructures, such as the requirement of cryogenic temperatures and the overall cost. Results from Monte Carlo simulations will drive the spectroscopic system designs carried out using different codes like GEANT4, FLUKA, and PHITS. The performance of the selected design will be evaluated using γ-ray calibration sources, and the obtained data will be compared with simulated results. The spectroscopic system will be coupled to a custom deposition target handling station, controlling the coupling of the disk with the beam line and the subsequent transportation towards the counting position. The whole system should be designed and assembled in order to be ready for commissioning before the first SPES RIBs will be delivered. Such system, called IRIS (ISOLPHARM Radionuclide Implantation Station), will open new experimental possibilities as it could be also used for the production of calibrated mono-isotopic radioactive sources, that can be employed for other applications. Such sources can be created collecting the high purity RIBs from SPES (especially if photo-ionization is used) on appropriate substrates.

6.3 Development, characterization and modifications of materials for applied nuclear physics

Several research activities are carried out at the AN2000, CN and Tandem-ALPI accelerators for nuclear physics applications. An overview of some experiments performed and of the communities involved is given hereafter. These research activities have a consolidated background at the LNL but also a florid perspective, considering the wide network of INFN divisions, Italian Universities and international groups involved. As an example, the new low-energy irradiation facilities ASIF and ASIDI will be fully operative in the next years at the AN2000 and CN accelerators, respectively; the material characterization experiments such as ANT and HIX has been recently started and will continue in the future, as long as the bounded nuclear physics studies will be pursued. In addition, novel HPGe detectors, developed in the framework of N3G as an example, already play a key role in nuclear physics and will increase their impact in the next years. Details of these applied and interdisciplinary research activities are given below.

6.3.1 Ion beam micro-analysis for nuclear targets development and cross section measurements for applied nuclear physics

In the last few years the constant growth request of isotopically enriched targets with specific characteristics imposed the Ion Beam Analysis (IBA) for advanced nuclear target development and characterization as a new specific research field of nuclear physics. In some cases, the target production processes may be driven by the IBA outcomes, that include Elastic Backscattering Spectrometry (EBS), Nuclear Raction Analysis (NRA), Elastic Recoil Detection Analysis (ERDA), Particle Induced X-ray Emission (PIXE), Particle-induced gamma emission (PIGE) and Ion beam-induced luminescence (IBIL) analysis, that are all part of LNL background. The experiments reported hereafter are examples where the IBA techniques are used as complementary tools to provide compositional information and dose measurements to support, or in some cases allow, nuclear physics experiments.

- ANT (Advanced Nuclear Target) involves IBA techniques for target characterization in the framework of LUNA collaboration for astrophysics experiments. The low background experiments require accurate characterization of targets' and substrates' composition and elemental composition for measurements with very low nuclear cross section, where Beam Induced Background (BIB) could compromise the measurement and therefore the experiment success. ANT has a new approach regarding targets preparation and characterization based on EBS and NRA techniques, focusing on contaminants reduction (oxygen, deuterium and fluorine) using high purity materials and specific LNL apparatus for high quality targets synthesis [575]. In collaboration with the LNL Target Service, the classical evaporated target are characterized with IBA, and the design, production and characterization of novel solid targets is carried out for each specific experiment to improve the LUNA cross section measurements quality.
- DES (Deposition of Elements on Substrates) since 2018 performs RBS measurements at the AN2000, using α-beams or protons at 2 MeV. The studied samples are prototypes of target systems designed for the next phase of the NUMEN experiment, based at the LNS. These target systems are composed by a 2 μm thick substrate made of Highly Oriented Pyrolytic Graphite, on which a very thin (few hundreds of nm) target layer is deposited. The RBS measurements are crucial to study the graphite substrate and target layer thicknesses, and their elemental composition [576].
- The HEAT (Hydrogen dEsorption from cArbon Targets) project [577], funded by INFN-CSN5 young researchers grant, aims to establish an effective and reproducible method for H and ^{2}H desorption in carbon targets via sample heating, up to 1200°C. The setup core is the fully programmable heater module, installed on linear actuators for XYZ motion and azimuth rotation to adopt different target-beam geometries depending on the Ion Beam Analysis of interest. To check the effectiveness of the desorption ERDA and NRA were performed before and after the sample heating. From preliminary results the glassy carbon targets show a significantly lower initial ^{2}H content, however the ^{2}H content was reduced by 40% in graphite targets. The HEAT setup have proved high performance and versatility and in next future the campaign on carbon targets for the planned measurement at the 3.5 MV accelerator of the of Bellotti Ion beam facility will be completed.
- The HIX (characterization of HIVIPP targets for REMIX) project deals with IBA characterization of isotopically enriched targets produced using the HIVIPP (High energy Vibrational Powder Plating) technique [578, 579]. Information regarding the precise knowledge of target properties, such as thickness (at/cm^2 or mg/cm^2), homogeneity over the surface, purity either isotopically or chemically, are essential for proper analysis of the experimental data. The targets characterized at the AN2000 accelerator with RBS and PIXE are then irradiated at the ARRONAX facility (Nantes, France) for nuclear cross section measurements [580]. Thin isotopically enriched ^{48,49,50}Ti targets to produce the theranostic radionuclide ^{47}Sc were prepared at LNL in the framework of PASTA and REMIX projects (funded by INFN-CSN5) [541]. In future the LARAMED beam line devoted to nuclear cross section measurements will be exploited.

The constant growth in the request of isotopically enriched target showed a lack of data concerning elastic scattering cross sections in the 0.3–5 MeV energy range. For several elements (e.g., ^{30}Si, ^{49}Ti, ^{25}Mg, ^{15}N, ^{17}O) there are few experimental data relative to the EBS nuclear cross section and, in some cases, there are no data. For these reasons a novel scattering chamber has been designed and will be soon available at the CN and AN2000 facilities to fill the gap of the EBS cross sections data. The new scattering chamber, funded by CSN5 with the SALVIA (Setup for AnaLysis with MeV accelerators of Isotopic tArgets and their preparation) young researcher grant, includes a cryogenic electron suppressor to improve the charge quality measurement and, at the same time, drastically reduce the carbon buildup induced by hydrocarbon cracking. A polarized sample holder allows the beam energy changement and thus to obtain high energy resolution cross section measurements. The same chamber could be used also for the analysis of AN2000 and CN beam characteristics, i.e., beam energy, energy spread and long-term stability.

6.3.2 Ion-solid interaction, development and radiation damage of materials, detectors and devices

The study of radiation effects (natural and artificial) on materials, detectors and devices is an important and lively field of scientific and technological research. Tolerance to radiation is an important issue in many applications of electronic devices and sensors (HEP at accelerators, space, telecommunications, avionics, nuclear plants, medical imaging, etc.). Furthermore, the improvement in the use of ion beams to study and tune material and devices properties for applications in quantum and detector and sensing technologies requires both the development of new sophisticated experimental techniques and apparatus.

The SIRAD facility at the Tandem-ALPI complex [581] is an example of apparatus routinely used by University and INFN groups to study Single Event Effects (SEE) and bulk damage effects in electronic devices, systems, and semiconductor detectors.

SIRAD was developed in 1997 to use p and Li beams for bulk damage studies; heavy ion beams experiments began in 1999 and have become the main activity. The facility was significantly upgraded in 2004 to perform SEE sensitivity micro-mapping. An additional post-acceleration foil stripping system was installed before the switching magnet to have SIRAD serviced by ALPI, significantly improving the energy, hence the range of all available ion beams at LNL. The SIRAD irradiation facility was continuously maintained and improved over the years to increase the flexibility for many types of users and experiments.

ASIF (ASI Supported Irradiation Facilities) facility [582] instead of SIRAD facility has been designed for large irradiated area (up to 400 cm^2) using light and monochromatic ion beams (H^+ and He^+) at lower energy (0.1–5.5 MeV) available using AN2000 and CN accelerators. The reason of a new facility development is aimed by the constant growth of low energy proton irradiation on materials, devices and optical components used in geosynchronous satellites. The new facility available at LNL provides a high uniform irradiation area with an accurate dose measurement (10^9-10^{16}) using multiple Faraday cup system, in order to simulate the damage effects of 10–15 years of natural space radiation exposure. Furthermore, ASIF facility has been designed in order to guarantee the ASI/ESA compliance tests.

ASIDI (Advances in Single Ion Deterministic Irradiation) is a new facility installed in AN2000 experimental room. The specific design of sub-micrometrical monolithic dual collimator allows the availability of an achromatic beam irradiation from single-ion hit up to 10^4 ions/s in 200–2200 keV energy range. Moreover, the high precision sample positioning system (50 nm in the beam plane) allows the reproducibility in the target positioning. The facility is involved in different research activities, which include detector development and tests (PIXEL, 3D, Microstrip, PDA, etc.), radiation damage studies (electronics, detectors), characterization of the electronic features of micro-devices and detectors with unprecedented level of resolution, material modification, functionalization (semiconductors, SC oxides, SC thin films), investigation of advanced SS material modifications at the sub-micron scale (QUANTUM), localized implantation (color centers in diamond and other high band-gap semiconductors, low D materials).

The set of available beams (CN and Tandem), or the incoming ones at SPES (NEPIR, see 6.1.3), can provide mono-energetic or quasi mono-energetic (QMN) neutron beams with energies from a few keV up to 70 MeV [583]. The neutrons are produced by bombarding low-Z targets (D,T, ^{7}Li, ^{8}Be) with light ions. At the CN facility the beam lines were recently upgraded with an electric kicker system that can throw out a sequence of proton beam bunches and deliver single well separated bunches onto neutron production targets, allowing well defined TOF measurements with an intrinsic time resolution well below 1 ns (sigma). This new tool adds more possibilities to the already rich basic and applied physics research programs. In particular, it is used to measure the *n* energy spectra of new tens-of-μm thin lithium targets (in a copper beam stopper), which has been especially designed to have low mass and thus low *n* spectra perturbation. Higher energy *n* are produced at Tandem using other nuclear reactions, e.g., ^{1}H(^{11}B,n)^{11}C, ^{1}H(^{15}N,n)^{15}O, to produce kinematically focused 11 and 14 MeV neutrons.

The HERETIC Experiment (HEat REsistance Test for Irradiated Cooled targets) [584] regards irradiated target studies for endurance test. It is aimed at validating a new kind of fixed target system for future nuclear physics experiments (NUMEN project) with high intensity beams (10^{13} pps) of swift heavy ions (Z<20 and energy>10 MeV/u). Thanks to the reduced total thickness of the target/substrate assembly (about 2.5 μm), it is a viable solution for high energy resolution measurements. The system is composed by an isotopically enriched thin target, deposited on a 2 μm thick Highly Oriented Pyrolytic Graphite (HOPG) substrate, and chilled using a dedicated cryocooler. In the experiment, the Tandem will provide 1 μA of ^{16}O ions at 50 MeV to irradiate up to 10 h Ge, Te, and HOPG targets to study their thermal behaviour and radiation damages.

6.3.3 Novel detectors development and test

LNL is involved in several research programs regarding design, development and validation of novel detectors for different applications in particle detection and spectroscopy. The prototype detectors are tested using different radiation sources available (ions, *n*, X-ray and γ-ray) at AN2000, CN and Tandem-XTU.

- N3G (Next Generation Germanium Gamma Detectors) aims to implement Pulsed Laser Melting (PLM) technology to produce complex Hyperpure Germanium (HPGE) segmented detectors and to test their potential to face the challenge of nuclear spectroscopy experiments under conditions of high flux and high damage [585]. The basic idea is to exploit the fast laser processing that does not contaminate HPGe to produce thin n-doped junctions that can be segmented to produce insolated contacts indispensable for localize γ event and allow the tracking. The challenge that is ongoing is to bring this technology to produce complex geometry γ detectors such as coaxial segmented detectors. In addition to innovative crystals processing, complete prototypes will be implemented with dedicated electronics and DAQ; cold ASIC preamplifier with smart functionalities for high flux γ managing are under prototyping. Besides the development of advanced instruments for science, the possibility of producing segmented γ detector with complex geometry and low-cost processes can produce future benefit in medicine and security.
- FIRE (Flexible organic Ionizing Radiation dEtectors) project [586], funded by the INFN-CSN5, aims at the fabrication of a fully flexible indirect dosimeter (NEPRO). The core element is a thin layer of stretchable siloxane scintillator, whose development has been studied and accomplished at the LNL. Optimal flexibility is known for siloxanes, besides their water equivalency nature, hence the possibility to use them in small-scale wearable devices to monitor dose rates has been pursued. The indirect device has been fabricated, coupling the siloxane scintillator synthesized at LNL with the flexible organic photo transistor manufactured at INFN-ROMA3. Optimal performance has been demonstrated by irradiation with 5 MeV H^+ (Labec-INFN) as for (i) linear response with proton flux, (ii) limit of detection (0.026 Gy/min), (iii) measurement repeatability, (iv) sensitivity in the dose rates

range used in proton-therapy (fluxes 10^6–10^9 H^+/cm^2s). In the next future, tests at the proton therapy facility APSS in Trento will be carried out using a NEPRO device installed in an anthropomorphic phantom.

- NEUNOSCINT (Neutron Interactions in Scintillators for Neutrino detection) experiments aim at study the neutron responses of liquid scintillators for neutrino physics experiments [587], such as JUNO, BOREXINO and SNO. Proton recoils due to neutron scattering form an important background for antineutrino detection, which is realized via inverse beta decay where an electron antineutrino scatters off a proton creating a positron and a neutron. Backgrounds to these signals are due to neutrons which scatter off protons during thermalisation before capture. If the proton recoil has sufficient energy, a signal similar to the coincidence signal of the inverse beta decay channel will be induced. A complete knowledge about proton quenching is necessary to understand the potential impact of this background. Furthermore, particle identification can be used, for instance, to identify neutrino-proton elastic scattering for supernova neutrino detection; another example is the identification of neutral current reactions of atmospheric neutrinos with neutron production, which form a severe background for the detection of the diffuse supernova neutrino background in our universe. A possible particle identification technique for background discrimination in large-scale liquid scintillator detectors is based on the time profile of scintillation light emitted in response to a recoiling proton as it may differ from electron-like events due to quenching effects. This could be exploited in a pulse-shape discrimination analysis leading to background reduction by orders of magnitude.
- IBIC (Ion Beam Induces Charge) detectors: High precision ion irradiation is a strategic tool for the study of radiation effects in very localized sites or regions at the (sub-)micrometer-scale; in particular, for single-atom device development or for single ion response and damage studies, the control over both the absolute number of ions and the accurate positioning is needed [588]. This control can be achieved through the development of diagnostic tools for the assessment of both the spatial resolution and the accuracy of the ion beam with single-ion sensitivity. Within the INFN-ASIDI experiment, two different strategies were pursued to develop position-sensitive detectors based on the IBIC technique. The former relies on the IBIC mapping of a Si photodiode expressly nano-machined by means of a keV Focused Ion Beam (FIB): the beam resolution is assessed by the analysis of CCE (Charge Collection Efficiency) profiles through these FIB microstructures, which act also as reference markers for the accurate location of the ion impact point. The second method is based on the analysis of the induced charge shared among three graphitic electrodes fabricated by Deep Ion Lithography in a diamond detector: the triangulation of the three signals allows the evaluation of the impact position of individual ions.
- RREACT (Reliability and Radiation Effects on Advanced Components and Technologies) experiment: Ionizing particle beam detection is a crucial issue in many applications, including space, high-energy physics, medical, etc. Recently, the implementation of a particle detector using 3D NAND Flash memories has raised significant interest in the radiation community [589]. The monitor operates detecting the number of affected cells in the array. The key advantage of using floating-gate-based memories over other memories is the fact that, with proper techniques, the cell threshold voltage can be measured, in addition to the digital content. Other advantages due to the non-volatility are the very low power consumption, the avoidance of data loss if a single event functional interrupt occurs, and the possibility of designing passive detectors to be measured offline with a separate reader. Being a simple memory, such detector could be used for various purposes inside a system (data/code storage) and a part of it could be dedicated to particle detection. As a semiconductor memory, it is compact and low-cost. Concerning the array architecture, there are several benefits of using a 3D array compared to a planar one. The most obvious advantage is that the direction of impinging particles can be tracked in a 3D volume. In addition, the analysis of threshold voltage shifts in 3D tracks potentially offers a larger set of information, allowing a higher precision in determining the beam features. The reported linearity between the linear energy transfer (LET) of the impinging particle and the threshold voltage shift can be exploited to measure the LET of the beam.

7 Conclusions

In conclusion, the Nuclear Physics Mid Term Plan in Italy was a great opportunity to trigger and coordinate new ideas from the whole international community, promoting the collaboration between groups working on different topics. There was also a large involvement of young nuclear physics researchers, that will lead nuclear research in the future. The four working groups of the LNL session - Nuclear Astrophysics, Nuclear Structure, Nuclear Dynamics and Applications - collected a wide range of science cases that can be realistically addressed in the upcoming years, exploiting both accelerator facilities that are already running and SPES. Alongside the wide range of beams available, LNL will host a variety of cutting edge detectors and target systems, both resident and itinerant. This puts the laboratory in a favourable condition to be at the forefront in nuclear science and technology.

Funding Open access funding provided by Università degli Studi di Padova within the CRUI-CARE Agreement.

Data availability No data associated in the manuscript.

References

1. https://www.lnl.infn.it/en/
2. A. Lombardi, G. Bassato, A. Battistella, A.M. Bellato, G. Bezzon, L. Bertazzo, G. Bisoffi, E. Bissiato, S. Canella, M. Cavenago, F. Cervellera, F. Chiurlotto, M. Comunian, A. Facco, P. Favaron, G. Fortuna, S. Gambalonga, M. Lollo, M.F. Moisio, V. Palmieri, R. Pengo, A. Pisent, M. Poggi, A.M. Porcellato, F. Scarpa, L. Ziomi, I. Kulik, A. Kolomiets, S. Yaramishev, H. Dewa, The new positive ion injector PIAVE at LNL, in *Proceedings of the 1997 Particle Accelerator Conference - Vancouver, B.C., Canada*, 12–16 May, p. 1129 (1997)
3. G. Fortuna, R. Pengo, G. Bassato, I. Ben-Zvi, J.D. Larson, J.S. Sokolowski, L. Badan, A. Battistella, G. Bisoffi, G. Buso, M. Cavenago, F. Cervellera, A. Dainelli, A. Facco, P. Favaron, A. Lombardi, S. Marigo, M.F. Moisio, V. Palmieri, A.M. Porcellato, K. Rudolph, R. Preciso, B. Tiveron, The alpi project at the laboratori nazionali di legnaro. Nucl. Instrum. Methods Phys. Res. Sect. A **287**(1), 253–256 (1990). https://doi.org/10.1016/0168-9002(90)91803-J
4. P. Russotto, L. Calabretta, G. Cardella, G. Cosentino, E.D. Filippo, B. Gnoffo, M.L. Cognata, N.S. Martorana, E.V. Pagano, R.G. Pizzone, L. Quattrocchi, S. Romano, A.D. Russo, D. Santonocito, Status and perspectives of the infn-lns in-flight fragment separator. J. Phys. Conf. Ser. **1014**(1), 012016 (2018). https://doi.org/10.1088/1742-6596/1014/1/012016
5. C. Broggini, O. Straniero, M.G.F. Taiuti, G. de Angelis, G. Benzoni, G.E. Bruno, S. Bufalino, G. Cardella, N. Colonna, M. Contalbrigo, G. Cosentino, S. Cristallo, C. Curceanu, E. De Filippo, R. Depalo, A. Di Leva, A. Feliciello, S. Gammino, A. Galatà, M. La Cognata, R. Lea, S. Leoni, I. Lombardo, V. Manzari, D. Mascali, C. Massimi, A. Mengoni, D. Mengoni, D.R. Napoli, S. Palmerini, S. Piano, S. Pirrone, R.G. Pizzone, G. Politi, P. Prati, G. Prete, P. Russotto, G. Tagliente, G.M. Urciuoli, Experimental nuclear astrophysics in Italy. Riv. Nuovo Cim. **42**, 103 (2019). https://doi.org/10.1393/ncr/i2019-10157-1. arXiv:1902.05262 [nucl-ex]
6. A. Badalà, M. La Cognata, R. Nania, M. Osipenko, S. Piantelli, R. Turrisi, L. Barion, S. Capra, D. Carbone, F. Carnesecchi, E.A.R. Casula, C. Chatterjee, G.F. Ciani, R. Depalo, A. Di Nitto, A. Fantini, A. Goasduff, G.L. Guardo, A.C. Kraan, A. Manna, L. Marsicano, N.S. Martorana, L. Morales-Gallegos, E. Naselli, A. Scordo, S. Valdré, G. Volpe, Trends in particle and nuclei identification techniques in nuclear physics experiments. Riv. Nuovo Cim. **45**, 189–276 (2022). https://doi.org/10.1007/s40766-021-00028-5
7. T. Marchi, G. Prete, F. Gramegna, A. Andrighetto, P. Antonini, M. Ballan, M. Bellato, L. Bellan, D. Benini, G. Bisoffi, J. Bermudez, G. Benzoni, D. Bortolato, F. Borgna, A. Calore, S. Canella, S. Carturan, N. Ciatara, M. Cinausero, P. Cocconi, A. Cogo, D. Conventi, V. Conte, M. Comunian, L. Costa, S. Corradetti, G. de Angelis, C.D. Martinis, P.D. Ruvo, J. Esposito, E. Fagotti, D. Fabris, P. Favaron, E. Fioretto, A. Galatá, F. Gelain, M. Giacchini, D. Giora, A. Gottardo, M. Gulmini, M. Lollo, A. Lombardi, M. Manzolaro, M. Maggiore, D. Maniero, P.F. Mastinu, A. Monetti, F. Pasquato, R. Pegoraro, A. Pisent, M. Poggi, S. Pavinato, L. Pranovi, D. Pedretti, C. Roncolato, M. Rossignoli, L. Sarchiapone, D. Scarpa, J.J.V. Dobón, V. Volpe, A. Vescovo, D. Zafiropoulos, The SPES facility at Legnaro National Laboratories. J. Phys. Conf. Ser. **1643**(1), 012036 (2020). https://doi.org/10.1088/1742-6596/1643/1/012036
8. https://agenda.infn.it/event/10539/
9. S. Akkoyun, A. Algora, B. Alikhani, F. Ameil, G. de Angelis, L. Arnold, A. Astier, A. Ataç, Y. Aubert, C. Aufranc, A. Austin, S. Aydin, F. Azaiez, S. Badoer, D.L. Balabanski, D. Barrientos, G. Baulieu, R. Baumann, D. Bazzacco, F.A. Beck, T. Beck, P. Bednarczyk, M. Bellato, M.A Bentley, G. Benzoni, R. Berthier, L. Berti, R. Beunard, G. Lo Bianco, B. Birkenbach, P.G. Bizzeti, A.M. Bizzeti-Sona, F. Le Blanc, J.M. Blasco, N. Blasi, D. Bloor, C. Boiano, M. Borsato, D. Bortolato, A.J. Boston, H.C. Boston, P. Bourgault, P. Boutachkov, A. Bouty, A. Bracco, S. Brambilla, I.P. Brawn, A. Brondi, S. Broussard, B. Bruyneel, D. Bucurescu, I. Burrows, A. Bürger, S. Cabaret, B. Cahan, E. Calore, F. Camera, A. Capsoni, F. Carrió, G. Casati, M. Castoldi, B. Cederwall, J.-L. Cercus, V. Chambert, M. El Chambit, R. Chapman, L. Charles, J. Chavas, E. Clément, P. Cocconi, S. Coelli, P.J. Coleman-Smith, A. Colombo, S. Colosimo, C. Commeaux, D. Conventi, R.J. Cooper, A. Corsi, A. Cortesi, L. Costa, F.C.L. Crespi, J.R. Cresswell, D.M. Cullen, D. Curien, A. Czermak, D. Delbourg, R. Depalo, T. Descombes, P. Désesquelles, P. Detistov, C. Diarra, F. Didierjean, M.R. Dimmock, Q.T. Doan, C. Domingo-Pardo, M. Doncel, F. Dorangeville, N. Dosme, Y. Drouen, G. Duchêne, B. Dulny, J. Eberth, P. Edelbruck, J. Egea, T. Engert, M.N. Erduran, S. Ertürk, C. Fanin, S. Fantinel, E. Farnea, T. Faul, M. Filliger, F. Filmer, C. Finck, G. de France, A. Gadea, W. Gast, A. Geraci, J. Gerl, R. Gernhäuser, A. Giannatiempo, A. Giaz, L. Gibelin, A. Givechev, N. Goel, V. González, A. Gottardo, X. Grave, J. Grębosz, R. Griffiths, A.N. Grint, P. Gros, L. Guevara, M. Gulmini, A. Görgen, H.T.M. Ha, T. Habermann, L.J. Harkness, H. Harroch, K. Hauschild, C. He, A. Hernández-Prieto, B. Hervieu, H. Hess, T. Hüyük, E. Ince, R. Isocrate, G. Jaworski, A. Johnson, J. Jolie, P. Jones, B. Jonson, P. Joshi, D.S. Judson, A. Jungclaus, M. Kaci, N. Karkour, M. Karolak, A. Kaşkaş, M. Kebbiri, R.S. Kempley, A. Khaplanov, S. Klupp, M. Kogimtzis, I. Kojouharov, A. Korichi, W. Korten, T. Kröll, R. Krücken, N. Kurz, B.Y. Ky, M. Labiche, X. Lafay, L. Lavergne, I.H. Lazarus, S. Leboutelier, F. Lefebvre, E. Legay, L. Legeard, F. Lelli, S.M. Lenzi, S. Leoni, A. Lermitage, D. Lersch, J. Leske, S.C. Letts, S. Lhenoret, R.M. Lieder, D. Linget, J. Ljungvall, A. Lopez-Martens, A. Lotodé, S. Lunardi, A. Maj, J. van der Marel, Y. Mariette, N. Mărginean, R. Marginean, G. Maron, A.R. Mather, W. Meczyński, V. Mendéz, P. Medina, B. Melon, R. Menegazzo, D. Mengoni, E. Merchan, L. Mihailescu, C. Michelagnoli, J. Mierzejewski, L. Milechina, B. Million, K. Mitev, P. Molini, D. Montanari, S. Moon, F. Morbiducci, R. Moro, P.S. Morrall, O. Möller, A. Nannini, D.R. Napoli, L. Nelson, M. Nespolo, V.L. Ngo, M. Nicoletto, R. Nicolini, Y. Le Noa, P.J. Nolan, M. Norman, J. Nyberg, A. Obertelli, A. Olariu, R. Orlandi, D.C. Oxley, C. Özben, M. Ozille, C. Oziol, E. Pachoud, M. Palacz, J. Palin, J. Pancin, C. Parisel, P. Pariset, G. Pascovici, R. Peghin, L. Pellegri, A. Perego, S. Perrier, M. Petcu, P. Petkov, C. Petrache, E. Pierre, N. Pietralla, S. Pietri, M. Pignanelli, I. Piqueras, Z. Podolyák, P. Le Pouhalec, J. Pouthas, D. Pugnére, V.F.E. Pucknell, A. Pullia, B. Quintana, R. Raine, G. Rainovski, L. Ramina, G. Rampazzo, G. La Rana, M. Rebeschini, F. Recchia, N. Redon, M. Reese, P. Reiter, P.H. Regan, S. Riboldi, M. Richer, M. Rigato, S. Rigby, G. Ripamonti, A.P. Robinson, J. Robin, J. Roccaz, J.-A. Ropert, B. Rossé, C. Rossi Alvarez, D. Rosso, B. Rubio, D. Rudolph, F. Saillant, E. Şahin, F. Salomon, M.-D.. Salsac, J. Salt, G. Salvato, J. Sampson, E. Sanchis, C. Santos, H. Schaffner, M. Schlarb, D.P. Scraggs, D. Seddon, M. Şenyiğit, M.-H. Sigward, G. Simpson, J. Simpson, M. Slee, J.F. Smith, P. Sona, B. Sowicki, P. Spolaore, C. Stahl, T. Stanios, E. Stefanova, O. Stézowski, J. Strachan, G., Suliman, P.-A. Söderström, J.L. Tain, S. Tanguy, S. Tashenov, C. Theisen, J. Thornhill, F. Tomasi, N. Toniolo, R. Touzery, B. Travers, A. Triossi, M. Tripon, K.M.M. Tun-Lanoë, M. Turcato, C. Unsworth, C.A. Ur, J.J. Valiente-Dobon, V. Vandone, E. Vardaci, R. Venturelli, F. Veronese, C. Veyssiere, E. Viscione, R. Wadsworth, P.M. Walker, N. Warr, C. Weber, D. Weisshaar, D. Wells, O. Wieland, A. Wiens, G. Wittwer, H.J. Wollersheim, F. Zocca, N.V. Zamfir, M. Ziębliński, A. Zucchiatti, AGATA—Advanced GAmma Tracking Array. Nucl. Instrum. Methods Phys. Res. A **668**, 26–58 (2012). https://doi.org/10.1016/j.nima.2011.11.081. arXiv:1111.5731 [physics.ins-det]
10. J.J. Valiente-Dobón, G. Jaworski, A. Goasduff, F.J. Egea, V. Modamio, T. Hüyük, A. Triossi, M. Jastrzab, P.A. Söderström, A. Di Nitto, G. de Angelis, G. de France, N. Erduran, A. Gadea, M. Moszyński, J. Nyberg, M. Palacz, R. Wadsworth, R. Aliaga, C. Aufranc, M. Bézard, G. Baulieu, E. Bissiato, A. Boujrad, I. Burrows, S. Carturan, P. Cocconi, G. Colucci, D. Conventi, M. Cordwell, S. Coudert, J.M. Deltoro, L. Ducroux, T. Dupasquier, S. Ertürk, X. Fabian, V. González, A. Grant, K. Hadyńska-Klęk, A. Illana, M.L. Jurado-Gomez, M. Kogimtzis, I. Lazarus, L. Legeard, J. Ljungvall, G. Pasqualato, R.M. Pérez-Vidal, A. Raggio, D. Ralet, N. Redon, F. Saillant, B. Sayğı, E. Sanchis, M. Scarcioffolo, M. Siciliano, D. Testov, O. Stézowski, M. Tripon, I. Zanon, NEDA-NEutron Detector Array. Nucl. Instrum. Methods Phys. Res. A **927**, 81–86 (2019). https://doi.org/10.1016/j.nima.2019.02.021
11. F. Camera, A. Maj, PARIS White Book. http://slcj.uw.edu.pl/en/the-paris-white-book/ (2021)
12. S. Carboni, S. Barlini, L. Bardelli, N. Le Neindre, M. Bini, B. Borderie, R. Bougault, G. Casini, P. Edelbruck, A. Olmi, G. Pasquali, G. Poggi, M.F. Rivet, A.A. Stefanini, G. Baiocco, R. Berjillos, E. Bonnet, M. Bruno, A. Chbihi, I. Cruceru, M. Degerlier, J.A. Dueñas, E. Galichet, F. Gramegna, A.

Kordyasz, T. Kozik, V.L. Kravchuk, O. Lopez, T. Marchi, I. Martel, L. Morelli, M. Parlog, H. Petrascu, E. Rosato, V. Seredov, E. Vient, M. Vigilante, R. Alba, D. Santonocito, C. Maiolino, Particle identification using the ΔE-E technique and pulse shape discrimination with the silicon detectors of the FAZIA project. Nucl. Instrum. Methods Phys. Res. A **664**(1), 251–263 (2012). https://doi.org/10.1016/j.nima.2011.10.061

13. S. Szilner, C.A. Ur, L. Corradi, N. Marginean, G. Pollarolo, A.M. Stefanini, S. Beghini, B.R. Behera, E. Fioretto, A. Gadea, B. Guiot, A. Latina, P. Mason, G. Montagnoli, F. Scarlassara, M. Trotta, G. de Angelis, F.D. Vedova, E. Farnea, F. Haas, S. Lenzi, S. Lunardi, R. Mărginean, R. Menegazzo, D.R. Napoli, M. Nespolo, I.V. Pokrovsky, F. Recchia, M. Romoli, M.-D. Salsac, N. Soić, J.J. Valiente-Dobón, Multinucleon transfer reactions in closed-shell nuclei. Phys. Rev. C **76**, 024604 (2007). https://doi.org/10.1103/PhysRevC.76.024604
14. D. Montanari, E. Farnea, S. Leoni, G. Pollarolo, L. Corradi, G. Benzoni, A. Gadea, E. Fioretto, A. Latina, G. Montagnoli, F. Scarlassara, A.M. Stefanini, S. Szilner, Response function of the magnetic spectrometer PRISMA. Eur. Phys. J. A **47**, 4 (2011). https://doi.org/10.1140/epja/i2011-11004-9
15. G. Montagnoli, A.M. Stefanini, M. Trotta, S. Beghini, M. Bettini, F. Scarlassara, V. Schiavon, L. Corradi, B.R. Behera, E. Fioretto, A. Gadea, A. Latina, S. Szilner, L. Donà, M. Rigato, N.A. Kondratiev, A.Y. Chizhov, G. Kniajeva, E.M. Kozulin, I.V. Pokrovskiy, V.M. Voskressensky, D. Ackermann, The large-area micro-channel plate entrance detector of the heavy-ion magnetic spectrometer PRISMA. Nucl. Instrum. Methods Phys. Res. A **547**(2), 455–463 (2005). https://doi.org/10.1016/j.nima.2005.03.158
16. S. Beghini, L. Corradi, E. Fioretto, A. Gadea, A. Latina, G. Montagnoli, F. Scarlassara, A.M. Stefanini, S. Szilner, M. Trotta, A.M. Vinodkumar, The focal plane detector of the magnetic spectrometer PRISMA. Nucl. Instrum. Methods Phys. Res. A **551**(2), 364–374 (2005). https://doi.org/10.1016/j.nima.2005.06.058
17. A. Gadea, N. Marginean, L. Corradi, S.M. Lenzi, C.A. Ur, E. Farnea, G. de Angelis, E. Fioretto, D.R. Napoli, A.M. Stefanini, S. Szilner, M. Axiotis, B.R. Behera, A. Latina, C. Rusu, W. Zhimin, D. Bazzacco, S. Beghini, S. Lunardi, G. Montagnoli, R. Menegazzo, F. Scarlassara, F.D. Vedova, M. Nespolo, A. Bracco, F. Camera, S. Leoni, B. Million, M. Pignanelli, G. Pollarolo, M. Trotta, P.G. Bizzeti, A.M. Bizzeti-Sona, D. Curien, P. Medina, M. Chambit, R. Chapman, X. Liang, S.J. Freeman, A. Smith, B.J. Varley, V. Pucknell, R. Lemmon, The CLARA-PRISMA setup installed at LNL: first results. J. Phys. G **31**(10), 1443–1448 (2005). https://doi.org/10.1088/0954-3899/31/10/011
18. A. Gadea, E. Farnea, J.J. Valiente-Dobón, B. Million, D. Mengoni, D. Bazzacco, F. Recchia, A. Dewald, T. Pissulla, W. Rother, G. de Angelis, A. Austin, S. Aydin, S. Badoer, M. Bellato, G. Benzoni, L. Berti, R. Beunard, B. Birkenbach, E. Bissiato, N. Blasi, C. Boiano, D. Bortolato, A. Bracco, S. Brambilla, B. Bruyneel, E. Calore, F. Camera, A. Capsoni, J. Chavas, P. Cocconi, S. Coelli, A. Colombo, D. Conventi, L. Costa, L. Corradi, A. Corsi, A. Cortesi, F.C.L. Crespi, N. Dosme, J. Eberth, S. Fantinel, C. Fanin, E. Fioretto, C. Fransen, A. Giaz, A. Gottardo, X. Grave, J. Gręgosz, R. Griffiths, E. Grodner, M. Gulmini, T. Habermann, C. He, H. Hess, R. Isocrate, J. Jolie, P. Jones, A. Latina, E. Legay, S. Lenzi, S. Leoni, F. Lelli, D. Lersch, S. Lunardi, G. Maron, R. Menegazzo, C. Michelagnoli, P. Molini, G. Montagnoli, D. Montanari, O. Möller, D.R. Napoli, M. Nicoletto, R. Nicolini, M. Ozille, G. Pascovici, R. Peghin, M. Pignanelli, V. Pucknell, A. Pullia, L. Ramina, G. Rampazzo, M. Rebeschini, P. Reiter, S. Riboldi, M. Rigato, C. Rossi Alvarez, D. Rosso, G. Salvato, J. Strachan, E. Sahin, F. Scarlassara, J. Simpson, A.M. Stefanini, O. Stézowski, F. Tomasi, N. Toniolo, A. Triossi, M. Turcato, C.A. Ur, V. Vandone, R. Venturelli, F. Veronese, C. Veyssiere, E. Viscione, O. Wieland, A. Wiens, F. Zocca, A. Zucchiatti, Conceptual design and infrastructure for the installation of the first AGATA sub-array at LNL. Nucl. Instrum. Methods Phys. Res. A **A654**, 88–96 (2011). https://doi.org/10.1016/j.nima.2011.06.004
19. A. Goasduff, D. Mengoni, F. Recchia, J.J. Valiente-Dobón, R. Menegazzo, G. Benzoni, D. Barrientos, M. Bellato, N. Bez, M. Biasotto, N. Blasi, C. Boiano, A. Boso, S. Bottoni, A. Bracco, S. Brambilla, D. Brugnara, F. Camera, S. Capra, A. Capsoni, P. Cocconi, S. Coelli, M.L. Cortés, F.C.L. Crespi, G. de Angelis, F.J. Egea, C. Fanin, S. Fantinel, A. Gadea, E.R. Gamba, A. Gambalonga, C. Gesmundo, G. Gosta, A. Gottardo, A. Gozzelino, E.T. Gregor, M. Gulmini, J. Ha, K. Hadyńska-Klęk, A. Illana, R. Isocrate, G. Jaworski, P.R. John, S.M. Lenzi, S. Leoni, S. Lunardi, M. Magalini, N. Marchini, B. Million, V. Modamio, A. Nannini, D.R. Napoli, G. Pasqualato, J. Pellumaj, R.M. Pérez-Vidal, S. Pigliapoco, M. Polettini, C. Porzio, A. Pullia, L. Ramina, G. Rampazzo, M. Rampazzo, M. Rebeschini, K. Rezynkina, M. Rocchini, M. Romanato, D. Rosso, A. Saltarelli, M. Scarcioffolo, M. Siciliano, D.A. Testov, D. Tomasella, F. Tomasi, N. Toniolo, C.A. Ur, S. Ventura, F. Veronese, E. Viscione, V. Volpe, O. Wieland, I. Zanon, S. Ziliani, G. Zhang, D. Bazzacco, The GALILEO γ-ray array at the Legnaro National Laboratories. Nucl. Instrum. Methods Phys. Res. A **1015**, 165753 (2021). https://doi.org/10.1016/j.nima.2021.165753
20. M. Rocchini, K. Hadyńska-Klęk, A. Nannini, J.J. Valiente-Dobón, A. Goasduff, D. Testov, D. Mengoni, P.R. John, M. Siciliano, B. Melon, P. Sona, M. Ottanelli, A. Perego, M. Chiari, M. Zielińska, D. Bazzacco, G. Benzoni, S. Bettarini, M. Brianzi, F. Camera, P. Cocconi, C. Czelusniak, D.T. Doherty, M. Komorowska, N. Marchini, M. Matejska-Minda, P.J. Napiorkowski, E. Pasquali, L. Ramina, M. Rampazzo, F. Recchia, D. Rosso, L. Sottili, A. Tredici, SPIDER: a Silicon PIe DEtectoR for low-energy Coulomb-excitation measurements. Nucl. Instrum. Methods Phys. Res. A **971**, 164030 (2020). https://doi.org/10.1016/j.nima.2020.164030
21. D. Testov, D. Mengoni, A. Goasduff, A. Gadea, R. Isocrate, P.R. John, G. de Angelis, D. Bazzacco, C. Boiano, A. Boso, P. Cocconi, J.A. Dueñas, L. Grassi, F.J. Egea Canet, K. Hadyńska-Klęk, G. Jaworski, S. Lunardi, R. Menegazzo, D.R. Napoli, F. Recchia, M. Siciliano, Valiente-Dobón: the 4π highly-efficient light-charged-particle detector EUCLIDES, installed at the GALILEO array for in-beam γ-ray spectroscopy. Eur. Phys. J. A **55**, 47 (2019). https://doi.org/10.1140/epja/i2019-12714-6
22. D. Mengoni, J.A. Dueñas, M. Assié, C. Boiano, P.R. John, R.J. Aliaga, D. Beaumel, S. Capra, A. Gadea, V. Gonzáles, A. Gottardo, L. Grassi, V. Herrero-Bosch, T. Houdy, I. Martel, V.V. Parkar, R. Perez-Vidal, A. Pullia, E. Sanchis, A. Triossi, J.J. Valiente Dobón, Digital pulse-shape analysis with a TRACE early silicon prototype. Nucl. Instrum. Methods Phys. Res. A **764**, 241–246 (2014). https://doi.org/10.1016/j.nima.2014.07.054
23. M. Bruno, F. Gramegna, T. Marchi, L. Morelli, G. Pasquali, G. Casini, U. Abbondanno, G. Baiocco, L. Bardelli, S. Barlini, M. Bini, S. Carboni, M. Cinausero, M. D'Agostino, M. Degerlier, V.L. Kravchuk, E. Geraci, P.F. Mastinu, A. Ordine, S. Piantelli, G. Poggi, A. Moroni, GARFIELD + RCo digital upgrade: a modern set-up for mass and charge identification of heavy-ion reaction products. Eur. Phys. J. A **49**, 128 (2013). https://doi.org/10.1140/epja/i2013-13128-2
24. T. Roger, J. Pancin, G.F. Grinyer, B. Mauss, A.T. Laffoley, P. Rosier, H. Alvarez-Pol, M. Babo, B. Blank, M. Caamaño, S. Ceruti, J. Daemen, S. Damoy, B. Duclos, B. Fernández-Domínguez, F. Flavigny, J. Giovinazzo, T. Goigoux, J.L. Henares, P. Konczykowski, T. Marchi, G. Lebertre, N. Lecesne, L. Legeard, C. Maugeais, G. Minier, B. Osmond, J.L. Pedroza, J. Pibernat, O. Poleshchuk, E.C. Pollacco, R. Raabe, B. Raine, F. Renzi, F. Saillant, P. Sénécal, P. Sizun, D. Suzuki, J.A. Swartz, C. Wouters, G. Wittwer, J.C. Yang, Demonstrator detection system for the active target and time projection chamber (ACTAR TPC) project. Nucl. Instrum. Methods Phys. Res. A **895**, 126–134 (2018). https://doi.org/10.1016/j.nima.2018.04.003
25. D. Dell'Aquila, I. Lombardo, G. Verde, M. Vigilante, G. Ausanio, A. Ordine, M. Miranda, M. De Luca, R. Alba, L. Augey, S. Barlini, E. Bonnet, B. Borderie, R. Bougault, M. Bruno, A. Camaiani, G. Casini, A. Chbihi, M. Cicerchia, M. Cinausero, D. Fabris, Q. Faible, L. Francalanza, J.D. Frankland, L. Grassi, F. Gramegna, D. Gruyer, A.J. Kordyasz, T. Kozik, R. LaTorre, N. Le Neindre, O. Lopez, T. Marchi, L. Morelli, P. Ottanelli, M. Parlog, G. Pastore, G. Pasquali, S. Piantelli, D. Santonocito, A.A. Stefanini, G. Tortone, S. Valdré, E. Vient, Oscar: a new modular device for the identification and correlation of low energy particles. Nucl. Instrum. Methods Phys. Res. Sect. A **877**, 227–237 (2018). https://doi.org/10.1016/j.nima.2017.09.046
26. S. Beghini, C. Signorini, S. Lunardi, M. Morando, G. Fortuna, A.M. Stefanini, W. Meczynski, R. Pengo, An electrostatic beam separator for evaporation residue detection. Nucl. Instrum. Methods Phys. Res. A **239**(3), 585–591 (1985). https://doi.org/10.1016/0168-9002(85)90040-3
27. M. Mazzocco, F. Farinon, T. Glodariu, H. Geissel, A. Guglielmetti, N. Iwasa, M. La Commara, B. Martin, C. Mazzocchi, D. Pierroutsakou, M. Romoli, M. Sandoli, C. Signorini, F. Soramel, L. Stroe, E. Vardaci, H. Weick, M. Winkler, Production and separation of light low-energy radioactive ion beams

with the EXOTIC beam-line at LNL. Nucl. Instrum. Methods Phys. Res. B **266**(19), 4665–4669 (2008). https://doi.org/10.1016/j.nimb.2008.05.112. (**Proceedings of the XVth International Conference on Electromagnetic Isotope Separators and Techniques Related to their Applications**)
28. D. Pierroutsakou, A. Boiano, C. Boiano, P. Di Meo, M. La Commara, C. Manea, M. Mazzocco, M. Nicoletto, C. Parascandolo, C. Signorini, F. Soramel, E. Strano, N. Toniolo, D. Torresi, G. Tortone, A. Anastasio, M. Bettini, C. Cassese, L. Castellani, D. Corti, L. Costa, B. De Fazio, G. Galet, T. Glodariu, J. Grebosz, A. Guglielmetti, P. Molini, G. Pontoriere, R. Rocco, M. Romoli, L. Roscilli, M. Sandoli, L. Stroe, M. Tessaro, P.G. Zatti, The experimental set-up of the rib in-flight facility exotic. Nucl. Instrum. Methods Phys. Res. Sect. A **834**, 46–70 (2016). https://doi.org/10.1016/j.nima.2016.07.019
29. E. Clément, C. Michelagnoli, G. de France, H.J. Li, A. Lemasson, C. Barthe Dejean, M. Beuzard, P. Bougault, J. Cacitti, J.-L. Foucher, G. Fremont, P. Gangnant, J. Goupil, C. Houarner, M. Jean, A. Lefevre, L. Legeard, F. Legruel, C. Maugeais, L. Ménager, N. Ménard, H. Munoz, M. Ozille, B. Raine, J.A. Ropert, F. Saillant, C. Spitaels, M. Tripon, P. Vallerand, G. Voltolini, W. Korten, M.-D. Salsac, C. Theisen, M. Zielińska, T. Joannem, M. Karolak, M. Kebbiri, A. Lotode, R. Touzery, C. Walter, A. Korichi, J. Ljungvall, A. Lopez-Martens, D. Ralet, N. Dosme, X. Grave, N. Karkour, X. Lafay, E. Legay, I. Kojouharov, C. Domingo-Pardo, A. Gadea, R.M. Pérez-Vidal, J.V. Civera, B. Birkenbach, J. Eberth, H. Hess, L. Lewandowski, P. Reiter, A. Nannini, G. de Angelis, G. Jaworski, P. John, D.R. Napoli, J.J. Valiente-Dobón, D. Barrientos, D. Bortolato, G. Benzoni, A. Bracco, S. Brambilla, F. Camera, F.C.L. Crespi, S. Leoni, B. Million, A. Pullia, O. Wieland, D. Bazzacco, S.M. Lenzi, S. Lunardi, R. Menegazzo, D. Mengoni, F. Recchia, M. Bellato, R. Isocrate, F.J. Egea Canet, F. Didierjean, G. Duchêne, R. Baumann, M. Brucker, E. Dangelser, M. Filliger, H. Friedmann, G. Gaudiot, J.-N. Grapton, H. Kocher, C. Mathieu, M.-H. Sigward, D. Thomas, S. Veeramootoo, J. Dudouet, O. Stézowski, C. Aufranc, Y. Aubert, M. Labiche, J. Simpson, I. Burrows, P.J. Coleman-Smith, A. Grant, I.H. Lazarus, P.S. Morrall, V.F.E. Pucknell, A. Boston, D.S. Judson, N. Lalović, J. Nyberg, J. Collado, V. González, I. Kuti, B.M. Nyakó, A. Maj, M. Rudigier, Conceptual design of the AGATA 1π array at GANIL. Nucl. Instrum. Methods Phys. Res. A **855**, 1–12 (2017). https://doi.org/10.1016/j.nima.2017.02.063
30. C. Müller-Gatermann, F. von Spee, A. Goasduff, D. Bazzacco, M. Beckers, T. Braunroth, A. Boso, P. Cocconi, G. de Angelis, A. Dewald, C. Fransen, A. Goldkuhle, A. Gottardo, A. Gozzelino, K. Hadyńska-Klęk, G. Jawroski, P.R. John, J. Jolie, S.M. Lenzi, J. Litzinger, R. Menegazzo, D. Mengoni, D.R. Napoli, F. Recchia, M. Siciliano, D. Testov, S. Thiel, J.J. Valiente-Dobón, K.O. Zell, A new dedicated plunger device for the GALILEO γ-ray detector array. Nucl. Instrum. Methods Phys. Res. A **920**, 95–99 (2019). https://doi.org/10.1016/j.nima.2018.12.077
31. A. Gottardo, J.J. Valiente-Dobón, A. Gadea, R. Chapman, P.H. Regan, S. Aydin, S. Brambilla, R.J. Casperson, G. de Angelis, F. Della Vedova, D. O'Donnel, E. Farnea, S.J. Freeman, G. Jones, N.A. Kondratiev, E.M. Kozulin, S. Lunardi, N. Marginean, D. Mengoni, D.R. Napoli, J. Ollier, R. Orlandi, S. Pietri, Z. Podolyak, F. Recchia, E. Sahin, J.F. Smith, R. Spohw, S.J. Steer, N. Thompson, C.A. Ur, P. Wady, Z. Wang, V. Werner, Performance of the DANTE detector. Nucl. Phys. A **805**, 606–608 (2008). https://doi.org/10.1016/j.nuclphysa.2008.02.206
32. R.J. Aliaga, V. Herrero-Bosch, S. Capra, A. Pullia, J.A. Dueñas, L. Grassi, A. Triossi, C. Domingo-Pardo, R. Gadea, V. González, T. Hüyük, E. Sanchís, A. Gadea, D. Mengoni, Conceptual design of the TRACE detector readout using a compact, dead time-less analog memory ASIC. Nucl. Instrum. Methods Phys. Res. A **800**, 34–39 (2015). https://doi.org/10.1016/j.nima.2015.07.067
33. M. Assié, E. Clément, A. Lemasson, D. Ramos, A. Raggio, I. Zanon, F. Galtarossa, C. Lenain, J. Casal, F. Flavigny, A. Matta, D. Mengoni, D. Beaumel, Y. Blumenfeld, R. Borcea, D. Brugnara, W. Catford, F. de Oliveira, F. Delaunay, N. De Séréville, F. Didierjean, C.A. Diget, J. Dudouet, B. Fernández-Domínguez, C. Fougères, G. Frémont, V. Girard-Alcindor, A. Giret, A. Goasduff, A. Gottardo, J. Goupil, F. Hammache, P.R. John, A. Korichi, L. Lalanne, S. Leblond, A. Lefevre, F. Legruel, L. Ménager, B. Million, C. Nicolle, F. Noury, E. Rauly, K. Rezynkina, E. Rindel, J.S. Rojo, M. Siciliano, M. Stanoiu, I. Stefan, L. Vatrinet, The MUGAST-AGATA-VAMOS campaign: set-up and performances. Nucl. Instrum. Methods Phys. Res. A **1014**, 165743 (2021). https://doi.org/10.1016/j.nima.2021.165743. arXiv:2104.10707 [physics.ins-det]
34. D. Mengoni, J.A. Dueñas, M. Assié, C. Boiano, P.R. John, R.J. Aliaga, D. Beaumel, S. Capra, A. Gadea, V. Gonzáles, A. Gottardo, L. Grassi, V. Herrero-Bosch, T. Houdy, I. Martel, V.V. Parkar, R. Perez-Vidal, A. Pullia, E. Sanchis, A. Triossi, J.J. Valiente-Dobón, N. Cieplicka-Orynczak, D. Mengoni, M. Ciemala, S. Leoni, B. Fornal, J.A. Duenas, S. Brambilla, C. Boiano, P.R. John, D. Bazzacco, G. Benzoni, G. Bocchi, S. Capra, F.C.L. Crespi, A. Goasduff, K. Hadyńska-Klęk, L.W. Iskra, G. Jaworski, F. Recchia, M. Siciliano, D. Testov, J.J. Valiente-Dobón, Towards the lowest-energy limit for light ions identification with silicon pixel-type detectors. Eur. Phys. J. A **54**, 209 (2018). https://doi.org/10.1140/epja/i2018-12644-9
35. M. Sedlak, A. Gottardo, A. Goasduff, R. Pengo, F. Crespi, I. Lombardo, I. Zanon, The Cryogenic TArgets for DIrect Reactions (CTADIR) project. Nuovo Cim. C **45**, 1–4 (2022). https://doi.org/10.1393/ncc/i2022-22108-6
36. F. Favela, L. Acosta, E. Andrade, V. Araujo, A. Huerta, O.G. de Lucio, G. Murillo, M.E. Ortiz, R. Policroniades, P. Santa Rita, A. Varela, E. Chávez, New supersonic gas jet target for low energy nuclear reaction studies. Phys. Rev. Accel. Beams **18**, 123502 (2015). https://doi.org/10.1103/PhysRevSTAB.18.123502
37. N. Marchini, A. Nannini, M. Ottanelli, A. Saltarelli, M. Rocchini, G. Benzoni, E.R. Gamba, A. Goasduff, A. Gottardo, T. Krings, M. Perri, SLICES: Spes Low-energy Internal Conversion Electron Spectrometer. Nucl. Instrum. Methods Phys. Res. A **1020**, 165860 (2021). https://doi.org/10.1016/j.nima.2021.165860
38. D. Bisello, J. Esposito, P. Mastinu, G. Prete, L. Silvestrin, J. Wyss, The Phase 0 of the NEPIR project at LNL. Nuovo Cim. C (2019). https://doi.org/10.1393/ncc/i2019-19072-3
39. http://www.ucans.org/link.html/
40. https://elena-neutron.iff.kfa-juelich.de/projects/
41. R. Alfonso Barrera, D. Bisello, J. Esposito, P.F. Mastinu, G. Prete, L. Silvestrin, J. Wyss, CoolGAL: a Galinstan bathed Be fast neutron production target at the NEPIR facility. Eur. Phys. J. Web Conf. **231**, 03002 (2020). https://doi.org/10.1051/epjconf/202023103002
42. P.F. Mastinu, D. Bisello, R.A. Barrera, I. Porras, G. Prete, J. Wyss, Fast neutrons at LNL Legnaro. J. Neutron Res. **22**, 233 (2020). https://doi.org/10.3233/JNR-200156
43. The QMN beam line of the neutron-induced single event effects facility at the 70 MeV cyclotron of LNL-INFN. Phys. Procedia **60**, 271–277 (2014). https://doi.org/10.1016/j.phpro.2014.11.037
44. A. Coc, E. Vangioni-Flam, P. Descouvemont, A. Adahchour, C. Angulo, Updated big bang nucleosynthesis compared with Wilkinson microwave anisotropy probe observations and the abundance of light elements. Astrophys. J. **600**(2), 544–552 (2004). https://doi.org/10.1086/380121. arXiv:astro-ph/0309480 [astro-ph]
45. R.H. Cyburt, B.D. Fields, K.A. Olive, T.-H. Yeh, Big bang nucleosynthesis: present status. Rev. Mod. Phys. **88**(1), 015004 (2016). https://doi.org/10.1103/RevModPhys.88.015004. arXiv:1505.01076 [astro-ph.CO]
46. R.J. Cooke, M. Pettini, C.C. Steidel, One percent determination of the primordial deuterium abundance. Astrophys. J. **855**, 102 (2018). https://doi.org/10.3847/1538-4357/aaab53. (**[astro-ph.CO]**)
47. R.J. Cooke, M. Pettini, K.M. Nollett, R. Jorgenson, The primordial deuterium abundance of the most metal-poor damped Lyα system. Astrophys. J. **830**, 148 (2016). https://doi.org/10.3847/0004-637X/830/2/148. (**[astro-ph.CO]**)
48. O. Pisanti, G. Mangano, G. Miele, P. Mazzella, Primordial deuterium after LUNA: concordances and error budget. J. Cosmol. Astropart. Phys. **04**, 020 (2021). https://doi.org/10.1088/1475-7516/2021/04/020. (**[astro-ph.CO]**)
49. T.-H. Yeh, K.A. Olive, B.D. Fields, The impact of new d(p,γ)^{3}He rates on Big Bang Nucleosynthesis. J. Cosmol. Astropart. Phys. **03**, 046 (2021). https://doi.org/10.1088/1475-7516/2021/03/046. (**[astro-ph.CO]**)

50. C. Pitrou, A. Coc, J.-P. Uzan, E. Vangioni, A new tension in the cosmological model from primordial deuterium? Mon. Not. R. Astron. Soc. **502**, 2474–2481 (2021). https://doi.org/10.1093/mnras/stab135. (**[astro-ph.CO]**)
51. J. Moscoso, R.S. de Souza, A. Coc, C. Iliadis, Bayesian estimation of the D(p,γ)^{3}He thermonuclear reaction rate. Astrophys. J. **923**, 49 (2021). https://doi.org/10.3847/1538-4357/ac1db0
52. F. Cavanna, P. Prati, Direct measurement of nuclear cross-section of astrophysical interest: results and perspectives. Int. J. Mod. Phys. A **33**, 1843010–346 (2018). https://doi.org/10.1142/S0217751X18430108
53. V. Mossa, K. Stöckel, F. Cavanna, F. Ferraro, M. Aliotta, F. Barile, D. Bemmerer, A. Best, A. Boeltzig, C. Broggini, C.G. Bruno, A. Caciolli, T. Chillery, G.F. Ciani, P. Corvisiero, L. Csedreki, T. Davinson, R. Depalo, A. Di Leva, Z. Elekes, E.M. Fiore, A. Formicola, Z. Fülöp, G. Gervino, A. Guglielmetti, C. Gustavino, G. Gyürky, G. Imbriani, M. Junker, A. Kievsky, I. Kochanek, M. Lugaro, L.E. Marcucci, G. Mangano, P. Marigo, E. Masha, R. Menegazzo, F.R. Pantaleo, V. Paticchio, R. Perrino, D. Piatti, O. Pisanti, P. Prati, L. Schiavulli, O. Straniero, T. Szücs, M.P. Takács, D. Trezzi, M. Viviani, S. Zavatarelli, The baryon density of the Universe from an improved rate of deuterium burning. Nature **587**, 210–213 (2020). https://doi.org/10.1038/s41586-020-2878-4
54. S. Turkat, S. Hammer, E. Masha, S. Akhmadaliev, D. Bemmerer, M. Grieger, T. Hensel, J. Julin, M. Koppitz, F. Ludwig, C. Möckel, S. Reinicke, R. Schwengner, K. Stöckel, T. Szücs, L. Wagner, K. Zuber, Measurement of the ^{2}H(p,γ)^{3}He S factor at 265–1094 keV. Phys. Rev. C **103**(4), 045805 (2021). https://doi.org/10.1103/PhysRevC.103.045805. arXiv:2104.06914 [nucl-ex]
55. L. Sbordone, P. Bonifacio, E. Caffau, H.-G. Ludwig, N.T. Behara, J.I. González Hernández, M. Steffen, R. Cayrel, B. Freytag, C. van't Veer, P. Molaro, B. Plez, T. Sivarani, M. Spite, F. Spite, T.C. Beers, N. Christlieb, P. François, V. Hill, The metal-poor end of the Spite plateau. I. Stellar parameters, metallicities, and lithium abundances. Astron. Astrophys. **522**, 26 (2010). https://doi.org/10.1051/0004-6361/200913282. arXiv:1003.4510 [astro-ph.GA]
56. M. Barbagallo, A. Musumarra, L. Cosentino, E. Maugeri, S. Heinitz, A. Mengoni, R. Dressler, D. Schumann, F. Käppeler, N. Colonna, P. Finocchiaro, M. Ayranov, L. Damone, N. Kivel, O. Aberle, S. Altstadt, J. Andrzejewski, L. Audouin, M. Bacak, J. Balibrea-Correa, S. Barros, V. Bécares, F. Bečvář, C. Beinrucker, E. Berthoumieux, J. Billowes, D. Bosnar, M. Brugger, M. Caamaño, M. Calviani, F. Calviño, D. Cano-Ott, R. Cardella, A. Casanovas, D.M. Castelluccio, F. Cerutti, Y.H. Chen, E. Chiaveri, G. Cortés, M.A. Cortés-Giraldo, S. Cristallo, M. Diakaki, C. Domingo-Pardo, E. Dupont, I. Duran, B. Fernandez-Dominguez, A. Ferrari, P. Ferreira, W. Furman, S. Ganesan, A. García-Rios, A. Gawlik, T. Glodariu, K. Göbel, I.F. Gonçalves, E. González-Romero, E. Griesmayer, C. Guerrero, F. Gunsing, H. Harada, T. Heftrich, J. Heyse, D.G. Jenkins, E. Jericha, T. Katabuchi, P. Kavrigin, A. Kimura, M. Kokkoris, M. Krtička, E. Leal-Cidoncha, J. Lerendegui, C. Lederer, H. Leeb, S. Lo Meo, S.J. Lonsdale, R. Losito, D. Macina, J. Marganiec, T. Martínez, C. Massimi, P. Mastinu, M. Mastromarco, A. Mazzone, E. Mendoza, P.M. Milazzo, F. Mingrone, M. Mirea, S. Montesano, R. Nolte, A. Oprea, A. Pappalardo, N. Patronis, A. Pavlik, J. Perkowski, M. Piscopo, A. Plompen, I. Porras, J. Praena, J. Quesada, K. Rajeev, T. Rauscher, R. Reifarth, A. Riego-Perez, P. Rout, C. Rubbia, J. Ryan, M. Sabate-Gilarte, A. Saxena, P. Schillebeeckx, S. Schmidt, P. Sedyshev, A.G. Smith, A. Stamatopoulos, G. Tagliente, J.L. Tain, A. Tarifeño-Saldivia, L. Tassan-Got, A. Tsinganis, S. Valenta, G. Vannini, V. Variale, P. Vaz, A. Ventura, V. Vlachoudis, R. Vlastou, J. Vollaire, A. Wallner, S. Warren, M. Weigand, C. Weiß, C. Wolf, P.J. Woods, T. Wright, P. Žugec, n_TOF collaboration: ^{7}Be(n,α)^{4}He reaction and the cosmological lithium problem: measurement of the cross section in a wide energy range at n_TOF at CERN. Phys. Rev. Lett. **117**(15), 152701 (2016). https://doi.org/10.1103/PhysRevLett.117.152701. arXiv:1606.09420 [nucl-ex]
57. L. Damone, M. Barbagallo, M. Mastromarco, A. Mengoni, L. Cosentino, E. Maugeri, S. Heinitz, D. Schumann, R. Dressler, F. Käppeler, N. Colonna, P. Finocchiaro, J. Andrzejewski, J. Perkowski, A. Gawlik, O. Aberle, S. Altstadt, M. Ayranov, L. Audouin, M. Bacak, J. Balibrea-Correa, J. Ballof, V. Bécares, F. Bečvář, C. Beinrucker, G. Bellia, A.P. Bernardes, E. Berthoumieux, J. Billowes, M.J.G. Borge, D. Bosnar, A. Brown, A. Brugger, M. Busso, M. Caamaño, F. Calviño, M. Calviani, D. Cano-Ott, R. Cardella, A. Casanovas, D.M. Castelluccio, R. Catherall, F. Cerutti, Y.H. Chen, E. Chiaveri, J.G.M. Correia, G. Cortés, M.A. Cortés-Giraldo, S. Cristallo, M. Diakaki, M. Dietz, C. Domingo-Pardo, A. Dorsival, E. Dupont, I. Duran, B. Fernandez-Dominguez, A. Ferrari, P. Ferreira, W. Furman, S. Ganesan, A. García-Rios, S. Gilardoni, T. Glodariu, K. Göbel, I.F. Gonçalves, E. González-Romero, T.D. Goodacre, E. Griesmayer, C. Guerrero, F. Gunsing, H. Harada, T. Heftrich, J. Heyse, D.G. Jenkins, E. Jericha, K. Johnston, Y. Kadi, A. Kalamara, T. Katabuchi, P. Kavrigin, A. Kimura, N. Kivel, U. Köster, M. Kokkoris, M. Krtička, S. Kurtulgil, E. Leal-Cidoncha, C. Lederer-Woods, H. Leeb, J. Lerendegui-Marco, S. Lo Meo, S.J. Lonsdale, R. Losito, D. Macina, J. Marganiec, B. Marsh, T. Martínez, A. Masi, C. Massimi, P. Mastinu, F. Matteucci, A. Mazzone, E. Mendoza, P.M. Milazzo, F. Mingrone, M. Mirea, A. Musumarra, A. Negret, R. Nolte, A. Oprea, N. Patronis, A. Pavlik, L. Piersanti, M. Piscopo, A. Plompen, I. Porras, J. Praena, J.M. Quesada, D. Radeck, K. Rajeev, T. Rauscher, R. Reifarth, A. Riego-Perez, S. Rothe, P. Rout, C. Rubbia, J. Ryan, M. Sabaté-Gilarte, A. Saxena, J. Schell, P. Schillebeeckx, S. Schmidt, P. Sedyshev, C. Seiffert, A.G. Smith, N.V. Sosnin, A. Stamatopoulos, T. Stora, G. Tagliente, J.L. Tain, A. Tarifeño-Saldivia, L. Tassan-Got, A. Tsinganis, S. Valenta, G. Vannini, V. Variale, P. Vaz, A. Ventura, V. Vlachoudis, R. Vlastou, A. Wallner, S. Warren, M. Weigand, C. Weiß, C. Wolf, P.J. Woods, T. Wright, P., Žugec, n_TOF collaboration: ^{7}Be(n,p)^{7}Li reaction and the cosmological lithium problem: measurement of the cross section in a wide energy range at n_TOF at CERN. Phys. Rev. Lett. **121**(4), 042701 (2018). https://doi.org/10.1103/PhysRevLett.121.042701. arXiv:1803.05701 [nucl-ex]
58. S.M. Ali, D. Gupta, K. Kundalia, S.K. Saha, O. Tengblad, J.D. Ovejas, A. Perea, I. Martel, J. Cederkall, J. Park, S. Szwec, Resonance excitations in ^{7}Be(d, p)^{8}be* to address the cosmological lithium problem. Phys. Rev. Lett. **128**, 252701 (2022). https://doi.org/10.1103/PhysRevLett.128.252701
59. A. Tumino, C.A. Bertulani, M. La Cognata, L. Lamia, R.G. Pizzone, S. Romano, S. Typel, The Trojan horse method: a nuclear physics tool for astrophysics. Annu. Rev. Nucl. Part. Sci. **71**(1), 345–376 (2021). https://doi.org/10.1146/annurev-nucl-102419-033642
60. L. Lamia, M. Mazzocco, R.G. Pizzone, S. Hayakawa, M. La Cognata, C. Spitaleri, C.A. Bertulani, A. Boiano, C. Boiano, C. Broggini, A. Caciolli, S. Cherubini, G. D'Agata, H. da Silva, R. Depalo, F. Galtarossa, G.L. Guardo, M. Gulino, I. Indelicato, M. La Commara, G. La Rana, R. Menegazzo, J. Mrazek, A. Pakou, C. Parascandolo, D. Piatti, D. Pierroutsakou, S.M.R. Puglia, S. Romano, G.G. Rapisarda, A.M. Sánchez-Benítez, M.L. Sergi, O. Sgouros, F. Soramel, V. Soukeras, R. Spartá, E. Strano, D. Torresi, A. Tumino, H. Yamaguchi, G.L. Zhang, Cross-section measurement of the cosmologically relevant ^{7}Be(n,α)^{4}He reaction over a broad energy range in a single experiment. Astrophys. J. **879**(1), 23 (2019). https://doi.org/10.3847/1538-4357/ab2234
61. L. Lamia, C. Spitaleri, C.A. Bertulani, S.Q. Hou, M. La Cognata, R.G. Pizzone, S. Romano, M.L. Sergi, A. Tumino, On the determination of the ^{7}Be(n,α)^{4}He reaction cross section at BBN energies. Astrophys. J. **850**(2), 175 (2017). https://doi.org/10.3847/1538-4357/aa965c
62. S. Hayakawa, M. La Cognata, L. Lamia, H. Yamaguchi, D. Kahl, K. Abe, H. Shimizu, L. Yang, O. Beliuskina, S.M. Cha, K.Y. Chae, S. Cherubini, P. Figuera, Z. Ge, M. Gulino, J. Hu, A. Inoue, N. Iwasa, A. Kim, D. Kim, G. Kiss, S. Kubono, M. La Commara, M. Lattuada, E.J. Lee, J.Y. Moon, S. Palmerini, C. Parascandolo, S.Y. Park, V.H. Phong, D. Pierroutsakou, R.G. Pizzone, G.G. Rapisarda, S. Romano, C. Spitaleri, X.D. Tang, O. Trippella, A. Tumino, N.T. Zhang, Constraining the primordial lithium abundance: new cross section measurement of the ^{7}Be + n reactions updates the total ^{7}Be destruction rate. Astrophys. J. Lett. **915**(1), 13 (2021). https://doi.org/10.3847/2041-8213/ac061f
63. G. Martín-Hernández, P. Mastinu, E. Musacchio González, R. Capote, H. Lubián, M. Macías, ^{7}Li(p, n)^{7}Be cross section from threshold to 1960 kev and precise measurement of the ^{197}Au(n, γ) spectrum-averaged cross section at 30 kev. Phys. Rev. C **99**, 034616 (2019). https://doi.org/10.1103/PhysRevC.99.034616
64. A. Coc, B. Davids, Comment on "Measurement of d + ^{7}Be cross sections for big-bang nucleosynthesis". arXiv e-prints, 1912-03933 (2019). arXiv:1912.03933 [astro-ph.CO]

65. M. Gai, The interaction of deuterons and neutrons with ^{7}Be and the "primordial ^{7}Li problem". Mem. Soc. Astron. Ital. **91**, 14 (2020)
66. N. Rijal, I. Wiedenhöver, J.C. Blackmon, M. Anastasiou, L.T. Baby, D.D. Caussyn, P. Höflich, K.W. Kemper, E. Koshchiy, G.V. Rogachev, Measurement of d + ^{7}Be cross sections for big-bang nucleosynthesis. Phys. Rev. Lett. **122**(18), 182701 (2019). https://doi.org/10.1103/PhysRevLett.122.182701. arXiv:1808.07893 [nucl-ex]
67. D. Pierroutsakou, A. Boiano, C. Boiano, P. Di Meo, M. La Commara, C. Manea, M. Mazzocco, M. Nicoletto, C. Parascandolo, C. Signorini, F. Soramel, E. Strano, N. Toniolo, D. Torresi, G. Tortone, A. Anastasio, M. Bettini, C. Cassese, L. Castellani, D. Corti, L. Costa, B. De Fazio, G. Galet, T. Glodariu, J. Gręboszc, A. Guglielmetti, P. Molini, G. Pontoriere, R. Rocco, M. Romoli, L. Roscilli, M. Sandoli, L. Stroe, M. Tessaro, P.G. Zatti, The experimental set-up of the RIB in-flight facility EXOTIC. Nucl. Instrum. Methods Phys. Res. A **834**, 46–70 (2016). https://doi.org/10.1016/j.nima.2016.07.019
68. W.C. Haxton, A.M. Serenelli, CN-cycle solar neutrinos and sun's primordial core metallicity. Astrophys. J. **687**, 678–691 (2008). https://doi.org/10.1086/591787
69. . M. Borexino Collaboration, K. Agostini, Altenmüller, S. Appel, V. Atroshchenko, Z. Bagdasarian, D. Basilico, G. Bellini, J. Benziger, R. Biondi, D. Bravo, B. Caccianiga, F. Calaprice, A. Caminata, P. Cavalcante, A. Chepurnov, D. D'Angelo, S. Davini, A. Derbin, A. Di Giacinto, V. Di Marcello, X.F. Ding, A. Di Ludovico, L. Di Noto, I. Drachnev, A. Formozov, D. Franco, C. Galbiati, C. Ghiano, M. Giammarchi, A. Goretti, A.S. Göttel, M. Gromov, D. Guffanti, A. Ianni, A. Ianni, A. Jany, D. Jeschke, V. Kobychev, G. Korga, S. Kumaran, M. Laubenstein, E. Litvinovich, P. Lombardi, I. Lomskaya, L. Ludhova, G. Lukyanchenko, L. Lukyanchenko, I. Machulin, J. Martyn, E. Meroni, M. Meyer, L. Miramonti, M. Misiaszek, V. Muratova, B. Neumair, M. Nieslony, R. Nugmanov, L. Oberauer, V. Orekhov, F. Ortica, M. Pallavicini, L. Papp, L. Pelicci, Ö. Penek, L. Pietrofaccia, N. Pilipenko, A. Pocar, G. Raikov, M.T. Ranalli, G. Ranucci, A. Razeto, A. Re, M. Redchuk, A. Romani, N. Rossi, S. Schönert, D. Semenov, G. Settanta, M. Skorokhvatov, A. Singhal, O. Smirnov, A. Sotnikov, Y. Suvorov, R. Tartaglia, G. Testera, J. Thurn, E. Unzhakov, F.L. Villante, A. Vishneva, R.B. Vogelaar, F. von Feilitzsch, M. Wojcik, M. Wurm, S. Zavatarelli, K. Zuber, G. Zuzel, Experimental evidence of neutrinos produced in the CNO fusion cycle in the Sun. Nature **587**(7835), 577–582 (2020). https://doi.org/10.1038/s41586-020-2934-0. arXiv:2006.15115 [hep-ex]
70. B. Frentz, A. Aprahamian, A.M. Clark, R.J. deBoer, C. Dulal, J.D. Enright, J. Görres, S.L. Henderson, J.D. Hinnefeld, K.B. Howard, R. Kelmar, K. Lee, L. Morales, S. Moylan, Z. Rahman, W. Tan, L.E. Weghorn, M. Wiescher, Lifetime measurements of excited states in ^{15}O. Phys. Rev. C **103**, 045802 (2021). https://doi.org/10.1103/PhysRevC.103.045802
71. P.F. Bertone, A.E. Champagne, D.C. Powell, C. Iliadis, S.E. Hale, V.Y. Hansper, Lifetime of the 6793-keV state in ^{15}O. Phys. Rev. Lett. **87**, 152501 (2001). https://doi.org/10.1103/PhysRevLett.87.152501
72. K. Yamada, T. Motobayashi, H. Akiyoshi, N. Aoi, Z. Fülöp, T. Gomi, Y. Higurashi, N. Imai, N. Iwasa, H. Iwasaki, Y. Iwata, H. Kobayashi, M. Kurokawa, Z. Liu, T. Minemura, S. Ozawa, H. Sakurai, M. Serata, S. Shimoura, S. Takeuchi, T. Teranishi, Y. Yanagisawa, K. Yoshida, M. Ishihara, E1 strength of the subthreshold $3/2^{+}$ state in ^{15}O studied by Coulomb excitation. Phys. Lett. B **579**, 265–270 (2004). https://doi.org/10.1016/j.physletb.2003.11.024
73. N. Galinski, S.K.L. Sjue, G.C. Ball, D.S. Cross, B. Davids, H. Al Falou, A.B. Garnsworthy, G. Hackman, U. Hager, D.A. Howell, M. Jones, R. Kanungo, R. Kshetri, K.G. Leach, J.R. Leslie, M. Moukaddam, J.N. Orce, E.T. Rand, C. Ruiz, G. Ruprecht, M.A. Schumaker, C.E. Svensson, S. Triambak, C.D. Unsworth, Lifetime measurements of states in ^{15}O. Phys. Rev. C **90**, 035803 (2014). https://doi.org/10.1103/PhysRevC.90.035803
74. M. Wiescher, J. Görres, E. Uberseder, G. Imbriani, M. Pignatari, The cold and hot CNO cycles. Annu. Rev. Nucl. Part. Sci. **60**(1), 381–404 (2010). https://doi.org/10.1146/annurev.nucl.012809.104505
75. G.G. Kiss, M. La Cognata, C. Spitaleri, R. Yarmukhamedov, I. Wiedenhöver, L.T. Baby, S. Cherubini, A. Cvetinović, G. D'Agata, P. Figuera, G.L. Guardo, M. Gulino, S. Hayakawa, I. Indelicato, L. Lamia, M. Lattuada, F. Mudò, S. Palmerini, R.G. Pizzone, G.G. Rapisarda, S. Romano, M.L. Sergi, R. Spartà, O. Trippella, A. Tumino, M. Anastasiou, S.A. Kuvin, N. Rijal, B. Schmidt, S.B. Igamov, S.B. Sakuta, K.I. Tursunmakhatov, Z. Fülöp, G. Gyürky, T. Szücs, Z. Halász, E. Somorjai, Z. Hons, J. Mrázek, R.E. Tribble, A.M. Mukhamedzhanov, Astrophysical s-factor for the ^{3}He(α, γ)^{7}Be reaction via the asymptotic normalization coefficient (ANC) method. Phys. Lett. B **807**, 135606 (2020). https://doi.org/10.1016/j.physletb.2020.135606
76. G. D'Agata, A.I. Kilic, V. Burjan, J. Mrazek, V. Glagolev, V. Kroha, G.L. Guardo, M. La Cognata, L. Lamia, S. Palmerini, R.G. Pizzone, G.G. Rapisarda, S. Romano, M.L. Sergi, R. Spartà, C. Spitaleri, I. Sivàček, A. Tumino, ^{26}Si(p, γ)^{27}P direct proton capture by means of the asymptotic normalization coefficients method for mirror nuclei. Phys. Rev. C **103**, 015806 (2021). https://doi.org/10.1103/PhysRevC.103.015806
77. F. Farinon, T. Glodariu, M. Mazzocco, A. Battistella, R. Bonetti, L. Costa, A. De Rosa, A. Guglielmetti, G. Inglima, M. La Commara, V.Z. Maidikov, B. Martin, C. Mazzocchi, D. Pierroutsakou, M. Romoli, M. Sandoli, C. Signorini, F. Soramel, L. Stroe, E. Vardaci, Commissioning of the EXOTIC beam line. Nucl. Instrum. Methods Phys. Res. B **266**(19), 4097–4102 (2008). https://doi.org/10.1016/j.nimb.2008.05.128. (**Proceedings of the XVth International Conference on Electromagnetic Isotope Separators and Techniques Related to their Applications**)
78. M. Freer, H.O.U. Fynbo, The Hoyle state in ^{12}C. Prog. Part. Nucl. Phys. **78**, 1–23 (2014). https://doi.org/10.1016/j.ppnp.2014.06.001
79. T. Kibédi, B. Alshahrani, A.E. Stuchbery, A.C. Larsen, A. Görgen, S. Siem, M. Guttormsen, F. Giacoppo, A.I. Morales, E. Sahin, G.M. Tveten, F.L.B. Garrote, L.C. Campo, T.K. Eriksen, M. Klintefjord, S. Maharramova, H.-T. Nyhus, T.G. Tornyi, T. Renstrøm, W. Paulsen, Radiative width of the Hoyle state from γ-ray spectroscopy. Phys. Rev. Lett. **125**, 182701 (2020). https://doi.org/10.1103/PhysRevLett.125.182701
80. G. Cardella, F. Favela, N.S. Martorana, L. Acosta, A. Camaiani, E. De Filippo, N. Gelli, E. Geraci, B. Gnoffo, C. Guazzoni, G. Immè, D.J. Marín-Lámbarri, G. Lanzalone, I. Lombardo, L. Lo Monaco, C. Maiolino, A. Nannini, A. Pagano, E.V. Pagano, M. Papa, S. Pirrone, G. Politi, E. Pollacco, L. Quattrocchi, F. Risitano, F. Rizzo, P. Russotto, V.L. Sicari, D. Santonocito, A. Trifirò, M. Trimarchi, Investigating γ-ray decay of excited ^{12}C levels with a multifold coincidence analysis. Phys. Rev. C **104**, 064315 (2021). https://doi.org/10.1103/PhysRevC.104.064315
81. M. Tsumura, T. Kawabata, Y. Takahashi, S. Adachi, H. Akimune, S. Ashikaga, T. Baba, Y. Fujikawa, H. Fujimura, H. Fujioka, T. Furuno, T. Hashimoto, T. Harada, M. Ichikawa, K. Inaba, Y. Ishii, N. Itagaki, M. Itoh, C. Iwamoto, N. Kobayashi, A. Koshikawa, S. Kubono, Y. Maeda, Y. Matsuda, S. Matsumoto, K. Miki, T. Morimoto, M. Murata, T. Nanamura, I. Ou, S. Sakaguchi, A. Sakaue, M. Sferrazza, K.N. Suzuki, T. Takeda, A. Tamii, K. Watanabe, Y.N. Watanabe, H.P. Yoshida, J. Zenihiro, First experimental determination of the radiative-decay probability of the 3_1 state in ^{12}C for estimating the triple alpha reaction rate in high temperature environments. Phys. Lett. B **817**, 136283 (2021). https://doi.org/10.1016/j.physletb.2021.136283
82. D. Chamberlin, D. Bodansky, W.W. Jacobs, D.L. Oberg, Upper limit on the radiative width of the 9.64-MeV state of ^{12}C. Phys. Rev. C **10**, 909–911 (1974). https://doi.org/10.1103/PhysRevC.10.909
83. G. Cardella, A. Bonasera, N.S. Martorana, L. Acosta, E. De Filippo, E. Geraci, B. Gnoffo, C. Guazzoni, L. Lo Monaco, C. Maiolino, A. Pagano, E.V. Pagano, M. Papa, S. Pirrone, G. Politi, F. Risitano, F. Rizzo, P. Russotto, M. Trimarchi, Search for rare 3-α decays in the region of the Hoyle state of ^{12}C. Nucl. Phys. A **1020**, 122395 (2022). https://doi.org/10.1016/j.nuclphysa.2022.122395
84. D. Dell'Aquila, I. Lombardo, G. Verde, M. Vigilante, L. Acosta, C. Agodi, F. Cappuzzello, D. Carbone, M. Cavallaro, S. Cherubini, A. Cvetinovic, G. D'Agata, L. Francalanza, G.L. Guardo, M. Gulino, I. Indelicato, M. La Cognata, L. Lamia, A. Ordine, R.G. Pizzone, S.M.R. Puglia, G.G. Rapisarda, S. Romano, G. Santagati, R. Spartà, G. Spadaccini, C. Spitaleri, A. Tumino, High-precision probe of the fully sequential decay width of the Hoyle state in ^{12}C. Phys. Rev. Lett. **119**(13), 132501 (2017). https://doi.org/10.1103/PhysRevLett.119.132501. arXiv:1705.09196 [nucl-ex]
85. M. Freer, I. Boztosun, C.A. Bremner, S.P.G. Chappell, R.L. Cowin, G.K. Dillon, B.R. Fulton, B.J. Greenhalgh, T. Munoz-Britton, M.P. Nicoli, W.D.M. Rae, S.M. Singer, N. Sparks, D.L. Watson, D.C. Weisser, Reexamination of the excited states of ^{12}C. Phys. Rev. C (2007). https://doi.org/10.1103/PhysRevC.76.034320

86. D.J. Marín-Lámbarri, R. Bijker, M. Freer, M. Gai, T. Kokalova, D.J. Parker, C. Wheldon, Evidence for triangular $\mathcal{D}_{3}$ symmetry in ^{12}C. Phys. Rev. Lett. (2014). https://doi.org/10.1103/PhysRevLett.113.012502
87. P. Hess, ^{12}C within the semimicroscopic algebraic cluster model. Eur. Phys. J. A (2018). https://doi.org/10.1140/epja/i2018-12468-7
88. A. Tumino, C. Spitaleri, M. La Cognata, S. Cherubini, G.L. Guardo, M. Gulino, S. Hayakawa, I. Indelicato, L. Lamia, H. Petrascu, R.G. Pizzone, S.M.R. Puglia, G.G. Rapisarda, S. Romano, M.L. Sergi, R. Spartá, L. Trache, An increase in the ^{12}C + ^{12}C fusion rate from resonances at astrophysical energies. Nature **557**(7707), 687–690 (2018). https://doi.org/10.1038/s41586-018-0149-4
89. S.E. Woosley, A. Heger, T.A. Weaver, The evolution and explosion of massive stars. Rev. Mod. Phys. **74**(4), 1015–1071 (2002). https://doi.org/10.1103/RevModPhys.74.1015
90. C.L. Jiang, B.B. Back, K.E. Rehm, K. Hagino, G. Montagnoli, A.M. Stefanini, Heavy-ion fusion reactions at extreme sub-barrier energies. Eur. Phys. J. A **57**(7), 235 (2021). https://doi.org/10.1140/epja/s10050-021-00536-2
91. A. Diaz-Torres, L.R. Gasques, M. Wiescher, Effects of nuclear molecular configurations on the astrophysical S-factor for ^{16}O + ^{16}O. Phys. Lett. B **652**(5–6), 255–258 (2007). https://doi.org/10.1016/j.physletb.2007.06.077. arXiv:0708.2317 [nucl-th]
92. J.J. Cowan, W.K. Rose, Production of ^{14}C and neutrons in red giants. Astrophys. J. **212**, 149–158 (1977). https://doi.org/10.1086/155030
93. G. Potel, F.M. Nunes, I.J. Thompson, Establishing a theory for deuteron-induced surrogate reactions. Phys. Rev. C **92**, 034611 (2015). https://doi.org/10.1103/PhysRevC.92.034611
94. F. Käppeler, A.A. Naqvi, M. Al-Ohali, Stellar krypton cross sections at kT=25 and 52 keV. Phys. Rev. C **35**, 936–941 (1987). https://doi.org/10.1103/PhysRevC.35.936
95. C. Abia, M. Busso, R. Gallino, I. Dominguez, O. Straniero, J. Isern, The ^{85}Kr s-process branching and the mass of carbon stars. Astrophys. J. **559**(2), 1117–1134 (2001). https://doi.org/10.1086/322383
96. S. Fiebiger, B. Baramsai, A. Couture, M. Krtička, S. Mosby, R. Reifarth, J. O'Donnell, G. Rusev, J. Ullmann, M. Weigand, C. Wolf, Neutron capture cross sections of Kr. J. Phys. Conf. Ser. **165**, 01023 (2017). https://doi.org/10.1051/epjconf/201716501023
97. R. Raut, A.P. Tonchev, G. Rusev, W. Tornow, C. Iliadis, M. Lugaro, J. Buntain, S. Goriely, J. Kelley, R. Schwengner, A. Banu, N. Tsoneva, Cross-section measurements of the ^{86}Kr(γ, n) reaction to probe the s-process branching at ^{85}Kr. Phys. Rev. Lett. **111**(11), 112501 (2013). https://doi.org/10.1103/PhysRevLett.111.112501
98. P.F. Mastinu, G. Martín Hernández, J. Praena, A method to obtain a Maxwell–Boltzmann neutron spectrum at kT=30 keV for nuclear astrophysics studies. Nucl. Instrum. Methods Phys. Res. A **601**(3), 333–338 (2009). https://doi.org/10.1016/j.nima.2009.01.005
99. G. Gervino, O. Aberle, A.-P. Bernardes, N. Colonna, S. Cristallo, M. Diakaki, S. Fiore, A. Manna, C. Massimi, P. Mastinu, A. Mengoni, R. Mucciola, E. Musacchio González, N. Patronis, E. Stamati, P. Vaz, R. Vlastou, NEAR: a new station to study neutron-induced reactions of astrophysical interest at CERN-n_TOF. Universe **8**(5), 255 (2022). https://doi.org/10.3390/universe8050255
100. C. Guerrero, A. Tsinganis, E. Berthoumieux, M. Barbagallo, F. Belloni, F. Gunsing, C. Weiß, E. Chiaveri, M. Calviani, V. Vlachoudis, S. Altstadt, S. Andriamonje, J. Andrzejewski, L. Audouin, V. Bécares, F. Bečvář, J. Billowes, V. Boccone, D. Bosnar, M. Brugger, F. Calviño, D. Cano-Ott, C. Carrapiço, F. Cerutti, M. Chin, N. Colonna, G. Cortés, M.A. Cortés-Giraldo, M. Diakaki, C. Domingo-Pardo, I. Duran, R. Dressler, N. Dzysiuk, C. Eleftheriadis, A. Ferrari, K. Fraval, S. Ganesan, A.R. García, G. Giubrone, K. Göbel, M.B. Gómez-Hornillos, I.F. Gonçalves, E. González-Romero, E. Griesmayer, P. Gurusamy, A. Hernández-Prieto, P. Gurusamy, D.G. Jenkins, E. Jericha, Y. Kadi, F. Käppeler, D. Karadimos, N. Kivel, P. Koehler, M. Kokkoris, M. Krtička, J. Kroll, C. Lampoudis, C. Langer, E. Leal-Cidoncha, C. Lederer, H. Leeb, L.S. Leong, R. Losito, A. Manousos, J. Marganiec, T. Martínez, C. Massimi, P.F. Mastinu, M. Mastromarco, M. Meaze, E. Mendoza, A. Mengoni, P.M. Milazzo, F. Mingrone, M. Mirea, W. Mondalaers, T. Papaevangelou, C. Paradela, A. Pavlik, J. Perkowski, A. Plompen, J. Praena, J.M. Quesada, T. Rauscher, R. Reifarth, A. Riego, F. Roman, C. Rubbia, M. Sabate-Gilarte, R. Sarmento, A. Saxena, P. Schillebeeckx, S. Schmidt, D. Schumann, P. Steinegger, G. Tagliente, J.L. Tain, D. Tarrío, L. Tassan-Got, S. Valenta, G. Vannini, V. Variale, P. Vaz, A. Ventura, R. Versaci, M.J. Vermeulen, R. Vlastou, A. Wallner, T. Ware, M. Weigand, T. Wright, P. Žugec, Performance of the neutron time-of-flight facility n_TOF at CERN. Eur. Phys. J. A **49**, 27 (2013). https://doi.org/10.1140/epja/i2013-13027-6
101. M. Arnould, S. Goriely, K. Takahashi, The r-process of stellar nucleosynthesis: astrophysics and nuclear physics achievements and mysteries. Phys. Rep. **450**(4–6), 97–213 (2007). https://doi.org/10.1016/j.physrep.2007.06.002. arXiv:0705.4512 [astro-ph]
102. T. Rauscher, Sensitivity of astrophysical reaction rates to nuclear uncertainties. Astrophys. J. Suppl. **201**(2), 26 (2012). https://doi.org/10.1088/0067-0049/201/2/26. arXiv:1205.0685 [astro-ph.SR]
103. M.R. Mumpower, R. Surman, G.C. McLaughlin, A. Aprahamian, The impact of individual nuclear properties on r-process nucleosynthesis. Prog. Part. Nucl. Phys. **86**, 86–126 (2016). https://doi.org/10.1016/j.ppnp.2015.09.001. arXiv:1508.07352 [nucl-th]
104. D. Vescovi, R. Reifarth, S. Cristallo, A. Couture, Candidates for direct neutron-capture measurements related to r-process in neutron star mergers. Front. Astron. Space Sci. (2022) (**in press**)
105. C.J. Horowitz, A. Arcones, B. Côté, I. Dillmann, W. Nazarewicz, I.U. Roederer, H. Schatz, A. Aprahamian, D. Atanasov, A. Bauswein, T.C. Beers, J. Bliss, M. Brodeur, J.A. Clark, A. Frebel, F. Foucart, C.J. Hansen, O. Just, A. Kankainen, G.C. McLaughlin, J.M. Kelly, S.N. Liddick, D.M. Lee, J. Lippuner, D. Martin, J.J. Mendoza-Temis, B.D. Metzger, M.R. Mumpower, G. Perdikakis, J. Pereira, B.W. O'Shea, R. Reifarth, A.M. Rogers, D.M. Siegel, A. Spyrou, R. Surman, X. Tang, T. Uesaka, M. Wang, r-process nucleosynthesis: connecting rare-isotope beam facilities with the cosmos. J. Phys. G **46**(8), 083001 (2019). https://doi.org/10.1088/1361-6471/ab0849. arXiv:1805.04637
106. J.J. Cowan, C. Sneden, J.E. Lawler, A. Aprahamian, M. Wiescher, K. Langanke, G. Martínez-Pinedo, F.-K. Thielemann, Origin of the heaviest elements: the rapid neutron-capture process. Rev. Mod. Phys. **93**(1), 015002 (2021). https://doi.org/10.1103/RevModPhys.93.015002. arXiv:1901.01410
107. P. Möller, B. Pfeiffer, K.-L. Kratz, New calculations of gross β-decay properties for astrophysical applications: speeding-up the classical r process. Phys. Rev. C **67**(5), 055802 (2003). https://doi.org/10.1103/PhysRevC.67.055802
108. T. Marketin, L. Huther, G. Martínez-Pinedo, Large-scale evaluation of β-decay rates of r-process nuclei with the inclusion of first-forbidden transitions. Phys. Rev. C **93**(2), 025805 (2016). https://doi.org/10.1103/PhysRevC.93.025805. arXiv:1507.07442
109. E.M. Ney, J. Engel, T. Li, N. Schunck, Global description of β-decay with the axially deformed Skyrme finite-amplitude method: extension to odd-mass and odd-odd nuclei. Phys. Rev. C **102**(3), 034326 (2020). https://doi.org/10.1103/PhysRevC.102.034326
110. A. Perego, S. Rosswog, R.M. Cabezon, O. Korobkin, R. Kappeli, A. Arcones, M. Liebendorfer, Neutrino-driven winds from neutron star merger remnants. Mon. Not. R. Astron. Soc. **443**(4), 3134–3156 (2014). https://doi.org/10.1093/mnras/stu1352. arXiv:1405.6730
111. D. Radice, A. Perego, K. Hotokezaka, S.A. Fromm, S. Bernuzzi, L.F. Roberts, Binary neutron star mergers: mass ejection, electromagnetic counterparts, and nucleosynthesis. Astrophys. J. **869**(2), 130 (2018). https://doi.org/10.3847/1538-4357/aaf054. arXiv:1809.11161
112. A. Perego, S. Bernuzzi, D. Radice, Thermodynamics conditions of matter in neutron star mergers. Eur. Phys. J. A **55**(8), 124 (2019). https://doi.org/10.1140/epja/i2019-12810-7. arXiv:1903.07898
113. A. Goasduff, A. Gottardo, R. Pengo, M. Rigato, The cryogenic target for direct reactions (CTADIR). INFN-LNL Rep. **262**, 41 (2021)
114. N. Cieplicka-Oryńczak, D. Mengoni, M. Ciemała, S. Leoni, B. Fornal, J.A. Dueñas, S. Brambilla, C. Boiano, P.R. John, D. Bazzacco, G. Benzoni, G. Bocchi, S. Capra, F.C.L. Crespi, A. Goasduff, K. Hadyńska-Klęk, ŁW. Iskra, G. Jaworski, F. Recchia, M. Siciliano, D. Testov, J.J. Valiente-Dobón,

Towards the lowest-energy limit for light ions identification with silicon pixel-type detectors. Eur. Phys. J. A **54**(12), 209 (2018). https://doi.org/10.1140/epja/i2018-12644-9
115. C. Travaglio, R. Gallino, E. Arnone, J. Cowan, F. Jordan, C. Sneden, Galactic evolution of Sr, Y, and Zr: a multiplicity of nucleosynthetic processes. Astrophys. J. **601**, 864 (2004). https://doi.org/10.1086/380507
116. T. Mishenina, M. Pignatari, T. Gorbaneva, C. Travaglio, B. Côté, F.-K. Thielemann, C. Soubiran, Enrichment of the galactic disc with neutron-capture elements: Mo and ru. Mon. Not. R. Astron. Soc. **489**, 1697–1708 (2019). https://doi.org/10.1093/mnras/stz2202
117. J. Bliss, A. Arcones, F. Montes, J. Pereira, Impact of (α, n) reactions on weak r-process in neutrino-driven winds. J. Phys. G **44**, 054003 (2017). https://doi.org/10.1088/1361-6471/aa63bd
118. S. Jin, Nuclear reaction sensitivity in magnetohydrodynamically driven supernovae. Astrophys. J. **927**, 116 (2022). https://doi.org/10.3847/1538-4357/ac4f4a
119. E. Pian, P. D'Avanzo, S. Benetti, M. Branchesi, E. Brocato, S. Campana, E. Cappellaro, S. Covino, V. D'Elia, J.P.U. Fynbo, F. Getman, G. Ghirlanda, G. Ghisellini, A. Grado, G. Greco, J. Hjorth, C. Kouveliotou, A. Levan, L. Limatola, D. Malesani, P.A. Mazzali, A. Melandri, P. Møller, L. Nicastro, E. Palazzi, S. Piranomonte, A. Rossi, O.S. Salafia, J. Selsing, G. Stratta, M. Tanaka, N.R. Tanvir, L. Tomasella, D. Watson, S. Yang, L. Amati, L.A. Antonelli, S. Ascenzi, M.G. Bernardini, M. Boër, F. Bufano, A. Bulgarelli, M. Capaccioli, P. Casella, A.J. Castro-Tirado, E. Chassande-Mottin, R. Ciolfi, C.M. Copperwheat, M. Dadina, G. De Cesare, A. Di Paola, Y.Z. Fan, B. Gendre, G. Giuffrida, A. Giunta, L.K. Hunt, G.L. Israel, Z.-P. Jin, M.M. Kasliwal, S. Klose, M. Lisi, F. Longo, E. Maiorano, M. Mapelli, N. Masetti, L. Nava, B. Patricelli, D. Perley, A. Pescalli, T. Piran, A. Possenti, L. Pulone, M. Razzano, R. Salvaterra, P. Schipani, M. Spera, A. Stamerra, L. Stella, G. Tagliaferri, V. Testa, E. Troja, M. Turatto, S.D. Vergani, D. Vergani, Spectroscopic identification of r-process nucleosynthesis in a double neutron-star merger. Nature **551**, 67–70 (2017). https://doi.org/10.1038/nature24298
120. D. Kasen, B. Metzger, J. Barnes, E. Quataert, E. Ramirez-Ruiz, Origin of the heavy elements in binary neutron-star mergers from a gravitational-wave event. Nature **551**, 80–84 (2017). https://doi.org/10.1038/nature24453
121. S. Bisterzo, C. Travaglio, R. Gallino, M. Wiescher, F. Käppeler, Galactic chemical evolution and solar s-process abundances: dependence on the ^{13}C-pocket structure. Astrophys. J. **787**(1), 10 (2014). https://doi.org/10.1088/0004-637X/787/1/10. arXiv:1403.1764 [astro-ph.SR]
122. N. Prantzos, C. Abia, S. Cristallo, M. Limongi, A. Chieffi, Chemical evolution with rotating massive star yields II. A new assessment of the solar s- and r-process components. Mon. Not. R. Astron. Soc. **491**(2), 1832–1850 (2020). https://doi.org/10.1093/mnras/stz3154. arXiv:1911.02545 [astro-ph.GA]
123. S. Cristallo, L. Piersanti, O. Straniero, R. Gallino, I. Domínguez, F. Käppeler, Asymptotic-giant-branch models at very low metallicity. Publ. Astron. Soc. Aust. **26**(3), 139–144 (2009). https://doi.org/10.1071/AS09003. arXiv:0904.4173 [astro-ph.SR]
124. M. Lugaro, S.W. Campbell, H. Van Winckel, K. De Smedt, A.I. Karakas, F. Käppeler, Post-AGB stars in the Magellanic Clouds and neutron-capture processes in AGB stars. Astron. Astrophys. **583**, 77 (2015). https://doi.org/10.1051/0004-6361/201526690. arXiv:1509.03518 [astro-ph.SR]
125. S. Cristallo, D. Karinkuzhi, A. Goswami, L. Piersanti, D. Gobrecht, Constraints of the physics of low-mass AGB stars from CH and CEMP stars. Astrophys. J. **833**(2), 181 (2016). https://doi.org/10.3847/1538-4357/833/2/181. arXiv:1610.05475 [astro-ph.SR]
126. A. Choplin, L. Siess, S. Goriely, The intermediate neutron capture process. I. Development of the i-process in low-metallicity low-mass AGB stars. Astron. Astrophys. **648**, 119 (2021). https://doi.org/10.1051/0004-6361/202040170. arXiv:2102.08840 [astro-ph.SR]
127. F. Herwig, M. Pignatari, P.R. Woodward, D.H. Porter, G. Rockefeller, C.L. Fryer, M. Bennett, R. Hirschi, Convective-reactive proton-^{12}C combustion in Sakurai's object (V4334 Sagittarii) and implications for the evolution and yields from the first generations of stars. Astrophys. J. **727**(2), 89 (2011). https://doi.org/10.1088/0004-637X/727/2/89. arXiv:1002.2241 [astro-ph.SR]
128. S. Jones, C. Ritter, F. Herwig, C. Fryer, M. Pignatari, M.G. Bertolli, B. Paxton, H ingestion into He-burning convection zones in super-AGB stellar models as a potential site for intermediate neutron-density nucleosynthesis. Mon. Not. R. Astron. Soc. **455**(4), 3848–3863 (2016). https://doi.org/10.1093/mnras/stv2488. arXiv:1510.07417 [astro-ph.SR]
129. I.U. Roederer, A.I. Karakas, M. Pignatari, F. Herwig, The diverse origins of neutron-capture elements in the metal-poor Star HD 94028: possible detection of products of I-process nucleosynthesis. Astrophys. J. **821**(1), 37 (2016). https://doi.org/10.3847/0004-637X/821/1/37. arXiv:1603.00036 [astro-ph.SR]
130. O. Clarkson, F. Herwig, M. Pignatari, Pop III i-process nucleosynthesis and the elemental abundances of SMSS J0313–6708 and the most iron-poor stars. Mon. Not. R. Astron. Soc. **474**(1), 37–41 (2018). https://doi.org/10.1093/mnrasl/slx190. arXiv:1710.01763 [astro-ph.SR]
131. P. Banerjee, Y.-Z. Qian, A. Heger, New neutron-capture site in Massive Pop III and Pop II stars as a source for heavy elements in the early galaxy. Astrophys. J. **865**(2), 120 (2018). https://doi.org/10.3847/1538-4357/aadb8c. arXiv:1711.05964 [astro-ph.SR]
132. P.A. Denissenkov, F. Herwig, U. Battino, C. Ritter, M. Pignatari, S. Jones, B. Paxton, I-process nucleosynthesis and mass retention efficiency in He-shell flash evolution of rapidly accreting white dwarfs. Astrophys. J. Lett. **834**(2), 10 (2017). https://doi.org/10.3847/2041-8213/834/2/L10. arXiv:1610.08541 [astro-ph.SR]
133. B. Côté, P. Denissenkov, F. Herwig, A.J. Ruiter, C. Ritter, M. Pignatari, K. Belczynski, i-process contribution of rapidly accreting white dwarfs to the solar composition of first-peak neutron-capture elements. Astrophys. J. **854**(2), 105 (2018). https://doi.org/10.3847/1538-4357/aaaae8. arXiv:1712.07551 [astro-ph.SR]
134. P.A. Denissenkov, F. Herwig, P. Woodward, R. Andrassy, M. Pignatari, S. Jones, The i-process yields of rapidly accreting white dwarfs from multicycle He-shell flash stellar evolution models with mixing parametrizations from 3D hydrodynamics simulations. Mon. Not. R. Astron. Soc. **488**(3), 4258–4270 (2019). https://doi.org/10.1093/mnras/stz1921. arXiv:1809.03666 [astro-ph.SR]
135. M.G. Bertolli, F. Herwig, M. Pignatari, T. Kawano, Systematic and correlated nuclear uncertainties in the i-process at the neutron shell closure N = 82. arXiv e-prints, 1310-4578 (2013). arXiv:1310.4578
136. S. Goriely, L. Siess, A. Choplin, The intermediate neutron capture process. II. Nuclear uncertainties. Astron. Astrophys. **654**, 129 (2021). https://doi.org/10.1051/0004-6361/202141575. arXiv:2109.00332 [astro-ph.SR]
137. P. Denissenkov, G. Perdikakis, F. Herwig, H. Schatz, C. Ritter, M. Pignatari, S. Jones, S. Nikas, A. Spyrou, The impact of (n, γ) reaction rate uncertainties of unstable isotopes near N = 50 on the i-process nucleosynthesis in He-shell flash white dwarfs. J. Phys. G **45**(5), 055203 (2018). https://doi.org/10.1088/1361-6471/aabb6e
138. J.E. McKay, P.A. Denissenkov, F. Herwig, G. Perdikakis, H. Schatz, The impact of (n,γ) reaction rate uncertainties on the predicted abundances of I-process elements with $32 \leq Z \leq 48$ in the metal-poor star HD94028. Mon. Not. R. Astron. Soc. **491**(4), 5179–5187 (2020). https://doi.org/10.1093/mnras/stz3322. arXiv:1909.07011 [astro-ph.SR]
139. P.A. Denissenkov, F. Herwig, G. Perdikakis, H. Schatz, The impact of (n,γ) reaction rate uncertainties of unstable isotopes on the i-process nucleosynthesis of the elements from Ba to W. Mon. Not. R. Astron. Soc. **503**(3), 3913–3925 (2021). https://doi.org/10.1093/mnras/stab772. arXiv:2010.15798 [astro-ph.SR]
140. E. Caurier, G. Martínez-Pinedo, F. Nowacki, A. Poves, A.P. Zuker, The shell model as a unified view of nuclear structure. Rev. Mod. Phys. **77**, 427–488 (2005). https://doi.org/10.1103/RevModPhys.77.427

141. G. Colò, Nuclear density functional theory. Adv. Phys. X **5**(1), 1740061 (2020). https://doi.org/10.1080/23746149.2020.1740061. arXiv:2012.01864 [nucl-ex]
142. L. Coraggio, S. Pastore, C. Barbieri, Editorial: the future of nuclear structure: challenges and opportunities in the microscopic description of nuclei. Front. Phys. **8**, 626976 (2021). https://doi.org/10.3389/fphy.2020.626976
143. L.E. Marcucci, Editorial: the long-lasting quest for nuclear interactions: the past, the present and the future. Front. Phys. **8**, 609907 (2020). https://doi.org/10.3389/fphy.2020.609907
144. R.F. Garcia Ruiz, M.L. Bissell, K. Blaum, A. Ekström, N. Frömmgen, G. Hagen, M. Hammen, K. Hebeler, J.D. Holt, G.R. Jansen, M. Kowalska, K. Kreim, W. Nazarewicz, R. Neugart, G. Neyens, W. Nörtershäuser, T. Papenbrock, J. Papuga, A. Schwenk, J. Simonis, K.A. Wendt, D.T. Yordanov, Unexpectedly large charge radii of neutron-rich calcium isotopes. Nat. Phys. **12**, 594 (2016). https://doi.org/10.1038/nphys3645
145. E. Leistenschneider, M.P. Reiter, S. Ayet San Andrés, B. Kootte, J.D. Holt, P. Navrátil, C. Babcock, C. Barbieri, B.R. Barquest, J. Bergmann, J. Bollig, T. Brunner, E. Dunling, A. Finlay, H. Geissel, L. Graham, F. Greiner, H. Hergert, C. Hornung, C. Jesch, R. Klawitter, Y. Lan, D. Lascar, K.G. Leach, W. Lippert, J.E. McKay, S.F. Paul, A. Schwenk, D. Short, J. Simonis, V. Somà, R. Steinbrügge, S.R. Stroberg, R. Thompson, M.E. Wieser, C. Will, M. Yavor, C. Andreoiu, T. Dickel, I. Dillmann, G. Gwinner, W.R. Plaß, C. Scheidenberger, A.A. Kwiatkowski, J. Dilling, Dawning of the $N = 32$ shell closure seen through precision mass measurements of neutron-rich titanium isotopes. Phys. Rev. Lett. **120**, 062503 (2018). https://doi.org/10.1103/PhysRevLett.120.062503
146. S. Chen, J. Lee, P. Doornenbal, A. Obertelli, C. Barbieri, Y. Chazono, P. Navrátil, K. Ogata, T. Otsuka, F. Raimondi, V. Somà, Y. Utsuno, K. Yoshida, H. Baba, F. Browne, D. Calvet, F. Château, N. Chiga, A. Corsi, M.L. Cortés, A. Delbart, J.-M. Gheller, A. Giganon, A. Gillibert, C. Hilaire, T. Isobe, J. Kahlbow, T. Kobayashi, Y. Kubota, V. Lapoux, H.N. Liu, T. Motobayashi, I. Murray, H. Otsu, V. Panin, N. Paul, W. Rodriguez, H. Sakurai, M. Sasano, D. Steppenbeck, L. Stuhl, Y.L. Sun, Y. Togano, T. Uesaka, K. Wimmer, K. Yoneda, N. Achouri, O. Aktas, T. Aumann, L.X. Chung, F. Flavigny, S. Franchoo, I. Gašparić, R.-B. Gerst, J. Gibelin, K.I. Hahn, D. Kim, T. Koiwai, Y. Kondo, P. Koseoglou, C. Lehr, B.D. Linh, T. Lokotko, M. MacCormick, K. Moschner, T. Nakamura, S.Y. Park, D. Rossi, E. Sahin, D. Sohler, P.-A. Söderström, S. Takeuchi, H. Törnqvist, V. Vaquero, V. Wagner, S. Wang, V. Werner, X. Xu, H. Yamada, D. Yan, Z. Yang, M. Yasuda, L. Zanetti, Quasifree neutron knockout from ^{54}Ca corroborates arising $N = 34$ neutron magic number. Phys. Rev. Lett. **123**(14), 142501 (2019). https://doi.org/10.1103/PhysRevLett.123.142501
147. Y.L. Sun, A. Obertelli, P. Doornenbal, C. Barbieri, Y. Chazono, T. Duguet, H.N. Liu, P. Navrátil, F. Nowacki, K. Ogata, T. Otsuka, F. Raimondi, V. Somà, Y. Utsuno, K. Yoshida, N. Achouri, H. Baba, F. Browne, D. Calvet, F. Château, S. Chen, N. Chiga, A. Corsi, M.L. Cortés, A. Delbart, J.-M. Gheller, A. Giganon, A. Gillibert, C. Hilaire, T. Isobe, T. Kobayashi, Y. Kubota, V. Lapoux, T. Motobayashi, I. Murray, H. Otsu, V. Panin, N. Paul, W. Rodriguez, H. Sakurai, M. Sasano, D. Steppenbeck, L. Stuhl, Y. Togano, T. Uesaka, K. Wimmer, K. Yoneda, O. Aktas, T. Aumann, L.X. Chung, F. Flavigny, S. Franchoo, I. Gašparić, R.-B. Gerst, J. Gibelin, K.I. Hahn, D. Kim, T. Koiwai, Y. Kondo, P. Koseoglou, J. Lee, C. Lehr, B.D. Linh, T. Lokotko, M. MacCormick, K. Moschner, T. Nakamura, S.Y. Park, D. Rossi, E. Sahin, D. Sohler, P.-A. Söderström, S. Takeuchi, H. Törnqvist, V. Vaquero, V. Wagner, S. Wang, V. Werner, X. Xu, H. Yamada, D. Yan, Z. Yang, M. Yasuda, L. Zanetti, Restoration of the natural $E(1/2^+_1) - E(3/2^+_1)$ energy splitting in odd-K isotopes towards $N = 40$. Phys. Lett. B **802**, 135215 (2020). https://doi.org/10.1016/j.physletb.2020.135215
148. V. Somà, C. Barbieri, T. Duguet, P. Navrátil, Moving away from singly-magic nuclei with Gorkov Green's function theory. Eur. Phys. J. A **57**(4), 135 (2021). https://doi.org/10.1140/epja/s10050-021-00437-4. arXiv:2009.01829 [nucl-th]
149. Á. Koszorús, X.F. Yang, W.G. Jiang, S.J. Novario, S.W. Bai, J. Billowes, C.L. Bennersley, M.L. Bissell, T.E. Cocolios, B.S. Cooper, R.P. de Groote, A. Ekström, K.T. Flanagan, C. Forssén, S. Franchoo, R.F. Garcia Ruiz, F.P. Gustafsson, G. Hagen, G.R. Jansen, M. Kanellakopulos, M. Kortelainen, W. Nazarewicz, G. Neyens, T. Papenbrock, P.-G. Reinhard, C.M. Ricketts, B.K. Sahoo, A.R. Vernon, S.G. Wilkins, Charge radii of exotic potassium isotopes challenge nuclear theory and the magic character of $N = 32$. Nat. Phys. **17**(4), 439–443 (2021). https://doi.org/10.1038/s41567-020-01136-5. (**Erratum: Nature Phys. 17, 539 (2021)**)
150. S.R. Stroberg, J.D. Holt, A. Schwenk, J. Simonis, Ab initio limits of atomic nuclei. Phys. Rev. Lett. **126**, 022501 (2021). https://doi.org/10.1103/PhysRevLett.126.022501
151. V. Somà, P. Navrátil, F. Raimondi, C. Barbieri, T. Duguet, Novel chiral Hamiltonian and observables in light and medium-mass nuclei. Phys. Rev. C **101**, 014318 (2020). https://doi.org/10.1103/PhysRevC.101.014318
152. P. Arthuis, C. Barbieri, M. Vorabbi, P. Finelli, Ab initio computation of charge densities for Sn and Xe isotopes. Phys. Rev. Lett. **125**, 182501 (2020). https://doi.org/10.1103/PhysRevLett.125.182501
153. B. Hu, W. Jiang, T. Miyagi, Z. Sun, A. Ekström, C. Forssén, G. Hagen, J.D. Holt, T. Papenbrock, S.R. Stroberg, I. Vernon, Ab initio predictions link the neutron skin of ^{208}Pb to nuclear forces. Nat. Phys. **18**, 1196–1200 (2022). https://doi.org/10.1038/s41567-022-01715-8. arXiv:2112.01125 [nucl-th]
154. J.W.T. Keeble, A. Rios, Machine learning the deuteron. Phys. Lett. B **809**, 135743 (2020). https://doi.org/10.1016/j.physletb.2020.135743
155. C. Adams, G. Carleo, A. Lovato, N. Rocco, Variational Monte Carlo calculations of $A \leq 4$ nuclei with an artificial neural-network correlator Ansatz. Phys. Rev. Lett. **127**, 022502 (2021). https://doi.org/10.1103/PhysRevLett.127.022502
156. J.M. Yao, B. Bally, J. Engel, R. Wirth, T.R. Rodríguez, H. Hergert, *Abinitio* treatment of collective correlations and the neutrinoless double beta decay of ^{48}Ca. Phys. Rev. Lett. **124**(23), 232501 (2020). https://doi.org/10.1103/PhysRevLett.124.232501. arXiv:1908.05424 [nucl-th]
157. S.J. Novario, G. Hagen, G.R. Jansen, T. Papenbrock, Charge radii of exotic neon and magnesium isotopes. Phys. Rev. C **102**, 051303 (2020). https://doi.org/10.1103/PhysRevC.102.051303
158. M. Frosini, T. Duguet, J.-P. Ebran, V. Somà, Multi-reference many-body perturbation theory for nuclei: I. Novel PGCM-PT formalism. Eur. Phys. J. A **58**(4), 62 (2022). https://doi.org/10.1140/epja/s10050-022-00692-z. arXiv:2110.15737 [nucl-th]
159. Q. Yuan, S.Q. Fan, B.S. Hu, J.G. Li, S. Zhang, S.M. Wang, Z.H. Sun, Y.Z. Ma, F.R. Xu, Deformed in-medium similarity renormalization group. Phys. Rev. C **105**, 061303 (2022). https://doi.org/10.1103/PhysRevC.105.L061303. arXiv:2204.07301 [nucl-th]
160. A. Idini, C. Barbieri, P. Navrátil, Ab initio optical potentials and nucleon scattering on medium mass nuclei. Phys. Rev. Lett. **123**, 092501 (2019). https://doi.org/10.1103/PhysRevLett.123.092501
161. J. Rotureau, Coupled-cluster computations of optical potential for medium-mass nuclei. Front. Phys. **8**, 285 (2020). https://doi.org/10.3389/fphy.2020.00285
162. M. Vorabbi, C. Barbieri, V. Somà, P. Finelli, C. Giusti, Microscopic optical potentials from chiral nuclear interactions (2022) (**in preparation**)
163. V. Manea, J. Karthein, D. Atanasov, M. Bender, K. Blaum, T.E. Cocolios, S. Eliseev, A. Herlert, J.D. Holt, W.J. Huang, Y.A. Litvinov, D. Lunney, J. Menéndez, M. Mougeot, D. Neidherr, L. Schweikhard, A. Schwenk, J. Simonis, A. Welker, F. Wienholtz, K. Zuber, First glimpse of the $N = 82$ shell closure below $Z = 50$ from masses of neutron-rich cadmium isotopes and isomers. Phys. Rev. Lett. **124**, 092502 (2020). https://doi.org/10.1103/PhysRevLett.124.092502
164. G. Salvioni, J. Dobaczewski, C. Barbieri, G. Carlsson, A. Idini, A. Pastore, Model nuclear energy density functionals derived from ab initio calculations. J. Phys. G **47**(8), 085107 (2020). https://doi.org/10.1088/1361-6471/ab8d8e
165. F. Marino, C. Barbieri, A. Carbone, G. Colò, A. Lovato, F. Pederiva, X. Roca-Maza, E. Vigezzi, Nuclear energy density functionals grounded in ab initio calculations. Phys. Rev. C **104**, 024315 (2021). https://doi.org/10.1103/PhysRevC.104.024315

166. W. von Oertzen, M. Freer, Y. Kanada-En'yo, Nuclear clusters and nuclear molecules. Phys. Rep. **432**(2), 43–113 (2006). https://doi.org/10.1016/j.physrep.2006.07.001
167. Y. Ayyad, B. Olaizola, W. Mittig, G. Potel, V. Zelevinsky, M. Horoi, S. Beceiro-Novo, M. Alcorta, C. Andreoiu, T. Ahn, M. Anholm, L. Atar, A. Babu, D. Bazin, N. Bernier, S.S. Bhattacharjee, M. Bowry, R. Caballero-Folch, M. Cortesi, C. Dalitz, E. Dunling, A.B. Garnsworthy, M. Holl, B. Kootte, K.G. Leach, J.S. Randhawa, Y. Saito, C. Santamaria, P. Šiurytė, C.E. Svensson, R. Umashankar, N. Watwood, D. Yates, Direct observation of proton emission in ^{11}Be. Phys. Rev. Lett. **123**, 082501 (2019). https://doi.org/10.1103/PhysRevLett.123.082501
168. N. Cieplicka-Oryńczak, Y. Jaganathen, B. Fornal, S. Leoni, M. Płoszajczak, M. Ciemała, S. Ziliani, M. Kmiecik, A. Maj, J. Łukasik, P. Pawłowski, B. Sowicki, B. Wasilewska, M. Zbliński, P. Bednarczyk, C. Boiano, S. Bottoni, A. Bracco, S. Brambilla, I. Burducea, F. Camera, I. Ciepał, C. Clisu, F.C.L. Crespi, K. Dhanmeher, N. Florea, E. Gamba, J. Grbosz, M.N. Harakeh, D.A. Iancu, ŁW. Iskra, M. Krzysiek, P. Kulessa, N. Marginean, R. Marginean, I. Matea, M. Matejska-Minda, K. Mazurek, B. Million, W. Parol, M. Sferrazza, L. Stan, B. Włoch, The decay of the 21.47-mev stretched resonance in 13c: a precise probe of the open nuclear quantum system description. Phys. Lett. B **834**, 137398 (2022). https://doi.org/10.1016/j.physletb.2022.137398
169. M. Wiescher, G.P.A. Berg, M. Couder, J.L. Fisker, Y. Fujita, J. Görres, M.N. Harakeh, K. Hatanaka, A. Matic, W. Tan, A.M. van den Berg, Astrophysical nuclear reactions and the break-out from the hot CNO cycles. Prog. Part. Nucl. Phys. **59**(1), 51–65 (2007). https://doi.org/10.1016/j.ppnp.2007.01.021. (**International Workshop on Nuclear Physics 28th Course**)
170. K. Wimmer, T. Kröll, R. Krücken, V. Bildstein, R. Gernhäuser, B. Bastin, N. Bree, J. Diriken, P. Van Duppen, M. Huyse, N. Patronis, P. Vermaelen, D. Voulot, J. Van de Walle, F. Wenander, L.M. Fraile, R. Chapman, B. Hadinia, R. Orlandi, J.F. Smith, R. Lutter, P.G. Thirolf, M. Labiche, A. Blazhev, M. Kalkühler, P. Reiter, M. Seidlitz, N. Warr, A.O. Macchiavelli, H.B. Jeppesen, E. Fiori, G. Georgiev, G. Schrieder, S. Das Gupta, G. Lo Bianco, S. Nardelli, J. Butterworth, J. Johansen, K. Riisager, Discovery of the shape coexisting 0^+ state in ^{32}Mg by a two neutron transfer reaction. Phys. Rev. Lett. **105**, 252501 (2010). https://doi.org/10.1103/PhysRevLett.105.252501
171. Y. Ayyad, W. Mittig, T. Tang, B. Olaizola, G. Potel, N. Rijal, N. Watwood, H. Alvarez-Pol, D. Bazin, M. Caamaño, J. Chen, M. Cortesi, B. Fernández-Domínguez, S. Giraud, P. Gueye, S. Heinitz, R. Jain, B.P. Kay, E.A. Maugeri, B. Monteagudo, F. Ndayisabye, S.N. Paneru, J. Pereira, E. Rubino, C. Santamaria, D. Schumann, J. Surbrook, L. Wagner, J.C. Zamora, V. Zelevinsky, Evidence of a near-threshold resonance in ^{11}B relevant to the β-delayed proton emission of ^{11}Be. Phys. Rev. Lett. **129**, 012501 (2022). https://doi.org/10.1103/PhysRevLett.129.012501
172. E. Lopez-Saavedra, S. Almaraz-Calderon, B.W. Asher, L.T. Baby, N. Gerken, K. Hanselman, K.W. Kemper, A.N. Kuchera, A.B. Morelock, J.F. Perello, E.S. Temanson, A. Volya, I. Wiedenhöver, Observation of a near-threshold proton resonance in ^{11}B. Phys. Rev. Lett. **129**, 012502 (2022). https://doi.org/10.1103/PhysRevLett.129.012502
173. J. Okołowicz, M. Płoszajczak, W. Nazarewicz, Convenient location of a near-threshold proton-emitting resonance in ^{11}B. Phys. Rev. Lett. **124**, 042502 (2020). https://doi.org/10.1103/PhysRevLett.124.042502
174. M.C. Atkinson, P. Navrátil, G. Hupin, K. Kravvaris, S. Quaglioni, Ab initio calculation of the β decay from ^{11}Be to a ^{10}Be + p resonance. Phys. Rev. C **105**, 054316 (2022). https://doi.org/10.1103/PhysRevC.105.054316
175. W.P. Tan, J. Görres, M. Beard, M. Couder, A. Couture, S. Falahat, J.L. Fisker, L. Lamm, P.J. LeBlanc, H.Y. Lee, S. O'Brien, A. Palumbo, E. Stech, E. Strandberg, M. Wiescher, Measurement of the decay branching ratios of the α-unbound states in ^{19}Ne and the ^{15}O(α, γ) reaction rate. Phys. Rev. C **79**, 055805 (2009). https://doi.org/10.1103/PhysRevC.79.055805
176. B. Mauss, P. Morfouace, T. Roger, J. Pancin, G.F. Grinyer, J. Giovinazzo, V. Alcindor, H. Álvarez-Pol, A. Arokiaraj, M. Babo, B. Bastin, C. Borcea, M. Caamaño, S. Ceruti, B. Fernández-Domínguez, E. Foulon-Moret, P. Gangnant, S. Giraud, A. Laffoley, G. Mantovani, T. Marchi, B. Monteagudo, J. Pibernat, O. Poleshchuk, R. Raabe, J. Refsgaard, A. Revel, F. Saillant, M. Stanoiu, G. Wittwer, J. Yang, Commissioning of the ACtive TARget and Time Projection Chamber (ACTAR TPC). Nucl. Instrum. Methods Phys. Res. A **940**, 498–504 (2019). https://doi.org/10.1016/j.nima.2019.06.067
177. O. Poleshchuk, R. Raabe, S. Ceruti, A. Ceulemans, H. De Witte, T. Marchi, A. Mentana, J. Refsgaard, J. Yang, The SpecMAT active target. Nucl. Instrum. Methods Phys. Res. A **1015**, 165765 (2021). https://doi.org/10.1016/j.nima.2021.165765
178. A. Fernández, D. Hufschmidt, J.L. Colaux, J.J. Valiente-Dobón, V. Godinho, M.C. Jiménez de Haro, D. Feria, A. Gadea, S. Lucas, Low gas consumption fabrication of ^{3}He solid targets for nuclear reactions. Mater. Des. **186**, 108337 (2020). https://doi.org/10.1016/j.matdes.2019.108337
179. C. Wheldon, T. Kokalova, W. von Oertzen, S. Thummerer, H.G. Bohlen, B. Gebauer, A. Tumino, T.N. Massey, G. de Angelis, M. Axiotis, A. Gadea, T. Kröll, N. Marginean, D.R. Napoli, M. De Poli, C. Ur, D. Bazzacco, S.M. Lenzi, C. RossiAlvarez, S. Lunardi, R. Menegazzo, P.G. Bizzeti, A.M. Bizzeti-Sona, Octupole-deformed molecular bands in ^{21}Ne. Eur. Phys. J. A **26**(3), 321–326 (2005). https://doi.org/10.1140/epja/i2005-10186-y
180. S. Ziliani, M. Ciemała, F.C.L. Crespi, S. Leoni, B. Fornal, T. Suzuki, T. Otsuka, A. Maj, P. Bednarczyk, G. Benzoni, A. Bracco, C. Boiano, S. Bottoni, S. Brambilla, M. Bast, M. Beckers, T. Braunroth, F. Camera, N. Cieplicka-Oryńczak, E. Clément, S. Coelli, O. Dorvaux, S. Erturk, G. de France, C. Fransen, A. Goldkuhle, J. Grębosz, M.N. Harakeh, L.W. Iskra, B. Jacquot, A. Karpov, M. Kicińska-Habior, Y. Kim, M. Kmiecik, A. Lemasson, S.M. Lenzi, M. Lewitowicz, H. Li, I. Matea, K. Mazurek, C. Michelagnoli, M. Matejska-Minda, B. Million, C. Müller-Gatermann, V. Nanal, P. Napiorkowski, D.R. Napoli, R. Palit, M. Rejmund, C. Schmitt, M. Stanoiu, I. Stefan, E. Vardaci, B. Wasilewska, O. Wieland, M. Zębliński, M. Zielińska, Complete set of bound negative-parity states in the neutron-rich nucleus ^{18}N. Phys. Rev. C **104**, 041301 (2021). https://doi.org/10.1103/PhysRevC.104.L041301
181. M. Ciemała, S. Ziliani, F.C.L. Crespi, S. Leoni, B. Fornal, A. Maj, P. Bednarczyk, G. Benzoni, A. Bracco, C. Boiano, S. Bottoni, S. Brambilla, M. Bast, M. Beckers, T. Braunroth, F. Camera, N. Cieplicka-Oryńczak, E. Clément, S. Coelli, O. Dorvaux, S. Erturk, G. de France, C. Fransen, A. Goldkuhle, J. Grębosz, M.N. Harakeh, L.W. Iskra, B. Jacquot, A. Karpov, M. Kicińska-Habior, Y. Kim, M. Kmiecik, A. Lemasson, S.M. Lenzi, M. Lewitowicz, H. Li, I. Matea, K. Mazurek, C. Michelagnoli, M. Matejska-Minda, B. Million, C. Müller-Gatermann, V. Nanal, P. Napiorkowski, D.R. Napoli, R. Palit, M. Rejmund, C. Schmitt, M. Stanoiu, I. Stefan, E. Vardaci, B. Wasilewska, O. Wieland, M. Zębliński, M. Zielińska, A. Ataç, D. Barrientos, B. Birkenbach, A.J. Boston, B. Cederwall, L. Charles, J. Collado, D.M. Cullen, P. Désesquelles, C. Domingo-Pardo, J. Dudouet, J. Eberth, V. González, J. Goupil, L.J. Harkness-Brennan, H. Hess, D.S. Judson, A. Jungclaus, W. Korten, M. Labiche, A. Lefevre, R. Menegazzo, D. Mengoni, J. Nyberg, R.M. Perez-Vidal, Z. Podolyak, A. Pullia, F. Recchia, P. Reiter, F. Saillant, M.D. Salsac, E. Sanchis, O. Stézowski, C. Theisen, J.J. Valiente-Dobón, J.D. Holt, J. Menéndez, A. Schwenk, J. Simonis, Testing ab initio nuclear structure in neutron-rich nuclei: Lifetime measurements of second 2^+ state in ^{16}C and ^{20}O. Phys. Rev. C **101**, 021303 (2020). https://doi.org/10.1103/PhysRevC.101.021303
182. V.I. Zagrebaev, B. Fornal, S. Leoni, W. Greiner, Formation of light exotic nuclei in low-energy multinucleon transfer reactions. Phys. Rev. C **89**, 054608 (2014). https://doi.org/10.1103/PhysRevC.89.054608
183. C. Forssén, R. Roth, P. Navrátil, Systematics of 2^+ states in C isotopes from the no-core shell model. J. Phys. G **40**(5), 055105 (2013). https://doi.org/10.1088/0954-3899/40/5/055105
184. I. Zanon, Testing three-body forces in the oxygen region via lifetime measurements. Nuovo Cimento della Societa Italiana di Fisica C (2022). https://doi.org/10.1393/ncc/i2022-22066-y
185. I. Stefan, B. Fornal, S. Leoni, F. Azaiez, C. Portail, J.C. Thomas, A.V. Karpov, D. Ackermann, P. Bednarczyk, Y. Blumenfeld, S. Calinescu, A. Chbihi, M. Ciemala, N. Cieplicka-Oryńczak, F.C.L. Crespi, S. Franchoo, F. Hammache, ŁW. Iskra, B. Jacquot, R.V.F. Janssens, O. Kamalou, T. Lauritsen, M. Lewitowicz, L. Olivier, S.M. Lukyanov, M. Maccormick, A. Maj, P. Marini, I. Matea, M.A. Naumenko, F. de Oliveira Santos, C. Petrone, Y.E.

Penionzhkevich, F. Rotaru, H. Savajols, O. Sorlin, M. Stanoiu, B. Szpak, O.B. Tarasov, D. Verney, Neutron-rich nuclei produced at zero degrees in damped collisions induced by a beam of 18o on a 238u target. Phys. Lett. B **779**, 456–459 (2018). https://doi.org/10.1016/j.physletb.2018.02.037
186. J.-P. Ebran, E. Khan, T. Nikšić, D. Vretenar, Density functional theory studies of cluster states in nuclei. Phys. Rev. C **90**, 054329 (2014). https://doi.org/10.1103/PhysRevC.90.054329
187. T. Furumoto, T. Suhara, N. Itagaki, Drastic change of inelastic scattering dependent on the development of dineutron correlations in ^{10}Be. Phys. Rev. C **104**, 034613 (2021). https://doi.org/10.1103/PhysRevC.104.034613
188. D.R. Bès, R.A. Broglia, Pairing vibrations. Nucl. Phys. **80**(2), 289–313 (1966). https://doi.org/10.1016/0029-5582(66)90090-3
189. R.A. Broglia, O. Hansen, C. Riedel, Two-neutron transfer reactions and the pairing model, in *Advances in nuclear physics*, vol. 6, ed. by M. Baranger, E. Vogt (Springer, New York, 1973), pp.287–457. https://doi.org/10.1007/978-1-4615-9041-5_3
190. M. Assié, C.H. Dasso, R.J. Liotta, A.O. Macchiavelli, A. Vitturi, The giant pairing vibration in heavy nuclei—present status and future studies. Eur. Phys. J. A **55**(12), 245 (2019). https://doi.org/10.1140/epja/i2019-12829-8
191. F. Cappuzzello, D. Carbone, M. Cavallaro, M. Bondì, C. Agodi, F. Azaiez, A. Bonaccorso, A. Cunsolo, L. Fortunato, A. Foti, S. Franchoo, E. Khan, R. Linares, J. Lubian, J.A. Scarpaci, A. Vitturi, Signatures of the giant pairing vibration in the ^{14}C and ^{15}C atomic nuclei. Nat. Commum. **6**(6743), 1–7 (2015). https://doi.org/10.1038/ncomms7743
192. M. Laskin, R.F. Casten, A.O. Macchiavelli, R.M. Clark, D. Bucurescu, Population of the giant pairing vibration. Phys. Rev. C **93**, 034321 (2016). https://doi.org/10.1103/PhysRevC.93.034321
193. U. Garg, G. Colò, The compression-mode giant resonances and nuclear incompressibility. Prog. Part. Nucl. Phys. **101**, 55–95 (2018). https://doi.org/10.1016/j.ppnp.2018.03.001
194. M.N. Harakeh, A. van der Woude, *Giant Resonances Fundamental High-Frequency Modes of Nuclear Excitation* (Oxford University Press, New York, 2001)
195. U. Garg, P. Bogucki, J.D. Bronson, Y.-W. Lui, C.M. Rozsa, D.H. Youngblood, Splitting of the giant monopole resonance with deformation in Sm nuclei. Phys. Rev. Lett. **45**, 1670–1673 (1980). https://doi.org/10.1103/PhysRevLett.45.1670
196. Y.K. Gupta, U. Garg, J.T. Matta, D. Patel, T. Peach, J. Hoffman, K. Yoshida, M. Itoh, M. Fujiwara, K. Hara, H. Hashimoto, K. Nakanishi, M. Yosoi, H. Sakaguchi, S. Terashima, S. Kishi, T. Murakami, M. Uchida, Y. Yasuda, H. Akimune, T. Kawabata, M.N. Harakeh, Splitting of ISGMR strength in the light-mass nucleus ^{24}Mg due to ground-state deformation. Phys. Lett. B **748**, 343–346 (2015). https://doi.org/10.1016/j.physletb.2015.07.021
197. T. Peach, U. Garg, Y.K. Gupta, J. Hoffman, J.T. Matta, D. Patel, P.V.M. Rao, K. Yoshida, M. Itoh, M. Fujiwara, K. Hara, H. Hashimoto, K. Nakanishi, M. Yosoi, H. Sakaguchi, S. Terashima, S. Kishi, T. Murakami, M. Uchida, Y. Yasuda, H. Akimune, T. Kawabata, M.N. Harakeh, G. Colò, Effect of ground-state deformation on isoscalar giant resonances in ^{28}Si. Phys. Rev. C **93**, 064325 (2016). https://doi.org/10.1103/PhysRevC.93.064325
198. M. Vandebrouck, J. Gibelin, E. Khan, N.L. Achouri, H. Baba, D. Beaumel, Y. Blumenfeld, M. Caamaño, L. Càceres, G. Colò, F. Delaunay, B. Fernandez-Dominguez, U. Garg, G.F. Grinyer, M.N. Harakeh, N. Kalantar-Nayestanaki, N. Keeley, W. Mittig, J. Pancin, R. Raabe, T. Roger, P. Roussel-Chomaz, H. Savajols, O. Sorlin, C. Stodel, D. Suzuki, J.C. Thomas, Measurement of the isoscalar monopole response in the neutron-rich nucleus ^{68}Ni. Phys. Rev. Lett. **113**, 032504 (2014). https://doi.org/10.1103/PhysRevLett.113.032504
199. E.K. Warburton, J.A. Becker, B.A. Brown, Mass systematics for A=29-44 nuclei: the deformed A∼32 region. Phys. Rev. C **41**, 1147–1166 (1990). https://doi.org/10.1103/PhysRevC.41.1147
200. Y. Utsuno, T. Otsuka, T. Mizusaki, M. Honma, Varying shell gap and deformation in $N\sim20$ unstable nuclei studied by the Monte Carlo shell model. Phys. Rev. C **60**, 054315 (1999). https://doi.org/10.1103/PhysRevC.60.054315
201. E. Caurier, F. Nowacki, A. Poves, Merging of the islands of inversion at $N = 20$ and $N = 28$. Phys. Rev. C **90**, 014302 (2014). https://doi.org/10.1103/PhysRevC.90.014302
202. A.N. Deacon, J.F. Smith, S.J. Freeman, R.V.F. Janssens, M.P. Carpenter, B. Hadinia, C.R. Hoffman, B.P. Kay, T. Lauritsen, C.J. Lister, D. O'Donnell, J. Ollier, T. Otsuka, D. Seweryniak, K.-M. Spohr, D. Steppenbeck, S.L. Tabor, V. Tripathi, Y. Utsuno, P.T. Wady, S. Zhu, Cross-shell excitations near the "island of inversion": structure of ^{30}Mg. Phys. Rev. C **82**, 034305 (2010). https://doi.org/10.1103/PhysRevC.82.034305
203. S. Leoni, B. Fornal, N. Mărginean, M. Sferrazza, Y. Tsunoda, T. Otsuka, G. Bocchi, F.C.L. Crespi, A. Bracco, S. Aydin, M. Boromiza, D. Bucurescu, N. Cieplicka-Oryńczak, C. Costache, S. Călinescu, N. Florea, D.G. Ghiţă, T. Glodariu, A. Ionescu, L.W. Iskra, M. Krzysiek, R. Mărginean, C. Mihai, R.E. Mihai, A. Mitu, A. Negreţ, C.R. Niţă, A. Olăcel, A. Oprea, S. Pascu, P. Petkov, C. Petrone, G. Porzio, A. Şerban, C. Sotty, L. Stan, I. Ştiru, L. Stroe, R. Şuvăil, S. Toma, A. Turturică, S. Ujeniuc, C.A. Ur, Multifaceted quadruplet of low-lying spin-zero states in ^{66}Ni: emergence of shape isomerism in light nuclei. Phys. Rev. Lett. **118**, 162502 (2017). https://doi.org/10.1103/PhysRevLett.118.162502
204. N. Mărginean, D. Little, Y. Tsunoda, S. Leoni, R.V.F. Janssens, B. Fornal, T. Otsuka, C. Michelagnoli, L. Stan, F.C.L. Crespi, C. Costache, R. Lica, M. Sferrazza, A. Turturica, A.D. Ayangeakaa, K. Auranen, M. Barani, P.C. Bender, S. Bottoni, M. Boromiza, A. Bracco, S. Călinescu, C.M. Campbell, M.P. Carpenter, P. Chowdhury, M. Ciemała, N. Cieplicka-Oryńczak, D. Cline, C. Clisu, H.L. Crawford, I.E. Dinescu, J. Dudouet, D. Filipescu, N. Florea, A.M. Forney, S. Fracassetti, A. Gade, I. Gheorghe, A.B. Hayes, I. Harca, J. Henderson, A. Ionescu, L.W. Iskra, M. Jentschel, F. Kandzia, Y.H. Kim, F.G. Kondev, G. Krishichayan, U. Korschinek, M. Köster, T. Krzysiek, J. Lauritsen, R. Li, E.A. Mărginean, C. Maugeri, R.E. Mihai, A. Mihai, P. Mitu, A. Mutti, C.R. Negret, A. Niţă, A. Olăcel, S. Oprea, C. Pascu, C. Petrone, D. Porzio, D. Rhodes, D. Seweryniak, C. Schumann, S.M. Sotty, R. Stolze, S. Şuvăilă, S. Toma, W.B. Ujeniuc, C.Y. Walters, J. Wu, S. Wu, S. Ziliani. Zhu, Shape coexistence at zero spin in ^{64}Ni driven by the monopole tensor interaction. Phys. Rev. Lett. **125**, 102502 (2020). https://doi.org/10.1103/PhysRevLett.125.102502
205. M. Bernas, P. Dessagne, M. Langevin, J. Payet, F. Pougheon, P. Roussel, Magic features of ^{68}Ni. Phys. Lett. B **113**(4), 279–282 (1982). https://doi.org/10.1016/0370-2693(82)90039-9
206. K. Nowak, K. Wimmer, S. Hellgartner, D. Mücher, V. Bildstein, J. Diriken, J. Elseviers, L.P. Gaffney, R. Gernhäuser, J. Iwanicki, J.G. Johansen, M. Huyse, J. Konki, T. Kröll, R. Krücken, R. Lutter, R. Orlandi, J. Pakarinen, R. Raabe, P. Reiter, T. Roger, G. Schrieder, M. Seidlitz, O. Sorlin, P. Van Duppen, N. Warr, H. De Witte, M. Zielińska, Spectroscopy of ^{46}Ar by the $(t,\ p)$ two-neutron transfer reaction. Phys. Rev. C **93**, 044335 (2016). https://doi.org/10.1103/PhysRevC.93.044335
207. S. Calinescu, L. Cáceres, S. Grévy, O. Sorlin, Z. Dombrádi, M. Stanoiu, R. Astabatyan, C. Borcea, R. Borcea, M. Bowry, W. Catford, E. Clément, S. Franchoo, R. Garcia, R. Gillibert, I.H. Guerin, I. Kuti, S. Lukyanov, A. Lepailleur, V. Maslov, P. Morfouace, J. Mrazek, F. Negoita, M. Niikura, L. Perrot, Z. Podolyák, C. Petrone, Y. Penionzhkevich, T. Roger, F. Rotaru, D. Sohler, I. Stefan, J.C. Thomas, Z. Vajta, E. Wilson, Coulomb excitation of ^{44}Ca and ^{46}Ar. Phys. Rev. C **93**, 044333 (2016). https://doi.org/10.1103/PhysRevC.93.044333
208. K. Langanke, D.J. Dean, S.E. Koonin, P.B. Radha, Pairing correlations in $N\sim Z$ pf-shell nuclei. Nucl. Phys. A **613**(3), 253–266 (1997). https://doi.org/10.1016/S0375-9474(96)00442-3
209. C.R. Alvarez, The GASP array. Nucl. Phys. News **3**(3), 10–13 (1993). https://doi.org/10.1080/10506899308221154
210. W. Korten, S. Lunardi, Achievements with the Euroball Spectrometer (1997). http://euroball.lnl.infn.it/
211. R.A. Broglia, V. Zelevinsky, *Fifty Years of Nuclear BCS* (World Scientific, Singapore, 2013). https://doi.org/10.1142/8526
212. S. Frauendorf, A.O. Macchiavelli, Overview of neutron-proton pairing. Prog. Part. Nucl. Phys. **78**, 24–90 (2014). https://doi.org/10.1016/j.ppnp.2014.07.001

213. K. Yoshida, Proton-neutron pairing vibrations in N = Z nuclei: precursory soft mode of isoscalar pairing condensation. Phys. Rev. C **90**, 031303 (2014). https://doi.org/10.1103/PhysRevC.90.031303
214. B.F. Bayman, N.M. Hintz, Analysis of two-neutron (L=0) transfer cross sections for calcium and nickel. Phys. Rev. **172**(4), 1113–1123 (1968). https://doi.org/10.1103/PhysRev.172.1113
215. P. Fröbich, Enhancement of deuteron transfer reactions by neutron–proton pairing correlations. Phys. Lett. B **37**(4), 338–340 (1971). https://doi.org/10.1016/0370-2693(71)90195-X
216. P. Van Isacker, D.D. Warner, A. Frank, Deuteron transfer in N=Z nuclei. Phys. Rev. Lett. **94**(16), 162502 (2005). https://doi.org/10.1103/PhysRevLett.94.162502
217. J.A. Lay, Y. Ayyad, A.O. Macchiavelli, Neutron–proton pair transfer reactions and corresponding Weisskopf-type units. Phys. Lett. B **824**, 136789 (2022). https://doi.org/10.1016/j.physletb.2021.136789
218. M. Sambataro, N. Sandulescu, Four-body correlations in nuclei. Phys. Rev. Lett. **115**(11), 112501 (2015). https://doi.org/10.1103/PhysRevLett.115.112501
219. M. Sambataro, N. Sandulescu, Quartet correlations in N = Z nuclei induced by realistic two-body interactions. Eur. Phys. J. A **53**, 47 (2017). https://doi.org/10.1140/epja/i2017-12240-7
220. D. Rudolph, C. Baktash, M.J. Brinkman, E. Caurier, D.J. Dean, M. Devlin, J. Dobaczewski, P.-H. Heenen, H.-Q. Jin, D.R. LaFosse, W. Nazarewicz, F. Nowacki, A. Poves, L.L. Riedinger, D.G. Sarantites, W. Satuła, C.-H. Yu, Rotational bands in the doubly magic nucleus ^{56}Ni. Phys. Rev. Lett. **82**(19), 3763–3766 (1999). https://doi.org/10.1103/PhysRevLett.82.3763
221. A.P. Zuker, A. Poves, F. Nowacki, S.M. Lenzi, Nilsson-SU3 self-consistency in heavy N = Z nuclei. Phys. Rev. C **92**, 024320 (2015). https://doi.org/10.1103/PhysRevC.92.024320
222. D.D. Dao, F. Nowacki, Nuclear structure within a discrete nonorthogonal shell model approach: new frontiers. Phys. Rev. C **105**, 054314 (2022). https://doi.org/10.1103/PhysRevC.105.054314
223. E. Wigner, On the consequences of the symmetry of the nuclear Hamiltonian on the spectroscopy of nuclei. Phys. Rev. **51**, 106–119 (1937). https://doi.org/10.1103/PhysRev.51.106
224. A.P. Zuker, S.M. Lenzi, G. Martínez-Pinedo, A. Poves, Isobaric multiplet yrast energies and isospin nonconserving forces. Phys. Rev. Lett. **89**(14), 142502 (2002). https://doi.org/10.1103/PhysRevLett.89.142502
225. M.A. Bentley, S.M. Lenzi, Coulomb energy differences between high-spin states in isobaric multiplets. Prog. Part. Nucl. Phys. **59**(2), 497–561 (2007). https://doi.org/10.1016/j.ppnp.2006.10.001
226. J. Ekman, D. Rudolph, C. Fahlander, A.P. Zuker, M.A. Bentley, S.M. Lenzi, C. Andreoiu, M. Axiotis, G. de Angelis, E. Farnea, A. Gadea, T. Kröll, N. Mărginean, T. Martinez, M.N. Mineva, C. Rossi-Alvarez, C.A. Ur, Unusual isospin-breaking and isospin-mixing effects in the A=35 mirror nuclei. Phys. Rev. Lett. **92**(13), 132502 (2004). https://doi.org/10.1103/PhysRevLett.92.132502
227. M.A. Bentley, S.M. Lenzi, S.A. Simpson, C. Aa. Diget, Isospin-breaking interactions studied through mirror energy differences. Phys. Rev. C **92**(2), 024310 (2015). https://doi.org/10.1103/PhysRevC.92.024310
228. S.M. Lenzi, M.A. Bentley, R. Lau, C. Aa. Diget, Isospin-symmetry breaking corrections for the description of triplet energy differences. Phys. Rev. C **98**(5), 054322 (2018). https://doi.org/10.1103/PhysRevC.98.054322
229. M.A. Bentley, Excited states in isobaric multiplets—experimental advances and the shell-model approach. Physics **4**(3), 995–1011 (2022). https://doi.org/10.3390/physics4030066
230. A. Boso, S.A. Milne, M.A. Bentley, F. Recchia, S.M. Lenzi, D. Rudolph, M. Labiche, X. Pereira-Lopez, S. Afara, F. Ameil, T. Arici, S. Aydin, M. Axiotis, D. Barrientos, G. Benzoni, B. Birkenbach, A.J. Boston, H.C. Boston, P. Boutachkov, A. Bracco, A.M. Bruce, B. Bruyneel, B. Cederwall, E. Clément, M.L. Cortés, D.M. Cullen, P. Désesquelles, Z. Dombràdi, C. Domingo-Pardo, J. Eberth, C. Fahlander, M. Gelain, V. González, P.R. John, J. Gerl, P. Golubev, M. Górska, A. Gottardo, T. Grahn, L. Grassi, T. Habermann, L.J. Harkness-Brennan, T.W. Henry, H. Hess, I. Kojouharov, W. Korten, N. Lalović, M. Lettmann, C. Lizarazo, C. Louchart-Henning, R. Menegazzo, D. Mengoni, E. Merchan, C. Michelagnoli, B. Million, V. Modamio, T. Moeller, D.R. Napoli, J. Nyberg, B.S. Nara Singh, H. Pai, N. Pietralla, S. Pietri, Z. Podolyak, R.M. Perez Vidal, A. Pullia, D. Ralet, G. Rainovski, M. Reese, P. Reiter, M.D. Salsac, E. Sanchis, L.G. Sarmiento, H. Schaffner, L.M. Scruton, P.P. Singh, C. Stahl, S. Uthayakumaar, J.J. Valiente-Dobón, O. Wieland, Isospin dependence of electromagnetic transition strengths among an isobaric triplet. Phys. Lett. B **797**, 134835 (2019). https://doi.org/10.1016/j.physletb.2019.134835
231. W.J. Marciano, A. Sirlin, Radiative corrections to β decay and the possibility of a fourth generation. Phys. Rev. Lett. **56**, 22–25 (1986). https://doi.org/10.1103/PhysRevLett.56.22
232. A. Falkowsky, M. González-Alonso, O. Navillat-Cuncic, Comprehensive analysis of beta decays within and beyond the standard model. J. High Energy Phys. (2021). https://doi.org/10.1007/JHEP04(2021)126
233. J.C. Hardy, I.S. Towner, Superallowed $0^+ \rightarrow 0^+$ nuclear β decays: 2014 critical survey, with precise results for V_{ud} and CKM unitarity. Phys. Rev. C **91**, 025501 (2015). https://doi.org/10.1103/PhysRevC.91.025501
234. N. Severijns, L. Hayen, V. De Leebeeck, S. Vanlangendonck, K. Bodek, D. Rozpedzik, I. Towner, $\mathcal{F}t$ values of the mirror β transitions and the weak magnetism induced current in allowed nuclear β decay (2021). arXiv:2109.08895 [nucl-th]
235. J.B. French, Adaptive selection methods for genetic algorithms, in *Proceedings of the International School of Physics Enrico Fermi, Varenna 1965*. ed. by C. Bloch (Academic Press, New York, 1966), p.36
236. M. Baranger, A definition of the single-nucleon potential. Nucl. Phys. A **149**(2), 225–240 (1970). https://doi.org/10.1016/0375-9474(70)90692-5
237. T. Duguet, G. Hagen, Ab-initio approach to effective single-particle energies in doubly closed shell nuclei. Phys. Rev. C **85**, 034330 (2012). https://doi.org/10.1103/PhysRevC.85.034330
238. T. Duguet, H. Hergert, J.D. Holt, V. Somà, Nonobservable nature of the nuclear shell structure: meaning, illustrations, and consequences. Phys. Rev. C **92**(3), 034313 (2015). https://doi.org/10.1103/PhysRevC.92.034313. arXiv:1411.1237 [nucl-th]
239. J.P. Schiffer, C.R. Hoffman, B.P. Kay, J.A. Clark, C.M. Deibel, S.J. Freeman, A.M. Howard, A.J. Mitchell, P.D. Parker, D.K. Sharp, J.S. Thomas, Test of sum rules in nucleon transfer reactions. Phys. Rev. Lett. **108**, 022501 (2012). https://doi.org/10.1103/PhysRevLett.108.022501
240. T. Duguet, A. Signoracci, V. Somà (2022) (**unpublished**)
241. M. Bender, P.-H. Heenen, P.-G. Reinhard, Self-consistent mean-field models for nuclear structure. Rev. Mod. Phys. **75**, 121–180 (2003). https://doi.org/10.1103/RevModPhys.75.121
242. L.M. Robledo, T.R. Rodríguez, R.R. Rodríguez-Guzmán, Mean field and beyond description of nuclear structure with the Gogny force: a review. J. Phys. G **46**(1), 013001 (2018). https://doi.org/10.1088/1361-6471/aadebd
243. J.L. Egido, State-of-the-art of beyond mean field theories with nuclear density functionals. Phys. Scr. **91**(7), 073003 (2016). https://doi.org/10.1088/0031-8949/91/7/073003
244. T. Nikšić, D. Vretenar, P. Ring, Relativistic nuclear energy density functionals: mean-field and beyond. Prog. Part. Nucl. Phys. **66**(3), 519–548 (2011). https://doi.org/10.1016/j.ppnp.2011.01.055

245. M. Bender, K. Rutz, P.-G. Reinhard, J.A. Maruhn, Pairing gaps from nuclear mean-field models. Eur. Phys. J. A **8**(1), 59–75 (2000). https://doi.org/10.1007/s10050-000-4504-z
246. T. Duguet, P. Bonche, P.-H. Heenen, J. Meyer, Pairing correlations. I. Description of odd nuclei in mean-field theories. Phys. Rev. C **65**, 014310 (2001). https://doi.org/10.1103/PhysRevC.65.014310
247. T. Duguet, P. Bonche, P.-H. Heenen, J. Meyer, Pairing correlations. II. Microscopic analysis of odd-even mass staggering in nuclei. Phys. Rev. C **65**, 014311 (2001). https://doi.org/10.1103/PhysRevC.65.014311
248. N. Schunck, J. Dobaczewski, J. McDonnell, J. Moré, W. Nazarewicz, J. Sarich, M.V. Stoitsov, One-quasiparticle states in the nuclear energy density functional theory. Phys. Rev. C **81**, 024316 (2010). https://doi.org/10.1103/PhysRevC.81.024316
249. L.M. Robledo, R. Bernard, G.F. Bertsch, Pairing gaps in the Hartree–Fock–Bogoliubov theory with the Gogny D1S interaction. Phys. Rev. C **86**, 064313 (2012). https://doi.org/10.1103/PhysRevC.86.064313
250. S. Perez-Martin, L.M. Robledo, Microscopic justification of the equal filling approximation. Phys. Rev. C **78**, 014304 (2008). https://doi.org/10.1103/PhysRevC.78.014304
251. G.F. Bertsch, C.A. Bertulani, W. Nazarewicz, N. Schunck, M.V. Stoitsov, Odd-even mass differences from self-consistent mean field theory. Phys. Rev. C **79**, 034306 (2009). https://doi.org/10.1103/PhysRevC.79.034306
252. R. Rodriguez-Guzman, P. Sarriguren, L.M. Robledo, Systematics of one-quasiparticle configurations in neutron-rich odd Sr, Zr, and Mo isotopes with the Gogny energy density functional. Phys. Rev. C **82**, 044318 (2010). https://doi.org/10.1103/PhysRevC.82.044318
253. B. Bally, B. Avez, M. Bender, P.-H. Heenen, Beyond mean-field calculations for odd-mass nuclei. Phys. Rev. Lett. **113**, 162501 (2014). https://doi.org/10.1103/PhysRevLett.113.162501
254. M. Borrajo, J.L. Egido, Ground-state properties of even and odd magnesium isotopes in a symmetry-conserving approach. Phys. Lett. B **764**, 328–334 (2017). https://doi.org/10.1016/j.physletb.2016.11.037
255. M. Borrajo, J.L. Egido, Symmetry conserving configuration mixing description of odd mass nuclei. Phys. Rev. C **98**, 044317 (2018). https://doi.org/10.1103/PhysRevC.98.044317
256. K.J. Pototzky, J. Erler, P.-G. Reinhard, V.O. Nesterenko, Properties of odd nuclei and the impact of time-odd mean fields: a systematic Skyrme–Hartree—Fock analysis. Eur. Phys. J. A **46**(2), 299–313 (2010). https://doi.org/10.1140/epja/i2010-11045-6
257. A.V. Afanasjev, H. Abusara, Time-odd mean fields in covariant density functional theory: nonrotating systems. Phys. Rev. C **81**, 014309 (2010). https://doi.org/10.1103/PhysRevC.81.014309
258. B. Bally, M. Bender, Projection on particle number and angular momentum: example of triaxial Bogoliubov quasiparticle states. Phys. Rev. C **103**, 024315 (2021). https://doi.org/10.1103/PhysRevC.103.024315
259. M. Anguiano, J.L. Egido, L.M. Robledo, Particle number projection with effective forces. Nucl. Phys. A **696**(3), 467–493 (2001). https://doi.org/10.1016/S0375-9474(01)01219-2
260. D. Lacroix, T. Duguet, M. Bender, Configuration mixing within the energy density functional formalism: removing spurious contributions from nondiagonal energy kernels. Phys. Rev. C **79**, 044318 (2009). https://doi.org/10.1103/PhysRevC.79.044318
261. M. Bender, T. Duguet, D. Lacroix, Particle-number restoration within the energy density functional formalism. Phys. Rev. C **79**, 044319 (2009). https://doi.org/10.1103/PhysRevC.79.044319
262. B. Bally, A. Sánchez-Fernández, T.R. Rodríguez, Variational approximations to exact solutions in shell-model valence spaces: calcium isotopes in the pf shell. Phys. Rev. C **100**, 044308 (2019). https://doi.org/10.1103/PhysRevC.100.044308
263. A. Sánchez-Fernández, B. Bally, T.R. Rodríguez, Variational approximations to exact solutions in shell-model valence spaces: systematic calculations in the sd shell. Phys. Rev. C **104**, 054306 (2021). https://doi.org/10.1103/PhysRevC.104.054306
264. B. Bally, A. Sáchez-Fernández, T.R. Rodríguez, Symmetry-projected variational calculations with the numerical suite taurus. Eur. Phys. J. A **57**(2), 69 (2021). https://doi.org/10.1140/epja/s10050-021-00369-z
265. M. Frosini, T. Duguet, J.-P. Ebran, B. Bally, T. Mongelli, T.R. Rodríguez, R. Roth, V. Somà, Multi-reference many-body perturbation theory for nuclei: II. Ab initio study of neon isotopes via PGCM and IM-NCSM calculations. Eur. Phys. J. A **58**(4), 63 (2022). https://doi.org/10.1140/epja/s10050-022-00693-y. arXiv:2111.00797 [nucl-th]
266. N. Shimizu, T. Mizusaki, K. Kaneko, Y. Tsunoda, Generator-coordinate methods with symmetry-restored Hartree–Fock–Bogoliubov wave functions for large-scale shell-model calculations. Phys. Rev. C **103**, 064302 (2021). https://doi.org/10.1103/PhysRevC.103.064302
267. R. Taniuchi, C. Santamaria, P. Doornenbal, A. Obertelli, K. Yoneda, G. Authelet, H. Baba, D. Calvet, F. Château, A. Corsi, A. Delbart, J.-M. Gheller, A. Gillibert, J.D. Holt, T. Isobe, V. Lapoux, M. Matsushita, J. Menéndez, S. Momiyama, T. Motobayashi, M. Niikura, F. Nowacki, K. Ogata, H. Otsu, T. Otsuka, C. Péron, S. Péru, A. Peyaud, E.C. Pollacco, A. Poves, J.-Y. Roussé, H. Sakurai, A. Schwenk, Y. Shiga, J. Simonis, S.R. Stroberg, S. Takeuchi, Y. Tsunoda, T. Uesaka, H. Wang, F. Browne, L.X. Chung, Z. Dombradi, S. Franchoo, F. Giacoppo, A. Gottardo, K. Hadyńska-Klęk, Z. Korkulu, S. Koyama, Y. Kubota, J. Lee, M. Lettmann, C. Louchart, R. Lozeva, K. Matsui, T. Miyazaki, S. Nishimura, L. Olivier, S. Ota, Z. Patel, E. Sahin, C. Shand, P.-A. Söderström, I. Stefan, D. Steppenbeck, T. Sumikama, D. Suzuki, Z. Vajta, V. Werner, J. Wu, Z.Y. Xu, ^{78}Ni revealed as a doubly magic stronghold against nuclear deformation. Nature **569**(7754), 53–58 (2019). https://doi.org/10.1038/s41586-019-1155-x
268. C. Delafosse, D. Verney, P. Marević, A. Gottardo, C. Michelagnoli, A. Lemasson, A. Goasduff, J. Ljungvall, E. Clément, A. Korichi, G. de Angelis, C. Andreoiu, M. Babo, A. Boso, F. Didierjean, J. Dudouet, S. Franchoo, A. Gadea, G. Georgiev, F. Ibrahim, B. Jacquot, T. Konstantinopoulos, S.M. Lenzi, G. Maquart, I. Matea, D. Mengoni, D.R. Napoli, T. Nikšić, L. Olivier, R.M. Pérez-Vidal, C. Portail, F. Recchia, N. Redon, M. Siciliano, I. Stefan, O. Stézowski, D. Vretenar, M. Zielińska, D. Barrientos, G. Benzoni, B. Birkenbach, A.J. Boston, H.C. Boston, B. Cederwall, L. Charles, M. Ciemała, J. Collado, D.M. Cullen, P. Désesquelles, G. de France, C. Domingo-Pardo, J. Eberth, V. González, L.J. Harkness-Brennan, H. Hess, D.S. Judson, A. Jungclaus, W. Korten, A. Lefevre, F. Legruel, R. Menegazzo, B. Million, J. Nyberg, B. Quintana, D. Ralet, P. Reiter, F. Saillant, E. Sanchis, C. Theisen, J.J. Valiente Dobon, Pseudospin symmetry and microscopic origin of shape coexistence in the ^{78}Ni region: a hint from lifetime measurements. Phys. Rev. Lett. **121**, 192502 (2018). https://doi.org/10.1103/PhysRevLett.121.192502
269. F. Nowacki, A. Poves, E. Caurier, B. Bounthong, Shape coexistence in ^{78}Ni as the portal to the fifth island of inversion. Phys. Rev. Lett. **117**, 272501 (2016). https://doi.org/10.1103/PhysRevLett.117.272501
270. J. Hakala, S. Rahaman, V.-V. Elomaa, T. Eronen, U. Hager, A. Jokinen, A. Kankainen, I.D. Moore, H. Penttilä, S. Rinta-Antila, J. Rissanen, A. Saastamoinen, T. Sonoda, C. Weber, J. Äystö, Evolution of the $N = 50$ shell gap energy towards ^{78}Ni. Phys. Rev. Lett. **101**, 052502 (2008). https://doi.org/10.1103/PhysRevLett.101.052502
271. S. Baruah, G. Audi, K. Blaum, M. Dworschak, S. George, C. Guénaut, U. Hager, F. Herfurth, A. Herlert, A. Kellerbauer, H.-J. Kluge, D. Lunney, H. Schatz, L. Schweikhard, C. Yazidjian, Mass measurements beyond the major r-process waiting point ^{80}Zn. Phys. Rev. Lett. **101**, 262501 (2008). https://doi.org/10.1103/PhysRevLett.101.262501
272. L. Olivier, S. Franchoo, M. Niikura, Z. Vajta, D. Sohler, P. Doornenbal, A. Obertelli, Y. Tsunoda, T. Otsuka, G. Authelet, H. Baba, D. Calvet, F. Château, A. Corsi, A. Delbart, J.-M. Gheller, A. Gillibert, T. Isobe, V. Lapoux, M. Matsushita, S. Momiyama, T. Motobayashi, H. Otsu, C. Péron, A. Peyaud, E.C. Pollacco, J.-Y. Roussé, H. Sakurai, C. Santamaria, M. Sasano, Y. Shiga, S. Takeuchi, R. Taniuchi, T. Uesaka, H. Wang, K. Yoneda, F. Browne,

L.X. Chung, Z. Dombradi, F. Flavigny, F. Giacoppo, A. Gottardo, K. Hadyńska-Klęk, Z. Korkulu, S. Koyama, Y. Kubota, J. Lee, M. Lettmann, C. Louchart, R. Lozeva, K. Matsui, T. Miyazaki, S. Nishimura, K. Ogata, S. Ota, Z. Patel, E. Sahin, C. Shand, P.-A. Söderström, I. Stefan, D. Steppenbeck, T. Sumikama, D. Suzuki, V. Werner, J. Wu, Z. Xu, Persistence of the $Z = 28$ shell gap around ^{78}Ni: first spectroscopy of ^{79}Cu. Phys. Rev. Lett. **119**, 192501 (2017). https://doi.org/10.1103/PhysRevLett.119.192501

273. D. Verney, D. Testov, F. Ibrahim, Y. Penionzhkevich, B. Roussière, V. Smirnov, F. Didierjean, K. Flanagan, S. Franchoo, E. Kuznetsova, R. Li, B. Marsh, I. Matea, H. Pai, E. Sokol, I. Stefan, D. Suzuki, Pygmy Gamow–Teller resonance in the $N = 50$ region: new evidence from staggering of β-delayed neutron-emission probabilities. Phys. Rev. C **95**, 054320 (2017). https://doi.org/10.1103/PhysRevC.95.054320
274. C. Delafosse, A. Goasduff, A. Kankainen, D. Verney, L. Al Ayoubi, O. Beliuskina, L. Cañete, T. Eronen, R.P. de Groote, M. Hukkanen, F. Ibrahim, A. Illana, A. Jaries, L. Lalanne, I.D. Moore, D. Nesterenko, H. Penttilä, S. Rinta-Antila, A. de Roubin, D. Thisse, R. Thoër, G. Tocabens, First trap-assisted decay spectroscopy of the ^{81}Ge ground state. Eur. Phys. J. A **58**(3), 51 (2022). https://doi.org/10.1140/epja/s10050-022-00698-7
275. D.K. Sharp, B.P. Kay, J.S. Thomas, S.J. Freeman, J.P. Schiffer, B.B. Back, S. Bedoor, T. Bloxham, J.A. Clark, C.M. Deibel, C.R. Hoffman, A.M. Howard, J.C. Lighthall, S.T. Marley, A.J. Mitchell, T. Otsuka, P.D. Parker, K.E. Rehm, D.V. Shetty, A.H. Wuosmaa, Neutron single-particle strength outside the $N = 50$ core. Phys. Rev. C **87**, 014312 (2013). https://doi.org/10.1103/PhysRevC.87.014312
276. J.S. Thomas, D.W. Bardayan, J.C. Blackmon, J.A. Cizewski, U. Greife, C.J. Gross, M.S. Johnson, K.L. Jones, R.L. Kozub, J.F. Liang, R.J. Livesay, Z. Ma, B.H. Moazen, C.D. Nesaraja, D. Shapira, M.S. Smith, First study of the level structure of the r-process nucleus ^{83}Ge. Phys. Rev. C **71**, 021302 (2005). https://doi.org/10.1103/PhysRevC.71.021302
277. K. Heyde, J.L. Wood, Shape coexistence in atomic nuclei. Rev. Mod. Phys. **83**, 1467–1521 (2011). https://doi.org/10.1103/RevModPhys.83.1467
278. J.L. Wood, E.F. Zganjar, C. De Coster, K. Heyde, Electric monopole transitions from low energy excitations in nuclei. Nucl. Phys. A **651**(4), 323–368 (1999). https://doi.org/10.1016/S0375-9474(99)00143-8
279. E.F. Zganjar, Conversion electron spectroscopy and its role in identifying shape coexisting structures in nuclei via E0 transitions. J. Phys. G **43**(2), 024013 (2016). https://doi.org/10.1088/0954-3899/43/2/024013
280. J.L. Wood, K. Heyde, A focus on shape coexistence in nuclei. J. Phys. G **43**(2), 020402 (2016). https://doi.org/10.1088/0954-3899/43/2/020402
281. H. Mach, M. Moszyński, R.L. Gill, F.K. Wohn, J.A. Winger, C. Hill, G. Molnár, K. Sistemich, Deformation and shape coexistence of 0^+ states in ^{98}Sr and ^{100}Zr. Phys. Lett. B **230**(1), 21–26 (1989). https://doi.org/10.1016/0370-2693(89)91646-8
282. N. Mărginean, D.L. Balabanski, D. Bucurescu, S. Lalkovski, L. Atanasova, G. Căta-Danil, I. Căta-Danil, J.M. Daugas, D. Deleanu, P. Detistov, G. Deyanova, D. Filipescu, G. Georgiev, D. Ghiţă, K.A. Gladnishki, R. Lozeva, T. Glodariu, M. Ivaşcu, S. Kisyov, C. Mihai, R. Mărginean, A. Negret, S. Pascu, D. Radulov, T. Sava, L. Stroe, G. Suliman, N.V. Zamfir, In-beam measurements of sub-nanosecond nuclear lifetimes with a mixed array of HPGe and LaBr 3: Ce detectors. Eur. Phys. J. A **46**(1), 329–336 (2010). https://doi.org/10.1140/epja/i2010-11052-7
283. J.-M. Régis, G. Pascovici, J. Jolie, M. Rudigier, The mirror symmetric centroid difference method for picosecond lifetime measurements via $\gamma - \gamma$ coincidences using very fast LaBr 3(Ce) scintillator detectors. Nucl. Instrum. Methods Phys. Res. A **622**(1), 83–92 (2010). https://doi.org/10.1016/j.nima.2010.07.047
284. P.-A. Söderström, S. Nishimura, P. Doornenbal, G. Lorusso, T. Sumikama, H. Watanabe, Z.Y. Xu, H. Baba, F. Browne, S. Go, G. Gey, T. Isobe, H.-S. Jung, G.D. Kim, Y.-K. Kim, I. Kojouharov, N. Kurz, Y.K. Kwon, Z. Li, K. Moschner, T. Nakao, H. Nishibata, M. Nishimura, A. Odahara, H. Sakurai, H. Schaffner, T. Shimoda, J. Taprogge, Z. Vajta, V. Werner, J. Wu, A. Yagi, K. Yoshinaga, Installation and commissioning of EURICA—Euroball-RIKEN cluster array. Nucl. Instrum. Methods Phys. Res. B **317**, 649–652 (2013). https://doi.org/10.1016/j.nimb.2013.03.018. (**XVIth International Conference on ElectroMagnetic Isotope Separators and Techniques Related to their Applications, December 2–7, 2012 at Matsue, Japan**)
285. M. Rudigier, Z. Podolyák, P.H. Regan, A.M. Bruce, S. Lalkovski, R.L. Canavan, E.R. Gamba, O. Roberts, I. Burrows, D.M. Cullen, L.M. Fraile, L. Gerhard, J. Gerl, M. Gorska, A. Grant, J. Jolie, V. Karayonchev, N. Kurz, W. Korten, I.H. Lazarus, C.R. Nita, V.F.E. Pucknell, J.-M. Régis, H. Schaffner, J. Simpson, P. Singh, C.M. Townsley, J.F. Smith, J. Vesic, FATIMA—FAst TIMing Array for DESPEC at FAIR. Nucl. Instrum. Methods Phys. Res. A **969**, 163967 (2020). https://doi.org/10.1016/j.nima.2020.163967
286. E.R. Gamba, A.M. Bruce, M. Rudigier, Treatment of background in $\gamma - \gamma$ fast-timing measurements. Nucl. Instrum. Methods Phys. Res. A **928**, 93–103 (2019). https://doi.org/10.1016/j.nima.2019.03.028
287. V. Werner, N. Cooper, M. Bonett-Matiz, E. Williams, J.-M. Régis, M. Rudigier, T. Ahn, V. Anagnostatou, Z. Berant, M. Bunce, M. Elvers, A. Heinz, G. Ilie, J. Jolie, D. Radeck, D. Savran, M. Smith, Excited state lifetime measurements in rare earth nuclei with fast electronics. J. Phys. Conf. Ser. **312**(9), 092062 (2011). https://doi.org/10.1088/1742-6596/312/9/092062
288. A.I. Morales, G. Benzoni, H. Watanabe, G. de Angelis, S. Nishimura, L. Coraggio, A. Gargano, N. Itaco, T. Otsuka, Y. Tsunoda, P. Van Isacker, F. Browne, R. Daido, P. Doornenbal, Y. Fang, G. Lorusso, Z. Patel, S. Rice, L. Sinclair, P.-A. Söderström, T. Sumikama, J.J. Valiente-Dobón, J. Wu, Z.Y. Xu, A. Yagi, R. Yokoyama, H. Baba, R. Avigo, F.L. Bello Garrote, N. Blasi, A. Bracco, A.M. Bruce, F. Camera, S. Ceruti, F.C.L. Crespi, M.-C. Delattre, Z. Dombradi, A. Gottardo, T. Isobe, I. Kojouharov, N. Kurz, I. Kuti, S. Lalkovski, K. Matsui, B. Melon, D. Mengoni, T. Miyazaki, V. Modamio-Hoybjor, S. Momiyama, D.R. Napoli, M. Niikura, R. Orlandi, Z. Podolyák, P.H. Regan, H. Sakurai, E. Sahin, D. Sohler, H. Schaffner, R. Taniuchi, J. Taprogge, Z. Vajta, O. Wieland, M. Yalcinkaya, Is seniority a partial dynamic symmetry in the first $\nu g_{9/2}$ shell? Phys. Lett. B **781**, 706–712 (2018). https://doi.org/10.1016/j.physletb.2018.04.049
289. F. Browne, A.M. Bruce, T. Sumikama, I. Nishizuka, S. Nishimura, P. Doornenbal, G. Lorusso, P.-A. Söderström, H. Watanabe, R. Daido, Z. Patel, S. Rice, L. Sinclair, J. Wu, Z.Y. Xu, A. Yagi, H. Baba, N. Chiga, R. Carroll, F. Didierjean, Y. Fang, N. Fukuda, G. Gey, E. Ideguchi, N. Inabe, T. Isobe, D. Kameda, I. Kojouharov, N. Kurz, T. Kubo, S. Lalkovski, Z. Li, R. Lozeva, H. Nishibata, A. Odahara, Z. Podolyák, P.H. Regan, O.J. Roberts, H. Sakurai, H. Schaffner, G.S. Simpson, H. Suzuki, H. Takeda, M. Tanaka, J. Taprogge, V. Werner, O. Wieland, Lifetime measurements of the first 2^+ states in ^{104,106}Zr: evolution of ground-state deformations. Phys. Lett. B **750**, 448–452 (2015). https://doi.org/10.1016/j.physletb.2015.09.043
290. M. Rudigier, P.M. Walker, R.L. Canavan, Z. Podolyák, P.H. Regan, P.-A. Söderström, M. Lebois, J.N. Wilson, N. Jovancevic, A. Blazhev, J. Benito, S. Bottoni, M. Brunet, N. Cieplicka-Orynczak, S. Courtin, D.T. Doherty, L.M. Fraile, K. Hadyńska-Klęk, M. Heine, L.W. Iskra, J. Jolie, V. Karayonchev, A. Kennington, P. Koseoglou, G. Lotay, G. Lorusso, M. Nakhostin, C.R. Nita, S. Oberstedt, L. Qi, J.-M. Régis, V. Sánchez-Tembleque, R. Shearman, W. Witt, V. Vedia, K.O. Zell, Multi-quasiparticle sub-nanosecond isomers in ^{178}W. Phys. Lett. B **801**, 135140 (2020). https://doi.org/10.1016/j.physletb.2019.135140
291. E.R. Gamba, A.M. Bruce, S. Lalkovski, M. Rudigier, S. Bottoni, M.P. Carpenter, S. Zhu, J.T. Anderson, A.D. Ayangeakaa, T.A. Berry, I. Burrows, M.C. Gallardo, R.J. Carroll, P. Copp, D.M. Cullen, T. Daniel, G.F. Martínez, J.P. Greene, L.A. Gurgi, D.J. Hartley, R. Ilieva, S. Ilieva, F.G. Kondev, T. Kröll, G.J. Lane, T. Lauritsen, I. Lazarus, G. Lotay, C.R. Niţă, Z. Podolyák, V. Pucknell, M. Reed, P.H. Regan, J. Rohrer, J. Sethi, D. Seweryniak, C.M. Shand, J. Simpson, M. Smoleń, E.A. Stefanova, V. Vedia, O. Yordanov, Fast-timing measurements in the ground-state band of ^{114}Pd. Phys. Rev. C **100**, 044309 (2019). https://doi.org/10.1103/PhysRevC.100.044309
292. D. Cline, Nuclear shapes studied by Coulomb excitation. Annu. Rev. Nucl. Part. Sci. **36**(1), 683–716 (1986). https://doi.org/10.1146/annurev.ns.36.120186.003343
293. K. Kumar, Intrinsic quadrupole moments and shapes of nuclear ground states and excited states. Phys. Rev. Lett. **28**(4), 249 (1972). https://doi.org/10.1103/PhysRevLett.28.249

294. E. Clément, M. Zielińska, A. Görgen, W. Korten, S. Péru, J. Libert, H. Goutte, S. Hilaire, B. Bastin, C. Bauer, A. Blazhev, N. Bree, B. Bruyneel, P.A. Butler, J. Butterworth, P. Delahaye, A. Dijon, D.T. Doherty, A. Ekström, C. Fitzpatrick, C. Fransen, G. Georgiev, R. Gernhäuser, H. Hess, J. Iwanicki, D.G. Jenkins, A.C. Larsen, J. Ljungvall, R. Lutter, P. Marley, K. Moschner, P.J. Napiorkowski, J. Pakarinen, A. Petts, P. Reiter, T. Renstrøm, M. Seidlitz, B. Siebeck, S. Siem, C. Sotty, J. Srebrny, I. Stefanescu, G.M. Tveten, J. Van de Walle, M. Vermeulen, D. Voulot, N. Warr, F. Wenander, A. Wiens, H. De Witte, K. Wrzosek-Lipska, Spectroscopic quadrupole moments in ^{96,98}Sr: evidence for shape coexistence in neutron-rich strontium isotopes at N= 60. Phys. Rev. Lett. **116**(2), 022701 (2016). https://doi.org/10.1103/PhysRevLett.116.022701
295. K. Hadyńska-Klęk, P.J. Napiorkowski, M. Zielińska, J. Srebrny, A. Maj, F. Azaiez, J.J. Valiente Dobón, M. Kicińska-Habior, F. Nowacki, H. Naïdja, B. Bounthong, T.R. Rodríguez, G. de Angelis, T. Abraham, G. Anil Kumar, D. Bazzacco, M. Bellato, D. Bortolato, P. Bednarczyk, G. Benzoni, L. Berti, B. Birkenbach, B. Bruyneel, S. Brambilla, F. Camera, J. Chavas, B. Cederwall, L. Charles, M. Ciemała, P. Cocconi, P. Coleman-Smith, A. Colombo, A. Corsi, F.C.L. Crespi, D.M. Cullen, A. Czermak, P. Désesquelles, D.T. Doherty, B. Dulny, J. Eberth, E. Farnea, B. Fornal, S. Franchoo, A. Gadea, A. Giaz, A. Gottardo, X. Grave, J. Grębosz, A. Görgen, M. Gulmini, T. Habermann, H. Hess, R. Isocrate, J. Iwanicki, G. Jaworski, D.S. Judson, A. Jungclaus, N. Karkour, M. Kmiecik, D. Karpiński, M. Kisieliński, N. Kondratyev, A. Korichi, M. Komorowska, M. Kowalczyk, W. Korten, M. Krzysiek, G. Lehaut, S. Leoni, J. Ljungvall, A. Lopez-Martens, S. Lunardi, G. Maron, K. Mazurek, R. Menegazzo, D. Mengoni, E. Merchán, W. Męczyński, C. Michelagnoli, J. Mierzejewski, B. Million, S. Myalski, D.R. Napoli, R. Nicolini, M. Niikura, A. Obertelli, S.F. Özmen, M. Palacz, L. Próchniak, A. Pullia, B. Quintana, G. Rampazzo, F. Recchia, N. Redon, P. Reiter, D. Rosso, K. Rusek, E. Sahin, M.-D. Salsac, P.-A. Söderström, I. Stefan, O. Stézowski, J. Styczeń, C. Theisen, N. Toniolo, C.A. Ur, V. Vandone, R. Wadsworth, B. Wasilewska, A. Wiens, J.L. Wood, K. Wrzosek-Lipska, M. Zięblíński, Superdeformed and triaxial states in ^{42}Ca. Phys. Rev. Lett. **117**(6), 062501 (2016). https://doi.org/10.1103/PhysRevLett.117.062501
296. L.P. Gaffney, P.A. Butler, M. Scheck, A.B. Hayes, F. Wenander, M. Albers, B. Bastin, C. Bauer, A. Blazhev, J. Cederkäll, T. Chupp, D. Cline, T.E. Cocolios, T. Davinson, H. De Witte, J. Diriken, T. Grahn, A. Herzan, M. Huyse, D.G. Jenkins, D.T. Joss, N. Kesteloot, J. Konki, M. Kowalczyk, T. Kröll, E. Kwan, R. Lutter, K. Moschner, P. Napiorkowski, J. Pakarinen, M. Pfeiffer, D. Radeck, P. Reiter, K. Reynders, S.V. Rigby, L.M. Robledo, M. Rudigier, S. Sambi, M. Seidlitz, B. Siebeck, T. Stora, P. Thoele, P. Van Duppen, M.J. Vermeulen, M. von Schmid, D. Voulot, N. Warr, K. Wimmer, K. Wrzosek-Lipska, C.Y. Wu, S. Zielińska, M. Bönig, N. Bree, Studies of pear-shaped nuclei using accelerated radioactive beams. Nature **497**(7448), 199–204 (2013)
297. T. Kibédi, R.H. Spear, Reduced electric octupole transition probabilities, $B(E3, 0_1^+ \rightarrow 3_1^-)$—an update. At. Data Nucl. Data Tables **80**, 35–82 (2002). https://doi.org/10.1006/adnd.2001.0871
298. H.J. Wollersheim, H. Emling, H. Grein, R. Kulessa, R.S. Simon, C. Fleischmann, J. de Boer, E. Hauber, C. Lauterbach, C. Schandera, P.A. Butler, T. Czosnyka, Coulomb excitation of ^{226}Ra. Nucl. Phys. A **556**(2), 261–280 (1993). https://doi.org/10.1016/0375-9474(93)90351-W
299. B. Bucher, S. Zhu, C.Y. Wu, R.V.F. Janssens, R.N. Bernard, L.M. Robledo, T.R. Rodríguez, D. Cline, A.B. Hayes, A.D. Ayangeakaa, M.Q. Buckner, C.M. Campbell, M.P. Carpenter, J.A. Clark, H.L. Crawford, H.M. David, C. Dickerson, J. Harker, C.R. Hoffman, B.P. Kay, F.G. Kondev, T. Lauritsen, A.O. Macchiavelli, R.C. Pardo, G. Savard, D. Seweryniak, R. Vondrasek, Direct evidence for octupole deformation in ^{146}Ba and the origin of large $E1$ moment variations in reflection-asymmetric nuclei. Phys. Rev. Lett. **118**, 152504 (2017). https://doi.org/10.1103/PhysRevLett.118.152504
300. P.A. Butler, L.P. Gaffney, P. Spagnoletti, K. Abrahams, M. Bowry, J. Cederkäll, G. de Angelis, H. De Witte, P.E. Garrett, A. Goldkuhle, C. Henrich, A. Illana, K. Johnston, D.T. Joss, J.M. Keatings, N.A. Kelly, M. Komorowska, J. Konki, T. Kröll, M. Lozano, B.S. Nara Singh, D. O'Donnell, J. Ojala, R.D. Page, L.G. Pedersen, C. Raison, P. Reiter, J.A. Rodriguez, D. Rosiak, S. Rothe, M. Scheck, M. Seidlitz, T.M. Shneidman, B. Siebeck, J. Sinclair, J.F. Smith, M. Stryjczyk, P. Van Duppen, S. Vinals, V. Virtanen, N. Warr, K. Wrzosek-Lipska, M. Zielińska, Evolution of octupole deformation in radium nuclei from Coulomb excitation of radioactive ^{222}Ra and ^{228}Ra beams. Phys. Rev. Lett. **124**, 042503 (2020). https://doi.org/10.1103/PhysRevLett.124.042503
301. M.M.R. Chishti, D. O'Donnell, G. Battaglia, M. Bowry, D.A. Jaroszynski, B.S. Nara Singh, M. Scheck, P. Spagnoletti, J.F. Smith, Direct measurement of the intrinsic electric dipole moment in pear-shaped thorium-228. Nat. Phys. **16**, 853–856 (2020). https://doi.org/10.1038/s41567-020-0899-4
302. T.E. Chupp, P. Fierlinger, M.J. Ramsey-Musolf, J.T. Singh, Electric dipole moments of atoms, molecules, nuclei, and particles. Rev. Mod. Phys. **91**, 015001 (2019). https://doi.org/10.1103/RevModPhys.91.015001
303. D. Rosiak, M. Seidlitz, P. Reiter, H. Naïdja, Y. Tsunoda, T. Togashi, F. Nowacki, T. Otsuka, G. Colò, K. Arnswald, T. Berry, A. Blazhev, M.J.G. Borge, J. Cederkäll, D.M. Cox, H. De Witte, L.P. Gaffney, C. Henrich, R. Hirsch, M. Huyse, A. Illana, K. Johnston, L. Kaya, T. Kröll, M.L.L. Benito, J. Ojala, J. Pakarinen, M. Queiser, G. Rainovski, J.A. Rodriguez, B. Siebeck, E. Siesling, J. Snäll, P. Van Duppen, A. Vogt, M. von Schmid, N. Warr, F. Wenander, K.O. Zell, Enhanced quadrupole and octupole strength in doubly magic ^{132}Sn. Phys. Rev. Lett. **121**(25), 252501 (2018). https://doi.org/10.1103/PhysRevLett.121.252501
304. J. Van de Walle, F. Aksouh, T. Behrens, V. Bildstein, A. Blazhev, J. Cederkäll, E. Clément, T.E. Cocolios, T. Davinson, P. Delahaye, J. Eberth, A. Ekström, D.V. Fedorov, V.N. Fedosseev, L.M. Fraile, S. Franchoo, R. Gernhauser, G. Georgiev, D. Habs, K. Heyde, G. Huber, M. Huyse, F. Ibrahim, O. Ivanov, J. Iwanicki, J. Jolie, O. Kester, U. Köster, T. Kröll, R. Krücken, M. Lauer, A.F. Lisetskiy, R. Lutter, B.A. Marsh, P. Mayet, O. Niedermaier, M. Pantea, R. Raabe, P. Reiter, M. Sawicka, H. Scheit, G. Schrieder, D. Schwalm, M.D. Seliverstov, T. Sieber, G. Sletten, N. Smirnova, M. Stanoiu, I. Stefanescu, J.-C. Thomas, J.J. Valiente-Dobón, P.V. Duppen, D. Verney, D. Voulot, N. Warr, D. Weisshaar, F. Wenander, B.H. Wolf, M. Zielińska, Low-energy Coulomb excitation of neutron-rich zinc isotopes. Phys. Rev. C **79**(1), 014309 (2009). https://doi.org/10.1103/PhysRevC.79.014309
305. P. Möller, R. Bengtsson, B.G. Carlsson, P. Olivius, T. Ichikawa, Global calculations of ground-state axial shape asymmetry of nuclei. Phys. Rev. Lett. **97**(16), 162502 (2006). https://doi.org/10.1103/PhysRevLett.97.162502
306. P. Möller, R. Bengtsson, B.G. Carlsson, P. Olivius, T. Ichikawa, H. Sagawa, A. Iwamoto, Axial and reflection asymmetry of the nuclear ground state. At. Data Nucl. Data Tables **94**(5), 758 (2008). https://doi.org/10.1016/j.adt.2008.05.002
307. R. Surman, J. Engel, J.R. Bennett, B.S. Meyer, Source of the rare-earth element peak in r-process nucleosynthesis. Phys. Rev. Lett. **79**(10), 1809 (1997). https://doi.org/10.1103/PhysRevLett.79.1809
308. S. Cruz, P.C. Bender, R. Krücken, K. Wimmer, F. Ames, C. Andreoiu, R.A.E. Austin, C.S. Bancroft, R. Braid, T. Bruhn, W.N. Catford, A. Cheeseman, A. Chester, D.S. Cross, C.A. Diget, T. Drake, A.B. Garnsworthy, G. Hackman, R. Kanungo, A. Knapton, W. Korten, K. Kuhn, J. Lassen, R. Laxdal, M. Marchetto, A. Matta, D. Miller, M. Moukaddam, N.A. Orr, N. Sachmpazidi, A. Sanetullaev, C.E. Svensson, N. Terpstra, C. Unsworth, P.J. Voss, Shape coexistence and mixing of low-lying 0^+ states in ^{96}Sr. Phys. Lett. B **786**, 94–99 (2018). https://doi.org/10.1016/j.physletb.2018.09.031
309. S. Cruz, K. Wimmer, P.C. Bender, R. Krücken, G. Hackman, F. Ames, C. Andreoiu, R.A.E. Austin, C.S. Bancroft, R. Braid, T. Bruhn, W.N. Catford, A. Cheeseman, A. Chester, D.S. Cross, C.A. Diget, T. Drake, A.B. Garnsworthy, R. Kanungo, A. Knapton, W. Korten, K. Kuhn, J. Lassen, R. Laxdal, M. Marchetto, A. Matta, D. Miller, M. Moukaddam, N.A. Orr, N. Sachmpazidi, A. Sanetullaev, C.E. Svensson, N. Terpstra, C. Unsworth, P.J. Voss, Single-particle structure of neutron-rich Sr isotopes via ^{2}H(^{94,95,96}Sr, p) reactions. Phys. Rev. C **100**, 054321 (2019). https://doi.org/10.1103/PhysRevC.100.054321
310. N. Cieplicka-Oryńczak, C. Michelagnoli, A. Gargano, B. Fornal, S. Leoni, G. Benzoni, A. Blanc, S. Bottoni, F.C.L. Crespi, L.W. Iskra, M. Jentschel, U. Köster, P. Mutti, N. Pietralla, E. Ruiz-Martinez, V. Werner, Contrasting properties of particle–particle and hole–hole excitations in ^{206}Tl and ^{210}Bi nuclei. Phys. Lett. B **802**, 135222 (2020). https://doi.org/10.1016/j.physletb.2020.135222

311. S. Bottoni, S. Leoni, B. Fornal, R. Raabe, K. Rusek, G. Benzoni, A. Bracco, F.C.L. Crespi, A.I. Morales, P. Bednarczyk, N. Cieplicka-Oryńczak, W. Królas, A. Maj, B. Szpak, M. Callens, J. Bouma, J. Elseviers, H. De Witte, F. Flavigny, R. Orlandi, P. Reiter, M. Seidlitz, N. Warr, B. Siebeck, S. Hellgartner, D. Mücher, J. Pakarinen, M. Vermeulen, C. Bauer, G. Georgiev, R.V.F. Janssens, D. Balabanski, M. Sferrazza, M. Kowalska, E. Rapisarda, D. Voulot, M. Lozano Benito, F. Wenander, Cluster-transfer reactions with radioactive beams: a spectroscopic tool for neutron-rich nuclei. Phys. Rev. C **92**, 024322 (2015). https://doi.org/10.1103/PhysRevC.92.024322
312. K.L. Jones, A.S. Adekola, D.W. Bardayan, J.C. Blackmon, K.Y. Chae, K.A. Chipps, J.A. Cizewski, L. Erikson, C. Harlin, R. Hatarik, R. Kapler, R.L. Kozub, J.F. Liang, R. Livesay, Z. Ma, B.H. Moazen, C.D. Nesaraja, F.M. Nunes, S.D. Pain, N.P. Patterson, D. Shapira, J.F. Shriner, M.S. Smith, T.P. Swan, J.S. Thomas, The magic nature of ^{132}Sn explored through the single-particle states of ^{133}Sn. Nature **465**(7297), 454–457 (2010). https://doi.org/10.1038/nature09048
313. J.M. Allmond, A.E. Stuchbery, J.R. Beene, A. Galindo-Uribarri, J.F. Liang, E. Padilla-Rodal, D.C. Radford, R.L. Varner, A. Ayres, J.C. Batchelder, A. Bey, C.R. Bingham, M.E. Howard, K.L. Jones, B. Manning, P.E. Mueller, C.D. Nesaraja, S.D. Pain, W.A. Peters, A. Ratkiewicz, K.T. Schmitt, D. Shapira, M.S. Smith, N.J. Stone, D.W. Stracener, C.-H. Yu, Double-magic nature of ^{132}Sn and ^{208}Pb through lifetime and cross-section measurements. Phys. Rev. Lett. **112**, 172701 (2014). https://doi.org/10.1103/PhysRevLett.112.172701
314. G. Bocchi, S. Leoni, B. Fornal, G. Colò, P.F. Bortignon, S. Bottoni, A. Bracco, C. Michelagnoli, D. Bazzacco, A. Blanc, G. de France, M. Jentschel, U. Köster, P. Mutti, J.-M. Régis, G. Simpson, T. Soldner, C.A. Ur, W. Urban, L.M. Fraile, R. Lozeva, B. Belvito, G. Benzoni, A. Bruce, R. Carroll, N. Cieplicka-Oryńczak, F.C.L. Crespi, F. Didierjean, J. Jolie, W. Korten, T. Kröll, S. Lalkovski, H. Mach, N. Mărginean, B. Melon, D. Mengoni, B. Million, A. Nannini, D. Napoli, B. Olaizola, V. Paziy, Z. Podolyák, P.H. Regan, N. Saed-Samii, B. Szpak, V. Vedia, The mutable nature of particle-core excitations with spin in the one-valence-proton nucleus 133sb. Phys. Lett. B **760**, 273–278 (2016). https://doi.org/10.1016/j.physletb.2016.06.065
315. P.F. Bortignon, A. Bracco, R.A. Broglia, *Giant Resonances: Nuclear Structure at Finite Temperature* (CRC Press, London, 1998)
316. D. Savran, T. Aumann, A. Zilges, Experimental studies of the pygmy dipole resonance. Prog. Part. Nucl. Phys. **70**, 210–245 (2013). https://doi.org/10.1016/j.ppnp.2013.02.003
317. A. Bracco, F.C.L. Crespi, E.G. Lanza, Gamma decay of pygmy states from inelastic scattering of ions. Eur. Phys. J. A **51**, 99 (2015). https://doi.org/10.1140/epja/i2015-15099-6
318. A. Maj, M. Kmiecik, A. Bracco, F. Camera, P. Bednarczyk, B. Herskind, S. Brambilla, G. Benzoni, M. Brekiesz, D. Curien, G. de Angelis, E. Farnea, J. Grębosz, M. Kicińska-Habior, S. Leoni, W. Męczyński, B. Million, D.R. Napoli, J. Nyberg, C.M. Petrache, J. Styczeń, O. Wieland, M. Ziębliński, K. Zuber, N. Dubray, J. Dudek, K. Pomorski, Evidence for the Jacobi shape transition in hot ^{46}Ti. Nucl. Phys. A **731**, 319–326 (2004). https://doi.org/10.1016/j.nuclphysa.2003.11.043
319. M. Kmiecik, A. Maj, J. Styczeń, P. Bednarczyk, M. Brekiesz, J. Grębosz, M. Lach, W. Męczyński, M. Ziębliński, K. Zuber, A. Bracco, F. Camera, G. Benzoni, B. Million, S. Leoni, O. Wieland, B. Herskind, D. Curien, N. Dubray, J. Dudek, N. Schunck, K. Mazurek, GDR feeding of the highly-deformed band in ^{42}Ca. Acta Phys. Pol. B **36**, 1169 (2005). https://www.actaphys.uj.edu.pl/R/36/4/1169
320. D. Pandit, S. Mukhopadhyay, S. Bhattacharya, S. Pal, A. De, S. Bhattacharya, C. Bhattacharya, K. Banerjee, S. Kundu, T.K. Rana, A. Dey, G. Mukherjee, T. Ghosh, D. Gupta, S.R. Banerjee, Extreme nuclear shapes examined via giant dipole resonance lineshapes in hot light-mass systems. Phys. Rev. C **81**, 061302 (2010). https://doi.org/10.1103/PhysRevC.81.061302
321. B. Dey, C. Ghosh, D. Pandit, A.K. Rhine Kumar, S. Pal, V. Nanal, R.G. Pillay, P. Arumugam, S. De, G. Gupta, H. Krishnamoorthy, E.T. Mirgule, S. Pal, P.C. Rout, Study of the Jacobi shape transition in $A\approx30$ nuclei. Phys. Rev. C **97**, 014317 (2018). https://doi.org/10.1103/PhysRevC.97.014317
322. E.G. Lanza, Personal communication
323. X. Roca-Maza, N. Paar, Nuclear equation of state from ground and collective excited state properties of nuclei. Prog. Part. Nucl. Phys. **101**, 96–176 (2018). https://doi.org/10.1016/j.ppnp.2018.04.001
324. P.F. Bortignon, G. Colò, QRPA plus phonon coupling model and the photoabsorption cross section for ^{18,20,22}O. Nucl. Phys. A **696**, 427–441 (2001). https://doi.org/10.1016/S0375-9474(01)01217-9
325. D. Gambacurta, M. Grasso, J. Engel, Subtraction method in the second random-phase approximation: first applications with a Skyrme energy functional. Phys. Rev. C **92**, 034303 (2015). https://doi.org/10.1103/PhysRevC.92.034303
326. E. Litvinova, P. Ring, V. Tselyaev, Relativistic quasiparticle time blocking approximation: dipole response of open-shell nuclei. Phys. Rev. C **78**, 014312 (2008). https://doi.org/10.1103/PhysRevC.78.014312
327. V.G. Soloviev, *Theory of Atomic Nuclei: Quasiparticles and Phonons* (Institute of Physics, Bristol, 1992)
328. G. Colò, X. Roca-Maza, User guide for the hfbcs-qrpa(v1) code. Arxiv (2021). arXiv:2102.06562 [nucl-th]
329. Z.Z. Li, Y.F. Niu, W.H. Long, Electric dipole polarizability in neutron-rich Sn isotopes as a probe of nuclear isovector properties. Phys. Rev. C **103**, 064301 (2021). https://doi.org/10.1103/PhysRevC.103.064301
330. X. Roca-Maza, Y.F. Niu, G. Colo, P.F. Bortignon, Towards a self-consistent dynamical nuclear model. J. Phys. G **44**, 044001 (2017). https://doi.org/10.1088/1361-6471/aa5669
331. J.S. Brzosko, E. Gierlik, A. Soltan Jr., Z. Wilhelmi, Effect of the pigmy resonance on the calculations of the neutron capture cross section. Can. J. Phys. **47**(24), 2849–2857 (1969). https://doi.org/10.1139/p69-348
332. B. Alex Brown, Neutron radii in nuclei and the neutron equation of state. Phys. Rev. Lett. **85**, 5296–5299 (2000). https://doi.org/10.1103/PhysRevLett.85.5296
333. R.J. Furnstahl, Neutron radii in mean-field models. Nucl. Phys. A **706**(1), 85–110 (2002). https://doi.org/10.1016/S0375-9474(02)00867-9
334. J. Piekarewicz, B.K. Agrawal, G. Colò, W. Nazarewicz, N. Paar, P.-G. Reinhard, X. Roca-Maza, D. Vretenar, Electric dipole polarizability and the neutron skin. Phys. Rev. C **85**, 041302 (2012). https://doi.org/10.1103/PhysRevC.85.041302
335. Grit, website: http://grit.in2p3.fr/
336. A. Maj, F. Azaiez, D. Jenkins, C. Schmitt, O.S.J.P. Wieleczko, D. Balabanski, P. Bednarczyk, S. Brambilla, F. Camera, D.R. Chakrabarty, M. Chełstowska, M. Ciemała, S. Courtin, M. Csatlos, Z. Dombradi, O. Dorvaux, J. Dudek, M.N. Erduran, S. Ertürk, B. Fornal, S. Franchoo, G. Georgiev, J. Gulyás, S. Harissopoulos, P. Joshi, M. Kicińska-Habior, M. Kmiecik, A. Krasznahorkay, G.A. Kumar, K. Suresh, M. Labiche, I. Mazumdar, K. Mazurek, W. Męczyński, S. Myalski, V. Nanal, P. Napiorkowski, J. Peyre, J. Pouthas, O. Roberts, M. Rousseau, J.A. Scarpaci, A. Smith, I. Stefan, J. Strachan, D. Watts, M. Ziębliński, The PARIS project. Acta Phys. Pol. B **40**(3), 565–575 (2009)
337. P. Adrich, A. Klimkiewicz, M. Fallot, K. Boretzky, T. Aumann, D. Cortina-Gil, U.D. Pramanik, T.W. Elze, H. Emling, H. Geissel, M. Hellström, K.L. Jones, J.V. Kratz, R. Kulessa, Y. Leifels, C. Nociforo, R. Palit, H. Simon, G. Surówka, K. Sümmerer, W. Waluś, Evidence for pygmy and giant dipole resonances in ^{130}Sn and ^{132}Sn. Phys. Rev. Lett. **95**, 132501 (2005). https://doi.org/10.1103/PhysRevLett.95.132501
338. M. Spieker, N. Tsoneva, V. Derya, J. Endres, D. Savran, M.N. Harakeh, S. Harissopulos, R.-D. Herzberg, A. Lagoyannis, H. Lenske, N. Pietralla, L. Popescu, M. Scheck, F. Schlüter, K. Sonnabend, V.I. Stoica, H.J. Wörtche, A. Zilges, The pygmy quadrupole resonance and neutron-skin modes in ^{124}Sn. Phys. Lett. B **752**, 102–107 (2016). https://doi.org/10.1016/j.physletb.2015.11.004

339. D. Savran, V. Derya, S. Bagchi, J. Endres, M.N. Harakeh, J. Isaak, N. Kalantar-Nayestanaki, E.G. Lanza, B. Löher, A. Najafi, S. Pascu, S.G. Pickstone, N. Pietralla, V.Y. Ponomarev, C. Rigollet, C. Romig, M. Spieker, A. Vitturi, A. Zilges, Multi-messenger investigation of the pygmy dipole resonance in ^{140}Ce. Phys. Lett. B **786**, 16–20 (2018). https://doi.org/10.1016/j.physletb.2018.09.025
340. N.S. Martorana, G. Cardella, E.G. Lanza, L. Acosta, M.V. Andrés, L. Auditore, F. Catara, E. De Filippo, S. De Luca, D. Dell' Aquila, B. Gnoffo, G. Lanzalone, I. Lombardo, C. Maiolino, S. Norella, A. Pagano, E.V. Pagano, M. Papa, S. Pirrone, G. Politi, L. Quattrocchi, F. Rizzo, P. Russotto, D. Santonocito, A. Trifirò, M. Trimarchi, M. Vigilante, A. Vitturi, First measurement of the isoscalar excitation above the neutron emission threshold of the pygmy dipole resonance in ^{68}Ni. Phys. Lett. B **782**, 112–116 (2018). https://doi.org/10.1016/j.physletb.2018.05.019
341. M. Weinert, M. Spieker, G. Potel, N. Tsoneva, M. Müscher, J. Wilhelmy, A. Zilges, Microscopic structure of the low-energy electric dipole response of ^{120}Sn. Phys. Rev. Lett. **127**, 242501 (2021). https://doi.org/10.1103/PhysRevLett.127.242501
342. E. Litvinova, H. Wibowo, Nuclear response in a finite-temperature relativistic framework. Eur. Phys. J. A **55**, 223 (2019). https://doi.org/10.1140/epja/i2019-12771-9
343. E. Yüksel, G. Colò, E. Khan, Nuclear excitations within microscopic EDF approaches: pairing and temperature effects on the dipole response. Eur. Phys. J. A **55**, 230 (2019). https://doi.org/10.1140/epja/i2019-12918-8
344. Y.F. Niu, N. Paar, D. Vretenar, J. Meng, Low-energy monopole and dipole response in nuclei at finite temperature. Phys. Lett. B **681**(4), 315–319 (2009). https://doi.org/10.1016/j.physletb.2009.10.046
345. A. Berceanu, Y. Xu, Y.F. Niu, Temperature effects on neutron-capture cross sections and rates through electric dipole transitions in hot nuclei. Phys. Rev. C **104**, 044332 (2021). https://doi.org/10.1103/PhysRevC.104.044332
346. M. Scheck, S. Mishev, V.Y. Ponomarev, R. Chapman, L.P. Gaffney, E.T. Gregor, N. Pietralla, P. Spagnoletti, D. Savran, G.S. Simpson, Investigating the pygmy dipole resonance using β decay. Phys. Rev. Lett. **116**, 132501 (2016). https://doi.org/10.1103/PhysRevLett.116.132501
347. K.R. Mashtakov, V.Y. Ponomarev, M. Scheck, S.W. Finch, J. Isaak, M. Zweidinger, O. Agar, C. Bathia, T. Beck, J. Beller, M. Bowry, R. Chapman, M.M.R. Chishti, U. Friman-Gayer, L.P. Gaffney, P.E. Garrett, E.T. Gregor, J.M. Keatings, U. Köster, B. Löher, A.D. MacLean, D. O'Donnell, H. Pai, N. Pietralla, G. Rainovski, M. Ramdhane, C. Romig, G. Rusev, D. Savran, G.S. Simpson, J. Sinclair, K. Sonnabend, P. Spagnoletti, A.P. Tonchev, W. Tornow, Structure of high-lying levels populated in the ^{96}Y$\rightarrow^{96}$Zr β decay. Phys. Lett. B **820**, 136569 (2021). https://doi.org/10.1016/j.physletb.2021.136569
348. K. Mazurek, J. Dudek, A. Maj, D. Rouvel, Nuclear Jacobi and Poincaré transitions at high spins and temperatures: account of dynamic effects and large-amplitude motion. Phys. Rev. C **91**, 034301 (2015). https://doi.org/10.1103/PhysRevC.91.034301
349. K. Pomorski, J. Dudek, Nuclear liquid-drop model and surface-curvature effects. Phys. Rev. C **67**, 044316 (2003). https://doi.org/10.1103/PhysRevC.67.044316
350. B. Wasilewska, M. Kmiecik, M. Ciemała, A. Maj, F.C.L. Crespi, A. Bracco, M.N. Harakeh, P. Bednarczyk, S. Bottoni, S. Brambilla, F. Camera, I. Ciepał, N. Cieplicka-Oryńczak, M. Csatlos, B. Fornal, V. Gaudilla, J. Gręboszj, J. Isaak, L.W. Iskra, M. Jeżabek, A.J. Krasznahorkay, S. Kihel, M. Krzysiek, P. Lasko, S. Leoni, M. Lewitowicz, J. Łukasik, M. Matejska-Minda, K. Mazurek, P.J. Napiorkowski, W. Parol, P. Pawłowski, L.Q. Qi, M. Saxena, C. Schmitt, Y. Sobolev, B. Sowicki, M. Stanoiu, A. Tamii, O. Wieland, M. Ziębliński, γ decay to the ground state from the excitations above the neutron threshold in the ^{208}Pb$(p,\ p'\gamma)$ reaction at 85 MeV. Phys. Rev. C **105**, 014310 (2022). https://doi.org/10.1103/PhysRevC.105.014310
351. J.R. Beene, F.E. Bertrand, M.L. Halbert, R.L. Auble, D.C. Hensley, D.J. Horen, R.L. Robinson, R.O. Sayer, T.P. Sjoreen, Heavy-ion excitation and photon decay of giant resonances in ^{208}Pb. Phys. Rev. C **39**, 1307–1319 (1989). https://doi.org/10.1103/PhysRevC.39.1307
352. W.L. Lv, Y.F. Niu, G. Colò, Learning about the structure of giant resonances from their γ decay. Phys. Rev. C **103**, 064321 (2021). https://doi.org/10.1103/PhysRevC.103.064321
353. A. Giaz, L. Pellegri, S. Riboldi, F. Camera, N. Blasi, C. Boiano, A. Bracco, S. Brambilla, S. Ceruti, S. Coelli, F.C.L. Crespi, M. Csatlòs, S. Frega, J. Gulyàs, A. Krasznahorkay, S. Lodetti, B. Million, A. Owens, F. Quarati, L. Stuhl, O. Wieland, Characterization of large volume 3.5Œ8 LaBr3:Ce detectors. Nucl. Instrum. Methods Phys. Res. Sect. A **729**, 910–921 (2013). https://doi.org/10.1016/j.nima.2013.07.084
354. S. Ceruti, F. Camera, A. Bracco, R. Avigo, G. Benzoni, N. Blasi, G. Bocchi, S. Bottoni, S. Brambilla, F.C.L. Crespi, A. Giaz, S. Leoni, A. Mentana, B. Million, A.I. Morales, R. Nicolini, L. Pellegri, A. Pullia, S. Riboldi, O. Wieland, B. Birkenbach, D. Bazzacco, M. Ciemała, P. Désesquelles, J. Eberth, E. Farnea, A. Görgen, A. Gottardo, H. Hess, D.S. Judson, A. Jungclaus, M. Kmiecik, W. Korten, A. Maj, R. Menegazzo, D. Mengoni, C. Michelagnoli, V. Modamio, D. Montanari, S. Myalski, D. Napoli, B. Quintana, P. Reiter, F. Recchia, D. Rosso, E. Sahin, M.D. Salsac, P.-A. Söderström, O. Stézowski, C. Theisen, C. Ur, J.J. Valiente-Dobón, M. Ziębliński, Isospin mixing in ^{80}Zr: from finite to zero temperature. Phys. Rev. Lett. **115**, 222502 (2015). https://doi.org/10.1103/PhysRevLett.115.222502
355. D.D. Warner, M.A. Bentley, P.V. Isacker, The role of isospin symmetry in collective nuclear structure. Nat. Phys. **2**, 853–856 (2006). https://doi.org/10.1038/nphys291
356. J.A. Behr, K.A. Snover, C.A. Gossett, M. Kicińska-Habior, J.H. Gundlach, Z.M. Drebi, M.S. Kaplan, D.P. Wells, Restoration of isospin symmetry in highly excited compound nuclei. Phys. Rev. Lett. **70**, 3201–3204 (1993). https://doi.org/10.1103/PhysRevLett.70.3201
357. M.N. Harakeh, D.H. Dowell, G. Feldman, E.F. Garman, R. Loveman, J.L. Osborne, K.A. Snover, Role of isospin in the statistical decay of the giant dipole resonance built on excited states. Phys. Lett. B **176**(3), 297–301 (1986). https://doi.org/10.1016/0370-2693(86)90167-X
358. M. Kicińska-Habior, E. Wójcik, O. Kijewska, M. Kisieliński, M. Kowalczyk, J. Choiński, Giant dipole radiation and isospin purity in highly excited ^{32}S nuclei. Nucl. Phys. A **731**, 138–145 (2004). https://doi.org/10.1016/j.nuclphysa.2003.11.026
359. I.S. Towner, J.C. Hardy, Comparative tests of isospin-symmetry-breaking corrections to superallowed $0^+\rightarrow0^+$ nuclear β decay. Phys. Rev. C **82**, 065501 (2010). https://doi.org/10.1103/PhysRevC.82.065501
360. W. Satuła, J. Dobaczewski, W. Nazarewicz, M. Rafalski, Microscopic calculations of isospin-breaking corrections to superallowed beta decay. Phys. Rev. Lett. **106**, 132502 (2011). https://doi.org/10.1103/PhysRevLett.106.132502
361. D. Glas, U. Mosel, On the critical distance in fusion reactions. Nucl. Phys. A **237**(3), 429–440 (1975). https://doi.org/10.1016/0375-9474(75)90409-1
362. R. Bass, *Nuclear Reactions with Heavy Ions*, 1st edn. (Springer, Sunderland, 1980)
363. S.J. Sanders, A. Szanto de Toledo, C. Beck, Binary decay of light nuclear systems. Phys. Rep. **311**(6), 487–551 (1999). https://doi.org/10.1016/S0370-1573(98)00092-1
364. B.B. Back, H. Esbensen, C.L. Jiang, K.E. Rehm, Influence of heavy-ion transfer on fusion reactions. Rev. Mod. Phys. **86**, 317 (2014). https://doi.org/10.1103/RevModPhys.86.317
365. V. Jha, V.V. Parkar, S. Kailas, Incomplete fusion reactions using strongly and weakly bound projectiles. Phys. Rep. **845**, 1–58 (2020). https://doi.org/10.1016/j.physrep.2019.12.003
366. A.V. Karpov, A.S. Denikin, M.A. Naumenko, A.P. Alekseev, V.A. Rachkov, V.V. Samarin, V.V. Saiko, V.I. Zagrebaev, NRV web knowledge base on low-energy nuclear physics. Nucl. Instrum. Methods Phys. Res. A **859**, 112–124 (2017). https://doi.org/10.1016/j.nima.2017.01.069
367. V.I. Zagrebaev, A.S. Denikin, A.V. Karpov, A.P. Alekseev, M.A. Naumenko, V.A. Rachkov, V.V. Samarin, V.V. Saiko, NRV web knowledge base on low-energy nuclear physics (1999). http://nrv.jinr.ru/

368. D. Horn, A.J. Ferguson, Compound-nucleus cross sections from nuclear charge-density distributions. Phys. Rev. Lett. **41**, 1529–1532 (1978). https://doi.org/10.1103/PhysRevLett.41.1529
369. M. Lozano, G. Madurga, Nuclear-structure dependence of the fusion cross section for heavy ions. Phys. Lett. B **90**, 50–52 (1980). https://doi.org/10.1016/0370-2693(80)90048-9
370. S. Kailas, S.K. Gupta, Empirical description of heavy-ion fusion cross sections. Z. Phys. A **302**, 355–357 (1981). https://doi.org/10.1007/BF01414268
371. F. Porto, S. Sambataro, Heavy-ion fusion cross-sections predicted by a phenomenological formula. Nuov. Cim. A **83**, 339 (1984). https://doi.org/10.1007/BF02902726
372. R. Giordano, S. Sambataro, A. Scalia, F. Porto, P. Figuera, S. Pirrone, A new approach to heavy-ion fusion. Nuov. Cim. A **103**, 269–276 (1990). https://doi.org/10.1007/BF02820599
373. P. Eudes, Z. Basrak, F. Sébille, V. de la Mota, G. Royer, Comprehensive analysis of fusion data well above the barrier. Phys. Rev. C **90**(3), 034609 (2014). https://doi.org/10.1103/PhysRevC.90.034609
374. P.-G. Reinhard, A.S. Umar, P.D. Stevenson, J. Piekarewicz, V.E. Oberacker, J.A. Maruhn, Sensitivity of the fusion cross section to the density dependence of the symmetry energy. Phys. Rev. C **93**(4), 044618 (2016). https://doi.org/10.1103/PhysRevC.93.044618
375. H. Zheng, S. Burrello, M. Colonna, D. Lacroix, G. Scamps, Connecting the nuclear equation of state to the interplay between fusion and quasifission processes in low-energy nuclear reactions. Phys. Rev. C **98**(2), 024622 (2018). https://doi.org/10.1103/PhysRevC.98.024622
376. T. Maruyama, A. Bonasera, M. Papa, S. Chiba, Lifetime of heavy composite systems formed by fusion between heavy nuclei. J. Nucl. Rad. Sci. **3**(1), 77 (2002). https://doi.org/10.14494/jnrs2000.3.77
377. Z.-Q. Feng, G.-M. Jin, F.-S. Zhang, Dynamical analysis on heavy-ion fusion reactions near coulomb barrier. Nucl. Phys. A **802**(1), 91–106 (2008). https://doi.org/10.1016/j.nuclphysa.2008.01.022
378. S.M. Lee, T. Matsuse, A. Arima, "Statistical Yrast Line" in heavy-ion fusion reactions. Phys. Rev. Lett. **45**(3), 165–168 (1980). https://doi.org/10.1103/PhysRevLett.45.165
379. T. Matsuse, A. Arima, S.M. Lee, Critical distance in fusion reactions. Phys. Rev. C **26**(5), 2338–2341 (1982). https://doi.org/10.1103/PhysRevC.26.2338
380. R. Bass, Nucleus-nucleus potential deduced from experimental fusion cross sections. Phys. Rev. Lett. **39**(5), 265–268 (1977). https://doi.org/10.1103/PhysRevLett.39.265
381. M. Russo, A distributed neuro-genetic programming tool. Swarm Evol. Comput. **27**, 145–155 (2016). https://doi.org/10.1016/j.swevo.2015.10.009
382. M. Russo, A novel technique to self-adapt parameters in parallel/distributed genetic programming. Soft. Comput. **24**(22), 16885–16894 (2020). https://doi.org/10.1007/s00500-020-04982-w
383. D. Dell'Aquila, M. Russo, Automatic classification of nuclear physics data via a constrained evolutionary clustering approach. Comput. Phys. Commun. **259**, 107667 (2021). https://doi.org/10.1016/j.cpc.2020.107667
384. D. Dell'Aquila, B. Gnoffo, I. Lombardo, F. Porto, M. Russo, Modeling heavy-ion fusion cross section data via a novel artificial intelligence approach. J. Phys. G Nucl. Part. Phys. **50**(1), 015101 (2022). https://doi.org/10.1088/1361-6471/ac9ad1
385. E. Buccheri, D. Dell'Aquila, M. Russo, Artificial intelligence in health data analysis: the Darwinian evolution theory suggests an extremely simple and zero-cost large-scale screening tool for prediabetes and type 2 diabetes. Diabetes Res. Clin. Pract. **174**, 108722 (2021). https://doi.org/10.1016/j.diabres.2021.108722
386. E. Buccheri, D. Dell'Aquila, M. Russo, Stratified analysis of the age-related waist circumference cut-off model for the screening of dysglycemia at zero-cost. Obes. Med. **31**, 100398 (2022). https://doi.org/10.1016/j.obmed.2022.100398
387. G. Campobello, D. Dell'Aquila, M. Russo, A. Segreto, Neuro-genetic programming for multigenre classification of music content. Appl. Soft Comput. **94**, 106488 (2020). https://doi.org/10.1016/j.asoc.2020.106488
388. M. Cicerchia, F. Gramegna, D. Fabris, M. Cinausero, T. Marchi, G. Andreetta, S. Barlini, M. Bini, R. Bolzonella, M. Bruno, Enhanced α-particle production from fusion evaporation reactions leading to ^{46}Ti. J. Phys. G. **48**, 045101 (2021). https://doi.org/10.1088/1361-6471/abe5f6
389. D.J. Hinde, R. du Rietz, Effects of nuclear structure in heavy element formation dynamics. AIP Conf. Proc. **1423**, 65 (2012). https://doi.org/10.1063/1.3688783
390. T.S. Tveter, J.J. Gaardhøje, A. Maj, T. Ramsøy, A. Ataç, J. Bacelar, A. Bracco, A. Buda, F. Camera, B. Herskind, W. Korten, W. Królas, A. Menthe, B. Million, H. Nifenecker, M. Pignanelli, J.A. Pinston, H. Ploeg, F. Schussler, G. Sletten, Collective dipole motion in highly excited ^{272}Hs ($Z = 108$) nuclei. Phys. Rev. Lett. **76**, 1035 (1996). https://doi.org/10.1103/PhysRevLett.76.1035
391. E.M. Kozulin, A.A. Bogachev, M.G. Itkis, I.M. Itkis, G.N. Knyazheva, N.A. Kondratiev, L. Kurpa, I.V. Pokrovsky, E.V. Prokhorova, The CORSET time-of-flight spectrometer for measuring binary products of nuclear reactions. Instrum. Exp. Tech. **51**, 44–58 (2008). https://doi.org/10.1134/S0020441208010041
392. E.M. Kozulin, I.M. Harca, E. Vardaci, I. Matea, A. Maj, I. Itkis, G. Knyazheva, K. Novikov, O. Dorvaux, M. Ciemała, S. Brambilla, N. Kozulina, I.V. Kolesov, E. Saveleva, V.V. Kirakosyan, C. Schmitt, C. Borcea, S. Calinescu, C. Petrone, M. Ashaduzzaman, B. DeCanditiis, A. Pulcini, D. Quero, P. Rath, A. di Nitto, G. La Rana, A. Bracco, F. Camera, O. Stézowski, J. Wilson, D. Verney, W.H. Trzaska, SPS and the PARIS collaboration: features of the fission fragments formed in the heavy ion induced ^{32}S+^{197}Au reaction near the interaction barrier. Eur. Phys. J. A **56**(1), 6 (2020). https://doi.org/10.1140/epja/s10050-019-00019-5
393. E. Vardaci, A. Pulcini, E.M. Kozulin, I. Matea, D. Verney, A. Maj, C. Schmitt, I.M. Itkis, G.N. Knyazheva, K. Novikov, N. Kozulina, I.M. Harca, I.V. Kolesov, K. Saveleva, V.V. Kirakosyan, O. Dorvaux, M. Ciemała, S. Brambilla, M. Ashaduzzaman, B. De Canditiis, A. Di Nitto, D. Quero, C. Parascandolo, D. Pierroutsakou, P.K. Rath, G. Sposito, G. La Rana, A. Bracco, F. Camera, O. Stézowski, C. Borcea, S. Calinescu, C. Petrone, J. Wilson, Using γ rays to disentangle fusion-fission and quasifission near the Coulomb barrier: a test of principle in the fusion–fission and quasielastic channels. Phys. Rev. C **101**, 064612 (2020). https://doi.org/10.1103/PhysRevC.101.064612
394. A.D. Nitto, A. Brondi, G.L. Rana, R. Moro, P.N. Nadtochy, E. Vardaci, N. Gelli, M. Cinausero, G. Prete, The role of isospin in fusion evaporation reactions. J. Phys. Conf. Ser. **267**, 012053 (2011). https://doi.org/10.1088/1742-6596/267/1/012053
395. P.N. Nadtochy, E. Vardaci, A. Di Nitto, A. Brondi, G. La Rana, R. Moro, M. Cinausero, G. Prete, N. Gelli, F. Lucarelli, Examination of isospin effects in multi-dimensional Langevin fission dynamics. Phys. Lett. B **685**, 258 (2010). https://doi.org/10.1016/j.physletb.2010.01.069
396. A. Moro, A. Brondi, N. Gelli, M. Barbui, A. Boiano, M. Cinausero, A. Di Nitto, D. Fabris, E. Fioretto, G. La Rana, F. Lucarelli, M. Lunardon, G. Montagnoli, A. Ordine, G. Prete, V. Rizzi, M. Trotta, E. Vardaci, Compound nucleus evaporative decay as a probe for the isospin dependence of the level density. Eur. Phys. J. A **48**, 159 (2012). https://doi.org/10.1140/epja/i2012-12159-5
397. A.J. Sierk, Macroscopic model of rotating nuclei. Phys. Rev. C **33**, 2039–2053 (1986). https://doi.org/10.1103/PhysRevC.33.2039
398. A.J. Sierk, Mass-asymmetric fission of light nuclei. Phys. Rev. Lett. **55**, 582–583 (1985). https://doi.org/10.1103/PhysRevLett.55.582
399. G. Ademard, J.P. Wieleczko, J. Gomez del Campo, M. La Commara, E. Bonnet, M. Vigilante, A. Chbihi, J.D. Frankland, E. Rosato, G. Spadaccini, S.A. Kalandarov, C. Beck, S. Barlini, B. Borderie, R. Bougault, R. Dayras, G. de Angelis, J. De Sanctis, V.L. Kravchuk, P. Lautesse, N. Le Neindre,

J. Moisan, A. D'Onofrio, M. Parlog, D. Pierroutsakou, M.F. Rivet, M. Romoli, R. Roy, G.G. Adamian, N.V. Antonenko, Decay of excited nuclei produced in ^{78,82}Kr +^{40} Ca reactions at 5.5 MeV/nucleon. Phys. Rev. C **83**, 054619 (2011). https://doi.org/10.1103/PhysRevC.83.054619
400. S. Pirrone, G. Politi, B. Gnoffo, M. La Commara, E. De Filippo, P. Russotto, M. Trimarchi, M. Vigilante, M. Colonna, S.A. Kalandarov, F. Amorini, L. Auditore, C. Beck, G. Cardella, A. D'Onofrio, E. Geraci, D. Lacroix, E. La Guidara, G. Lanzalone, A. Pagano, E.V. Pagano, M. Papa, E. Piasecki, L. Quattrocchi, F. Rizzo, E. Rosato, G. Spadaccini, A. Trifirò, Isospin influence on fragments production in ^{78}Kr + ^{40}Ca and ^{86}Kr + ^{48}Ca collisions at 10 MeV/nucleon. Eur. Phys. J. A **55**(2), 22 (2019). https://doi.org/10.1140/epja/i2019-12695-4
401. B. Gnoffo, Isospin influence on the IMFs production in the ^{78,86}Kr+^{40,48}Ca reactions at 10 AMeV. Nuovo Cim. C **39**, 275 (2016). https://doi.org/10.1393/ncc/i2016-16275-0
402. P.N. Nadtochy, A. Kelić, K.-H. Schmidt, Fission rate in multi-dimensional Langevin calculations. Phys. Rev. C **75**, 064614 (2007). https://doi.org/10.1103/PhysRevC.75.064614
403. J. Gómez del Campo, C. Baktash, H.-Q. Jin, D. Rudolph, A. D'Onofrio, F. Terrasi, G. de Angelis, M. De Poli, C. Fahlander, A. Gadea, D.R. Napoli, Q. Pan, P. Spolaore, L. De Acuna, D. Bazzacco, S. Lunardi, P. Pavan, C. Rossi-Alvarez, A. Buscemi, R. Zanon, A. De Rosa, L. Campajola, M. La Commara, G. Inglima, V. Roca, M. Romano, M. Sandoli, M. Romoli, A. Ordine, D. Pierroutsakou, Emission of intermediate mass fragments using γ-spectroscopic techniques. Phys. Rev. C **57**, 457 (1998). https://doi.org/10.1103/PhysRevC.57.R457
404. S.A. Kalandarov, G.G. Adamian, N.V. Antonenko, W. Scheid, Emission of charged particles from excited compound nuclei. Phys. Rev. C **82**, 044603 (2010). https://doi.org/10.1103/PhysRevC.82.044603
405. A.S. Zubov, G.G. Adamian, N.V. Antonenko, S.P. Ivanova, W. Scheid, Competition between evaporation channels in neutron-deficient nuclei. Phys. Rev. C **68**, 014616 (2003). https://doi.org/10.1103/PhysRevC.68.014616
406. H. Hauser, H. Feshback, The inelastic scattering of neutrons. Phys. Rev. **87**, 366–373 (1952). https://doi.org/10.1103/PhysRev.87.366
407. L.G. Moretto, Statistical emission of large fragments: a general theoretical approach. Nucl. Phys. A **247**(2), 211–230 (1975). https://doi.org/10.1016/0375-9474(75)90632-6
408. D. Lacroix, A. Van Lauwe, D. Durand, Event generator for nuclear collisions at intermediate energies. Phys. Rev. C **69**, 054604 (2004). https://doi.org/10.1103/PhysRevC.69.054604
409. P. Napolitani, M. Colonna, Inhomogeneity growth in two-component fermionic systems. Phys. Rev. C **96**, 054609 (2017). https://doi.org/10.1103/PhysRevC.96.054609
410. N. Itagaki, T. Naito, Y. Hirata, Persistence of cluster structure in the ground state of ^{11}B. Phys. Rev. C **105**, 024304 (2022). https://doi.org/10.1103/PhysRevC.105.024304
411. G. Baiocco, L. Morelli, F. Gulminelli, M. D'Agostino, M. Bruno, U. Abbondanno, S. Barlini, M. Bini, S. Carboni, G. Casini, M. Cinausero, M. Degerlier, F. Gramegna, V.L. Kravchuk, T. Marchi, A. Olmi, G. Pasquali, S. Piantelli, A.R. Raduta, α-clustering effects in dissipative ^{12}C +^{12}C reactions at 95 MeV. Phys. Rev. C **87**, 054614 (2013). https://doi.org/10.1103/PhysRevC.87.054614
412. P. Kaur, M. Maiti, T.N. Nag, S. Sodaye, Reaction dynamics of the ^{12}C +^{181} Ta system near the coulomb barrier: evidence of fusion–fission events. Phys. Rev. C **105**, 014629 (2022). https://doi.org/10.1103/PhysRevC.105.014629
413. S. Manna, T.K. Rana, C. Bhattacharya, S. Bhattacharya, S. Kundu, K. Banerjee, P. Roy, R. Pandey, V. Srivastava, A. Chaudhuri, T. Roy, T.K. Ghosh, G. Mukherjee, J.K. Meena, S.K. Pandit, K. Mahata, A. Shrivastava, V. Nanal, Survival of cluster correlation in dissipative binary breakup of ^{24,25}Mg*. Phys. Rev. C **94**, 051601 (2016). https://doi.org/10.1103/PhysRevC.94.051601
414. L. Morelli, M. Bruno, M. D'Agostino, G. Baiocco, F. Gulminelli, S. Barlini, A. Buccola, A. Camaiani, G. Casini, C. Ciampi, C. Frosin, N. Gelli, A. Olmi, P. Ottanelli, G. Pasquali, S. Piantelli, S. Valdré, M. Cicerchia, M. Cinausero, F. Gramegna, G. Mantovani, T. Marchi, M. Degerlier, D. Fabris, V.L. Kravchuk, Full disassembly of excited ^{24}Mg into six α particles. Phys. Rev. C **99**, 054610 (2019). https://doi.org/10.1103/PhysRevC.99.054610
415. A. Camaiani, G. Casini, L. Morelli, S. Barlini, S. Piantelli, G. Baiocco, M. Bini, M. Bruno, A. Buccola, M. Cinausero, M. Cicerchia, M. D'Agostino, M. Degelier, D. Fabris, C. Frosin, F. Gramegna, F. Gulminelli, G. Mantovani, T. Marchi, A. Olmi, P. Ottanelli, G. Pasquali, G. Pastore, S. Valdré, G. Verde, Experimental study of precisely selected evaporation chains in the decay of excited ^{25}Mg. Phys. Rev. C **97**, 044607 (2018). https://doi.org/10.1103/PhysRevC.97.044607
416. K. Schmidt, X. Cao, E.J. Kim, K. Hagel, M. Barbui, J. Gauthier, S. Wuenschel, G. Giuliani, M.R.D. Rodrigues, H. Zheng, M. Huang, N. Blando, A. Bonasera, R. Wada, C. Botosso, G. Liu, G. Viesti, S. Moretto, G. Prete, S. Pesente, D. Fabris, Y. El Masri, T. Keutgen, S. Kowalski, A. Kumar, G. Zhang, J.B. Natowitz, α-conjugate neck structures in the collisions of 35 MeV/nucleon ^{40}Ca with ^{40}Ca. Phys. Rev. C **95**, 054618 (2017). https://doi.org/10.1103/PhysRevC.95.054618
417. S. Zhang, A. Bonasera, M. Huang, H. Zheng, D.X. Wang, J.C. Wang, L. Lu, G. Zhang, Z. Kohley, Y.G. Ma, S.J. Yennello, Strongly resonating bosons in hot nuclei. Phys. Rev. C **99**, 044605 (2019). https://doi.org/10.1103/PhysRevC.99.044605
418. R. Han, Z. Chen, R. Wada, A. Ono, G. Tian, F. Shi, X. Zhang, B. Liu, H. Sun, Effects of cluster correlations on fragment emission in ^{12}C +^{12} C at 50 mev/nucleon. Phys. Rev. C **102**, 064617 (2020). https://doi.org/10.1103/PhysRevC.102.064617
419. M. Kimura, Y. Taniguchi, α+^{28}Si and ^{16}O+^{16}O molecular states and their isoscalar monopole strengths. Phys. Rev. C **102**, 024325 (2020). https://doi.org/10.1103/PhysRevC.102.024325
420. W. Scheid, W. Greiner, R. Lemmer, Quasimolecular structure in elastic O^{16} + O^{16} scattering. Phys. Rev. Lett. **25**, 176–180 (1970). https://doi.org/10.1103/PhysRevLett.25.176
421. M.-D. Salsac, F. Haas, S. Courtin, A. Algora, C. Beck, S. Beghini, B.R. Behera, R. Chapman, L. Corradi, Z. Dombradi, E. Farnea, E. Fioretto, A. Gadea, D.G. Jenkins, A. Latina, D. Lebhertz, S. Lenzi, X. Liang, N. Marginean, G. Montagnoli, D. Napoli, P. Papka, I. Pokrovski, G. Pollarolo, M. Rousseau, E. Sahin, A. Sanchez i Zafra, F. Scarlassara, D. Sohler, A.M. Stefanini, S. Szilner, M. Trotta, C. Ur, F.D. Vedova, Z.M. Wang, K.T. Wiedemann, Decay of a narrow and high spin ^{24}Mg+^{24}Mg resonance. Nucl. Phys. A **801**(1), 1–20 (2008). https://doi.org/10.1016/j.nuclphysa.2007.12.007
422. M. Rousseau, C. Beck, C. Bhattacharya, V. Rauch, O. Dorvaux, K. Eddahbi, C. Enaux, R.M. Freeman, F. Haas, D. Mahboub, R. Nouicer, P. Papka, O. Stézowski, S. Szilner, A. Hachem, E. Martin, S.J. Sanders, A.K. Dummer, A. Szanto de Toledo, Highly deformed ^{40}Ca configurations in ^{28}Si+^{12}C. Phys. Rev. C **66**, 034612 (2002). https://doi.org/10.1103/PhysRevC.66.034612
423. P. Papka, C. Beck, F. Haas, V. Rauch, M. Rousseau, P. Bednarczyk, S. Courtin, O. Dorvaux, K. Eddahbi, J. Robin, A. Sànchez i Zafra, O. Stézowski, A. Prévost, Cluster emission and extremely deformed shapes in the N=Z nucleus ^{44}Ti. Acta Phys. Pol. B **34**, 2343 (2003)
424. C. Bhattacharya, M. Rousseau, C. Beck, V. Rauch, R.M. Freeman, D. Mahboub, R. Nouicer, P. Papka, O. Stézowski, A. Hachem, E. Martin, A.K. Dummer, S.J. Sanders, A. SzantoD Toledo, Deformation effects in ^{56}Ni nuclei produced in ^{28}Si+^{28}Si at 112 MeV. Phys. Rev. C **65**, 014611 (2001). https://doi.org/10.1103/PhysRevC.65.014611
425. G. La Rana, R. Moro, A. Brondi, P. Cuzzocrea, A. D'Onofrio, E. Perillo, M. Romano, F. Terrasi, E. Vardaci, H. Dumont, Unexpected large deformations in ^{60}Ni nuclei produced in the reaction 120 MeV ^{30}Si+^{30}Si. Phys. Rew. C **37**, 1920–1925 (1988). https://doi.org/10.1103/PhysRevC.37.1920
426. W. von Oertzen, B. Gebauer, G. Efimov, V. Zherebchevsky, T. Kokalova, S. Thummerer, C. Schulz, H.G. Bohlen, D. Kamanin, C. Beck, D. Curien, P. Papka, M. Rousseau, G. Royer, G. de Angelis, Fission and ternary cluster decay of hyper-deformed ^{56}Ni. Eur. Phys. J. A **36**, 279–288 (2008). https://doi.org/10.1140/epja/i2008-10592-7

427. A. Maj et al., Nucl. Phys. A **731**, 319 (2004)
428. M. Kicińska-Habior, K.A. Snover, J.A. Behr, C.A. Gossett, Y. Alhassid, N. Whelan, Search for a phase transition in the nuclear shape at finite temperature and rapid rotation. Phys. Lett. B **308**, 225–230 (1993). https://doi.org/10.1016/0370-2693(93)91276-S
429. G. Benzoni, A. Bracco, F. Camera, S. Leoni, B. Million, A. Maj, A. Algora, A. Axelsson, M. Bergström, N. Blasi, M. Castoldi, S. Frattini, A. Gadea, B. Herskind, M. Kmiecik, G. Lo Bianco, J. Nyberg, M. Pignanelli, J. Styczeń, O. Wieland, M. Zięblíński, A. Zucchiatti, Effect of e1 decay in the population of superdeformed structures. Phys. Lett. B **540**(3), 199–206 (2002). https://doi.org/10.1016/S0370-2693(02)02175-5
430. E. Ideguchi, D.G. Sarantites, W. Reviol, A.V. Afanasjev, M. Devlin, C. Baktash, R.V.F. Janssens, D. Rudolph, A. Axelsson, M.P. Carpenter, A. Galindo-Uribarri, D.R. LaFosse, T. Lauritsen, F. Lerma, C.J. Lister, P. Reiter, D. Seweryniak, M. Weiszflog, J.N. Wilson, Superdeformation in the doubly magic nucleus $^{40}_{20}Ca_{20}$. Phys. Rev. Lett. **87**, 222501 (2001). https://doi.org/10.1103/PhysRevLett.87.222501
431. C. Beck, Molecular resonance phenomena and alpha-clustering: recent progress and perspectives. Nucl. Phys. A **738**, 24–30 (2004). https://doi.org/10.1016/j.nuclphysa.2004.04.007. (**Proceedings of the 8th International Conference on Clustering Aspects of Nuclear Structure and Dynamics**)
432. C. Beck, Nuclear alpha-clustering, superdeformation, and quasimolecular resonances. Int. J. Mod. Phys. E **13**, 9–18 (2004). https://doi.org/10.1142/S0218301304001679
433. N.N. Ajitanand, G. La Rana, R. Lacey, D.J. Moses, L.C. Vaz, G.F. Peaslee, D.M. de Castro Rizzo, M. Kaplan, J.M. Alexander, Clues to the shapes of very hot nuclei: calculated patterns for evaporative emission from deformed nuclei. Phys. Rev. C **34**, 877–889 (1986). https://doi.org/10.1103/PhysRevC.34.877
434. M. Kmiecik, A. Maj, M. Brekiesz, K. Mazurek, P. Bednarczyk, J. Gręgosz, W. Męczyński, J. Styczeń, M. Zięblíński, K. Zuber, P. Papka, C. Beck, D. Curien, F. Haas, V. Rauch, M. Rousseau, J. Dudek, N. Schunck, A. Bracco, F. Camera, G. Benzoni, O. Wieland, B. Herskind, E. Farnea, G. de Angelis, Strong deformation effects in hot rotating ^{46}Ti*. Acta Phys. Pol. B **38**, 1437 (2007)
435. I. Lombardo, D. Dell'Aquila, M. Cinausero, L.R. Gasques, M. Vigilante, V.A.B. Zagatto, S. Barlini, R. Bolzonella, M. Bruno, A. Buccola, A. Camaiani, S.M. Carturan, G. Casini, C. Ciampi, M. Cicerchia, M. D'Andrea, M. Degerlier, D. Fabris, C. Frosin, F. Gramegna, A. Lepine-Szily, G. Maggioni, G. Mantovani, T. Marchi, A. Ordine, P. Ottanelli, G. Pasquali, S. Piantelli, V. Rigato, M. Russo, L. Scomparin, S. Valdrè, G. Verde, Study of the ^{33}Cl spectroscopic factors via the ^{32}S(^{3}He, d)^{33}Cl one-proton transfer reaction. J. Phys. G **48**(6), 065101 (2021). https://doi.org/10.1088/1361-6471/abdee4
436. A.M. Mukhamedzhanov, R.E. Tribble, Connection between asymptotic normalization coefficients, subthreshold bound states, and resonances. Phys. Rev. C **59**, 3418–3424 (1999). https://doi.org/10.1103/PhysRevC.59.3418
437. F. Hammache, N. de Séréville, Transfer reactions as a tool in nuclear astrophysics. Front. Phys. **8**, 602920 (2021). https://doi.org/10.3389/fphy.2020.602920
438. L. Corradi, G. Pollarolo, S. Szilner, Multinucleon transfer processes in heavy-ion reactions. J. Phys. G **36**(11), 113101 (2009). https://doi.org/10.1088/0954-3899/36/11/113101
439. A. Gadea, D.R. Napoli, G. de Angelis, R. Menegazzo, A.M. Stefanini, L. Corradi, M. Axiotis, L. Berti, E. Fioretto, T. Kroell, A. Latina, N. Mărginean, G. Maron, T. Martinez, D. Rosso, C. Rusu, N. Toniolo, S. Szilner, M. Trotta, D. Bazzacco, S. Beghini, M. Bellato, F. Brandolini, E. Farnea, R. Isocrate, S.M. Lenzi, S. Lunardi, G. Montagnoli, P. Pavan, C. Rossi Alvarez, F. Scarlassara, C. Ur, N. Blasi, A. Bracco, F. Camera, S. Leoni, B. Million, M. Pignanelli, G. Pollarolo, A. DeRosa, G. Inglima, M. La Commara, G. La Rana, D. Pierroutsakou, M. Romoli, M. Sandoli, P.G. Bizzeti, A.M. Bizzeti-Sona, G. Lo Bianco, C.M. Petrache, A. Zucchiatti, P. Cocconi, B. Quintana, C. Beck, D. Curien, G. Duchene, F. Haas, P. Medina, P. Papka, J. Durell, S.J. Freeman, A. Smith, B. Varley, K. Fayz, V. Pucknell, J. Simpson, W. Gelletly, P. Regan, PRISMA-2 collaboration and EUROBALL collaboration: coupling a CLOVER detector array with the PRISMA magnetic spectrometer. Eur. Phys. J. A **20**, 193–197 (2003). https://doi.org/10.1140/epja/i2002-10352-9
440. A. Bracco, G. Duchene, Z. Podolyak, P. Reiter, Gamma spectroscopy with AGATA in its first phases: new insights in nuclear excitations along the nuclear chart. Prog. Part. Nucl. Phys. **121**, 103887 (2021). https://doi.org/10.1016/j.ppnp.2021.103887
441. L. Corradi, A.M. Stefanini, C.J. Lin, S. Beghini, G. Montagnoli, F. Scarlassara, G. Pollarolo, A. Winther, Multinucleon transfer processes in ^{64}Ni+^{238}U. Phys. Rev. C **59**, 261–268 (1999). https://doi.org/10.1103/PhysRevC.59.261
442. A. Vogt, B. Birkenbach, P. Reiter, L. Corradi, T. Mijatović, D. Montanari, S. Szilner, D. Bazzacco, M. Bowry, A. Bracco, B. Bruyneel, F.C.L. Crespi, G. de Angelis, P. Désesquelles, J. Eberth, E. Farnea, E. Fioretto, A. Gadea, K. Geibel, A. Gengelbach, A. Giaz, A. Görgen, A. Gottardo, J. Gręgosz, H. Hess, P.R. John, J. Jolie, D.S. Judson, A. Jungclaus, W. Korten, S. Leoni, S. Lunardi, R. Menegazzo, D. Mengoni, C. Michelagnoli, G. Montagnoli, D. Napoli, L. Pellegri, G. Pollarolo, A. Pullia, B. Quintana, F. Radeck, F. Recchia, D. Rosso, E. Sahin, M.D. Salsac, F. Scarlassara, P.-A. Söderström, A.M. Stefanini, T. Steinbach, O. Stézowski, B. Szpak, C. Theisen, C. Ur, J.J. Valiente-Dobón, V. Vandone, A. Wiens, Light and heavy transfer products in ^{136}Xe+^{238}U multinucleon transfer reactions. Phys. Rev. C **92**, 024619 (2015). https://doi.org/10.1103/PhysRevC.92.024619
443. Y.X. Watanabe, Y.H. Kim, S.C. Jeong, Y. Hirayama, N. Imai, H. Ishiyama, H.S. Jung, H. Miyatake, S. Choi, J.S. Song, E. Clément, G. de France, A. Navin, M. Rejmund, C. Schmitt, G. Pollarolo, L. Corradi, E. Fioretto, D. Montanari, M. Niikura, D. Suzuki, H. Nishibata, J. Takatsu, Pathway for the production of neutron-rich isotopes around the $N = 126$ shell closure. Phys. Rev. Lett. **115**, 172503 (2015). https://doi.org/10.1103/PhysRevLett.115.172503
444. T. Mijatović, S. Szilner, L. Corradi, D. Montanari, G. Pollarolo, E. Fioretto, A. Gadea, A. Goasduff, D.J. Malenica, N. Marginean, M. Milin, G. Montagnoli, F. Scarlassara, N. Soic, A.M. Stefanini, C.A. Ur, J.J. Valiente-Dobón, Multinucleon transfer reactions in the ^{40}Ar +^{208} Pb system. Phys. Rev. C **94**, 064616 (2016). https://doi.org/10.1103/PhysRevC.94.064616
445. P. Čolović, S. Szilner, A. Illana, J.J. Valiente-Dobón, L. Corradi, G. Pollarolo, T. Mijatović, A. Goasduff, G. Benzoni, M.J.G. Borge, A. Boso, A. Boukhari, S. Ceruti, J.G. Cubiss, G. de Angelis, H. De Witte, E. Fioretto, C. Fransen, F. Galtarossa, L.P. Gaffney, E. Giannopoulos, H. Hess, M.L. Jurado-Gomez, L. Kaya, T. Kroll, T. Marchi, R. Menegazzo, D. Mengoni, D.R. Napoli, G. O'Neill, J. Pakarinen, Z. Podolyák, F. Recchia, P. Reiter, D. Rosiak, J. Snall, P. Spagnoletti, D. Testov, S. Thiel, N. Warr, R. Zidarova, Population of lead isotopes in binary reactions using a ^{94}Rb radioactive beam. Phys. Rev. C **102**, 054609 (2020). https://doi.org/10.1103/PhysRevC.102.054609
446. A.M. Stefanini, L. Corradi, G. Maron, A. Pisent, M. Trotta, A.M. Vinodkumar, S. Beghini, G. Montagnoli, F. Scarlassara, G.F. Segato, A.D. Rosa, G. Inglima, D. Pierroutsakou, M. Romoli, M. Sandoli, G. Pollarolo, A. Latina, The heavy-ion magnetic spectrometer PRISMA. Nucl. Phys. A **701**(1), 217–221 (2002). https://doi.org/10.1016/S0375-9474(01)01578-0
447. E. Fioretto, F. Galtarossa, L. Corradi, H.M. Jia, F. Collini, T. Marchi, G. Colucci, T. Mijatović, G. Montagnoli, D. Montanari, F. Scarlassara, A.M. Stefanini, E. Strano, S. Szilner, G. Pasquali, J. Gręgosz, A gas detection system for fragment identification in low-energy heavy-ion collisions. Nucl. Instrum. Methods Phys. Res. A **899**, 73–79 (2018). https://doi.org/10.1016/j.nima.2018.05.011
448. F. Galtarossa, L. Corradi, S. Szilner, E. Fioretto, G. Pollarolo, T. Mijatović, D. Montanari, D. Ackermann, D. Bourgin, S. Courtin, G. Fruet, A. Goasduff, J. Gręgosz, F. Haas, D. Jelavić Malenica, S.C. Jeong, H.M. Jia, P.R. John, D. Mengoni, M. Milin, G. Montagnoli, F. Scarlassara, N. Skukan, N. Soić, A.M. Stefanini, E. Strano, V. Tokić, C.A. Ur, J.J. Valiente-Dobón, Y.X. Watanabe, Mass correlation between light and heavy reaction products in multinucleon transfer ^{197}Au +^{130} Te collisions. Phys. Rev. C **97**, 054606 (2018). https://doi.org/10.1103/PhysRevC.97.054606

449. L. Corradi, S. Szilner, G. Pollarolo, G. Colò, P. Mason, E. Farnea, E. Fioretto, A. Gadea, F. Haas, D. Jelavić-Malenica, N. Marginean, C. Michelagnoli, G. Montagnoli, D. Montanari, F. Scarlassara, N. Soić, A.M. Stefanini, C.A. Ur, J.J. Valiente-Dobón, Single and pair neutron transfers at sub-barrier energies. Phys. Rev. C **84**, 034603 (2011). https://doi.org/10.1103/PhysRevC.84.034603
450. D. Montanari, L. Corradi, S. Szilner, G. Pollarolo, E. Fioretto, G. Montagnoli, F. Scarlassara, A.M. Stefanini, S. Courtin, A. Goasduff, F. Haas, D. Jelavić Malenica, C. Michelagnoli, T. Mijatović, N. Soić, C.A. Ur, M. Varga Pajtler, Neutron pair transfer in ^{60}Ni +^{116} Sn far below the Coulomb barrier. Phys. Rev. Lett. **113**, 052501 (2014). https://doi.org/10.1103/PhysRevLett.113.052501
451. D. Montanari, L. Corradi, S. Szilner, G. Pollarolo, A. Goasduff, T. Mijatović, D. Bazzacco, B. Birkenbach, A. Bracco, L. Charles, S. Courtin, P. Désesquelles, E. Fioretto, A. Gadea, A. Gorgen, A. Gottardo, J. Grębosz, F. Haas, H. Hess, D. Jelavić Malenica, A. Jungclaus, M. Karolak, S. Leoni, A. Maj, R. Menegazzo, D. Mengoni, C. Michelagnoli, G. Montagnoli, D.R. Napoli, A. Pullia, F. Recchia, P. Reiter, D. Rosso, M.D. Salsac, F. Scarlassara, P.-A. Söderström, N. Soić, A.M. Stefanini, O. Stézowski, C. Theisen, C.A. Ur, J.J. Valiente-Dobón, M. Varga Pajtler, Pair neutron transfer in ^{60} Ni + ^{116} Sn probed via γ-particle coincidences. Phys. Rev. C **93**, 054623 (2016). https://doi.org/10.1103/PhysRevC.93.054623
452. T. Mijatović, S. Szilner, L. Corradi, F. Galtarossa, D. Montanari, G. Pollarolo, P. Čolović, G. Colucci, E. Fioretto, A. Goasduff, J.D. Malenica, T. Marchi, G. Montagnoli, N. Soić, F. Scarlassara, A.M. Stefanini, J.J. Valiente-Dobón, Nucleon–nucleon correlation studies in heavy-ion transfer reactions. J. Phys. Conf. Ser. **1643**(1), 012097 (2020). https://doi.org/10.1088/1742-6596/1643/1/012097
453. L. Corradi, S. Szilner, G. Pollarolo, E. Fioretto, F. Galtarossa, T. Mijatović, A. Gottardo, A.I. Sison, G. Jaworski, T. Marchi, A.M. Stefanini, D. Testov, J.J. Valiente-Dobón, G. Colucci, A. Goasduff, D. Mengoni, G. Montagnoli, D. Montanari, F. Scarlassara, M. Siciliano, P. Čolović, D.J. Malenica, N. Soić, N. Vukman, D. Nurkić, M. de la Luz Jurado Gomez, Probing nucleon–nucleon correlations in heavy ion transfer reactions using large solid angle magnetic spectrometers. JPS Conf. Proc. **32**, 010043 (2020). https://doi.org/10.7566/JPSCP.32.010043
454. K. Sekizawa, TDHF theory and its extensions for the multinucleon transfer reaction: a mini review. Front. Phys. **7**, 20 (2019). https://doi.org/10.3389/fphy.2019.00020
455. K. Sekizawa, S. Ayik, Quantal diffusion approach for multinucleon transfer processes in the ^{58,64}Ni+^{208}Pb reactions: toward the production of unknown neutron-rich nuclei. Phys. Rev. C **102**, 014620 (2020). https://doi.org/10.1103/PhysRevC.102.014620
456. S. Ayik, K. Sekizawa, Kinetic energy dissipation and fluctuations in strongly-damped heavy-ion collisions within the stochastic mean-field approach. Phys. Rev. C **102**, 064619 (2020). https://doi.org/10.1103/PhysRevC.102.064619
457. E. Williams, K. Sekizawa, D.J. Hinde, C. Simenel, M. Dasgupta, I.P. Carter, K.J. Cook, D.Y. Jeung, S.D. McNeil, C.S. Palshetkar, D.C. Rafferty, K. Ramachandran, A. Wakhle, Exploring zeptosecond quantum equilibration dynamics: from deep-inelastic to fusion–fission outcomes in ^{58}Ni+^{60}Ni reactions. Phys. Rev. Lett. **120**, 022501 (2018). https://doi.org/10.1103/PhysRevLett.120.022501
458. P. Magierski, K. Sekizawa, G. Wlazłowski, Novel role of superfluidity in low-energy nuclear reactions. Phys. Rev. Lett. **119**, 042501 (2017). https://doi.org/10.1103/PhysRevLett.119.042501
459. G. Potel, F. Barranco, E. Vigezzi, R.A. Broglia, Quantum entanglement in nuclear cooper-pair tunneling with γ rays. Phys. Rev. C **103**, 021601 (2021). https://doi.org/10.1103/PhysRevC.103.L021601
460. R.A. Broglia, F. Barranco, G. Potel, E. Vigezzi, Transient weak links between superconducting nuclei: coherence length. Nucl. Phys. News **31**(4), 24–29 (2021). https://doi.org/10.1080/10619127.2021.1990668
461. P. Magierski, The tiniest superfluid circuit in nature. Physics **14**, 27 (2021)
462. W. Henning, F.L.H. Wolfs, J.P. Schiffer, K.E. Rehm, Subbarrier nucleon transfer: doorway to heavy-ion fusion. Phys. Rev. Lett. **58**, 318 (1987). https://doi.org/10.1103/PhysRevLett.58.318
463. M. Beckerman, M. Salomaa, A. Sperduto, H. Enge, J. Ball, A. DiRienzo, S. Gazes, Y. Chen, J.D. Molitoris, M. Nai-feng, Dynamic influence of valence neutrons upon the complete fusion of massive nuclei. Phys. Rev. Lett. **45**, 1472 (1980). https://doi.org/10.1103/PhysRevLett.45.1472
464. H.M. Jia, C.J. Lin, F. Yang, X.X. Xu, H.Q. Zhang, Z.H. Liu, L. Yang, S.T. Zhang, P.F. Bao, L.J. Sun, Fusion of the ^{16}O+^{76}Ge and ^{18}O+^{74}Ge systems and the role of positive Q-value neutron transfers. Phys. Rev. C **86**, 044621 (2012). https://doi.org/10.1103/PhysRevC.86.044621
465. G. Montagnoli, F. Scarlassara, S. Beghini, A.D. Bello, G.F. Segato, A.M. Stefanini, D. Ackermann, L. Corradi, J.H. He, C.J. Lin, The time-of-flight spectrometer for heavy ions PISOLO. Nucl. Instrum. Methods Phys. Res. A **454**, 306 (2000)
466. E. Strano, G. Montagnoli, A.M. Stefanini, M. Mazzocco, G.L. Zhang, I. Zanon, G. Colucci, D. Ackermann, A. Boiano, L. Corradi, E. Fioretto, F. Galtarossa, M. La Commara, G. La Rana, C. Parascandolo, D. Pierroutsakou, F. Scarlassara, F. Soramel, D. Torresi, Use of the facility EXOTIC for fusion-evaporation studies. Nucl. Instrm. Methods Phys. Res. A **877**, 293 (2018). https://doi.org/10.1016/j.nima.2017.10.008
467. L. Moschini, A. Diaz-Torres, Tracing the dynamical interplay of low-energy reaction processes of exotic nuclei using a two-center molecular continuum. Phys. Lett. B **820**, 136513 (2021). https://doi.org/10.1016/j.physletb.2021.136513
468. N.K. Timofeyuk, D. Baye, P. Descouvemont, R. Kamouni, I.J. Thompson, ^{15}C- ^{15}F charge symmetry and the ^{14}C(n, γ)^{15}C reaction puzzle. Phys. Rev. Lett. **96**, 162501 (2006). https://doi.org/10.1103/PhysRevLett.96.162501
469. J. Yang, Ph.D. thesis, https://lirias.kuleuven.be/retrieve/553027
470. J. Yang, P. Capel, Systematic analysis of the peripherality of the ^{10}Be(d, p)^{11}Be transfer reaction and extraction of the asymptotic normalization coefficient of ^{11}Be bound states. Phys. Rev. C **98**, 054602 (2018). https://doi.org/10.1103/PhysRevC.98.054602
471. L. Moschini, J. Yang, P. Capel, ^{15}C: from halo effective field theory structure to the study of transfer, breakup, and radiative-capture reactions. Phys. Rev. C **100**, 044615 (2019). https://doi.org/10.1103/PhysRevC.100.044615
472. A. Calci, P. Navrátil, R. Roth, J. Dohet-Eraly, S. Quaglioni, G. Hupin, Can ab initio theory explain the phenomenon of parity inversion in ^{11}Be? Phys. Rev. Lett. **117**, 242501 (2016). https://doi.org/10.1103/PhysRevLett.117.242501
473. L. Moschini, P. Capel, Reliable extraction of the dB(E1)/dE for ^{11}Be from its breakup at 520 MeV/nucleon. Phys. Lett. B **790**, 367–371 (2019). https://doi.org/10.1016/j.physletb.2019.01.041
474. A. Bhattacharyya, U. Datta, A. Rahaman, S. Chakraborty, T. Aumann, S. Beceiro-Novo, K. Boretzky, C. Caesar, B.V. Carlson, W.N. Catford, M. Chartier, D. Cortina-Gil, P. Das, G. de Angelis, P.D. Fernandez, H. Emling, H. Geissel, D. Gonzalez-Diaz, M. Heine, H. Johansson, B. Jonson, N. Kalantar-Nayestanaki, T. Kröll, R. Krücken, J. Kurcewicz, C. Langer, T. Le Bleis, Y. Leifels, J. Marganiec, G. Münzenberg, T. Nilsson, C. Nociforo, V. Panin, S. Paschalis, R. Plag, R. Reifarth, M.V. Ricciardi, C. Rigollet, D. Rossi, C. Scheidenberger, H. Scheit, H. Simon, Y. Togano, S. Typel, Y. Utsuno, A. Wagner, F. Wamers, H. Weick, J.S. Winfield, Neutron capture cross sections of light neutron-rich nuclei relevant for r-process nucleosynthesis. Phys. Rev. C **104**, 045801 (2021). https://doi.org/10.1103/PhysRevC.104.045801
475. C.A. Bertulani, H.-W. Hammer, U. van Kolck, Effective field theory for halo nuclei: shallow p-wave states. Nucl. Phys. A **712**(1), 37–58 (2002). https://doi.org/10.1016/S0375-9474(02)01270-8
476. H.-W. Hammer, C. Ji, D.R. Phillips, Effective field theory description of halo nuclei. J. Phys. G **44**(10), 103002 (2017). https://doi.org/10.1088/1361-6471/aa83db
477. P. Capel, D.R. Phillips, H.-W. Hammer, Dissecting reaction calculations using halo effective field theory and ab initio input. Phys. Rev. C **98**, 034610 (2018). https://doi.org/10.1103/PhysRevC.98.034610

478. E.M. Burbidge, G.R. Burbidge, W.A. Fowler, F. Hoyle, Synthesis of the elements in stars. Rev. Mod. Phys. **29**, 547–650 (1957). https://doi.org/10.1103/RevModPhys.29.547
479. M. Terasawa, K. Sumiyoshi, T. Kajino, G.J. Mathews, I. Tanihata, New nuclear reaction flow during r-process nucleosynthesis in supernovae: critical role of light, neutron-rich nuclei. Astrophys. J. **562**(1), 470–479 (2001). https://doi.org/10.1086/323526
480. W. Liu, X. Bai, S. Zhou, Z. Ma, Z. Li, Y. Wang, A. Li, Z. Ma, B. Chen, X. Tang, Y. Han, Q. Shen, Angular distribution for the ^{7}Be(d, n)^{8}B reaction at $E_{c.m.} = 5.8$ MeV and the $S_{17}(0)$ factor for the ^{7}Be(p, γ)^{8}B reaction. Phys. Rev. Lett. **77**, 611–614 (1996). https://doi.org/10.1103/PhysRevLett.77.611
481. A. Pakou, N. Keeley, F. Cappuzzello, L. Acosta, C. Agodi, X. Aslanoglou, S. Calabrese, D. Carbone, M. Cavallaro, A. Foti, G. Marquanez-Durřn, I. Martel, M. Mazzocco, C. Parascandolo, D. Pierroutsakou, K. Rusek, O. Sgouros, V. Soukeras, E. Strano, V.A.B. Zagatto, The ^{7}Li(d, p)^{8}Li reaction in inverse kinematics at 5.44 MeV/u. Eur. Phys. J. A **53**, 167 (2017). https://doi.org/10.1140/epja/i2017-12361-y
482. R.B. Firestone, Z. Revay, Thermal neutron radiative cross sections for ^{6,7}Li, ^{9}Be, ^{10,11}B, ^{12,13}C, and ^{14,15}N. Phys. Rev. C **93**, 054306 (2016). https://doi.org/10.1103/PhysRevC.93.054306
483. R. Buompane, N. De Cesare, A. Di Leva, A. D'Onofrio, L. Gialanella, M. Romano, M. De Cesare, J.G. Duarte, Z. Fžlp, L. Morales-Gallegos, G. Gyžrky, L.R. Gasques, F. Marzaioli, G. Palumbo, G. Porzio, D. Rapagnani, V. Roca, D. Rogalla, M. Romoli, C. Sabbarese, D. Schžrmann, F. Terrasi, Test measurement of ^{7}Be(p,γ)^{8}B with the recoil mass separator ERNA. Eur. Phys. J. A **54**, 92 (2018). https://doi.org/10.1140/epja/i2018-12522-6
484. M. Igarashi, M. Toyama, Computer program TWOFNR. University of Surrey version (2008)
485. A.J. Koning, J.P. Delaroche, Local and global nucleon optical models from 1 keV to 200 MeV. Nucl. Phys. A **713**(3), 231–310 (2003). https://doi.org/10.1016/S0375-9474(02)01321-0
486. R.E. Hester, R.E. Pixley, W.A.S. Lamb, Radiative capture of protons in oxygen at 140 to 170 kev. Phys. Rev. **111**, 1604–1606 (1958). https://doi.org/10.1103/PhysRev.111.1604
487. N. Tanner, Direct radiative capture of protons by O^{16} and Ne^{20}. Phys. Rev. **114**, 1060–1064 (1959). https://doi.org/10.1103/PhysRev.114.1060
488. P. Corvisiero, M. Anghinolfi, M.M. Giannini, G. Ricco, M. Sanzone, M. Taiuti, Proton and deuteron radiative capture in light nuclei. Nucl. Phys. A **483**(1), 9–22 (1988). https://doi.org/10.1016/0375-9474(88)90062-0
489. C.R. Brune, W.H. Geist, R.W. Kavanagh, K.D. Veal, Sub-Coulomb α transfers on ^{12}C and the $^{12}C(\alpha, \gamma)^{16}OS$ factor. Phys. Rev. Lett. **83**, 4025–4028 (1999). https://doi.org/10.1103/PhysRevLett.83.4025
490. A.N. Andreyev, K. Nishio, K.-H. Schmidt, Nuclear fission: a review of experimental advances and phenomenology. Rep. Prog. Phys. **81**, 016301 (2018). https://doi.org/10.1088/1361-6633/aa82eb
491. G. Scamps, C. Simenel, Impact of pear-shaped fission fragments on mass-asymmetric fission in actinides. Nature **564**, 382 (2018). https://doi.org/10.1038/s41586-018-0780-0
492. A. Bulgac, P. Magierski, K.J. Roche, I. Stetcu, Induced fission of ^{240}Pu within a real-time microscopic framework. Phys. Rev. Lett. **116**, 122504 (2016). https://doi.org/10.1103/PhysRevLett.116.122504
493. A. Chatillon, J. Taïeb, H. Alvarez-Pol, L. Audouin, Y. Ayyad, G. Bélier, J. Benlliure, G. Boutoux, M. Caamaño, E. Casarejos, D. Cortina-Gil, A. Ebran, F. Farget, B. Fernández-Domínguez, T. Gorbinet, L. Grente, A. Heinz, H.T. Johansson, B. Jurado, A. Kelić-Heil, N. Kurz, B. Laurent, J.-F. Martin, C. Nociforo, C. Paradela, E. Pellereau, S. Pietri, A. Prochazka, J.L. Rodríguez-Sánchez, D. Rossi, H. Simon, L. Tassan-Got, J. Vargas, B. Voss, H. Weick, Evidence for a new compact symmetric fission mode in light thorium isotopes. Phys. Rev. Lett. **124**, 202502 (2020). https://doi.org/10.1103/PhysRevLett.124.202502
494. J.-F. Martin, J. Taïeb, G. Boutoux, A. Chatillon, T. Gorbinet, E. Pellereau, L. Audouin, A. Heinz, H. Alvarez-Pol, Y. Ayyad, G. Bélier, J. Benlliure, M. Caamaño, E. Casarejos, D. Cortina-Gil, A. Ebran, F. Farget, B. Fernández-Domínguez, L. Grente, H.T. Johansson, B. Jurado, A. Kelić-Heil, N. Kurz, B. Laurent, C. Nociforo, C. Paradela, S. Pietri, A. Prochazka, J.L. Rodríguez-Sánchez, D. Rossi, H. Simon, L. Tassan-Got, J. Vargas, B. Voss, H. Weick, Fission-fragment yields and prompt-neutron multiplicity for Coulomb-induced fission of ^{234,235}U and ^{237,238}Np. Phys. Rev. C **104**, 044602 (2021). https://doi.org/10.1103/PhysRevC.104.044602
495. C. Rodríguez-Tajes, F. Farget, X. Derkx, M. Caamaño, O. Delaune, K.-H. Schmidt, E. Clément, A. Dijon, A. Heinz, T. Roger, L. Audouin, J. Benlliure, E. Casarejos, D. Cortina, D. Doré, B. Fernández-Domínguez, B. Jacquot, B. Jurado, A. Navin, C. Paradela, D. Ramos, P. Romain, M.D. Salsac, C. Schmitt, Transfer reactions in inverse kinematics: an experimental approach for fission investigations. Phys. Rev. C **89**, 024614 (2014). https://doi.org/10.1103/PhysRevC.89.024614
496. M. Caamaño, F. Farget, O. Delaune, K.-H. Schmidt, C. Schmitt, L. Audouin, C.-O. Bacri, J. Benlliure, E. Casarejos, X. Derkx, B. Fernández-Domínguez, L. Gaudefroy, C. Golabek, B. Jurado, A. Lemasson, D. Ramos, C. Rodríguez-Tajes, T. Roger, A. Shrivastava, Characterization of the scission point from fission-fragment velocities. Phys. Rev. C **92**, 034606 (2015). https://doi.org/10.1103/PhysRevC.92.034606
497. M. Caamaño, F. Farget, Energy balance and deformation at scission in ^{240}Pu fission. Phys. Lett. B **770**, 72 (2017). https://doi.org/10.1016/j.physletb.2017.04.041
498. D. Ramos, M. Caamaño, F. Farget, C. Rodríguez-Tajes, L. Audouin, J. Benlliure, E. Casarejos, E. Clément, D. Cortina, O. Delaune, X. Derkx, A. Dijon, D. Doré, B. Fernández-Domínguez, G. de France, A. Heinz, B. Jacquot, A. Navin, C. Paradela, M. Rejmund, T. Roger, M.-D. Salsac, C. Schmitt, Isotopic fission-fragment distributions of ^{238}U, ^{239}Np, ^{240}Pu, ^{244}Cm, and ^{250}Cf produced through inelastic scattering, transfer, and fusion reactions in inverse kinematics. Phys. Rev. C **97**, 054612 (2018). https://doi.org/10.1103/PhysRevC.97.054612
499. D. Ramos, M. Caamaño, A. Lemasson, M. Rejmund, L. Audouin, H. Álvarez-Pol, J.D. Frankland, B. Fernández-Domínguez, E. Galiana-Baldó, J. Piot, D. Ackermann, S. Biswas, E. Clément, D. Durand, F. Farget, M.O. Fregeau, D. Galaviz, A. Heinz, A.I. Henriques, B. Jacquot, B. Jurado, Y.H. Kim, P. Morfouace, D. Ralet, T. Roger, C. Schmitt, P. Teubig, I. Tsekhanovich, First direct measurement of isotopic fission-fragment yields of ^{239}U. Phys. Rev. Lett. **123**, 092503 (2019). https://doi.org/10.1103/PhysRevLett.123.092503
500. C. Schmitt, A. Lemasson, K.-H. Schmidt, A. Jhingan, S. Biswas, Y.H. Kim, D. Ramos, A.N. Andreyev, D. Curien, M. Ciemała, E. Clément, O. Dorvaux, B. De Canditiis, F. Didierjean, G. Duchêne, J. Dudouet, J. Frankland, B. Jacquot, C. Raison, D. Ralet, B.-M. Retailleau, L. Stuttgé, I. Tsekhanovich, Experimental evidence for common driving effects in low-energy fission from sublead to actinides. Phys. Rev. Lett. **126**, 132502 (2020). https://doi.org/10.1103/PhysRevLett.126.132502
501. A. Latina, A.M. Stefanini, S. Beghini, B.R. Behera, L. Corradi, G. de Angelis, A. De Rosa, E. Fioretto, A. Gadea, M. Gulmini, G. Inglima, M. La Commara, G. Maron, R. Menegazzo, N. Marginean, G. Montagnoli, D.R. Napoli, D. Pierroutsakou, G. Pollarolo, M. Romoli, M. Sandoli, F. Scarlassara, S. Szilner, N. Toniolo, M. Trotta, Y.W. Wu, PRISMA—a magnetic spectrometer for heavy ions at LNL. Nucl. Phys. A **734**, 1–4 (2004). https://doi.org/10.1016/j.nuclphysa.2004.03.005. (**Proceedings of the Eighth International Conference on Nucleus-Nucleus Collisions (NN2003)**)
502. J. Khuyagbaatar, D.J. Hinde, I.P. Carter, M. Dasgupta, C.E. Düllmann, M. Evers, D.H. Luong, R. du Rietz, A. Wakhle, E. Williams, A. Yakushev, Experimental study of the quasifission, fusion–fission, and de-excitation of Cf compound nuclei. Phys. Rev. C **91**, 054608 (2015). https://doi.org/10.1103/PhysRevC.91.054608
503. K. Hirose, K. Nishio, S. Tanaka, R. Léguillon, H. Makii, I. Nishinaka, R. Orlandi, K. Tsukada, J. Smallcombe, M.J. Vermeulen, S. Chiba, Y. Aritomo, T. Ohtsuki, K. Nakano, S. Araki, Y. Watanabe, R. Tatsuzawa, N. Takaki, N. Tamura, S. Goto, I. Tsekhanovich, A.N. Andreyev, Role of multichance fission

in the description of fission-fragment mass distributions at high energies. Phys. Rev. Lett. **119**, 222501 (2017). https://doi.org/10.1103/PhysRevLett.119.222501
504. P. Möller, J. Randrup, Calculated fission-fragment yield systematics in the region 74≤Z≤94 and 90≤N≤150. Phys. Rev. C **91**, 044316 (2015). https://doi.org/10.1103/PhysRevC.91.044316
505. D. Ramos, C. Rodríguez-Tajes, M. Caamaño, F. Farget, L. Audouin, J. Benlliure, E. Casarejos, E. Clément, D. Cortina, O. Delaune, X. Derkx, A. Dijon, D. Doré, B. Fernández-Domínguez, G. de France, A. Heinz, B. Jacquot, A. Navin, C. Paradela, M. Rejmund, T. Roger, M.D. Salsac, C. Schmitt, Dependence of fission-fragment properties on excitation energy for neutron-rich actinides. EPJ Web Conf. **111**, 10001 (2016). https://doi.org/10.1051/epjconf/201611110001
506. D. Ramos, C. Rodrguez-Tajes, M. Caamaño, F. Farget, L. Audouin, J. Benlliure, E. Casarejos, E. Clément, D. Cortina, O. Delaune, X. Derkx, A. Dijon, D. Dorl', B. Fernŕndez-Domnguez, G. de France, A. Heinz, B. Jacquot, A. Navin, C. Paradela, M. Rejmund, T. Roger, M.-D. Salsac, C. Schmitt, Excitation-energy influence at the scission configuration. EPJ Web Conf. **146**, 04019 (2017). https://doi.org/10.1051/epjconf/201714604019
507. S. Mişicu, H. Esbensen, Hindrance of heavy-ion fusion due to nuclear incompressibility. Phys. Rev. Lett. **96**, 112701 (2006). https://doi.org/10.1103/PhysRevLett.96.112701
508. S. Mişicu, H. Esbensen, Signature of shallow potentials in deep sub-barrier fusion reactions. Phys. Rev. C **75**, 034606 (2007). https://doi.org/10.1103/PhysRevC.75.034606
509. C. Simenel, A.S. Umar, K. Godbey, M. Dasgupta, D.J. Hinde, How the Pauli exclusion principle affects fusion of atomic nuclei. Phys. Rev. C **95**, 031601 (2017). https://doi.org/10.1103/PhysRevC.95.031601
510. T. Ichikawa, K. Hagino, A. Iwamoto, Existence of a one-body barrier revealed in deep subbarrier fusion. Phys. Rev. C **75**, 057603 (2007). https://doi.org/10.1103/PhysRevC.75.057603
511. T. Ichikawa, K. Hagino, A. Iwamoto, Signature of smooth transition from sudden to adiabatic states in heavy-ion fusion reactions at deep sub-barrier energies. Phys. Rev. Lett. **103**, 2027401 (2009). https://doi.org/10.1103/PhysRevLett.103.202701
512. T. Ichikawa, K. Matsuyanagi, Damping of quantum vibrations revealed in deep sub-barrier fusion. Phys. Rev. C **88**, 011602 (2013). https://doi.org/10.1103/PhysRevC.88.011602
513. T. Ichikawa, K. Matsuyanagi, Universal damping mechanism of quantum vibrations in deep sub-barrier fusion reactions. Phys. Rev. C **92**, 021602 (2015). https://doi.org/10.1103/PhysRevC.92.021602
514. G. Montagnoli, A.M. Stefanini, Recent experimental results in sub- and near-barrier heavy-ion fusion reactions. Eur. Phys. J. A **53**, 169 (2017). https://doi.org/10.1140/epja/i2017-12350-2
515. I.Y. Lee, The GAMMASPHERE. Nucl. Phys. A **520**, 641 (1990). https://doi.org/10.1016/0375-9474(90)91181-P
516. C.L. Jiang, D. Santiago-Gonzalez, S. Almaraz-Calderon, K.E. Rehm, B.B. Back, K. Auranen, M.L. Avila, A.D. Ayangeakaa, S. Bottoni, M.P. Carpenter, C. Dickerson, B. DiGiovine, J.P. Greene, C.R. Hoffman, R.V.F. Janssens, B.P. Kay, S.A. Kuvin, T. Lauritsen, R.C. Pardo, J. Sethi, D. Seweryniak, R. Talwar, C. Ugalde, S. Zhu, D. Bourgin, S. Courtin, F. Haas, M. Heine, G. Fruet, D. Montanari, D.G. Jenkins, L. Morris, A. Lefebvre-Schuhl, M. Alcorta, X. Fang, X.D. Tang, B. Bucher, C.M. Deibel, S.T. Marley, Reaction rate for carbon burning in massive stars. Phys. Rev. C **97**, 012801 (2018). https://doi.org/10.1103/PhysRevC.97.012801
517. A.M. Stefanini, G. Montagnoli, L. Corradi, S. Courtin, E. Fioretto, A. Goasduff, F. Haas, P. Mason, R. Silvestri, P.P. Singh, F. Scarlassara, S. Szilner, Fusion hindrance for ^{58}Ni +^{54} Fe. Phys. Rev. C **82**, 014614 (2010). https://doi.org/10.1103/PhysRevC.82.014614
518. G. Montagnoli, A.M. Stefanini, C.L. Jiang, K. Hagino, F. Galtarossa, G. Colucci, S. Bottoni, C. Broggini, A. Caciolli, P. Čolović, L. Corradi, S. Courtin, R. Depalo, E. Fioretto, G. Fruet, A. Gal, A. Goasduff, M. Heine, S.P. Hu, M. Kaur, T. Mijatović, M. Mazzocco, D. Montanari, F. Scarlassara, E. Strano, S. Szilner, G.X. Zhang, Fusion hindrance for the positive q-value system ^{12}C +^{30} Si. Phys. Rev. C **97**, 024610 (2018). https://doi.org/10.1103/PhysRevC.97.024610
519. D. Shapira, J.F. Liang, C.J. Gross, R.L. Varner, H. Amro, C. Harlin, J.J. Kolata, S. Novotny, A high-efficiency compact setup to study evaporation residues formed in reactions induced by low-intensity radioactive ion beams. Nucl. Instrum. Methods Phys. Res. A **551**, 330 (2005). https://doi.org/10.1016/j.nima.2005.05.079
520. J.F. Liang, D. Shapira, J.R. Beene, C.J. Gross, R.L. Varner, A. Galindo-Uribarri, J.G. Campo, P.A. Hausladen, P.E. Mueller, D.W. Stracener, H. Amro, J.J. Kolata, J.D. Bierman, A.L. Caraley, K.L. Jones, Y. Larochelle, W. Loveland, D. Peterson, Fusion of radioactive ^{132}Sn with ^{64}Ni. Phys. Rev. C **75**, 054607 (2007). https://doi.org/10.1103/PhysRevC.75.054607
521. G. Fruet, S. Courtin, M. Heine, D.G. Jenkins, P. Adsley, A. Brown, R. Canavan, W.N. Catford, E. Charon, D. Curien, S. Della Negra, J. Duprat, F. Hammache, J. Lesrel, G. Lotay, A. Meyer, D. Montanari, L. Morris, M. Moukaddam, J. Nippert, Z. Podolyák, P.H. Regan, I. Ribaud, M. Richer, M. Rudigier, R. Shearman, N. de Séréville, C. Stodel, Advances in the direct study of carbon burning in massive stars. Phys. Rev. Lett. **124**, 0192701 (2020). https://doi.org/10.1103/PhysRevLett.124.192701
522. P.F.F. Carnelli, S. Almaraz-Calderon, K.E. Rehm, M. Albers, M. Alcorta, P.F. Bertone, B. Digiovine, H. Esbensen, J. Fernŕndez Niello, D. Henderson, C.L. Jiang, J. Lai, S.T. Marley, O. Nusair, T. Palchan-Hazan, R.C. Pardo, M. Paul, C. Ugalde, Multi-sampling ionization chamber (MUSIC) for measurements of fusion reactions with radioactive beams. Nucl. Instrum. Methods Phys. Res. A **799**, 197 (2015). https://doi.org/10.1016/j.nima.2015.07.030
523. B.W. Asher, S. Almaraz-Calderon, V. Tripathi, K.W. Kemper, L.T. Baby, N. Gerken, E. Lopez-Saavedra, A.B. Morelock, J.F. Perello, I. Wiedenhöver, N. Keeley, Experimental study of the ^{17}F +^{12} C fusion reaction and its implications for fusion of proton-halo systems. Phys. Rev. C **103**, 044615 (2021). https://doi.org/10.1103/PhysRevC.103.044615
524. G. Montagnoli, A.M. Stefanini, C.L. Jiang, G. Colucci, S. Bottoni, D. Brugnara, P. Čolović, L. Corradi, E. Fioretto, F. Galtarossa, A. Goasduff, O.S. Khwairakpam, M. Heine, G. Jaworski, M. Mazzocco, T. Mijatović, M. Siciliano, F. Scarlassara, S. Szilner, T. Van Patten, I. Zanon, Fusion of ^{12}C+^{24}Mg far below the barrier: evidence for the hindrance effect. Phys. Rev. C **101**, 044608 (2020). https://doi.org/10.1103/PhysRevC.101.044608
525. S. Almaraz-Calderon, K.E. Rehm, N. Gerken, M.L. Avila, B.P. Kay, R. Talwar, A.D. Ayangeakaa, S. Bottoni, A.A. Chen, C.M. Deibel, C. Dickerson, K. Hanselman, C.R. Hoffman, C.L. Jiang, S.A. Kuvin, O. Nusair, R.C. Pardo, D. Santiago-Gonzalez, J. Sethi, C. Ugalde, Study of the ^{26}Al$^{m}(d,\ p)^{27}$Al reaction and the influence of the ^{26}Al0^{+} isomer on the destruction of ^{26}Al in the galaxy. Phys. Rev. Lett. **119**, 072701 (2017). https://doi.org/10.1103/PhysRevLett.119.072701
526. J. Esposito, D. Bettoni, A. Boschi, M. Calderolla, S. Cisternino, G. Fiorentini, G. Keppel, P. Martini, M. Maggiore, L. Mou, M. Pasquali, L. Pranovi, G. Pupillo, C. Rossi Alvarez, L. Sarchiapone, G. Sciacca, H. Skliarova, P. Favaron, A. Lombardi, P. Antonini, A. Duatti, LARAMED a laboratory for radioisotopes of medical interest. Molecules (2019). https://doi.org/10.3390/molecules24010020
527. A. Andrighetto, M. Tosato, M. Ballan, S. Corradetti, F. Borgna, V.D. Marco, The ISOLPHARM project: ISOL-based production of radionuclides for medical applications. J. Radioanal. Nucl. Chem. **322**, 73–77 (2019). https://doi.org/10.1007/s10967-019-06698-0
528. PRISMAP consortium. Web page (2021). https://www.prismap.eu/
529. G. Pupillo, L. Mou, S. Manenti, F. Groppi, J. Esposito, F. Haddad, Nuclear data for light charged particle induced production of emerging medical radionuclides. Radiochim. Acta (2022). https://doi.org/10.1515/ract-2022-0011

530. S.M. Qaim, Theranostic radionuclides: recent advances in production methodologies. J. Radioanal. Nucl. Chem. **322**, 1257–1266 (2019). https://doi.org/10.1007/s10967-019-06797-y
531. A. Hermanne, A.V. Ignatyuk, R. Capote, B.V. Carlson, J.W. Engle, M.A. Kellett, T. Kibédi, G. Kim, F.G. Kondev, M. Hussain, O. Lebeda, A. Luca, Y. Nagai, H. Naik, A.L. Nichols, F.M. Nortier, S.V. Suryanarayana, S. Takács, F.T. Tárkányi, M. Verpelli, Reference cross sections for charged-particle monitor reactions. Nucl. Data Sheets **148**, 338–382 (2018). https://doi.org/10.1016/j.nds.2018.02.009
532. IAEA: Monitor Reactions. Web page (2019). https://www-nds.iaea.org/medical/monitor_reactions.html
533. L. Mou, P. Martini, G. Pupillo, I. Cieszykowska, C.S. Cutler, R. Mikołajczak, ^{67}Cu production capabilities: a mini review. Molecules (2022). https://doi.org/10.3390/molecules27051501
534. R.A. Jalilian, A.M. Gizawy, C. Alliot, S. Takacs, S. Chakarborty, R.A.M. Rovais, G. Pupillo, K. Nagatsu, H.J. Park, U.M. Khandaker, R. Mikolajczak, A. Bilewicz, S. Okarvi, K. Gagnon, H.A. Al Rayyes, E.S. Lapi, V. Starovoitova, A. Korde, O.A. Joao, IAEA activities on ^{67}Cu, ^{186}Re, ^{47}Sc theranostic radionuclides and radiopharmaceuticals. Curr. Radiopharm. (2021). https://doi.org/10.2174/1874471013999200928162322
535. G. Pupillo, L. Mou, P. Martini, M. Pasquali, A. Boschi, G. Cicoria, A. Duatti, F. Haddad, J. Esposito, Production of ^{67}Cu by enriched ^{70}Zn targets: first measurements of formation cross sections of ^{67}Cu, ^{64}Cu, ^{67}Ga, ^{66}Ga, ^{69m}Zn and ^{65}Zn in interactions of ^{70}Zn with protons above 45 MeV. Radiochim. Acta **108**(8), 593–602 (2020). https://doi.org/10.1515/ract-2019-3199
536. G. Pupillo, T. Sounalet, N. Michel, L. Mou, J. Esposito, F. Haddad, New production cross sections for the theranostic radionuclide ^{67}Cu. Nucl. Instrum. Methods Phys. Res. B **415**, 41–47 (2018). https://doi.org/10.1016/j.nimb.2017.10.022
537. S.M. Qaim, M. Hussain, I. Spahn, B. Neumaier, Continuing nuclear data research for production of accelerator-based novel radionuclides for medical use: a mini-review. Front. Phys. (2021). https://doi.org/10.3389/fphy.2021.639290
538. L. De Nardo, G. Pupillo, L. Mou, J. Esposito, A. Rosato, L. Meléndez-Alafort, A feasibility study of the therapeutic application of a mixture of $^{67/64}$Cu radioisotopes produced by cyclotrons with proton irradiation. Med. Phys. (2022). https://doi.org/10.1002/mp.15524
539. F. Barbaro, L. Canton, M.P. Carante, A. Colombi, L. De Dominicis, A. Fontana, F. Haddad, L. Mou, G. Pupillo, New results on proton-induced reactions on vanadium for ^{47}Sc production and the impact of level densities on theoretical cross sections. Phys. Rev. C **104**, 044619 (2021). https://doi.org/10.1103/PhysRevC.104.044619
540. S.M. Qaim, B. Scholten, B. Neumaier, New developments in the production of theranostic pairs of radionuclides. J. Radioanal. Nucl. Chem. **318**(3), 1493–1509 (2018). https://doi.org/10.1007/s10967-018-6238-x
541. G. Pupillo, L. Mou, A. Boschi, S. Calzaferri, L. Canton, S. Cisternino, L. De Dominicis, A. Duatti, A. Fontana, F. Haddad, P. Martini, M. Pasquali, H. Skliarova, J. Esposito, Production of ^{47}Sc with natural vanadium targets: results of the PASTA project. J. Radioanal. Nucl. Chem. (2019). https://doi.org/10.1007/s10967-019-06844-8
542. L. De Nardo, G. Pupillo, L. Mou, D. Furlanetto, A. Rosato, J. Esposito, L. Meléndez-Alafort, Preliminary dosimetric analysis of DOTA-folate radiopharmaceutical radiolabelled with ^{47}Sc produced through ^{nat}V(p, x)^{47}Sc cyclotron irradiation. Phys. Med. Biol. **66**(2), 025003 (2021). https://doi.org/10.1088/1361-6560/abc811
543. C. Müller, K.A. Domnanich, C.A. Umbricht, N.P. van der Meulen, Scandium and terbium radionuclides for radiotheranostics: current state of development towards clinical application. Br. J. Radiol. (2018). https://doi.org/10.1259/bjr.20180074
544. C. Favaretto, Z. Talip, F. Borgna, P.V. Grundler, G. Dellepiane, A. Sommerhalder, H. Zhang, R. Schibli, S. Braccini, C. Müller, N.P. van der Meulen, Cyclotron production and radiochemical purification of terbium-155 for SPECT imaging. EJNMMI Radiopharm. Chem. (2021). https://doi.org/10.1186/s41181-021-00153-w
545. N. Mlynczyk, A. Konefal, ^{117m}Sn the promising radioisotope for use in nuclear medicine. Acta Phys. Pol. B Suppl. (2020). https://doi.org/10.5506/APhysPolBSupp.13.943
546. P. Randhawa, A.P. Olson, S. Chen, K.L. Gower-Fry, C. Hoehr, J.W. Engle, C.F. Ramogida, V. Radchenko, Meitner-Auger electron emitters for targeted radionuclide therapy: Mercury-197m/g and Antimony-119. Curr. Radiopharm. **14**(4), 394–419 (2021). https://doi.org/10.2174/1874471014999210111201630
547. M.A. Mosby, E.R. Birnbaum, F.M. Nortier, J.W. Engle, Cross sections for proton-induced reactions on ^{nat}Sb up to 68 MeV. Nucl. Instrum. Methods Phys. Res. B **412**, 34–40 (2017). https://doi.org/10.1016/j.nimb.2017.08.038
548. E. Aluicio-Sarduy, R. Hernandez, A.P. Olson, T.E. Barnhart, W. Cai, P.A. Ellison, J.W. Engle, Production and in vivo PET/CT imaging of the theranostic pair $^{132/135}$La. Sci. Rep. (2019). https://doi.org/10.1038/s41598-019-47137-0
549. B.J.B. Nelson, J. Wilson, J.D. Andersson, F. Wuest, High yield cyclotron production of a novel $^{133/135}$La theranostic pair for nuclear medicine. Sci. Rep. (2020). https://doi.org/10.1038/s41598-020-79198-x
550. B. Nelson, S. Ferguson, M. Wuest, J. Wilson, J. Duke, S. Richter, H.-S. Jans, J. Andersson, F. Juengling, F. Wuest, First in vivo and phantom imaging of cyclotron produced ^{133}La as a theranostic radionuclide for ^{225}Ac and ^{135}La. J. Nucl. Med. (2021). https://doi.org/10.2967/jnumed.121.262459
551. J. Fonslet, B.Q. Lee, T.A. Tran, M. Siragusa, M. Jensen, T. Kibédi, A.E. Stuchbery, G.W. Severin, ^{135}La as an Auger-electron emitter for targeted internal radiotherapy. Phys. Med. Biol. **63**(1), 015026 (2017). https://doi.org/10.1088/1361-6560/aa9b44
552. F. Tárkányi, A. Hermanne, F. Ditrói, S. Takács, I. Spahn, S. Spellerberg, Activation cross-section measurement of proton induced reactions on cerium. Nucl. Instrum. Methods Phys. Res. B **412**, 46–53 (2017). https://doi.org/10.1016/j.nimb.2017.09.008
553. F. Tárkányi, F. Ditrói, B. Király, S. Takács, A. Hermanne, H. Yamazaki, M. Baba, A. Mohammadi, A.V. Ignatyuk, Study of activation cross sections of proton induced reactions on barium: production of ^{131}Ba→ ^{131}Cs. Appl. Radiat. Isot. **68**(10), 1869–1877 (2010). https://doi.org/10.1016/j.apradiso.2010.03.010
554. A. Colombi, M.P. Carante, F. Barbaro, L. Canton, A. Fontana, Production of high-purity ^{52g}Mn from ^{nat}V targets with α beams at cyclotrons. Nucl. Technol. **208**, 735–752 (2022). https://doi.org/10.1080/00295450.2021.1947122
555. S. Goriely, S. Hilaire, A.J. Koning, Improved predictions of nuclear reaction rates with the TALYS reaction code for astrophysical applications. Astron. Astrophys. **487**, 767 (2008). https://doi.org/10.1051/0004-6361:20078825
556. M. Herman, R. Capote, B.V. Carlson, P. Obložinskỳ, M. Sin, A. Trkov, H. Wienke, V. Zerkin, EMPIRE: nuclear reaction model code system for data evaluation. Nucl. Data Sheets **108**, 2655–715 (2007). https://doi.org/10.1016/j.nds.2007.11.003
557. T.T. Böhlen, F. Cerutti, M.P.W. Chin, A. Fassò, A. Ferrari, P.G. Ortega, A. Mairani, P.R. Sala, G. Smirnov, V. Vlachoudis, The FLUKA code: developments and challenges for high energy and medical applications. Nucl. Data Sheets **120**, 211–214 (2014). https://doi.org/10.1016/j.nds.2014.07.049
558. T. Sato, Y. Iwamoto, S. Hashimoto, T. Ogawa, T. Furuta, S. Abe, T. Kai, P.E. Tsai, N. Matsuda, H. Iwase, N. Shigyo, L. Sihver, K. Niita, Features of particle and heavy ion transport code system (PHITS) version 3.02. J. Nucl. Sci. Technol. **55**, 684–690 (2018). https://doi.org/10.1080/00223131.2017.1419890
559. F. Barbaro, L. De Dominicis, L. Canton, M.P. Carante, A. Colombi, A. Fontana, A. Stolarz, Theoretical study for a ^{117m}Sn production experiment with a 30 MeV α-beam cyclotron. Nuovo Cim. C **43**, 136 (2020). https://doi.org/10.1393/ncc/i2020-20136-x

560. L. De Dominicis, F. Barbaro, L. Canton, M.P. Carante, A. Colombi, A. Fontana, L. Mou, G. Pupillo, A. Stolarz, P.J. Napiorkowski, Production of ^{117m}Sn in ^{nat}Cd and ^{nat}In targets with an α-beam. Nuovo Cim. C **44**, 129 (2021). https://doi.org/10.1393/ncc/i2021-21129-y
561. A. Yu. Konobeyev, U. Fischer, P.E. Pereslavtsev, A.J. Koning, Implementation of GDH model in TALYS-1.7 code. Report KIT Scientific Working Papers 45 (2016)
562. M. Blann, Importance of the nuclear density distribution on pre-equilibrium decay. Phys. Rev. Lett. **28**(12), 757 (1972). https://doi.org/10.1103/PhysRevLett.28.757
563. M. Blann, H.K. Vonach, Global test of modified precompound decay models. Phys. Rev. C **28**, 1475–1492 (1983). https://doi.org/10.1103/PhysRevC.28.1475
564. M.B. Fox, A.S. Voyles, J.T. Morrell, L.A. Bernstein, A.M. Lewis, A.J. Koning, J.C. Batchelder, E.R. Birnbaum, C.S. Cutler, D.G. Medvedev, F.M. Nortier, E.M. O'Brien, C. Vermeulen, Investigating high-energy proton-induced reactions on spherical nuclei: implications for the preequilibrium exciton model. Phys. Rev. C **103**, 034601 (2021). https://doi.org/10.1103/PhysRevC.103.034601
565. M. Nicolaidis, *Soft Errors in Modern Electronic Systems*, vol. 41 (Springer, New York, 2011). https://doi.org/10.1007/978-1-4419-6993-4
566. T. Nakamura, M. Baba, E. Ibe, Y. Yahagi, H. Kameyama, *Terrestrial Neutron-Induced Soft Errors in Advanced Memory Devices* (World Scientific, Singapore, 2008)
567. J.-L. Autran, D. Munteanu, *Soft Errors: From Particles to Circuits* (CRC Press, Boca Raton, 2015)
568. E.N. Gonzalez, Radiotrazadores para el estudio de Ecosistemas Marinos y Oceánicos (GVA-THINKINAZUL/2021/036). Web page (2021). https://www.csic.es/es/investigacion/proyectos-de-investigacion/radiotrazadores-para-el-estudio-de-ecosistemas-marinos-y
569. F. Houlbreque, S. Reynaud, C. Godinot, F. Oberhansli, R. Rodolfo-Metalpa, C. Ferrer-Pages, Ocean acidification reduces feeding rates in the scleractinian coral Stylophora pistillata. Limnol. Oceanogr. **60**(1), 89–99 (2015). https://doi.org/10.1002/lno.10003
570. G. de Angelis, G. Fiorentini, The Legnaro National Laboratories and the SPES facility: nuclear structure and reactions today and tomorrow. Phys. Scr. (2016). https://doi.org/10.1088/0031-8949/91/11/113001
571. F. Borgna, M. Ballan, S. Corradetti, E. Vettorato, A. Monetti, M. Rossignoli, M. Manzolaro, D. Scarpa, U. Mazzi, N. Realdon, A. Andrighetto, A preliminary study for the production of high specific activity radionuclides for nuclear medicine obtained with the isotope separation on line technique. Appl. Radiat. Isot. **127**, 214–216 (2017). https://doi.org/10.1016/j.apradiso.2017.06.022
572. M. Ballan, M. Tosato, M. Verona, M. Caeran, F. Borgna, E. Vettorato, S. Corradetti, L. Zangrando, M. Sgaravatto, M. Verlato, M. Asti, G. Marzaro, F. Mastrotto, V. Di Marco, D. Maniglio, A. Bisio, A. Motta, A. Quaranta, A. Zenoni, P. Pastore, N. Realdon, A. Andrighetto, Preliminary evaluation of the production of non-carrier added ^{111}Ag as core of a therapeutic radiopharmaceutical in the framework of ISOLPHARM_Ag experiment. Appl. Radiat. Isot. (2020). https://doi.org/10.1016/j.apradiso.2020.109258
573. M. Ballan, E. Vettorato, L. Morselli, M. Tosato, S. Nardella, F. Borgna, S. Corradetti, A. Monetti, M. Lunardon, A. Zenoni, V. Di Marco, N. Realdon, A. Andrighetto, Development of implantation substrates for the collection of radionuclides of medical interest produced via ISOL technique at INFN-LNL. Appl. Radiat. Isot. (2021). https://doi.org/10.1016/j.apradiso.2021.109795
574. G. Franchin, H. Elsayed, R. Botti, K. Huang, J. Schmidt, G. Giometti, A. Zanini, A.D. Marzi, M. D'Agostini, P. Scanferla, Y. Feng, P. Colombo, Additive manufacturing of ceramics from liquid feedstocks. Chin. J. Mech. Eng. Addit. Manuf. Front. **1**, 100012 (2022). https://doi.org/10.1016/j.cjmeam.2022.100012
575. A.H.F. Muggleton, Deposition techniques for the preparation of thin film nuclear targets. Vacuum **37**, 785–817 (1987). https://doi.org/10.1016/0042-207X(87)90180-1
576. F. Pinna, D. Calvo, M. Campostrini, V. Capirossi, F. Delaunay, M. Fisichella, F. Iazzi, V. Rigato, Evaluation of target non-uniformity and dispersion effects on energy measurement resolution in NUMEN experiment. Phys. Scr. (2020). https://doi.org/10.1088/1402-4896/aba779
577. R. Depalo, C. Broggini, A. Caciolli, A. Guglielmetti, R. Menegazzo, V. Rigato, The HEAT project: study of hydrogen desorption from carbon targets, in *Nuclei in the Cosmos XV. Springer Proceedings in Physics*, vol. 219 (2019). https://doi.org/10.1007/978-3-030-13876-9_61
578. H. Skliarova, S. Cisternino, L. Pranovi, L. Mou, G. Pupillo, V. Rigato, C.R. Alvarez, HIVIPP deposition and characterization of isotopically enriched ^{48}Ti targets for nuclear cross-section measurements. Nucl. Instrum. Methods Phys. Res. A (2020). https://doi.org/10.1016/j.nima.2020.164371
579. S. Cisternino, H. Skliarova, P. Antonini, J. Esposito, L. Mou, L. Pranovi, G. Pupillo, G. Sciacca, Upgrade of the HIVIPP deposition apparatus for nuclear physics thin targets manufacturing. Instruments (2022). https://doi.org/10.3390/instruments6030023
580. G. Pupillo, A. Fontana, L. Canton, F. Haddad, H. Skliarova, S. Cisternino, P. Martini, M. Pasquali, A. Boschi, J. Esposito, A. Duatti, L. Mou, Preliminary results of the PASTA project. Nuovo Cim. C (2019). https://doi.org/10.1393/ncc/i2019-19139-1
581. J. Wyss, D. Bisello, D. Pantano, SIRAD: an irradiation facility at the lnl tandem accelerator for radiation damage studies on semiconductor detectors and electronic devices and systems. Nucl. Instrum. Methods Phys. Res. A **462**, 426–434 (2001). https://doi.org/10.1016/S0168-9002(01)00193-0
582. ASIF: ASI Supported Irradiation Facilities: Accordi ASI-ENEA, ASI-INFN. Web page. https://www.asi.it/tecnologia-e-ingegneria/lingegneria/asif/
583. P. Mastinu, D. Bisello, R.A. Barrera, I. Porras, G. Prete, L. Silvestrin, J. Wyss, ICANS-XXIII, hosted by the Oak Ridge National Laboratory Neutron Sciences Directorate. J. Neutron Res. **22**, 233–247 (2020). https://doi.org/10.3233/JNR-200156
584. F. Pinna, V. Capirossi, F. Delaunay, F. Iazzi, O. Brunasso, D. Calvo, M. Fisichella, Tests of a cooling system for thin targets submitted to intense ion beams for the NUMEN experiment. Acta Phys. Pol. B (2020). https://doi.org/10.5506/APhysPolB.51.655
585. S. Bertoldo, G. Maggioni, W. Raniero, C. Carraro, S. Riccetto, F. Sgarbossa, D. Scarpa, A. Andrighetto, A. Mazzolari, A. Gadea, D.R. Napoli, E. Napolitani, D. De Salvador, New method for the production of thin and stable, segmented n+ contacts in HPGe detectors. Eur. Phys. J. A **57**, 177 (2021). https://doi.org/10.1140/epja/s10050-021-00487-8
586. S.M. Carturan, A. Quaranta, Polysiloxane-based scintillators, in *Plastic Scintillators. Topics in Applied Physics*, vol. 140, ed. by M. Hamel (Springer, Cham, 2021), pp.169–199. https://doi.org/10.1007/978-3-030-73488-6_5
587. LiquidO Consortium, Neutrino physics with an opaque detector. Commun. Phys. **4**, 273 (2021). https://doi.org/10.1038/s42005-021-00763-5
588. A. Lo Giudice, P. Olivero, C. Manfredotti, M. Marinelli, E. Milani, F. Picollo, G. Prestopino, A. Re, V. Rigato, C. Verona, G. Verona-Rinati, E. Vittone, Lateral IBIC characterization of single crystal synthetic diamond detectors. Phys. Status Solidi RRL **5**, 80–82 (2011). https://doi.org/10.1002/pssr.201004488
589. M. Bagatin, S. Gerardin, A. Paccagnella, S. Beltrami, A. Costantino, C. Poivey, G. Santin, V. Ferlet-Cavrois, C. Cazzaniga, C. Frost, A heavy-ion detector based on 3-D NAND flash memories. IEEE Trans. Nucl. Sci. **67**(1), 154–160 (2020). https://doi.org/10.1109/TNS.2019.2955776